IDENTIFICATION AND CHARACTERIZATION OF YOUNG, NEARBY, SOLAR-TYPE STARS

by

Eric Earl Mamajek

A Dissertation Submitted to the Faculty of the

DEPARTMENT OF ASTRONOMY

In Partial Fulfillment of the Requirements
For the Degree of

DOCTOR OF PHILOSOPHY

In the Graduate College

THE UNIVERSITY OF ARIZONA

2004

The University of Arizona ®
Graduate College

As members of the Final Examination Committee, we certify that we have read the dissertation prepared by Eric Earl Mamajek

entitled Identification and Characterization of Young, Nearby, Solar-Type Stars

and recommend that it be accepted as fulfilling the dissertation requirement for the Degree of Doctor of Philosophy

Michael R. Meyer	7-1-04 date
James Liebert	7/1/04 date
John Bieging	7/1/04 date
Dennis Zaritsky	7/1/04 date
Philip Hinz	7/1/04 date

Final approval and acceptance of this dissertation is contingent upon the candidate's submission of the final copies of the dissertation to the Graduate College.

I hereby certify that I have read this dissertation prepared under my direction and recommend that it be accepted as fulfilling the dissertation requirement.

Dissertation Director: Michael R. Meyer July 16, 2004 date

STATEMENT BY AUTHOR

This dissertation has been submitted in partial fulfillment of requirements for an advanced degree at The University of Arizona and is deposited in the University Library to be made available to borrowers under rules of the Library.

Brief quotations from this dissertation are allowable without special permission, provided that accurate acknowledgment of source is made. Requests for permission for extended quotation from or reproduction of this manuscript in whole or in part may be granted by the head of the major department or the Dean of the Graduate College when in his or her judgment the proposed use of the material is in the interests of scholarship. In all other instances, however, permission must be obtained from the author.

SIGNED: 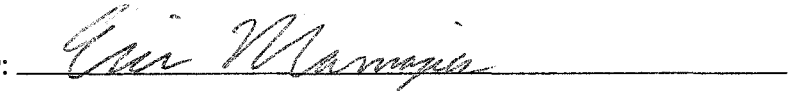

ACKNOWLEDGMENTS

First[1], I would like to thank my parents, Karen and Ronald Mamajek, for almost three decades of constant encouragement and support. I know they have been waiting a *long time* for me to be no longer considered a "student". I would like to thank my advisor Michael Meyer for his endless support and patience over the past few years. Mike has a gift for teaching how to be, and think, like a scientist. I suspect many more graduate students will benefit from his gift during his career. I would also like to thank Jim Liebert for our many conversations over the years. Jim is the heart of the astronomy graduate program at Steward, and I thank him on behalf of all of the graduate students who have benefited from his efforts. I would like to thank my previous research advisors for helping me reach where I'm at today: Eric Feigelson, Warrick Lawson, and Larry Ramsey. Among other things, I am particularly indebted to Eric, for taking a chance on me as an undergrad researcher, to Warrick, for teaching me how to be an observer, and to both, for guiding my MSc research projects. I have been inspired, influenced, and helped over the past 2+ decades or by many excellent scientists, educators, and enthusiasts. I would like to thank (in $\alpha\beta$ order): AAAP, D. Arnett, J. Bechtold, J. Beiging, Bethel Park school teachers, A. Blaauw, A. Burrows, J. Carpenter, J. Charlton, L. Close, J. Cocke, C. Corbally, J. de Bruijne, P. Deutsch, T. de Zeeuw, D. Eisenstien, X. Fan, T. Fleming, B. Green, R. Griffiths, L. Hillenbrand, D. Hines, P. Hinz, W. Hoffmann, R. Hoogerwerf, B. Januzzi, R. Kennicutt, L. Lebofsky, F. Melia, J. Monroe, Mrs. Nunes, E. Olszewski, P. Pinto, K. Ratnatunga, G. Rieke, C. Sagan, G. Schmidt, D. Schneider, G. Schneider, D. Soderblom, J. Stauffer, M. Steinmetz, P. Strittmatter, S. Strom, M. Sykes, L. Takahashi, G. Wargo, G. Wayne, R. White, S. Wolff, C. Wu, and D. Zaritsky. Among the students and "young" folks at Steward, LPL, and NOAO, I would like to thank everyone who has shared in the many good times over the past five years ($\alpha\beta$ order): J. Bailin, M. Brown, F. Ceisla, C. Cooper, C. Drouet D'Aubigny, K. Eriksen, M. Freed, N. Gorlova, C. Groppi, J. Hinz, V. Ivanov, M. "Fishboy" Kenworthy, S. Kim, K. Knierman, C. Kulesa, J. Lee, A. Leistra, W. Liu, A. Marble, C. Meakin, D. Miller, I. Momcheva, J. Monkiewicz, A. Moro-Martin, J. Moustakas, J. Murphy, D. O'Brien, E. Offerdahl, B. Oppenheimer, C. Peng, T. Pickering, G. Rudnick, N. Seigler, H.-J. Seo, M. Silverstone, A. Stutz, T. Thompson, M. Turnbull, G. Williams, K. Williams, P. Withers, & P. Young. I warmly thank the excellent people at Steward who have helped keep me on track ($\alpha\beta$ order): M. Cournoyer, C. Diaz-Silva, B. Duffy, J. Facio, J. Flores, J. Fookson, B. Fridena, A. Koski, N. Lauver, K. Morse, S. Thomas. Last, but certainly not least, I thank my love Lissa Miller for putting up with me while I finished this thesis. I don't know how she did it, but I love her for it.

[1]It is a ludicrous policy that one can write a thesis of unlimited length, but there is a page limit (1) for acknowledgments – *especially when the thesis formatting requires so much empty space!*

DEDICATION

This thesis is dedicated to my parents Karen and Ronald Mamajek.

TABLE OF CONTENTS

TABLE OF CONTENTS — *Continued*

TABLE OF CONTENTS — *Continued*

LIST OF FIGURES

LIST OF TABLES

ABSTRACT

Post-T Tauri stars (PTTSs) are low-mass, pre-MS stars which have ceased accreting, and are not necessarily near star-forming molecular clouds. Historically, they have been difficult to identify due to their benign spectroscopic signatures. With recent all-sky X-ray surveys and proper motion catalogs, it is now possible to find PTTSs in large numbers. The nearest PTTSs will be important targets for future imaging surveys characterizing dust disks and planetary systems around young solar analogs. The goal of this work is to systematically identify samples of PTTSs, investigate the evolution of circumstellar disks, to infer the fossil star-formation history of molecular clouds, and to estimate kinematic distances to young stars lacking trigonometric parallaxes. We present the results of a spectroscopic survey which identified 110 PTTS members of the nearest OB association (Sco-Cen). We find that 2/3rds of the low-mass star-formation in each OB subgroup occurred in <5 Myr, and that only ~1% of solar-type stars with mean age ~13 Myr shows signs of accretion from a circumstellar disk. In order to assess how long circumstellar material is detectable around PTTSs, we conducted a 10μm imaging survey of post-T Tauri members of the ~30-Myr-old Tuc-Hor association. The goal was to find evidence of either remnant accretion disks or dusty debris disks with orbital radii of $\lesssim$10 AU. Combined with data from other surveys, we conclude that mid-IR emission from warm dust grains in the terrestrial planet zones around young stars become undetectable compared to the stellar photosphere for nearly all stars by age ~20 Myr. Lastly, we present a technique for calculating distances isolated young field stars that currently lack trigonometric parallax measurements. The technique is a generalization of the classical cluster parallax method, but can handle anisotropic velocity dispersions

and non-zero Oort parameters. Distances and isochronal ages are estimated for a subsample of PTTSs included in the *Formation and Evolution of Planetary Systems* (FEPS) Spitzer Space Telescope (SST) Legacy Science program. The techniques developed in this thesis will allow one to efficiently conduct a systematic survey to identify the nearest, youngest stars to the Sun using existing databases.

CHAPTER 1

INTRODUCTION

Understanding the origins of stars and planetary systems is one of the most important goals of modern astronomy. We would like to know: how do molecular clouds form stars and circumstellar disks, and how do circumstellar disks evolve into planets? The specific goals of this thesis are to (1) investigate the fossil record of star-formation in the nearest OB association, and (2) study the evolution of circumstellar environments within 10 AU of young solar-type stars. In order to achieve these goals, we need to develop and employ techniques for efficiently selecting young solar-type stars from among field stars. By "young solar-type stars", we refer to adolescent stars similar in mass to our Sun (FGK stars, $\sim$0.5-1.5 $M_{\odot}$) with ages between a few Myr (actively-accreting Classical T Tauri stars) and $\sim$100 Myr (zero-age main sequence, or "ZAMS" stars). We will often refer to these objects, at least those that lack accretion disks, as "post-T Tauri stars" (PTTSs) throughout this work.

Identifying stellar adolescents has historically been a thorny problem due to their lack of obvious spectral signatures in low-resolution optical spectra (e.g. objective prism Hα surveys). Two recent breakthroughs have now made it possible to find these objects efficiently: multi-wavelength all-sky surveys (e.g. the *ROSAT* X-ray and EUV surveys), and high accuracy proper motion catalogs (e.g. Tycho-2; Høg et al., 2000a). The rapid rotation of young stars drives a vigorous stellar dynamo, producing copious, coronal X-ray emission. Young stars are also born in groups with small velocity dispersions, and the Galactic potential has not

had time to thoroughly scatter their space motion vectors. The convergence of their proper motions enhances their visibility in proper motion catalogs. We exploit the combination of X-ray brightness and kinematic coherence of the post-T Tauri stars in order to efficiently identify them for follow-up spectroscopy.

Finding and studying post-T Tauri stars is crucial to elucidating the evolution of circumstellar disks, the evolution of stellar angular momentum, and the the formation and destruction(?) of planets and planetesimals. Furthermore, *the nearest post-T Tauri stars are arguably the best targets for resolving circumstellar disks, and identifying young, luminous Jovian planets.* While the benefits of studying post-T Tauri stars are large for stellar astrophysics, their greatest potential value may well prove to be for planetary science. Understanding the evolution of stars, their circumstellar disks, and planetary systems, is crucial for placing our solar system, and Earth, in context.

Post-T Tauri stars also represent the recently-finished end-products of the star-formation process. In this context, the age spread of post-Tauri star populations can reveal how long the epoch of star-formation lasted within a given molecular cloud. There currently exists a debate as to whether molecular clouds form stars and dissipate over a short timescale (<few Myr) or much longer (>10 Myr), and whether high-mass and low-mass stars form contemporaneously, or sequentially. The view that molecular clouds form stars over a wide spectrum of masses within a short timescale (<few Myr), and then are dispersed by stellar winds and supernovae, appears to be favored. However, more observational data are needed to confirm this picture.

In what follows, we review the basic star-formation process, post-T Tauri stars, circumstellar disks and planet formation, and well as problems inherent in deriving distances to isolated young stars, in order to set the stage for this

thesis.

1.1 From Molecular Clouds to T Tauri Stars

Imagine yourself looking down on our Milky Way galaxy from above. Our Sun would be an inconspicuous faint point of light situated about 8 kpc from the Galactic center, and roughly half way between two spiral arms (Perseus and Sagittarius). You would notice that most luminous, blue, OB-type stars, H II regions, reflection nebulae, and dark (molecular) clouds, are concentrated along these spiral arms. The Sun appears to be situated in an inter-arm clump of molecular clouds and young stellar complexes. This inter-arm spiral arc is often called the "Orion Arm" or "Local Arm". While most of these bright, short-lived blue stars and molecular clouds are concentrated near the dense spiral arms, we are fortunate to have, up close within the Local Arm, many examples of OB associations and molecular clouds within a few hundred parsecs of the Sun. Ironically the Sun is situated in a local *under-density* of the interstellar medium (the "Local Bubble"). The nearest molecular clouds and OB associations are situated roughly 150 pc distant in Taurus-Auriga in the 2nd Galactic quadrant, and towards the Sco-Cen complex in the 4th Galactic quadrant (including the Chamaeleon, Lupus, Ophiuchus, and Corona Australis molecular cloud complexes).

A wealth of observational evidence demonstrates that stars are formed in the densest portions of molecular cloud complexes (e.g. Kenyon & Hartmann, 1995; Evans, 1999; Myers, 1999). In dense molecular clouds cores, self-gravity overcomes thermal, magnetic, and turbulent pressure, and collapses to form a flattened, rotating disk of gas and dust: a protostar (Shu, Adams, & Lizano, 1987; Shu et al., 1999, and references therein). The dust surrounding the protostar radiates (and re-radiates) much of the thermal energy from gravitational collapse

in the form of infrared and millimeter wavelength radiation (e.g. Lada & Wilking, 1984; Beichman et al., 1986; Motte, Andre, & Neri, 1998). One classification system of young stellar objects (YSOs) is based primarily on the shape of the spectral energy distribution (Lada, 1987; Adams, Lada, & Shu, 1987). An evolutionary sequence seems to exist whereby the coolest and most heavily embedded (extincted) objects are younger, and evolve into objects whose spectral energy distributions (SEDs) resemble reddened stellar photospheres. The material in the protostellar disk either viscously accretes onto the protostar, is ejected via interaction with the protostar's bipolar jets or stellar winds, or is photoevaporated by UV radiation (Hollenbach, Yorke, & Johnstone, 2000). As the extinction along the line-of-sight between the nascent star and the observer decreases, the young star becomes visible at optical wavelengths, and is called a "T Tauri star".

T Tauri stars were first identified as a stellar class by their variability and strong emission lines (Joy, 1945). The case for their classification as newly-formed, low-mass, pre-main sequence stars comes from the following: (1) proximity to dark or bright nebulae (both spatially, and in velocity), (2) spatial coincidence with unbound, short-lived (<tens Myr), OB associations, (3) luminosities above the main sequence on a Hertzsprung-Russell diagram, and (4) high Li abundance[1]. T Tauri stars exhibit near-infrared excess emission, first identified and attributed to circumstellar dust by Mendoza (1968). The most popular model for explaining the characteristics of T Tauri stars is that of a pre-main sequence star which accretes gas along magnetic field lines from a truncated circumstellar disk (e.g. Koenigl, 1991). Periodic variability can be caused by the rotational

[1]The very youngest stars have a Li abundance similar to that observed in meteorites in our own solar system (Strom et al., 1989), suggesting that the Galactic ISM [Li/H] ratio has changed little over its history. The two prevalent isotopes of Li (^{6}Li and ^{7}Li) are efficiently destroyed at $\sim 2 \times 10^6$ K in stellar interiors. Pre-MS low-mass stars are mostly convective, and can expose the gas in the outer covective layer to zones with the high temperatures and densities required for Li burning. In this sense, the photospheric abundance of Li can be used as a rough chronometer.

modulation of dark starspots (magnetically cooled regions) and bright regions (heated ($\sim 10^4$ K) boundary regions between the star and magnetospheric accretion columns). Non-periodic variability is also seen in many T Tauri stars, and may be due to variations in accretion rate and extinction. Several hundred T Tauri stars have been found clustered among nearby dark clouds via their variability or strong emission lines (e.g. Herbig & Bell, 1988).

Comparing the positions of T Tauri stars in the Hertzsprung-Russell diagram (HRD; i.e. effective temperature vs. luminosities) to theoretical evolutionary tracks, one surmises that the majority are less than a few Myr-old (Cohen & Kuhi, 1979; Hartmann, 2001). As the dark clouds associated with T Tauri stars are thought to survive for tens of Myr (e.g. Blitz & Shu, 1980) in order to account for the present star-formation rate in the Galactic disk compared to the number of molecular clouds observed, it is reasonable to ask: where are the evolutionary descendants of the T Tauri stars? If ambipolar diffusion is constraining which parts of a cloud proceed to collapse, presumably a range of initial conditions will lead to a wide range of formation times for the stars formed in a cloud complex. Is such a range of age observed?

Herbig (1978) logically pointed out that T Tauri stars must lose their signatures of activity (as manifested through IR excess and emission lines) at some point, separate themselves from star-forming molecular clouds, and join the field population. If the majority of T Tauri stars were observed to have isochronal ages of $\lesssim$3 Myr, and the ambipolar diffusion timescale is (coincidently) similar in duration to the Kelvin-Helmholtz time for a $\sim 1\ M_\odot$ star to reach the main sequence ($\sim$30 Myr), where are the 90% of pre-MS stars which are older ($\sim$3-30 Myr) than the observed T Tauri star populations? There was little evidence of this "missing" pre-MS stellar population at the time of Herbig's study. Very few candidates were

then known which had characteristics intermediate between that of T Tauri stars (<few Myr) and zero-age main sequence stars (like those found in the Pleiades cluster; ages ~100 Myr). So where are Herbig's"post-T Tauri" stars?

1.2 "Weak-lined" T Tauri Stars = Post-T Tauri Stars?

Observations with the *Einstein* X-ray observatory in the early 1980's yielded a surprise. Nearby star-forming clouds had the appearance of "X-ray Christmas trees" (Montmerle et al., 1983). The T Tauri star populations in molecular clouds were strong, variable X-ray sources, with luminosities roughly 2-4 orders of magnitude brighter than that of the Sun (e.g Feigelson & Kriss, 1981). Interspersed among the X-ray-luminous T Tauri stars was *another*, separate population of X-ray-luminous, Li-rich, pre-MS stars (Feigelson & Kriss, 1981; Walter & Kuhi, 1981). These new objects ("weak-lined T Tauri stars" ; WTTSs) lack evidence of accretion from a circumstellar disk, i.e. strong emission lines, and strong near-IR and UV excess emission. While many of the WTTSs were co-spatial with the "Classical" T Tauri stars (CTTSs) near molecular cloud cores, others were widely distributed tens of parsecs from active star-forming clouds. The isochronal ages of the WTTSs initially suggested a wide range of ages, between ~1-40 Myr (Walter et al., 1988). The existence of WTTSs with ages of ~1 Myr and CTTSs with ages of ~5 Myr was already an indication that low-mass stars have a wide range of accretion disk lifetimes.

From the number density of WTTSs discovered in the Einstein survey fields around the Taurus-Auriga molecular clouds, the total population of WTTSs was extrapolated to outnumber that of CTTSs by 10:1 (Walter et al., 1988), in agreement with Herbig's predictions. Many believed that the WTTSs found in the Einstein surveys were the tip of the iceberg of the long-sought post-T Tauri pop-

ulation. Yet, large scale surveys using spectroscopic or proper motion selection (Jones & Herbig, 1979; Herbig, Vrba, & Rydgren, 1986; Hartmann et al., 1991) failed to identify the population predicted to exist by the Einstein studies. Conflicting data suggested that the post-T Tauri problem was not yet solved.

In the mid-1990's, the *ROSAT* All-Sky Survey identified hundreds of new X-ray sources both inside and outside of the nearest molecular clouds. The stellar counterparts to these X-ray sources are predominantly Li-rich, late-type stars, and they were originally thought to be the population postulated to exist by Walter et al. (1988) (e.g. Wichmann et al., 1996; Alcalá et al., 1995). However, subsequent studies using high resolution spectroscopy (Wichmann et al., 2000; Covino et al., 1997), astrometry (Frink, 1999), as well as arguments regarding the star-formation history of the local Galactic disk (Briceño et al., 1997), suggested that these objects were a heterogeneous mix of bona fide T Tauri stars associated with dark clouds, as well as young field stars. At present, there appears to be little evidence for the existence of substantial numbers of older pre-MS stars (>3 Myr) centered on existing molecular clouds.

One unexpected result from the *ROSAT* All-Sky Survey was the discovery of isolated ~5-30 Myr-old low-mass stars *unassociated with known star-forming clouds*. Several of these groups were found within 100 pc of the Sun: the η Cha cluster (Mamajek, Lawson, & Feigelson, 1999), the TW Hya association (Webb et al., 1999), the β Pic moving group (Zuckerman, Song, Bessell, & Webb, 2001), and the Tucana-Horologium association (Zuckerman & Webb, 2000; Torres et al., 2000). It appears that the molecular clouds that formed these isolated stellar groups have been destroyed and star-formation has ceased, explaining why they escaped detection until recently.

Observations suggest that the formation of stars in molecular clouds is re-

markably synchronized, with age spreads of <3 Myr within the stellar populations associated with the nearest T Associations (e.g. Ballesteros-Paredes, Hartmann, & Vázquez-Semadeni, 1999). The small number of stars with ages >3 Myr suggested to exist in the nearest molecular clouds can be largely attributed to uncertainties in HRD positions (Hartmann, 2001), and possibly unassociated young field stars. The classical theory of star-formation suggests that the cloud cores producing low-mass stars are magnetically supported (Shu, Adams, & Lizano, 1987), and hence the lifetime of molecular clouds should be limited by the ambipolar diffusion timescale (~10-20 Myr; Palla & Galli, 1997). While most of the gas in dark clouds is molecular, a small fraction of the particules are ions, and the motions of the ions along magnetic field lines impedes the collapse of the molecular component. For typical parameters of molecular clouds, the ambipolar diffusion timescale is always larger than the free-fall collapse timescale by roughly an order of magnitude (McKee et al., 1993). The ambipolar diffusion timescale is controlled by the density of ions and neutral gas, magnetic field strength, and the diameter of the cloud. It is unclear why this combination of variables should conspire to produce all stars in a molecular cloud within a few Myr. It has been proposed that magnetic field pressure may not be the dominant factor controlling the star-formation timescale (and hence the average star-formation rate of the Galaxy), but perhaps collisions between large parcels of mostly neutral ISM, resulting in the rapid formation of clouds with and large turbulent pressure (Hartmann, Ballesteros-Paredes, & Bergin, 2001). In order to place quantitative constraints on this scenario, we need to sample the entire stellar population associated with a fossil giant molecular cloud - including any older PTTSs if they exist.

1.3 Finding Samples of Post-T Tauri Stars

Although strict observational criteria do not exist for classifying Post-T Tauri stars (PTTSs), a working definition is a low-mass star ($<2\ M_{\odot}$) that is Li-rich compared to stars on the ZAMS such as the $\sim$125 Myr-old Pleiades, and whose theoretical HR diagram position is above the main sequence (Herbig, 1978; Jensen, 2001). Since these criteria would also include CTTSs and WTTSs, one could argue that PTTSs should have ages >3 Myr, the typical lifetime of accretion disks that are responsible for CTTS activity. The lack of observational evidence for PTTSs *within* existing molecular cloud complexes (Hartmann, Ballesteros-Paredes, & Bergin, 2001) suggests that if they exist, they are outside of these clouds interspersed among the field population. Classifying PTTSs by these criteria has complications: (1) few young field stars not associated with well-studied molecular clouds currently have accurately measured distances (i.e. known luminosities), (2) unresolved binarity can make stars with known distances appear more luminous, and thus younger, (3) there is a dispersion in observed Li abundances among stars with the same masses and ages in coeval open clusters, and (4) other rare objects, such as evolved, tidally-locked binaries (RS CVns) can lie above the main sequence, be Li-rich, and X-ray bright, masquerading as PTTSs. X-ray surveys (*Einstein* and *ROSAT*) have proven to be the most efficient means of first identifying pre-MS candidates to date. Ideally, one would like additional criteria for separating *bona fide* young stars from other species of X-ray-luminous objects.

In §2 we describe a unique survey undertaken in the Sco-Cen OB association for identifying the largest and nearest sample of solar-type, post-T Tauri stars ever assembled. We predicted that low-mass Sco-Cen members should be X-ray luminous and have proper motions parallel to those of the higher mass members found by Hipparcos. The near-simultaneous availability of an all-sky catalog of

X-ray sources (*ROSAT* All-Sky Survey) and relatively deep proper motion catalog (Tycho) made it possible to not only isolate active stars from the field population, but select only those whose motions were convergent with the B-type subgroup members. Selection by X-ray emission and astrometry proved very fruitful – over 90% of the candidates selected proved to be Li-rich, pre-MS stars. Our study was able to place constraints on the star-formation history of the Sco-Cen OB subgroups, as well as determine the incidence of accretion disks around older pre-MS stars (~10-15 Myr).

1.4 Circumstellar Disk Evolution

One important question that can be addressed with representative samples of PTTSs is the timescale for disk evolution with a few AU. For example, it is thought that the bulk of the mass accretion for the solar system's terrestrial planets took place during the first $\sim 10^7$-10^8 yr of its history (Agnor, Canup, & Levison, 1999; Chambers, 2001). From observations of young stars in nearby molecular clouds, we now know that circumstellar disks are a nearly ubiquitous by-product of the star-formation process. Most low-mass stars in the youngest star-formation regions (e.g. the ~1-Myr-old Orion Nebula Cluster) have spectroscopic or photometric evidence of a circumstellar disk (Hillenbrand et al., 1998). The masses of circumstellar disks found around some T Tauri stars are similar to that of the minimum mass solar nebula (Beckwith et al., 1990) – the amount of H, He, and metals required to form the planets in our solar system. The physical sizes of circumstellar disks around T Tauri stars are similar to that of our own solar system (10s-100s AU; McCaughrean & O'Dell, 1996). Considering their masses, dimensions, and appearance at the very earliest stages of stellar evolution, these disks are hypothesized to be "protoplanetary". Radial velocity surveys of nearby solar-type stars

indicate that at least ~5% have at least one Jupiter-mass planet orbiting within a few AU (Marcy & Butler, 2000). We conclude that the formation of gas giant planets is one likely outcome of circumstellar disk evolution.

The incidence of inner protoplanetary accretion disks diminishes with age, being very common at ages <1 Myr, and very rare at >10 Myr (e.g. §2). The fraction of low-mass stars with disks, as manifested by IR excess (in the L-band; 3.5 μm), diminishes with age, with half losing their inner disks ($\lesssim$0.1 AU) within ~3 Myr (e.g. Haisch, Lada, & Lada, 2001a). Using population statistics of pre-MS stars in the Taurus molecular clouds, multiple studies have demonstrated that the transition time for disks inside of ~1 AU to go from optically-thick to optically-thin is $\sim 10^5$ yr (Skrutskie et al., 1990; Wolk & Walter, 1996).

While some studies argue that accretion terminates by age ~6 Myr (Haisch, Lada, & Lada, 2001a), others suggest that it may continue at lower accretion rates around some stars until at least ~10 Myr (§2, Muzerolle et al., 2000; Lawson et al., 2002; Lawson, Lyo, & Muzerolle , 2004). There are preliminary indications that disks may persist longer for stars in associations which lack massive OB stars and for the lowest mass stars (e.g. Lyo et al., 2003; Haisch, Lada, & Lada, 2001b). The question of whether cooler, remnant disks at larger orbital radii ($\gtrsim$1 AU) exist around stars that have stopped accreting, remains unanswered. How much dust exists within a few AU of post-T Tauri stars, and how does it compare with models of terrestrial planet formation?

In §3, we present the results of a mid-IR survey of members of a newly-discovered post-T Tauri star association (Tucana-Horologium) in order to search for evidence of circumstellar dust. Although it appears that accretion disks (and the near-IR excesses that accompany them) disappear by age ~10 Myr, our survey, combined with the results of other recent surveys, suggest that detectable

10 μm emission from either accretion disks or debris disks, becomes very rare after ~20 Myr. Our survey finds that typical ~30-Myr-old have less than a few thousand times the dust grain surface area that our inner solar system has today. At these levels, the amount of warm dust is undetectable through photometric modeling of spectral energy distributions.

1.5 Secular Parallaxes to Young Field Stars

While kinematic groups can provide important stellar samples for studying the star-formation history of a region and circumstellar disk evolution, they might represent only a small fraction of the integrated young stellar population in the solar neighborhood. Post-T Tauri stars in the field (outside of known clusters and associations) are much harder to find and characterize.

Distances to stars are essential if one wants to derive its luminosity, and potentially estimate its age through the use of theoretical evolutionary tracks. Direct determination of distances to stars through the measurement of trigonometric parallax are limited to stars either bright enough to have been measured by the Hipparcos satellite (V > 7-9^{mag} ESA, 1997), or "special" enough to be included in ground-based parallax measurement programs (usually high proper motion stars, or stars essential for standard candle calibration, e.g. Cepheids). Most isolated, young, Li-rich field stars have either poor parallax determinations from the Tycho experiment on the *Hipparcos* satellite, or no published values at all. While most Li-rich field stars are likely to have absolute magnitudes within a few tenths of the ZAMS, we would like to determine whether any of these field stars are so young that they are still demonstrably pre-main sequence. Very nearby pre-MS stars are highly desirable for studies of the early evolution of stars and circumstellar disks (and the search for planets), however they remain a difficult population

to identify.

In §4, we attempt to estimate distances to young isolated field stars using a variation of the cluster parallax technique. The cluster parallax technique is typically used on only the nearest clusters and OB associations (de Bruijne, 1999b; Madsen, Dravins, & Lindegren, 2002), whose members have large, statistically significant proper motions, and whose internal velocity dispersions ($\leq$1 km s^{-1}) are much smaller than their heliocentric space motions ($\sim$10-50 km s^{-1}). To estimate distances to young field stars which have accurate proper motions (but lack trigonometric parallaxes), we exploit the fact that the youngest ($\lesssim$100 Myr-old) field stars that *do* have accurate trigonometric parallaxes have similar 3D space motions with a relatively small velocity dispersion ($\sim$5 km s^{-1}) compared to their heliocentric speed ($\sim$20 km s^{-1}). These young stars are often called the "Local Association" or "Gould Belt" depending on how restrictive the group is defined in position, age, and velocity. Although the young field stars do not form a cluster in the classical sense (i.e. a spatially compact group of co-moving, co-eval stars formed in the same star-formation event), the coherence of the space motion vectors for the Local Association allows us to use similar techniques for selecting members and estimating distances. We develop an iterative algorithm which can be used to determine membership probabilities and distances for stars that belong to groups with previously determined velocity fields (mean space motion, velocity dispersion, and Oort parameters). We find that many of the Li-rich stars in the "Formation and Evolution of Planetary Systems" (FEPS) Spitzer Legacy Science program are likely members of the Local Association. The kinematic distances that we calculate imply luminosities that are either on the ZAMS or pre-MS. The iterative algorithm developed in §4, along with other spectroscopic and kinematic selection criteria, will be extremely useful for future surveys intent on

systematically identifying the youngest, closest, post-T Tauri and ZAMS stars to the Sun.

CHAPTER 2

FINDING POST-T TAURI STARS IN THE NEAREST OB ASSOCIATION

The contents of this chapter were previously published in Mamajek, Meyer, & Liebert (2002) and Mamajek (2003).

2.1 Introduction

Investigations of pre-main sequence evolution have been hampered by a lack of large samples of well-characterized PTTSs. This deficit has impacted studies of pre-MS angular momentum evolution (e.g. Rebull et al., 2001; Bouvier et al., 1997), stellar multiplicity (e.g. Köhler et al., 2000), and circumstellar disk evolution (e.g. Spangler et al., 2001; Haisch, Lada, & Lada, 2001a). The nearest post-T Tauri stars also provide optimal targets for young exoplanet and brown dwarf searches (e.g. Lowrance et al., 2000). These objects are much more luminous early in their evolution, and the closest targets enable characterization of the smallest orbital radii. With a post-T Tauri population in a nearby OB association, we can address basic questions such as: How long does star-formation persist in a giant molecular cloud? What is the duration of the accretion phase for young solar-type stars?

Identifying a bona fide PTTS sample can be accomplished by searching for low-mass members of nearby fossil OB associations. The Sco-Cen OB complex (Sco OB2) is the nearest OB association to the Sun (mean subgroup distances

range from 118-145 pc; de Zeeuw et al. (1999), hereafter Z99), and covers roughly 2000 square degrees (~5%) of the sky. The complex is comprised of three kinematic subgroups (Blaauw, 1946) with nuclear ages ranging from 5 to 15 Myr, a molecular cloud currently undergoing star-formation (the ρ Oph complex, Wilking, Lada, & Young , 1989; Blaauw, 1991; de Geus, 1992), and several smaller cloud complexes in the vicinity (e.g. the Lupus, Corona Australis, Chamaeleon, Musca, and Coalsack clouds). The three subgroups are Upper Scorpius (US; age 5-6 Myr), Upper Centaurus-Lupus (UCL; age 14-15 Myr), and Lower Centaurus-Crux (LCC; age 11-12 Myr, de Geus et al., 1989). US has been studied extensively in recent years (e.g. Preibisch & Zinnecker, 1999, and references therein), however UCL and LCC have received relatively little attention.

In this work, we investigate the low-mass ($<2\,M_{\odot}$) membership of the two oldest Sco-Cen OB subgroups (LCC and UCL) utilizing recently available astrometric catalogs (*Hipparcos*, Astrographic Catalog-Tycho (ACT), Tycho Reference Catalog (TRC), and *Tycho*-2), the 2 Micron All Sky Survey (2MASS), and the *ROSAT* All-Sky Survey (RASS). We conduct a spectroscopic survey of two samples: (1) an X-ray-selected sample of late-type stars from the kinematic candidate membership lists of Hoogerwerf (2000), and (2) the G-K type *Hipparcos* members of the OB subgroups from Z99. In §2.2, we discuss the procedure for selecting candidate pre-MS stars from both samples, and §2.3 discusses the observations and assembled database. §2.4 describes the data analysis and characterization of our stellar sample, and §2.5 discusses the selection of pre-MS stars, sample contamination, and completeness. §2.6 describes how we construct an H-R diagram for the subgroups, and §2.7 presents results regarding the ages of the subgroups, their age spreads, and the frequency of accretion disks around pre-MS stars. §2.8

discusses the star-formation history of LCC and UCL, and §2.9 summarizes the findings of our survey.

2.2 Selection of Candidate Pre-MS Stars

2.2.1 The *Hipparcos* Sample

Z99 lists *Hipparcos* Sco-Cen members that were selected using *both* de Bruijne's (1999a) refurbished convergent point method and Hoogerwerf & Aguilar's "spaghetti" method (1999). Their membership lists contained 31 G-K stars in UCL and 21 G-K stars in LCC (their Table C1). Most of these bright stars have been classified in the Michigan Spectral Survey (e.g. Houk & Cowley, 1975), however SIMBAD[1] reveals that most have been studied no further. We limit the survey to the 30 G-K candidates with Michigan luminosity classes IV or V (see Table 2.1). Stars with borderline F/G Michigan types were not observed. HIP 63962 and 73777 met the criteria, but were not observed. Z99 estimated the contamination by G-K-type interlopers of all luminosity classes to be 32% for LCC and 24% for UCL. Of these 31 stars, 17 also have RASS-BSC X-ray counterparts within 40″.

[1]http://simbad.u-strasbg.fr/Simbad

Table 2.1. Properties of de Zeeuw et al. (1999) Sco-Cen G-K Candidate Members

(1)	(2)	(3)	(4)	(5)	(6)	(7)	(8)	(9)	(10)	(11)
Name	OB	α, δ (ICRS)	$\mu_{\alpha*}$, μ_δ	V	$(B-V)$	SpT	J	H	K_s	notes
HIP	Grp.	h m s ° ′ ″	(mas yr^{-1})	(mag)	(mag)	MSS	(mag)	(mag)	(mag)	...
57524	LCC	11:47:24.55 -49:53:03.0	-33.7±0.8 -10.2±1.0	9.07	0.63±0.02	G3/5VPq2	7.91±0.02	7.59±0.06	7.51±0.02	1RXS J114724.3-495250, TWA 19A
58996	LCC	12:05:47.48 -51:00:12.1	-37.5±0.8 -11.5±0.8	8.89	0.63±0.02	G1Vq1	7.67±0.01	7.37±0.03	7.27±0.01	var(0.06), 1RXS J120547.8-510007
59854	LCC	12:16:27.84 -50:08:35.8	-29.1±1.3 -8.6±1.0	9.34	0.67±0.02	G3Vq1	8.04±0.01	7.69±0.02	7.61±0.03	1RXS J121627.9-500829
60885	LCC	12:28:40.05 -55:27:19.3	-34.9±0.8 -16.0±0.7	8.89	0.64±0.02	G1q4	7.68±0.02	7.40±0.05	7.28±0.03	var(0.02), 1RXS J122840.3-552707
60913	LCC	12:29:02.25 -64:55:00.6	-37.5±1.2 -11.4±0.9	9.04	0.73±0.02	G5Vq1	7.60±0.01	7.26±0.01	7.14±0.01	...
62445	LCC	12:47:51.87 -51:26:38.2	-30.4±1.0 -8.7±1.0	9.52	0.80±0.03	G8/K0Vq3	7.79±0.01	7.38±0.03	7.25±0.01	var(0.10), 1RXS J124751.7-512638
63797	LCC	13:04:30.96 -65:55:18.5	-42.4±1.0 -14.2±0.8	8.48	0.74±0.01	G3Vq1	7.02±0.04	6.79±0.02	6.71±0.01	...
63847	LCC	13:05:05.29 -64:13:55.3	-36.5±1.1 -19.5±1.3	9.18	0.73±0.02	G5Vq4	7.78±0.01	7.44±0.03	7.36±0.03	var(0.03)
65423	LCC	13:24:35.12 -55:57:24.2	-29.0±1.0 -13.0±1.0	9.59	0.66±0.03	(G3w)F7q2	8.45±0.01	8.16±0.03	8.10±0.01	1RXS J132435.3-555719
65517	LCC	13:25:47.83 -48:14:57.9	-39.0±1.2 -20.3±1.0	9.76	0.60±0.04	K0/2V+(G)q3	8.50±0.02	8.18±0.03	8.08±0.03	var(0.05, P=1.09d),V966 Cen,1RXS J132548.2-481451
66001	LCC	13:31:53.61 -51:13:33.1	-29.0±1.5 -20.1±1.1	9.84	0.72±0.04	G5/6Vq3	8.43±0.01	8.00±0.03	7.83±0.01	1RXS J133152.6-511335
66941	LCC	13:43:08.69 -69:07:39.5	-32.7±0.7 -19.8±0.9	7.57	0.74±0.01	G2IV/Vq2	6.21±0.01	5.85±0.03	5.77±0.01	var(0.08),CCDM 1343-6908,1RXS J134306.8-690754
67522	UCL	13:50:06.28 -40:50:08.8	-29.3±1.5 -22.9±1.0	9.79	0.67±0.04	G1Vq2	8.58±0.01	8.30±0.04	8.16±0.02	1RXS J135005.7-405001
68726	UCL	14:04:07.12 -37:15:50.5	-16.9±0.8 -16.7±0.7	7.11	0.72±0.02	G3IV/Vq3	5.29±0.00	5.40±0.04	4.92±0.05	CCDM 14041-3716
71178	UCL	14:33:25.78 -34:32:37.7	-28.1±1.6 -28.0±1.4	10.18	0.81±0.06	G8/K0Vq3	8.52±0.01	8.06±0.02	7.94±0.02	var(0.15), V1009 Cen
72070	UCL	14:44:30.96 -39:59:20.6	-20.9±1.5 -24.0±1.4	9.32	0.64±0.03	G3Vq3	8.19±0.01	7.93±0.02	7.81±0.01	...
74501	UCL	15:13:29.22 -55:43:54.6	-16.1±0.8 -24.0±0.8	7.47	0.78±0.01	G2IVq1	5.86±0.01	5.48±0.02	5.20±0.01	...
75924	UCL	15:30:26.29 -32:18:11.6	-31.7±2.4 -31.9±2.3	8.80	0.65±0.03	G6Vq2	7.37±0.01	7.05±0.03	6.92±0.02	1RXS J153026.1-321815

2.2.2 The RASS-ACT/TRC Sample

To identify low-mass members of an OB association, one can search for stars whose proper motions are similar to those of high-mass members. The high-mass membership and moving group solution for each OB subgroup were determined by Z99 and de Bruijne (1999b). Thousands of faint stars in the ACT and TRC astrometric catalogs[2] were identified by Hoogerwerf (2000) as candidate low-mass LCC and UCL members. A high degree of contamination from interlopers is expected due to the similarity of the space motions of the subgroups to that of the Local Standard of Rest, compounded by the low galactic latitude of the subgroups. The selection of ACT/TRC candidate members is described in detail in §4 of Hoogerwerf (2000).

The Hoogerwerf ACT/TRC membership lists for LCC and UCL were slightly modified, and filtered, to produce the final target list. First, we requested from R. Hoogerwerf (personal communication) candidate membership lists with different color-magnitude constraints from that described in Hoogerwerf (2000). The new color-magnitude selection box is essentially a polygon defined by the Schmidt-Kaler (1982) empirical zero-age main sequence ($(B-V)$ vs. M_V) at the mean distance for each subgroup (Z99), where we take all stars $\Delta M_V = 3$ mag above and $\Delta M_V = 1$ mag below the ZAMS line. Hoogerwerf originally selected only those stars within $\Delta M_V = 1.5$ mag above the ZAMS, however this could inadvertently omit younger members or binaries. The selection box contained 1353 ACT and TRC stars in LCC, and 1874 stars in UCL. In order to target low-mass solar-type stars with G-K spectral types, we retained only those stars with John-

[2]The ACT (Urban et al., 1998) and TRC catalogs (Høg et al., 1998) were used for target selection for this project in 1999/2000, however we use the photometry and astrometry from the Tycho-2 catalog (available in 2000; Høg et al., 2000a,b) in the data analysis. The Tycho-2 catalog was a joint USNO/Copenhagen project, and its data supercede the contents of the ACT and TRC catalogs.

Table 2.1—Continued

(1)	(2)	(3)	(4)	(5)	(6)	(7)	(8)	(9)	(10)	(11)
Name	OB	α, δ (ICRS)	μ_{α^*}, μ_δ	V	$(B-V)$	SpT	J	H	K_s	notes
HIP	Grp.	h m s ° ′ ″	(mas yr^{-1})	(mag)	(mag)	MSS	(mag)	(mag)	(mag)	...
76472	UCL	15:37:04.66 -40:09:22.1	-20.2±1.7 -27.6±1.4	9.39	0.73±0.03	G5Vq2	7.98±0.01	7.63±0.05	7.52±0.01	1RXS J153706.0-400929
77015	UCL	15:43:29.86 -38:57:38.6	-20.5±1.6 -31.7±1.2	9.66	0.61±0.03	G3Vq1	8.61±0.01	8.34±0.03	8.32±0.02	...
77081	UCL	15:44:21.05 -33:18:55.0	-19.1±1.8 -29.5±1.4	9.69	0.75±0.04	G8Vq2	8.27±0.02	7.86±0.03	7.79±0.02	...
77135	UCL	15:44:57.69 -34:11:53.7	-20.6±3.3 -25.9±2.5	9.88	0.78±0.02	G6/G8IV/Vq3	8.43±0.02	8.04±0.02	8.23±0.04	CCDM 15450-3412,1RXS J154458.0-341143
77144	UCL	15:45:01.83 -40:50:31.0	-19.4±1.3 -31.1±1.4	9.46	0.57±0.03	G1Vq1	8.30±0.01	7.97±0.03	7.88±0.02	var(0.11),1RXS J154502.0-405043
77524	UCL	15:49:44.98 -39:25:09.1	-24.5±2.0 -25.2±1.8	10.64	1.09±0.12	K0(V)q3	8.81±0.01	8.27±0.02	8.13±0.02	1RXS J154944.7-392509
77656	UCL	15:51:13.73 -42:18:51.3	-18.0±1.2 -30.0±1.0	9.58	0.74±0.04	G8Vq3	8.15±0.03	7.78±0.06	7.67±0.02	1RXS J155113.5-421858
79610	UCL	16:14:43.02 -38:38:43.5	-14.1±3.4 -29.4±3.2	9.24	0.52±0.03	G1/G2Vq1	8.07±0.01	7.85±0.03	7.98±0.03	CCDM 16147-3839
80636	UCL	16:27:52.34 -35:47:00.4	-13.1±2.1 -25.5±1.2	9.37	0.68±0.03	G6Vq2	8.04±0.01	7.71±0.01	7.62±0.01	1RXS J162752.8-354702
81380	UCL	16:37:12.87 -39:00:38.1	-14.4±2.1 -21.5±1.6	9.82	0.66±0.05	G2/5Vq3	8.45±0.02	8.09±0.04	7.99±0.03	...
81447	UCL	16:38:05.53 -34:01:10.6	-11.3±1.5 -23.9±1.0	9.08	0.54±0.05	G1IV/Vq1	7.91±0.02	7.66±0.03	7.55±0.03	...
81775	UCL	16:42:10.36 -31:30:15.0	-14.1±1.5 -18.3±1.3	9.44	0.64±0.04	G5Vq2	8.36±0.02	8.37±0.05	8.08±0.04	...

Note. — Columns: (1) *Hipparcos* ID, (2) OB subgroup region, (3) Hipparcos position (ICRS, epoch 2000.0), (4) proper motion components (mas yr^{-1}; where $\mu_{\alpha^*} = \mu_\alpha \cos\delta$), (5) Johnson V magnitude, (6) Johnson $(B-V)$ color, (7) Spectral types from the Michigan Spectral Survey (Vol. 1-3); "q1" indicates the flag "quality = 1" in the MSS catalog, where q=1,2 stars are judged to have reliable spectral types, (8-10) 2MASS JHK_s magnitudes, (11) Notes on variability, X-ray counterparts, and multiple star system name (CCDM) from *Hipparcos*. *"Var.(N.NN)"* indicates that the H6 field in the *Hipparcos* catalog is identified as being variable in the broad H_P pass-band. The magnitude scatter *N.NN* in H_P is listed, and period *P* if found. Near-IR photometry is from the preliminary 2MASS database. The name is given of RASS-BSC X-ray sources within 40″ of *Hipparcos* stars; many of the variable stars are also *ROSAT* sources. Astrometric data and optical photometry are from from the *Hipparcos* catalog ESA (1997).

son $(B-V) \geq 0.58$ mag (the unreddened color of G0 dwarfs; Drilling & Landolt, 2000). No red $(B-V)$ limit was imposed. After the color-magnitude selection, we retained only those stars which were identified as kinematic members in *both* the ACT and TRC astrometric catalogs. This final color-selection of the ACT/TRC lists resulted in 785 UCL candidates and 679 LCC candidates.

In order to further filter the target list, we selected only those ACT/TRC candidates which had *ROSAT* All-Sky Survey Bright Source Catalog (RASS-BSC) X-ray counterparts. Voges et al. (1999) cross-referenced the RASS-BSC with the Tycho catalog and found that 68% of the optical-X-ray correlations were within 13″, and 90% of the correlations were within 25″. In plotting a histogram of the separation distance between RASS-BSC X-ray sources and ACT/TRC stars, we independently find 40″ to be an optimal search radius. No constraints on X-ray hardness ratio were imposed in the target selection. In order to calculate X-ray luminosities, we assume the X-ray energy conversion factor for the *ROSAT* PSPC detector from Fleming et al. (1995). The linearity of this X-ray efficiency relation spans the temperature range of stellar coronae from inactive subdwarf stars to extremely active RS CVns and T Tauri stars. Unsurprisingly, the kinematic selection of ACT/TRC stars also selected many of the same stars as in the *Hipparcos* sample (HIP 57524, 59854, 62445, 65423, 66001, 66941, 67522, 75924, 76472, 77135, 77524, 77656, 80636). These stars are retained in the *Hipparcos* sample (Table 2.1), and omitted from the RASS-ACT/TRC list (Table 2.2). The final target list of 96 RASS-ACT/TRC stars (40 LCC, 56 UCL) is given in Table 2.2.

Table 2.2. Properties of RASS-ACT/TRC Candidates

(1)	(2)	(3)	(4)	(5)	(6)	(7)	(8)	(9)	(10)	(11)	(12)	(13)	(14)
Name	OB	α, δ (ICRS)	μ_{α^*} μ_δ	V_T	$(B_T - V_T)$	J	H	K_s	1RXS	sep.	X-ray	Hrdns.	Table 5
TYC	Grp.	h m s ° ′ ″	(mas yr^{-1})	(mag)	(mag)	(mag)	(mag)	(mag)	Name	(″)	(ct s^{-1})	HR1	#
9212-2011-1	LCC	10:57:49.38 -69:13:59.9	-36.1±2.4 5.7±2.3	10.49±0.04	1.09±0.08	8.49±0.03	8.02±0.05	7.79±0.01	J105751.2-691402	10	1.61e-01	0.31	1
8625-388-1	LCC	11:32:08.34 -58:03:20.0	-41.6±3.1 -1.4±3.0	10.02±0.03	1.02±0.06	8.09±0.02	7.64±0.04	7.48±0.02	J113209.3-580319	7	8.25e-02	0.03	2
8222-105-1	LCC	11:35:03.76 -48:50:22.0	-24.7±2.0 -7.0±1.9	10.35±0.03	0.75±0.05	9.22±0.02	8.93±0.03	8.86±0.03	J113501.5-485011	24	1.01e-01	0.49	...
8982-3046-1	LCC	12:04:14.42 -64:18:51.7	-28.9±3.9 -4.7±3.7	10.09±0.03	0.75±0.05	8.82±0.01	8.50±0.02	8.40±0.02	J120413.3-641837	16	2.77e-01	0.32	...
8982-3213-1	LCC	12:04:48.87 -64:09:55.4	-32.9±3.5 +0.8±3.1	9.49±0.02	0.79±0.03	8.05±0.01	7.71±0.01	7.61±0.01	J120448.2-640942	13	3.47e-01	0.46	3
8640-2515-1	LCC	12:06:13.54 -57:02:16.8	-24.6±2.8 -7.7±2.6	10.77±0.05	0.81±0.08	9.25±0.03	8.84±0.03	8.77±0.03	J120613.9-570215	3	1.44e-01	0.27	4
8644-802-1	LCC	12:09:41.86 -58:54:45.0	-33.8±3.1 -11.8±2.8	10.21±0.03	1.26±0.07	8.31±0.01	7.81±0.01	7.66±0.01	J120941.5-585440	5	2.33e-01	0.16	5
8644-340-1	LCC	12:11:31.43 -58:16:53.2	-36.0±2.6 -8.7±1.8	10.29±0.04	1.00±0.07	8.58±0.01	8.09±0.03	7.96±0.02	J121131.9-581651	4	2.41e-01	0.09	6
9231-1566-1	LCC	12:11:38.14 -71:10:36.0	-38.9±1.4 -8.3±1.4	9.23±0.02	0.79±0.03	7.68±0.01	7.31±0.04	7.19±0.02	J121137.3-711032	5	2.68e-01	0.34	7
8636-2515-1	LCC	12:12:35.75 -55:20:27.3	-34.5±2.1 -13.4±2.3	10.58±0.04	1.11±0.08	8.73±0.02	8.25±0.03	8.13±0.02	J121236.4-552037	11	1.83e-01	-0.02	8
8242-1324-1	LCC	12:14:34.09 -51:10:12.5	-35.7±2.1 -12.9±1.9	10.38±0.03	1.05±0.06	8.69±0.01	8.26±0.04	8.13±0.02	J121434.2-511004	8	1.77e-01	0.32	9
8637-2610-1	LCC	12:14:52.31 -55:47:03.6	-38.3±3.6 -7.2±3.4	9.73±0.02	0.92±0.04	8.04±0.02	7.66±0.02	7.52±0.01	J121452.4-554704	0	5.65e-01	0.37	10
8645-1339-1	LCC	12:18:27.64 -59:43:12.9	-41.6±3.7 -1.9±3.3	10.82±0.05	0.95±0.09	8.45±0.01	7.84±0.01	7.73±0.01	J121828.6-594307	8	1.78e-01	0.39	11
8641-2187-1	LCC	12:18:58.02 -57:37:19.2	-36.5±1.8 -10.2±1.5	9.96±0.03	1.02±0.05	7.96±0.01	7.47±0.04	7.31±0.01	J121858.2-573713	5	2.93e-01	0.23	12
8983-98-1	LCC	12:19:21.64 -64:54:10.4	-37.0±3.0 -11.2±2.8	10.21±0.04	1.01±0.07	8.03±0.01	7.55±0.01	7.38±0.01	J121919.4-645406	14	2.55e-01	0.26	13
8633-508-1	LCC	12:21:16.48 -53:17:44.9	-36.8±1.9 -7.7±1.8	9.41±0.02	0.76±0.03	8.08±0.01	7.74±0.02	7.65±0.02	J122116.7-531747	3	4.34e-01	-0.03	14
8238-1462-1	LCC	12:21:55.65 -49:46:12.5	-37.4±1.5 -14.2±1.3	10.10±0.03	0.90±0.05	8.49±0.02	8.05±0.02	8.02±0.03	J122155.9-494609	3	1.13e-01	0.59	15
8234-2856-1	LCC	12:22:04.30 -48:41:24.9	-30.0±2.0 -12.1±1.9	10.59±0.04	0.95±0.06	8.78±0.02	8.27±0.03	8.17±0.01	J122204.0-484118	7	1.10e-01	0.88	16
8633-28-1	LCC	12:22:33.23 -53:33:49.0	-31.7±1.5 -7.7±1.5	9.49±0.02	0.72±0.03	8.18±0.01	7.91±0.04	7.78±0.02	J122233.4-533347	2	1.43e-01	0.00	17

Table 2.2—Continued

(1) Name TYC	(2) OB Grp.	(3) α, δ (ICRS) h m s ° ′ ″	(4) μ_{α^*} μ_δ (mas yr^{-1})	(5) V_T (mag)	(6) $(B_T - V_T)$ (mag)	(7) J (mag)	(8) H (mag)	(9) K_s (mag)	(10) 1RXS Name	(11) sep. (″)	(12) X-ray (ct s^{-1})	(13) Hrdns. HR1	(14) Table 5 #
8641-1281-1	LCC	12:23:40.13 -56:16:32.5	-33.1±3.3 -14.0±3.0	10.94±0.06	0.94±0.09	9.02±0.02	8.53±0.05	8.37±0.03	J122339.9-561628	4	8.03e-02	0.15	18
8992-605-1	LCC	12:36:38.97 -63:44:43.5	-37.8±2.0 -9.7±1.9	9.98±0.03	1.10±0.05	8.02±0.01	7.51±0.01	7.35±0.01	J123637.5-634446	10	2.17e-01	0.09	19
8646-166-1	LCC	12:36:58.97 -54:12:18.0	-32.3±3.3 -13.9±3.0	10.50±0.04	1.07±0.07	8.75±0.04	8.28±0.03	8.16±0.02	J123657.4-541217	13	1.06e-01	0.44	20
8654-1115-1	LCC	12:39:37.96 -57:31:40.7	-35.2±2.5 -21.9±2.4	10.21±0.03	0.88±0.05	8.67±0.01	8.23±0.04	8.13±0.03	J123938.4-573141	3	2.34e-01	0.33	21
8659-2604-1	LCC	12:41:18.17 -58:25:56.0	-37.7±2.5 -17.6±2.3	10.01±0.03	0.81±0.05	8.40±0.01	8.02±0.02	7.89±0.01	J124118.5-582556	2	1.19e-01	0.81	22
8992-420-1	LCC	12:44:34.82 -63:31:46.2	-31.2±3.3 -7.7±3.0	10.91±0.05	1.40±0.14	8.54±0.01	8.01±0.01	7.87±0.01	J124432.6-633139	16	2.11e-01	0.39	23
8249-52-1	LCC	12:45:06.76 -47:42:58.2	-31.2±1.3 -14.4±1.3	10.48±0.04	0.86±0.06	8.70±0.02	8.23±0.02	8.10±0.01	J124506.9-474254	4	2.22e-01	0.30	24
7783-1908-1	LCC	12:48:07.79 -44:39:16.8	-39.7±1.3 -18.0±1.3	9.82±0.03	0.93±0.05	8.12±0.01	7.69±0.05	7.51±0.02	J124807.6-443913	4	4.33e-01	0.05	25
8655-149-1	LCC	12:48:48.18 -56:35:37.8	-29.4±1.7 -9.4±1.7	10.31±0.03	0.92±0.05	8.88±0.01	8.48±0.02	8.39±0.02	J124847.4-563525	13	9.77e-02	0.77	26
9245-617-1	LCC	12:58:25.58 -70:28:49.2	-43.1±1.5 -18.7±1.5	10.01±0.03	0.98±0.06	8.20±0.02	7.70±0.06	7.56±0.02	J125824.6-702848	4	2.30e-01	0.11	27
8648-446-1	LCC	13:01:50.70 -53:04:58.3	-32.6±4.4 -19.5±4.0	11.18±0.06	1.02±0.13	9.44±0.02	8.91±0.02	8.78±0.02	J130153.7-530446	29	8.19e-02	0.12	28
8652-1791-1	LCC	13:02:37.54 -54:59:36.8	-25.5±2.0 -6.6±2.0	10.35±0.03	0.72±0.05	8.86±0.01	8.57±0.03	8.48±0.02	J130237.2-545933	4	1.59e-01	0.92	29
8258-1878-1	LCC	13:06:40.12 -51:59:38.6	-33.3±2.4 -15.7±2.2	10.62±0.04	0.91±0.07	8.90±0.01	8.44±0.04	8.27±0.01	J130638.5-515948	17	8.46e-02	0.58	30
8990-701-1	LCC	13:13:28.11 -60:00:44.6	-26.6±3.0 -5.3±2.8	10.08±0.02	0.70±0.04	8.76±0.01	8.45±0.02	8.42±0.02	J131327.3-600032	13	1.23e-01	0.36	...
8259-689-1	LCC	13:14:23.84 -50:54:01.9	-27.4±2.1 -16.4±1.9	10.48±0.04	0.96±0.08	8.68±0.03	8.27±0.03	8.10±0.04	J131424.3-505402	4	2.72e-01	0.41	31
8649-251-1	LCC	13:17:56.94 -53:17:56.2	-23.4±3.4 -8.3±3.2	10.48±0.05	0.72±0.08	8.86±0.03	8.49±0.05	8.39±0.03	J131754.9-531758	18	1.60e-01	0.36	32
8248-539-1	LCC	13:22:04.46 -45:03:23.1	-26.7±1.6 -13.3±1.4	10.10±0.03	0.77±0.06	8.97±0.03	8.63±0.05	8.55±0.03	J132204.7-450312	10	7.06e-02	0.53	33
9246-971-1	LCC	13:22:07.54 -69:38:12.3	-40.8±2.5 -23.0±2.3	10.54±0.04	1.08±0.08	8.28±0.03	7.65±0.02	7.31±0.01	J132207.2-693812	1	1.58e-01	0.59	34
8663-1375-1	LCC	13:34:20.26 -52:40:36.1	-33.4±1.6 -21.1±1.3	9.37±0.02	0.71±0.03	8.04±0.01	7.69±0.04	7.56±0.03	J133420.0-524032	4	2.51e-01	0.44	35
7796-1788-1	UCL	13:37:57.29 -41:34:41.9	-36.7±1.2 -24.2±1.2	10.17±0.04	0.97±0.06	8.47±0.01	8.03±0.04	7.89±0.02	J133758.0-413448	10	2.22e-01	0.27	36

Table 2.2—Continued

(1) Name TYC	(2) OB Grp.	(3) α, δ (ICRS) h m s ° ′ ″	(4) μ_{α^*} μ_δ (mas yr^{-1})	(5) V_T (mag)	(6) $(B_T - V_T)$ (mag)	(7) J (mag)	(8) H (mag)	(9) K_s (mag)	(10) 1RXS Name	(11) sep. (″)	(12) X-ray (ct s^{-1})	(13) Hrdns. HR1	(14) Table 5 #
8667-283-1	LCC	13:43:28.53 -54:36:43.5	-44.0±1.8 -20.8±1.8	9.39±0.02	0.77±0.03	8.03±0.01	7.68±0.01	7.63±0.02	J134332.7-543638	36	4.81e-01	0.22	37
8270-2015-1	UCL	13:47:50.55 -49:02:05.5	-24.3±2.2 -14.7±2.0	10.91±0.07	0.90±0.11	9.30±0.01	8.81±0.05	8.70±0.03	J134748.0-490158	26	1.50e-01	-0.10	38
8263-2453-1	UCL	13:52:47.80 -46:44:09.2	-22.7±1.3 -18.9±1.4	9.69±0.03	0.72±0.04	8.41±0.02	8.07±0.04	7.94±0.01	J135247.0-464412	8	1.96e-01	0.67	39
7811-2909-1	UCL	14:02:20.73 -41:44:50.8	-27.6±2.0 -19.4±1.9	10.80±0.06	0.90±0.10	8.99±0.02	8.55±0.04	8.42±0.03	J140220.9-414435	15	9.68e-02	0.37	40
7815-2029-1	UCL	14:09:03.58 -44:38:44.4	-20.9±1.1 -22.6±1.1	9.46±0.02	0.71±0.04	8.25±0.01	7.98±0.05	7.86±0.02	J140902.6-443838	12	1.73e-01	0.67	41
9244-814-1	LCC	14:16:05.67 -69:17:36.0	-29.4±2.4 -16.0±2.3	10.21±0.03	0.72±0.06	8.74±0.01	8.39±0.02	8.36±0.02	J141605.3-691756	20	6.10e-02	0.47	42
8285-847-1	UCL	14:16:57.91 -49:56:42.3	-23.2±1.1 -22.1±1.1	8.77±0.01	0.71±0.02	7.43±0.02	7.12±0.02	7.03±0.01	J141658.4-495648	7	1.59e-01	0.15	...
8282-516-1	UCL	14:27:05.56 -47:14:21.8	-25.5±1.7 -21.2±1.6	10.68±0.05	0.95±0.08	9.06±0.03	8.65±0.03	8.52±0.03	J142705.3-471420	3	1.53e-01	-0.12	43
7817-622-1	UCL	14:28:09.30 -44:14:17.4	-18.4±2.0 -20.6±1.9	9.87±0.03	0.90±0.05	8.31±0.01	7.93±0.03	7.78±0.03	J142809.6-441438	20	1.45e-01	0.13	44
7813-224-1	UCL	14:28:19.38 -42:19:34.1	-19.7±1.5 -19.8±1.7	10.55±0.05	0.79±0.09	8.92±0.01	8.51±0.03	8.40±0.03	J142817.6-421958	31	2.23e-01	0.34	45
7814-1450-1	UCL	14:37:04.22 -41:45:03.0	-21.5±2.0 -19.1±1.9	9.77±0.02	0.72±0.04	8.26±0.01	7.90±0.02	7.80±0.03	J143704.6-414504	4	1.68e-01	0.58	46
8683-242-1	UCL	14:37:50.23 -54:57:41.1	-18.3±2.5 -25.8±2.4	10.80±0.06	0.77±0.09	8.94±0.01	8.46±0.02	8.32±0.02	J143750.9-545708	33	2.20e-01	0.07	47
8283-264-1	UCL	14:41:35.00 -47:00:28.8	-29.6±1.3 -27.4±1.2	10.09±0.03	0.88±0.04	8.43±0.01	7.98±0.03	7.88±0.03	J144135.3-470039	11	6.12e-01	0.15	48
8283-2795-1	UCL	14:47:31.77 -48:00:05.7	-29.6±2.3 -16.7±2.3	10.79±0.06	0.75±0.09	9.37±0.01	9.04±0.01	8.96±0.03	J144732.2-480019	14	7.37e-02	0.50	49
7305-380-1	UCL	14:50:25.81 -35:06:48.6	-18.2±2.6 -15.8±2.6	10.83±0.07	0.97±0.13	8.75±0.03	8.24±0.02	8.11±0.03	J145025.4-350645	6	9.03e-02	0.35	50
7828-2913-1	UCL	14:52:41.98 -41:41:55.2	-22.6±2.2 -21.4±2.1	11.02±0.09	1.35±0.22	9.05±0.02	8.40±0.02	8.29±0.03	J145240.7-414206	17	1.30e-01	0.21	51
7310-2431-1	UCL	14:57:19.63 -36:12:27.4	-26.6±1.6 -22.3±1.7	10.36±0.05	0.97±0.09	8.78±0.03	8.44±0.04	8.30±0.03	J145720.4-361242	17	8.67e-02	0.69	52
7310-503-1	UCL	14:58:37.70 -35:40:30.4	-21.4±2.2 -26.0±2.3	10.88±0.07	1.37±0.20	8.65±0.01	8.08±0.03	7.90±0.01	J145837.6-354036	5	8.30e-02	0.60	53
7824-1291-1	UCL	14:59:22.76 -40:13:12.1	-26.0±1.4 -26.5±1.6	9.80±0.04	0.86±0.07	8.34±0.01	7.97±0.04	7.82±0.02	J145923.0-401319	7	1.87e-01	0.35	54
7833-2037-1	UCL	15:00:51.88 -43:31:21.0	-20.1±2.1 -19.1±2.0	11.23±0.08	0.81±0.13	9.31±0.03	8.88±0.02	8.75±0.03	J150052.5-433107	15	7.57e-02	0.39	55

Table 2.2—Continued

(1) Name TYC	(2) OB Grp.	(3) α, δ (ICRS) h m s ° ′ ″	(4) μ_{α^*} μ_δ (mas yr^{-1})	(5) V_T (mag)	(6) $(B_T - V_T)$ (mag)	(7) J (mag)	(8) H (mag)	(9) K_s (mag)	(10) 1RXS Name	(11) sep. (″)	(12) X-ray (ct s^{-1})	(13) Hrdns. HR1	(14) Table 5 #
7829-504-1	UCL	15:01:11.56 -41:20:40.6	-14.9±1.7 -15.1±1.7	10.09±0.03	0.77±0.06	8.78±0.03	8.47±0.05	8.33±0.03	J150112.0-412040	4	1.78e-01	0.41	56
8297-1613-1	UCL	15:01:58.82 -47:55:46.4	-22.2±1.7 -18.2±1.6	10.22±0.04	0.71±0.07	8.91±0.01	8.59±0.02	8.51±0.02	J150158.5-475559	13	5.07e-02	0.42	57
7319-749-1	UCL	15:07:14.81 -35:04:59.6	-34.1±2.4 -30.1±2.5	10.59±0.06	1.00±0.11	8.87±0.01	8.42±0.05	8.35±0.03	J150714.5-350500	3	7.39e-02	0.71	58
7833-1106-1	UCL	15:08:00.55 -43:36:24.9	-21.8±1.4 -16.5±1.4	9.93±0.03	0.87±0.06	8.20±0.01	7.86±0.04	7.71±0.02	J150759.9-433642	18	8.84e-02	0.88	...
7833-2400-1	UCL	15:08:37.75 -44:23:16.9	-17.9±2.1 -17.6±2.0	10.91±0.07	0.80±0.11	9.33±0.03	8.95±0.02	8.81±0.03	J150836.0-442325	20	1.73e-01	0.45	59
7833-2559-1	UCL	15:08:38.50 -44:00:52.1	-23.5±2.1 -24.2±1.9	10.61±0.05	0.70±0.09	8.95±0.02	8.54±0.03	8.54±0.03	J150838.5-440048	4	1.21e-01	0.19	60
8293-92-1	UCL	15:09:27.93 -46:50:57.2	-19.9±2.1 -16.1±2.0	10.60±0.05	1.09±0.09	8.39±0.04	7.83±0.04	7.72±0.02	J150928.2-465109	12	7.77e-02	1.00	...
8294-2230-1	UCL	15:12:50.18 -45:08:04.5	-19.8±2.1 -22.4±2.0	10.79±0.07	0.85±0.11	9.13±0.01	8.74±0.03	8.67±0.02	J151250.0-450822	17	1.45e-01	0.19	61
8694-1685-1	UCL	15:18:01.74 -53:17:28.8	-28.7±2.5 -28.3±2.3	10.21±0.04	0.86±0.07	8.51±0.02	8.12±0.04	8.01±0.02	J151802.0-531719	10	2.23e-01	-0.04	62
7822-158-1	UCL	15:18:26.91 -37:38:02.1	-22.5±2.6 -28.3±2.6	11.11±0.09	0.87±0.15	9.07±0.03	8.63±0.04	8.53±0.03	J151827.3-373808	7	1.30e-01	0.37	63
8295-1530-1	UCL	15:25:59.65 -45:01:15.8	-21.9±2.2 -21.3±2.0	10.98±0.07	0.88±0.12	9.45±0.02	8.98±0.02	8.88±0.02	J152600.9-450113	13	6.10e-02	-0.15	64
7326-928-1	UCL	15:29:38.58 -35:46:51.3	-21.7±2.0 -26.1±2.1	10.54±0.06	1.07±0.11	8.77±0.01	8.27±0.03	8.19±0.03	J152937.7-354656	11	1.05e-01	0.21	65
7318-593-1	UCL	15:31:21.93 -33:29:39.5	-25.8±2.5 -31.5±2.5	10.99±0.08	0.72±0.12	9.39±0.03	8.95±0.06	8.81±0.03	J153121.8-333002	23	9.34e-02	0.06	...
7327-1934-1	UCL	15:37:02.14 -31:36:39.8	-17.8±1.6 -29.0±1.6	10.06±0.04	0.70±0.06	8.28±0.03	7.76±0.04	7.72±0.02	J153701.9-313647	7	3.92e-01	0.32	66
7840-1280-1	UCL	15:37:11.30 -40:15:56.8	-16.7±1.9 -22.5±1.9	10.55±0.05	1.24±0.10	8.98±0.01	8.46±0.05	8.31±0.03	J153711.6-401608	11	2.27e-01	-0.14	67
7848-1659-1	UCL	15:38:43.06 -44:11:47.4	-23.2±1.6 -28.4±1.5	10.36±0.05	0.85±0.08	8.81±0.05	8.36±0.04	8.22±0.03	J153843.1-441149	1	1.41e-01	-0.01	68
6785-510-1	UCL	15:39:24.41 -27:10:21.9	-20.2±1.7 -29.8±1.6	9.65±0.03	0.81±0.05	8.04±0.03	7.64±0.03	7.53±0.01	J153924.0-271035	14	2.33e-01	0.59	69
7331-782-1	UCL	15:44:03.77 -33:11:11.2	-22.2±2.6 -29.7±2.6	10.97±0.07	0.95±0.12	9.05±0.02	8.55±0.01	8.41±0.03	J154404.1-331120	10	7.72e-02	0.42	70
7845-1174-1	UCL	15:45:52.25 -42:22:16.5	-18.0±1.5 -30.4±1.6	10.61±0.05	1.15±0.09	8.69±0.02	8.09±0.04	7.94±0.02	J154552.7-422227	11	4.13e-01	0.07	71
8317-551-1	UCL	15:46:51.79 -49:19:04.7	-19.7±1.6 -27.9±1.5	10.29±0.04	1.04±0.08	8.69±0.01	8.36±0.03	8.31±0.02	J154651.5-491922	17	1.78e-01	0.07	72

Table 2.2—Continued

(1) Name TYC	(2) OB Grp.	(3) α, δ (ICRS) h m s ° ′ ″	(4) μ_{α^*} μ_δ (mas yr^{-1})	(5) V_T (mag)	(6) $(B_T - V_T)$ (mag)	(7) J (mag)	(8) H (mag)	(9) K_s (mag)	(10) 1RXS Name	(11) sep. (″)	(12) X-ray (ct s^{-1})	(13) Hrdns. HR1	(14) Table 5 #
7842-250-1	UCL	15:56:59.05 -39:33:43.1	-15.1±2.0 -21.6±2.0	10.90±0.07	0.94±0.12	9.20±0.02	8.83±0.03	8.70±0.03	J155659.0-393400	16	9.87e-02	-0.02	73
7333-1260-1	UCL	16:01:07.93 -32:54:52.5	-18.3±1.4 -29.6±1.5	9.58±0.02	0.73±0.04	8.46±0.01	8.16±0.04	8.08±0.02	J160108.0-325455	3	1.93e-01	0.34	74
7333-719-1	UCL	16:01:08.97 -33:20:14.2	-12.3±2.1 -23.0±2.2	10.99±0.07	1.15±0.16	9.01±0.02	8.55±0.03	8.46±0.03	J160108.9-332021	7	9.66e-02	0.75	75
7863-1629-1	UCL	16:03:45.37 -43:55:49.2	-12.5±1.1 -22.6±1.4	9.74±0.03	1.06±0.05	7.93±0.02	7.42±0.03	7.30±0.01	J160345.8-435544	6	4.09e-01	0.21	76
7855-1106-1	UCL	16:03:52.50 -39:39:01.3	-16.4±2.4 -28.4±2.3	11.12±0.08	1.15±0.18	8.98±0.03	8.35±0.03	8.21±0.03	J160352.0-393901	5	1.29e-01	-0.02	77
7851-1-1	UCL	16:05:45.00 -39:06:06.5	-16.8±2.2 -31.1±2.2	10.63±0.06	1.00±0.10	8.93±0.02	8.52±0.04	8.36±0.03	J160545.8-390559	11	1.57e-01	0.46	78
7355-317-1	UCL	16:13:58.02 -36:18:13.4	-18.4±2.0 -32.3±2.1	11.26±0.09	1.17±0.21	9.41±0.02	8.98±0.03	8.84±0.03	J161357.9-361813	1	1.74e-01	0.03	79
8319-1687-1	UCL	16:14:52.01 -50:26:18.5	-19.9±2.1 -29.2±2.0	10.50±0.05	0.96±0.09	8.38±0.01	7.91±0.01	7.76±0.01	J161451.3-502621	7	2.37e-01	0.15	80
7852-51-1	UCL	16:18:38.56 -38:39:11.8	-25.9±1.3 -34.0±1.5	9.09±0.02	0.69±0.03	8.02±0.01	7.79±0.05	7.69±0.02	J161839.0-383927	16	1.62e-01	-0.06	81
7857-648-1	UCL	16:21:12.19 -40:30:20.6	-9.1±1.4 -28.1±1.4	10.67±0.05	1.01±0.09	8.97±0.02	8.55±0.02	8.43±0.02	J162112.0-403032	11	1.29e-01	0.13	82
7857-514-1	UCL	16:23:29.55 -39:58:00.8	-12.5±2.1 -24.1±2.1	10.73±0.06	0.88±0.09	9.47±0.02	9.10±0.03	8.99±0.03	J162330.1-395806	8	7.93e-02	0.18	83
7853-227-1	UCL	16:27:30.55 -37:49:21.6	-10.0±2.5 -23.4±2.6	11.05±0.07	0.84±0.12	9.29±0.02	8.81±0.04	8.66±0.03	J162730.0-374929	9	6.24e-02	1.00	84
7353-2640-1	UCL	16:31:42.03 -35:05:17.2	-16.2±1.9 -27.6±2.0	10.72±0.05	0.81±0.08	9.19±0.02	8.75±0.02	8.63±0.02	J163143.7-350521	20	8.92e-02	0.52	85
7349-2191-1	UCL	16:35:35.99 -33:26:34.7	-6.0±1.8 -23.0±2.1	11.09±0.07	0.93±0.13	8.99±0.02	8.44±0.03	8.28±0.02	J163533.9-332631	25	1.65e-01	0.37	86
7858-526-1	UCL	16:38:38.47 -39:33:03.5	-10.4±1.3 -19.2±1.3	9.05±0.02	0.73±0.04	7.52±0.01	7.25±0.02	7.15±0.01	J163839.2-393307	9	8.45e-02	0.61	...
7858-830-1	UCL	16:39:59.30 -39:24:59.2	-9.7±2.2 -18.9±2.2	10.68±0.08	0.84±0.12	8.67±0.02	8.26±0.04	8.12±0.02	J163958.7-392457	7	7.39e-02	0.96	87
7871-1282-1	UCL	16:42:24.00 -40:03:29.7	-11.1±1.5 -20.2±1.3	9.70±0.03	0.88±0.06	8.03±0.03	7.63±0.05	7.46±0.02	J164224.5-400329	5	9.83e-02	0.44	88

2.3 Observations

Blue and red optical spectra of the pre-MS candidates were taken simultaneously with the Dual-Beam Spectrograph (DBS) on the Siding Springs 2.3-m telescope on the nights of 20-24 April 2000. The DBS instrument is detailed in Rodgers, Conroy, & Bloxham (1988). Using a 2″ wide slit, we used the B600 l/mm grating in first order on the blue channel, yielding 2.8Å FWHM resolution from 3838–5423Å. The red channel observations were done with the R1200 l/mm grating in first order, yielding 1.3Å FWHM resolution over 6205–7157Å. The five nights of bright time were predominantly clear to partly cloudy. Signal-to-noise ratios of ~50-200 per resolution element were typically reached with integration times of 120-720 s. Flat-fields and bias-frames were observed at the beginning and end of each night. NeAr λ-calibration arcs and spectrophotometric standards were observed every few hours. The spectra were reduced using standard IRAF routines. In order to remove low-order chromatic effects from the band-ratio measurements, we spectrophotometrically calibrated all of the target spectra using 2 standard stars from Hamuy et al. (1994). A total of 118 program stars (§2.2.1 and §2.2.2) and 20 MK spectral standards (§2.4.1.1) were observed. The major stellar absorption features of one of the single standard G stars were shifted to a zero-velocity wavelength scale. The spectra of all of the stars were then cross-correlated against this standard star using the IRAF task *fxcor*, and then shifted to the common, rest-frame wavelength scale. This was done to ensure proper identification of weak lines, as well as to make sure that the band-ratio measurements were sampling the same spectral range in each stellar spectrum.

Table 2.2—Continued

(1)	(2)	(3)						(4)		(5)	(6)	(7)	(8)	(9)	(10)	(11)	(12)	(13)	(14)
Name	OB	α, δ (ICRS)						μ_{α^*}	μ_δ	V_T	$(B_T - V_T)$	J	H	K_s	1RXS	sep.	X-ray	Hrdns.	Table 5
TYC	Grp.	h	m	s	°	′	″	(mas yr^{-1})		(mag)	(mag)	(mag)	(mag)	(mag)	Name	(″)	(ct s^{-1})	HR1	#

Note. — Columns: (1) Tycho-2 name, (2) OB subgroup region, (3) Tycho-2 position (ICRS, epoch 2000.0) (4) proper motion (α, δ components) in mas yr^{-1}(where $\mu_{\alpha^*} = \mu_\alpha \cos\delta$), (5) V_T magnitude, (6) $(B_T - V_T)$ color, (7-9) 2MASS JHK_s magnitudes, (10) X-ray counterpart name in RASS-BSC, (11) optical-X-ray separation, (12) X-ray count rate (ct s^{-1}), (13) Hardness ratio HR1, (14) Number in Table 5 if star is found to be "pre-MS" or "pre-MS?" in nature. X-ray data is from *ROSAT* All-Sky Survey BSC (Voges et al., 1999), astrometry and optical photometry are from *Tycho-2* catalog (Høg et al., 2000a), and near-IR photometry is from 2MASS (Cutri et al., 2003).

2.4 Analysis of Spectra

2.4.1 Spectral Types and Luminosity Classification

2.4.1.1 Standard Stars

We observed 20 spectral standards including dwarfs and subgiants (luminosity classes IV and V) and a few giants (III). A summary of their properties is listed in Table 2.3. To permit quantitative examination of trends in the strengths of spectral features, as well as interpolation between spectral types, we adopt the numerical subtype scaling of Keenan (1984; i.e. here listed as "SpT", where G0 = 30, G2 = 31, K0 = 34, etc.). All of the standard stars are classified on the MK system by Keenan & McNeil (1989), except for HR 7061 (Garcia, 1989). Table 2.3 also lists their spectral types as given in the Michigan Spectral Survey atlases of N. Houk (e.g. 1978). The sample standard deviation of a linear fit between the Keenan and Houk spectral types for dwarfs and subgiants, on Keenan's subtype scale, is σ(SpT) = 0.6 subtypes. The $\sim$0.6 subtype uncertainty probably represents the best that can be done using visual spectral types determined by different authors.

The adopted spectral types are those of Keenan & McNeil's, however the luminosity classification was verified (and some times changed) by virtue of (1) position of the stars on a color-magnitude diagram based on *Hipparcos* data, (2) position in a temperature vs. Sr II λ4077/Fe I λ4071 ratio diagram (see §2.4.1.3, Fig. 2.1), and (3) published $\log g$ estimates. Although changing the classification of some standards may appear imprudent, *the H-R diagram positions, Sr/Fe line ratio, and derived log g values (Cayrel de Strobel et al., 2001) are all consistent with our new adopted luminosity classes*[3]. In every case the difference was only half of a

[3] *Hipparcos* data also led Keenan & Barnbaum (1999) to revise the luminosity classes of a few giant star standards at the half luminosity class level.

luminosity class, and only 5/20 of the stars were changed. Notes on the revised luminosity classifications are given in Appendix B.

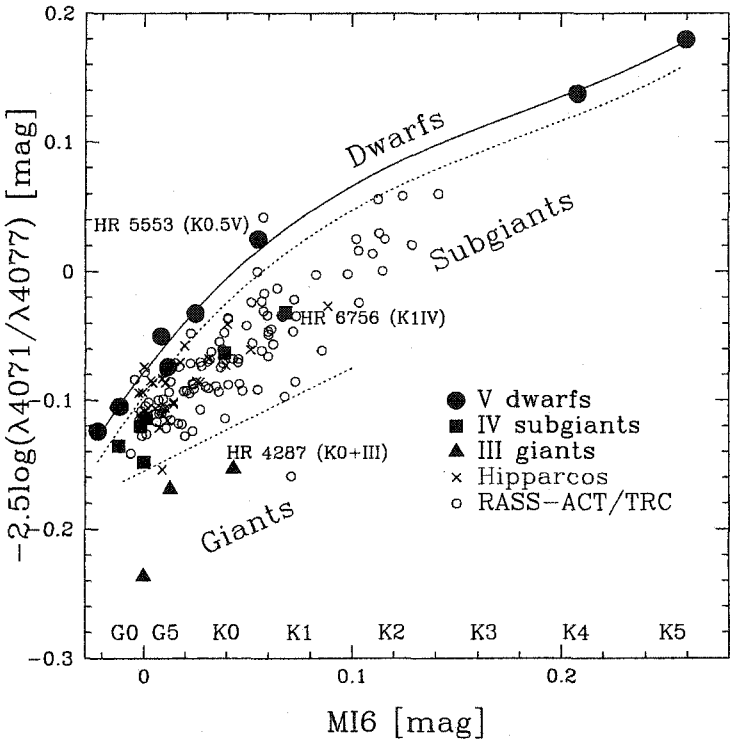

Figure 2.1: The MI6 band-ratio (T_{eff} indicator) vs. the band-ratio of Fe I λ4071/ Sr II λ4077 (surface gravity indicator). The solid line is a polynomial fit to only the dwarf standards. The dashed lines separate dwarfs, subgiants, and giants. The dwarf-subgiant dashed line is -2$\times$ the σ-residual below the dwarf regression, whereas the subgiant-giant boundary is placed somewhat arbitrarily to resolve the observed subgiant and giant loci. Empirically, this diagram suggests that most of the target stars are consistent with being G and K-type subgiants, with few giant and dwarf interlopers. A few early-K standards are noted for reference.

Table 2.3. Spectral Standard Stars

(1) Name HD	(2) Name HR	(3) MK Sp.Type	(4) V (mag)	(5) $\pi \pm \sigma_\pi$ (mas)	(6) $(B-V)$ (mag)	(7) [Fe/H] adopted	(8) MSS Sp.Type	(9) Adopted Sp.Type	(10) notes ...
182640	7377	F0IV	3.36	65.1 ± 0.8	0.32	...	F2V	F0IV	a,*b*
173677	7061	F6V	4.19	52.4 ± 0.7	0.48	–0.1	...	F6IV-V	c
84117	3862	F9V	4.93	67.2 ± 0.7	0.53	...	G0V	F9V	...
121370	5235	G0IV	2.68	88.2 ± 0.8	0.58	0.2	...	G0IV	b
89010	4030	G1.5IV-V	5.95	32.9 ± 0.9	0.66	0.0	...	G1.5IV-V	...
126868	5409	G2IV	4.84	24.2 ± 1.0	0.69	0.0	G3V	G2III-IV	a,*d*
161239	6608	G2IIIb	5.73	26.1 ± 0.6	0.68	...	...	G2IV	...
146233	6060	G2Va	5.49	71.3 ± 0.9	0.65	0.0	G5V	G2V	a
94481	4255	G4III	5.65	8.0 ± 0.8	0.83	...	K0III+(G)	G4III	...
117176	5072	G4V	4.97	55.2 ± 0.7	0.71	–0.1	...	G4IV-V	e
188376	7597	G5IV	4.70	42.0 ± 0.9	0.75	–0.1	G3/5III	G5IV	
115617	5019	G6.5V	4.74	117.3 ± 0.7	0.71	0.0	G5V	G6.5V	...
114946	4995	G7IV-V	5.31	25.9 ± 0.7	0.86	–0.1:	G8III/IV	G7IV	...
188512	7602	G8IV	3.71	73.0 ± 0.8	0.86	0.0:	...	G8IV	a
165760	6770	G8III	4.64	13.7 ± 0.8	0.95	–0.1	...	G8III	...
95272	4287	K0+III	4.08	18.7 ± 1.0	1.08	–0.1:	K1III	K0+III	...
131511	5553	K0.5V	6.00	86.7 ± 0.8	0.84	...	...	K0.5V	a
165438	6756	K1IV	5.74	28.6 ± 0.8	0.97	0.0	K0IV	K1IV	...
131977	5568	K4V	5.72	169.3 ± 1.7	1.02	0.0	K4V	K4V	...
120467	...	K6Va	8.16	70.5 ± 1.0	1.26	...	...	K6V	...

Note. — SB1,2 = spectroscopic binary in either SIMBAD or Duquennoy & Mayor (1991). MSS = Michigan Spectral Survey Vols. 1-5 = Houk & Cowley (1975), Houk (1978), Houk (1982), Houk & Smith-Moore (1988), Houk & Swift (1999). The [Fe/H] estimate is adopted from the compilation of published values in Cayrel de Strobel et al. (2001). A semi-colon after the [Fe/H] value indicates considerable scatter (>0.2 dex) in the published estimates.

[a]SIMBAD lists as variable or suspected var., however *Hipparcos* finds scatter in Hp $\leq$ 0.015 mag. The typical scatter for the other standard stars was 0.005 mag in Hp (Hipparcos magnitude), with none greater than 0.01 mag.

[b]Spectroscopic binary

[c]From standard list of Garcia (1989), and originally in Johnson & Morgan (1953), but not listed in either Keenan & Yorka (1988) or Keenan & McNeil (1989).

[d]HR 5409 is a resolved binary (sep. 5") listed by SIMBAD as a variable star, however *Hipparcos* found the scatter in the Hp band to be only 0.015 mag.

[e]Keenan & McNeil (1989) call it G4V, however it is G5V in virtually every other reference (e.g. Gray, Graham, & Hoyt, 2001). We retain Keenan's classification.

2.4.1.2 Visual Classification

The blue spectrum of each star was assigned a spectral type visually by E.M. through comparison with the standards in Table 2.3. In order to distinguish subtypes, we focused on several features such as the G band (λ4310), Ca I λ4227, Cr I λ4254 and nearby Fe lines, and the Mg b lines λ5167, λ5173, λ5184. Balmer lines were ignored due to possible chromospheric emission. After making an initial guess through comparison with a wide range of spectral types, a final visual spectral type was assigned through comparison to standards within $\pm$2 subtypes of the initial guess.

To test the accuracy of our visual classification, we compared our spectral types to those of quality 1 or 2 in the Michigan Spectral Survey. The average difference is not significant: -0.4 ± 0.6 (1σ sample standard deviation) subtypes (on Keenan's scale). The 12 *Hipparcos* stars were later visually typed a second time. Between the two estimates for each star, we estimate that the 1σ uncertainty in our visual spectral types is 0.6 subtypes. This is comparable to the dispersion between the Keenan and Houk spectral types for the standards themselves.

2.4.1.3 Quantitative Spectral Type Estimation

A two-dimensional quantitative spectral type (subtype plus luminosity class) can be estimated using integrated fluxes over narrow bands sensitive to temperature and surface gravity. We tested various ratios defined by Malyuto & Schmidt-Kaler (1997) and Rose (1984) for this purpose, as well as from Gray's spectral atlas (2000). In testing band-ratios as temperature indicators for our standards, we noticed that some had slight surface gravity dependencies. A surface gravity dependence in our temperature indicators could systematically affect our T_{eff}

estimates. We first discuss our surface gravity indicator and then define our temperature estimators using only subgiant and dwarf standards, thus mitigating the effects of surface gravity.

The most widely used surface gravity diagnostic for G and K stars is the ratio between Sr II λ4077 and nearby Fe lines (e.g. Keenan & McNeil, 1976; Gray, 2000). In thin and thick disk dwarfs, the abundance ratio [Sr/Fe] is within $\sim$0.1 dex of solar for most stars (Mashonkina & Gehren, 2001). A quantitative surface gravity (luminosity class) indicator was established by Rose (1984) from low-resolution spectra using the maximum absorption line depth for Sr II λ4077 and the average for the atomic Fe λ4045 and λ4063 lines. We measure the fluxes in 3 Å bands centered on the Sr II λ4077 line and the Fe I λ4071 line. Ratios between the λ4077 line and the other nearby Fe lines (λ4045, λ4063) did not distinguish subgiants and giants.

For a temperature estimator, we adopted Index 6 of Malyuto & Schmidt-Kaler (1997) ($\lambda\lambda$5125-5245/$\lambda\lambda$5245-5290) hereafter referred to as "MI6". The temperature sensitivity of this indicator largely reflects differing amounts of line-blanketing in these two wavelength regimes – mainly by the Mg b lines (λ5167, λ5173, and λ5184), and many Fe lines (e.g. Fe I λ5270). Although the Mg b lines are somewhat surface gravity sensitive, within the $\log g$ and T_{eff} regime of our standards and program stars, the temperature sensitivity is dominant. The difference in central wavelength between the two bandpasses is only 82Å, and the effects of reddening are negligible (Mathis, 1990). For a temperature indicator, we fit a low-order polynomial to MI6 vs. SpT for the dwarf and subgiant standard stars (see Appendix C) which has a 1σ sample standard deviation of 0.6 subtypes.

Fig. 2.1 plots the temperature-sensitive MI6 index versus our surface gravity discriminant (Sr II λ4077/Fe I λ4071). The dwarf standards form a very narrow sequence in Fig. 2.1, *confirming the lack of cosmic scatter in [Sr/Fe] values among field stars and the insensitivity of log g to spectral type for G-K dwarfs.* The polynomial fit to the dwarf data is given in Appendix C. There is a gap between the dwarf and subgiant loci between $\sim$1-2.5σ (sample standard deviation) of the dwarf locus polynomial, and we set the subgiant/dwarf separation at 2σ. We classify stars within 2σ of the solid dwarf line in Fig. 2.1 as dwarfs (4 of 96 RASS-ACT/TRC stars, 4 of 20 HIP stars), and three stars near the giant locus (TYC 8992-605-1, HIP 68726, and HIP 74501) as giants. We classify the rest as subgiants.

Gray (2000) suggests Y II λ4376/Fe I λ4383 as a surface gravity indicator for late-G stars using low-resolution spectra. From the solar spectral atlas of Wallace, Hinkle, & Livingston (1998), it appears that Gray's low-resolution Y II λ4376 feature is actually a blend of several lines of nearly equal strength. In order to test the properties of this band-ratio, we measure the flux in 3Å windows centered on wavelengths 4383.6Å and 4374.5Å. Plotting this ratio against spectral type for the standard stars showed a very tight locus for the dwarfs, however luminosity classes IV-V, IV, and III were indistinguishable from the dwarfs and each other. We found this ratio unsuitable for the purposes of luminosity classification of our targets, but we find it to be an excellent temperature estimator for FGK dwarfs, subgiants, and giants. Among the 20 standards, the measurement of the λ4374/λ4383 band-ratio vs. spectral type gives a tight correlation (sample standard deviation 1σ = 0.6 subtypes). We adopt the λ4374/λ4383 band ratio as our third, independent estimator of spectral type (polynomial fit is given in Appendix C).

2.4.1.4 Final Spectral Types

The three temperature-type estimates agree well for the majority of the program stars. The mean difference between the MI6 and visual spectral types is 0.7 subtypes. The mean difference between the λ4374/λ4383 band-ratio types and the visual types is 0.6 subtypes. We calculate a mean spectral type and standard error of the mean using the three classifications. The mean is unweighted since all three relations appeared to have 1σ sample standard deviations of $\approx$0.6 subtypes in their accuracy. The average standard error of the mean is 0.5 subtypes. We believe that using multiple techniques mitigates the effects that rapid rotation, binarity, etc. can introduce into visual classification alone. The spectral types are listed in Tables 2.6, 2.5 and 2.7.

2.4.2 Additional Spectroscopic Diagnostics

2.4.2.1 Chromospheric Hα Emission

Medium-to-low resolution spectra of chromospherically active stars show the Hα line to be partially filled-in, or even fully in emission. We measure the EW of the entire Hα feature; our resolution is insufficient to separate the "core" chromospheric emission from the photospheric Hα absorption line. A significant number of our stars show Hα emission (19% of the RASS-ACT/TRC G-K type stars). We characterize our targets stars as chromospherically active or inactive through comparing the Hα EW to that of standards of identical spectral type. Fig. 2.2 shows the EW(Hα) data for our targets and standard stars. Stars more than 2σ above the dwarf/subgiant EW(Hα) relation (a quadratic regression; see Appendix C) are considered to be active. The stars with Hα in emission (negative

EWs) have an "e" appended to their spectral types in Tables 2.6, 2.5 and 2.7. The Hα EWs for each star are also listed in these tables.

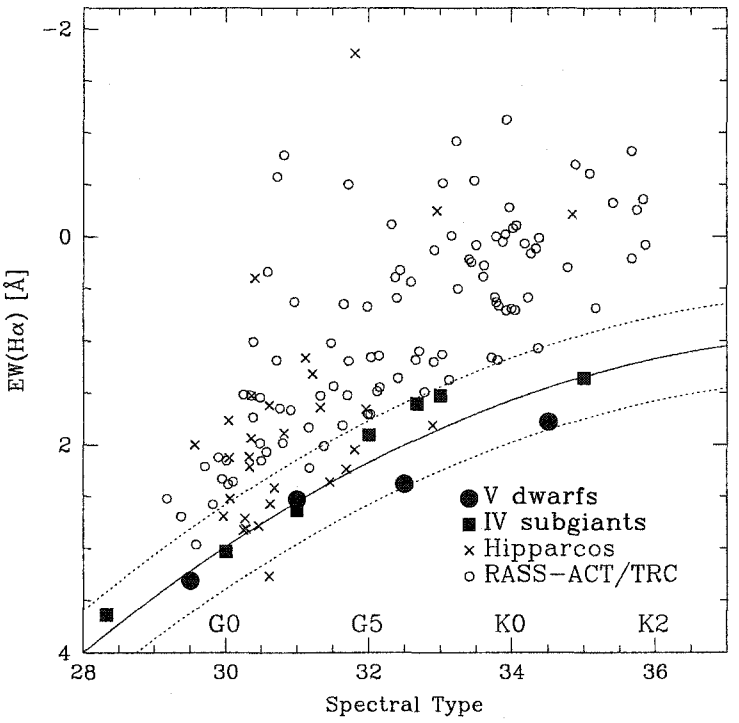

Figure 2.2: Hα EWs for the pre-MS candidates compared to inactive field dwarfs and subgiants. Symbols are the same as for Fig. 2.1. The solid line is the average EW(Hα) for dwarf and subgiant standard stars. The dashed line represents the $\pm 2\sigma$ residual scatter in the relation (encompassing all of the standards). Stars above this line are clearly chromospherically active, however those within the 2σ scatter have Hα emission similar to older field stars.

2.4.2.2 Li I λ6707 Equivalent Width

The presense of strong Li absorption in the spectra of late-type stars is a well-known diagnostic of stellar youth. Because of the extended timescale for significant Li depletion in stars of $\sim$1 $M_{\odot}$, *strong Li absorption is necessary, but not sufficient*

indicator of pre-MS nature for G stars. However it is a powerful age descriminent when combined with our surface gravity indicator.

Many studies have shown that the equivalent width (EW) of Li I λ6707 can be overestimated at low spectral resolution (e.g. Covino et al., 1997), especially for G-K stars. With a resolution of 1.3Å, we consider our EWs to be approximate. The EWs were measured with Voigt profiles in the IRAF routine *splot*. The continuum level was estimated from nearby pseudo-continuum peaks. We subtract the contribution from the neighboring Fe I λ6707.4Å feature using the prescription of Soderblom et al. (1993). In order to test the validity of our Li EWs, we divided several of our Li-rich targets by standard stars of the same spectral type. The ratioed spectra exhibit only a major absorption feature at λ6707. The division also removes the effects of blending by Fe lines (assuming the same stars have similar EWs). The EWs of this feature in the divided spectra corresponded well with our previous measurements, however the uncertainties in the EW appear to be ~20-50 mÅ (with the maximum value being for spectroscopic binaries).

Fig. 2.3 shows the Li I λ6707 EWs for our RASS-ACT/TRC and *Hipparcos* targets, separated according to their luminosity class (§2.4.1.3). Effective temperatures (T_{eff}) come from the final spectral type (see §2.6.2). Most points lie above the Li I λ6707 EWs that characterize young open clusters, plotted as low-order polynomial fits for the IC 2602 (30 Myr; Randich et al., 1997), Pleiades (70-125 Myr; Soderblom et al., 1993; Basri, Marcy, & Graham, 1996), and M34 clusters (250 Myr; Jones et al., 1997). The comparison is not completely fair, however, since the cluster ZAMS stars will be roughly 10% less massive than the corresponding pre-MS stars. Even if most of our program stars were older ZAMS stars, they still

would be Li-rich compared to stars in the well-studied open clusters. We select as "Li-rich" those stars above the solid line in Fig. 2.3. Considering the uncertainties in our EW(Li) measurements, and the lack of any other ~10-20 Myr-old pre-MS G-K-type stellar samples with which to compare, we are not compelled to subdivide our sample further. For the present, we are content to have demonstrated that we have identified a population which appears to be more Li-rich than ZAMS stars.

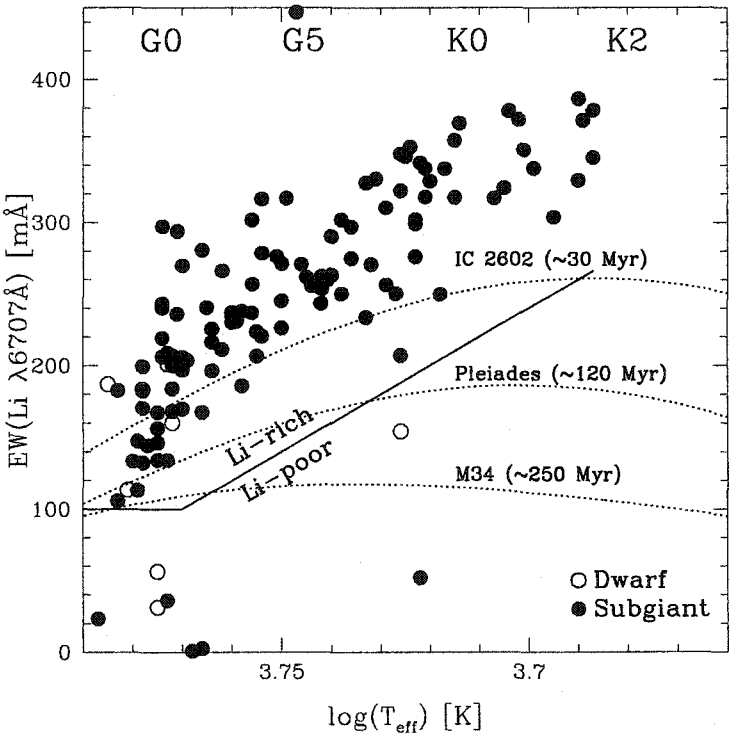

Figure 2.3: EWs for Li I λ6707 for the program stars compared to regression fits for stars in young open clusters (see §2.4.2.2). We discuss assignment of dwarf and subgiant luminosity classes in §2.4.1.3. The pre-MS candidates form an obvious locus, and we select all stars above the solid line as "Li-rich".

2.5 Defining the PTTS Sample

2.5.1 Membership Status

Our survey was designed to identify the pre-MS G and K-type stars in the Sco-Cen OB association. We classified the late-type stars according to their positions in Figs. 2.1, 2.2 and 2.3 (Table 2.4). We consider the 110 stars (85/96 RASS-ACT/TRC and 16/30 *Hipparcos*) classified as "Li-rich", "subgiant", and "active" as bona fide post-T Tauri stars ("pre-MS"). Li-rich stars with subgiant surface gravities and Hα EWs similar to the standard field stars (i.e. "inactive") are called "pre-MS?". Only 3 of the RASS-ACT/TRC stars, and 6 of the HIP stars are classified as "pre-MS?". The lone object with giant-like surface gravity in the RASS-ACT/TRC X-ray-selected sample (TYC 8992-605-1) is Li-rich, and we also classify it as a pre-MS PTTS. The 9 "pre-MS?" stars were included in our statistics concerning the star-formation history and disk-frequency of the sample (§2.7) for a total of 110 candidate lower-mass members of the LCC and UCL subgroups. All 13 stars selected in the RASS-ACT/TRC sample which overlaped with Z99's membership lists were found to be pre-MS candidates. Our RASS-ACT/TRC sample (including the 13 Z99 stars also selected) yielded a pre-MS hit-rate of (88+13)/(96+13) = 93%. Of the 30 Z99 candidates we observed, 22/30 (73%) are classified as pre-MS or "pre-MS?". The numbers of stars by membership class are listed in Table 2.4. Pre-MS stars in the *Hipparcos* sample are listed in Table 2.5, and those in the RASS-ACT/TRC sample are given in Table 2.6. Li-rich stars with dwarf-like surface gravity (N = 5) were considered young main sequence field stars ("ZAMS"), and are listed along with other interlopers in Table 2.7.

2.5.2 Sample Contamination

The primary contaminants one would expect from an X-ray- and proper motion-selected sample are X-ray-luminous ZAMS stars (ages $\approx$ 0.1-1 Gyr). Field ZAMS stars could occupy the same region of UVW velocity space, and be selected in our study by virtue of their proper motions and X-ray emission. However, our selection of candidate Sco-Cen members utilizes a surface gravity criterion which should minimize contamination. Even if our surface gravity indicator was in error, we claim ZAMS stars do not dominate our sample. Field ZAMS stars exhibit a large spread in Li EWs (especially for the late-G and early-K stars), however this is not observed in Fig. 2.3. The star just below the "Li-rich" line in Fig. 2.3 (TYC 7318-593-1; G9, EW(Li) $\simeq$ 150 mÅ) happens to be the sole RASS-ACT/TRC star with inferred $\log g$ *higher* than that of the dwarf standards in Fig. 2.1. We consider TYC 7318-593-1 to be a field ZAMS star candidate due to its intermediate Li strength and high surface gravity.

Table 2.4. Stellar Classification Scheme

(1) Li-Rich	(2) Hα Excess	(3) Lum. Class	(4) N(R-T) #	(5) N(HIP) #	(6) Adopted Class.
Yes	Yes	IV	94	7	Pre-main sequence (PMS)
Yes	No	IV	3	6	Probably pre-main sequence? (PMS?)
Yes	Strong	IV	1	0	Pre-MS Classical T Tauri star (CTTS)[a]
Yes	Yes/No	V	4	1	Young Dwarf (ZAMS)
No	Yes	V	1	0	Active Dwarf
No	Yes	IV	4	0	Active Subgiant
No	No	IV	1	2	Subgiant
No	No	III	0	2	Giant
No	No	V	0	2	Dwarf (MS)
No	No(Wide)	IV	2	0	Chromosph.-Active Binary (CAB)[b]
...	...	...	107	20	Total

Note. — N(R-T) is number in RASS-ACT/TRC sample. N(HIP) is number in *Hipparcos* sample. "Li-rich" implies significant Li absorption, and above the line in Fig.2.3. "Active" means that the Hα equivalent widths are >2 × the σ-residual above the regression of values for field, standard stars (Fig. 2.2; Appendix C), implying that chromospheric emission is filling in the absorption line. Luminosity classes are assigned according to a star's placement in Fig. 2.1.

[a]included in Pre-MS sample count.

[b]included in subgiant sample count.

Table 2.5. LCC & UCL Pre-Main Sequence Members from de Zeeuw et al. (1999) List

(1)	(2)	(3)	(4)	(5)	(6)	(7)	(8)	(9)	(10)	(11)	(12)	(13)	(14)	(15)	(16)	(17)	(18)	(19)
Name	OB	α, δ (ICRS)	π_{HIP}	π_{sec}	P_1	Spec.	$\log(T_{eff})$	$\log L/L_\odot$	A_V	EW(Hα)	EW(Li)	$\log(L_X)$	$\log(L_X/$	DM97	PS01	SDF00	Class	Notes
HIP	Grp	h m s ° ′ ″	(mas)	(mas)	%	Type	(K)	(dex)	(mag)	(Å)	(Å)	(erg s^{-1})	$L_{bol})$	$\tau, \mathcal{M}$	$\tau, \mathcal{M}$	$\tau, \mathcal{M}$	...	...
57524	LCC	11:47:24.55 -49:53:03.0	9.62(1.39)	8.83(0.60)	81	F9IV	3.783(4)	0.44(6)	0.30(10)	2.0	0.18	30.8	-3.3	16 1.3	16 1.2	20 1.3	PMS	...
58996	LCC	12:05:47.48 -51:00:12.1	9.78(1.16)	9.79(0.52)	91	G1IV	3.772(5)	0.43(5)	0.14(4)	3.3	0.21	30.5	-3.6	14 1.3	13 1.3	18 1.3	PMS?	...
59854	LCC	12:16:27.84 -50:08:35.8	8.24(1.78)	7.67(0.61)	99	G1IV	3.772(6)	0.49(7)	0.37(11)	1.6	0.20	30.9	-3.2	13 1.4	12 1.3	17 1.3	PMS	a
60885	LCC	12:28:40.05 -55:27:19.3	7.06(1.13)	9.49(0.52)	14	G0IV	3.778(5)	0.46(5)	0.16(5)	2.7	0.13	30.3	-3.8	14 1.3	13 1.3	18 1.3	PMS?	...
60913	LCC	12:29:02.25 -64:55:00.6	10.48(1.12)	9.82(0.58)	100	G4.5IV	3.758(8)	0.43(5)	0.21(4)	2.0	0.19	<29.7	<-4.3	11 1.4	12 1.3	16 1.3	PMS?	...
62445	LCC	12:47:51.87 -51:26:38.1	6.61(1.54)	7.70(0.55)	13	G4.5IVe	3.758(13)	0.62(6)	0.66(6)	-1.8	0.24	30.7	-3.4	7 1.6	5 1.6	11 1.5	PMS	SB3?
63847	LCC	13:05:05.29 -64:13:55.3	9.56(1.35)	10.18(0.61)	48	G3IV	3.764(7)	0.36(6)	0.33(6)	1.6	0.22	<29.7	<-4.3	14 1.3	15 1.2	19 1.3	PMS	...
65517	LCC	13:25:47.83 -48:14:57.9	9.59(1.44)	10.56(0.57)	50	G1.5IV	3.770(6)	0.02(5)	0.14(8)	1.9	0.17	30.4	-3.3	.. 1.0	39 1.0	...1.0	PMS	b
66001	LCC	13:31:53.61 -51:13:33.1	5.99(1.71)	7.88(0.62)	82	G2.5IV	3.766(11)	0.33(7)	0.11(10)	1.2	0.28	30.6	-3.2	15 1.2	18 1.2	21 1.2	PMS	...
66941	LCC	13:43:08.69 -69:07:39.5	8.05(0.95)	9.37(0.52)	97	G0.5IV	3.775(8)	1.09(5)	0.38(4)	2.1	0.16	31.1	-3.5	3 2.4	4 2.0	5 2.1	PMS	c
67522	UCL	13:50:06.28 -40:50:08.8	7.94(1.64)	7.91(0.60)	93	G0.5IV	3.775(6)	0.25(7)	0.02(10)	2.2	0.15	30.4	-3.5	20 1.2	25 1.1	29 1.2	PMS	...
71178	UCL	14:33:25.78 -34:32:37.6	9.76(1.90)	8.71(0.56)	99	G8IVe	3.741(12)	0.16(6)	0.35(8)	-0.2	0.26	<29.8	<-3.9	14 1.2	18 1.1	23 1.1	PMS	...
75924	UCL	15:30:26.29 -32:18:11.6	10.91(3.21)	9.79(0.79)	16	G2.5IV	3.765(6)	0.69(7)	0.37(7)	1.3	0.24	30.9	-2.9	7 1.6	5 1.7	11 1.5	PMS	d
76472	UCL	15:37:04.66 -40:09:22.1	5.70(1.63)	7.24(0.49)	95	G1IV	3.774(8)	0.60(6)	0.29(10)	0.4	0.24	30.8	-3.3	11 1.4	11 1.4	14 1.4	PMS	...
77081	UCL	15:44:21.05 -33:18:55.0	6.63(1.61)	7.66(0.59)	69	G7.5IV	3.742(8)	0.35(7)	0.15(6)	1.8	0.25	<29.9	<-4.1	9 1.4	11 1.3	15 1.3	PMS?	...
77135	UCL	15:44:57.69 -34:11:53.7	6.98(2.92)	7.20(0.96)	91	G4IV	3.760(6)	0.42(12)	0.08(5)	2.2	0.23	30.5	-3.4	12 1.4	12 1.3	17 1.3	PMS?	e
77144	UCL	15:45:01.83 -40:50:31.0	6.45(1.42)	8.00(0.53)	43	G0IV	3.778(7)	0.36(6)	0.08(5)	1.8	0.17	30.6	-3.4	17 1.2	20 1.2	23 1.3	PMS	...
77524	UCL	15:49:44.98 -39:25:09.1	6.63(1.93)	6.63(0.76)	96	K1-IVe	3.705(13)	0.23(10)	-0.03(10)	-0.2	0.32	30.5	-3.3	4 1.4	9 1.3	10 1.4	PMS	f

Table 2.5—Continued

(1)	(2)	(3)		(4)	(5)	(6)	(7)	(8)	(9)	(10)	(11)	(12)	(13)	(14)	(15)	(16)	(17)	(18)	(19)
Name	OB	α, δ (ICRS)		π_{HIP}	π_{sec}	P_1	Spec.	$\log(T_{eff})$	$\log L/L_\odot$	A_V	EW(Hα)	EW(Li)	$\log(L_X)$	$\log(L_X/$	DM97	PS01	SDF00	Class	Notes
HIP	Grp	h m s	° ′ ″	(mas)	(mas)	%	Type	(K)	(dex)	(mag)	(Å)	(Å)	(erg s^{-1})	$L_{bol})$	$\tau, \mathcal{M}$	$\tau, \mathcal{M}$	$\tau, \mathcal{M}$	...	...
77656	UCL	15:51:13.73	-42:18:51.3	6.52(1.37)	7.70(0.52)	100	G5IV	3.756(9)	0.41(6)	0.52(9)	1.7	0.30	30.3	-3.8	11 1.4	12 1.3	16 1.3	PMS	SB2
80636	UCL	16:27:52.34	-35:47:00.4	8.54(1.64)	6.56(0.52)	33	G0.5IV	3.774(7)	0.65(7)	0.39(8)	1.5	0.21	30.9	-3.3	10 1.5	10 1.4	13 1.5	PMS	...
81380	UCL	16:37:12.87	-39:00:38.1	7.27(1.91)	4.99(0.53)	92	G0IV	3.777(9)	0.74(10)	0.33(9)	2.5	0.14	<30.3	<-4.0	9 1.6	5 1.7	11 1.5	PMS	...
81447	UCL	16:38:05.53	-34:01:10.6	5.90(1.41)	5.80(0.52)	87	G0.5IV	3.775(5)	0.78(8)	0.03(7)	2.8	0.13	<30.2	<-4.3	8 1.6	5 1.7	10 1.6	PMS?	...

Note. — Columns: (1) *Hipparcos* catalog ID, (2) OB subgroup, (3) Hipparcos position (ICRS, epoch 2000.0), (4) *Hipparcos* astrometric parallax (mas), (5) Secular parallax estimate (mas) (see §2.6.3), (6) Membership probability (with v_{disp} = 1 km s^{-1}), (7) Spectral type (see §2.4.1), (8) Effective temperature (see §2.6.2), (9) Luminosity (see §2.6.5), (10) Extinction A_V (see §2.6.5), (11) Equivalent Width of Hα λ6562.8 (Å), (12) Corrected EW of Li I λ6707.8 (Å), (13) X-ray luminosity (erg s^{-1}) (see §2.2.2; approximate upper limits assume RASS PSPC detection limit of 0.05 ct s^{-1} and HR1 = 0), (14) Logarithm of ratio between X-ray and bolometric luminosities, (15) Age τ (in Myr) and Mass $\mathcal{M}$ (in $M/M_\odot$) using DM97 tracks, (16) Age τ (in Myr) and Mass $\mathcal{M}$ (in $M/M_\odot$) using PS01 tracks, (17) Age τ (in Myr) and Mass $\mathcal{M}$ (in $M/M_\odot$) using SDF00 tracks, (18) Class – PMS = pre-main sequence, PMS? = pre-main sequence? (see §2.5.1), (19) Notes – SB = spectroscopic binary.

[a]HIP 59854 = CCDM J12165-5009AB. Unresolved binary (ρ = 0.2″).

[b]HIP 65517. The Michigan Spectral Survey (Houk, 1978) classifies this star as K0/2(V)+(G) (quality = 3). We found it to be much earlier (G1.5), and note that the published $(b-y)$ and $(B-V)$colors support an early G classification.

[c]HIP 66941 = HD 119022 = Star "E" of Soderblom et al.'s (1998) high resolution survey of active southern stars. It is the most Li-rich of the very active stars in the Soderblom sample. We did not resolve this tight, equal-brightness binary (ρ = 0.2″; CCDM J13431-6908AB).

[d]HIP 75924 = CCDM J15304-3218AB. Both stars were on the slit (ρ = 1.5″).

[e]HIP 77135 = [KWS97] Lupus 1 26 = CCDM J15450-3412AB. Binary is resolved (ρ = 3.4″) but both were on-slit.

[f]HIP 77524 = [KWS97] TTS 79 = CCDM J15450-3412AB. Unresolved binary (ρ = 0.2″).

Table 2.6. Pre-Main Sequence LCC & UCL RASS-ACT/TRC Members

(1)	(2)	(3)	(4)	(5)	(6)	(7)	(8)	(9)	(10)	(11)	(12)	(13)	(14)	(15)	(16)	(17)	(18)	(19)
ID	Name	OB	α, δ (ICRS)	π_{sec}	P_1	Spec.	$\log(T_{eff})$	$\log L/L_\odot$	A_V	EW(Hα)	EW(Li)	$\log(L_X)$	$\log(L_X/$	DM97	PS01	SDF00	Class	Notes
#	TYC	Grp	h m s ° ′ ″	(mas)	%	Type	(K)	(dex)	(mag)	(Å)	(Å)	(erg s^{-1})	$L_{bol})$	$\tau, \mathcal{M}$	$\tau, \mathcal{M}$	$\tau, \mathcal{M}$	...	...
1	9212-2011-1	LCC	10:57:49.38 -69:13:59.9	9.76(101)	79	K1+IV	3.699(10)	0.02(9)	0.35(6)	0.7	0.34	30.3	-3.3	7 1.2	13 1.1	15 1.2	PMS	...
2	8625-388-1	LCC	11:32:08.34 -58:03:20.0	10.78(121)	59	G7IV	3.747(13)	0.19(10)	0.68(13)	0.4	0.45	29.9	-3.7	15 1.2	19 1.1	23 1.2	PMS	...
3	8982-3213-1	LCC	12:04:48.87 -64:09:55.4	8.36(127)	12	G1IV	3.773(5)	0.44(13)	0.60(11)	1.5	0.21	30.8	-3.2	14 1.3	13 1.3	18 1.3	PMS	...
4	8640-2515-1	LCC	12:06:13.54 -57:02:16.8	6.48(106)	90	G4IV	3.760(7)	0.15(14)	1.45(6)	0.6	0.23	30.6	-3.1	21 1.1	25 1.1	28 1.2	PMS	...
5	8644-802-1	LCC	12:09:41.86 -58:54:45.0	9.00(114)	65	K0IVe	3.720(13)	0.20(11)	0.28(10)	-0.1	0.33	30.5	-3.2	7 1.4	12 1.2	15 1.3	PMS	...
6	8644-340-1	LCC	12:11:31.43 -58:16:53.2	9.29(91)	95	G9IV	3.729(8)	0.05(9)	0.28(10)	0.3	0.31	30.5	-3.2	14 1.2	21 1.1	24 1.1	PMS	...
7	9231-1566-1	LCC	12:11:38.14 -71:10:36.0	10.15(68)	91	G3.5IV	3.762(5)	0.39(6)	0.48(8)	1.4	0.27	30.5	-3.5	13 1.3	13 1.3	18 1.3	PMS	...
8	8636-2515-1	LCC	12:12:35.75 -55:20:27.3	9.24(90)	50	K0+IV	3.717(7)	0.00(9)	0.48(12)	0.2	0.34	30.3	-3.2	11 1.2	19 1.1	23 1.1	PMS	...
9	8242-1324-1	LCC	12:14:34.09 -51:10:12.5	9.41(83)	82	G9IV	3.733(8)	0.01(8)	-0.02(5)	0.2	0.33	30.4	-3.2	17 1.1	25 1.0	28 1.1	PMS	...
10	8637-2610-1	LCC	12:14:52.31 -55:47:03.6	9.72(131)	62	G6IV	3.750(7)	0.28(12)	0.87(12)	0.6	0.27	30.9	-2.9	13 1.3	15 1.2	20 1.2	PMS	a
11	8645-1339-1	LCC	12:18:27.64 -59:43:12.9	10.42(132)	4	K1.5IVe	3.695(10)	0.03(11)	0.12(8)	-0.3	0.30	30.3	-3.1	6 1.2	12 1.2	14 1.2	PMS	...
12	8641-2187-1	LCC	12:18:58.02 -57:37:19.2	9.46(74)	97	G9.5IV	3.724(13)	0.32(7)	0.49(14)	0.1	0.35	30.6	-3.2	6 1.5	10 1.3	12 1.4	PMS	...
13	8983-98-1	LCC	12:19:21.64 -64:54:10.4	9.74(113)	89	K1-IV	3.707(10)	0.26(10)	0.25(5)	0.3	0.32	30.5	-3.2	4 1.5	8 1.3	10 1.4	PMS	...
14	8633-508-1	LCC	12:21:16.48 -53:17:44.9	9.31(78)	27	G1.5IV	3.770(7)	0.31(7)	0.44(7)	1.6	0.21	30.7	-3.3	17 1.2	20 1.2	23 1.2	PMS	...
15	8238-1462-1	LCC	12:21:55.65 -49:46:12.5	9.85(66)	86	G5.5IV	3.754(7)	0.08(6)	0.14(6)	1.5	0.28	30.2	-3.4	22 1.1	28 1.0	30 1.1	PMS	...
16	8234-2856-1	LCC	12:22:04.30 -48:41:24.9	7.96(81)	85	K0IVe	3.721(12)	0.10(9)	0.21(7)	-0.1	0.34	30.4	-3.2	10 1.3	15 1.1	19 1.2	PMS	...
17	8633-28-1	LCC	12:22:33.23 -53:33:49.0	8.07(69)	53	G0IV	3.778(5)	0.41(8)	0.41(11)	2.2	0.20	30.3	-3.7	16 1.3	17 1.2	20 1.3	PMS	...
18	8641-1281-1	LCC	12:23:40.13 -56:16:32.5	8.92(119)	66	K0+IV	3.715(17)	-0.09(12)	0.44(9)	1.1	0.36	30.0	-3.4	14 1.1	24 1.0	28 1.0	PMS	...
19	8992-605-1	LCC	12:36:38.97 -63:44:43.5	9.73(82)	56	K0+III	3.717(17)	0.25(8)	0.39(6)	0.6	0.37	30.4	-3.4	5 1.5	10 1.3	12 1.3	PMS?	b
20	8646-166-1	LCC	12:36:58.97 -54:12:18.0	8.64(118)	92	K0IV	3.721(6)	0.04(12)	0.11(5)	0.7	0.32	30.3	-3.4	11 1.2	18 1.1	22 1.1	PMS	...

Table 2.6—Continued

(1)	(2)	(3)	(4)			(5)	(6)	(7)	(8)	(9)	(10)	(11)	(12)	(13)	(14)	(15)	(16)	(17)	(18)	(19)
ID	Name	OB	α, δ (ICRS)			π_{sec}	P_1	Spec.	$\log(T_{eff})$	$\log L/L_\odot$	A_V	EW(Hα)	EW(Li)	$\log(L_X)$	$\log(L_X/$	DM97	PS01	SDF00	Class	Notes
#	TYC	Grp	h m s	° ′ ″		(mas)	%	Type	(K)	(dex)	(mag)	(Å)	(Å)	(erg s^{-1})	L_{bol})	$\tau, \mathcal{M}$	$\tau, \mathcal{M}$	$\tau, \mathcal{M}$	...	...
21	8654-1115-1	LCC	12:39:37.96	-57:31:40.7		10.22(96)	3	G7.5IV	3.742(12)	-0.06(8)	0.30(7)	0.1	0.26	30.4	-3.1	24 1.0	34 0.9	47 1.1	PMS	...
22	8659-2604-1	LCC	12:41:18.17	-58:25:56.0		10.26(95)	58	G1.5IVe	3.771(11)	0.14(8)	0.67(14)	-0.6	0.29	30.2	-3.4	24 1.1	30 1.1	300 1.2	PMS	...
23	8992-420-1	LCC	12:44:34.82	-63:31:46.2		7.97(119)	59	K1IVe	3.704(12)	0.25(13)	0.27(8)	-0.7	0.38	30.6	-3.0	4 1.4	8 1.3	9 1.4	PMS	c
24	8249-52-1	LCC	12:45:06.76	-47:42:58.2		8.34(62)	94	G8.5IV	3.738(11)	0.13(7)	0.38(14)	0.0	0.30	30.6	-3.1	14 1.2	19 1.1	23 1.1	PMS	...
25	7783-1908-1	LCC	12:48:07.79	-44:39:16.8		10.97(59)	21	G6IVe	3.751(13)	0.14(5)	0.18(8)	-0.1	0.28	30.6	-3.1	18 1.1	23 1.1	26 1.1	PMS	...
26	8655-149-1	LCC	12:48:48.18	-56:35:37.8		7.56(73)	56	G5IV	3.755(8)	0.14(9)	0.53(13)	1.2	0.22	30.4	-3.4	20 1.1	24 1.1	27 1.1	PMS	...
27	9245-617-1	LCC	12:58:25.58	-70:28:49.2		11.73(69)	80	K0+IV	3.714(10)	-0.01(6)	0.46(12)	0.0	0.37	30.3	-3.3	11 1.2	18 1.1	22 1.1	PMS	d
28	8648-446-1	LCC	13:01:50.70	-53:04:58.3		9.22(151)	75	K2-IV	3.690(8)	-0.37(14)	0.55(10)	0.2	0.33	30.0	-3.3	19 0.9	39 0.8	41 0.9	PMS	...
29	8652-1791-1	LCC	13:02:37.54	-54:59:36.8		6.40(81)	16	G1IV	3.772(6)	0.35(11)	0.38(5)	2.1	0.17	30.8	-3.1	16 1.2	18 1.2	21 1.3	PMS	...
30	8258-1878-1	LCC	13:06:40.12	-51:59:38.6		8.91(90)	94	K0IVe	3.722(19)	-0.05(9)	0.17(9)	-0.3	0.34	30.2	-3.4	15 1.1	24 1.0	28 1.0	PMS	...
31	8259-689-1	LCC	13:14:23.84	-50:54:01.9		7.70(81)	87	G5.5IV	3.754(10)	0.25(10)	0.27(9)	1.1	0.32	30.8	-2.9	15 1.2	18 1.1	22 1.2	PMS	...
32	8649-251-1	LCC	13:17:56.94	-53:17:56.2		5.99(121)	56	G1IV	3.774(8)	0.43(18)	0.22(11)	1.0	0.30	30.7	-3.2	14 1.3	14 1.3	19 1.3	PMS	...
33	8248-539-1	LCC	13:22:04.46	-45:03:23.1		7.16(67)	71	G0IV	3.779(6)	0.18(8)	0.22(8)	2.1	0.15	30.3	-3.6	26 1.2	30 1.1	...1.2	PMS	...
34	9246-971-1	LCC	13:22:07.54	-69:38:12.3		11.57(95)	82	K1IVe	3.702(17)	0.00(8)	0.17(7)	-39.9	0.37	30.2	-3.2	8 1.2	14 1.1	17 1.2	PMS	e
35	8663-1375-1	LCC	13:34:20.26	-52:40:36.1		9.50(66)	100	G1IV	3.774(7)	0.32(6)	0.45(10)	1.7	0.22	30.5	-3.4	18 1.2	21 1.2	24 1.3	PMS	...
36	7796-1788-1	UCL	13:37:57.29	-41:34:41.9		10.23(52)	49	K0IV	3.723(7)	0.00(5)	-0.07(5)	0.7	0.30	30.4	-3.2	14 1.2	21 1.0	25 1.1	PMS	...
37	8667-283-1	LCC	13:43:28.53	-54:36:43.5		11.70(75)	2	G2IV	3.769(7)	0.13(6)	0.28(12)	1.7	0.20	30.6	-3.2	24 1.1	30 1.1	200 1.2	PMS	...
38	8270-2015-1	UCL	13:47:50.55	-49:02:05.5		6.75(79)	73	G8IVe	3.740(11)	0.05(10)	0.45(13)	-0.5	0.29	30.5	-3.2	18 1.1	25 1.0	28 1.1	PMS	...
39	8263-2453-1	UCL	13:52:47.80	-46:44:09.2		6.92(57)	74	G0IV	3.778(8)	0.44(7)	0.34(8)	2.4	0.18	30.8	-3.3	15 1.3	15 1.3	19 1.3	PMS	...
40	7811-2909-1	UCL	14:02:20.73	-41:44:50.8		7.69(71)	58	G9IV	3.733(13)	0.07(8)	0.90(12)	0.2	0.23	30.3	-3.3	14 1.2	21 1.1	25 1.1	PMS	...

Table 2.6—Continued

(1)	(2)	(3)	(4)	(5)	(6)	(7)	(8)	(9)	(10)	(11)	(12)	(13)	(14)	(15)	(16)	(17)	(18)	(19)
ID	Name	OB	α, δ (ICRS)	π_{sec}	P_1	Spec.	$\log(T_{eff})$	$\log L/L_\odot$	A_V	EW(Hα)	EW(Li)	$\log(L_X)$	$\log(L_X/$	DM97	PS01	SDF00	Class	Notes
#	TYC	Grp	h m s ° ′ ″	(mas)	%	Type	(K)	(dex)	(mag)	(Å)	(Å)	(erg s^{-1})	$L_{bol})$	$\tau, \mathcal{M}$	$\tau, \mathcal{M}$	$\tau, \mathcal{M}$ ...	...	...
41	7815-2029-1	UCL	14:09:03.58 -44:38:44.4	7.05(49)	9	F9IV	3.783(5)	0.50(6)	0.38(6)	3.0	0.11	30.7	-3.5	14 1.3	13 1.3	18 1.3	PMS?	...
42	9244-814-1	LCC	14:16:05.67 -69:17:36.0	8.15(92)	11	G1IV	3.773(7)	0.19(10)	0.62(8)	2.2	0.13	30.1	-3.7	23 1.1	27 1.1	58 1.2	PMS	...
43	8282-516-1	UCL	14:27:05.56 -47:14:21.8	7.57(63)	89	G7IV	3.745(10)	0.06(8)	0.17(4)	1.1	0.26	30.4	-3.3	19 1.1	26 1.0	29 1.1	PMS	...
44	7817-622-1	UCL	14:28:09.30 -44:14:17.4	6.23(71)	52	G5.5IV	3.754(8)	0.54(10)	0.33(7)	1.4	0.22	30.6	-3.5	8 1.5	9 1.4	12 1.4	PMS	...
45	7813-224-1	UCL	14:28:19.38 -42:19:34.1	6.27(61)	87	G3.5IV	3.762(8)	0.33(9)	0.37(7)	1.0	0.21	30.8	-3.0	14 1.3	16 1.2	20 1.2	PMS	...
46	7814-1450-1	UCL	14:37:04.22 -41:45:03.0	6.41(70)	88	G0.5IV	3.775(8)	0.59(10)	0.18(6)	1.5	0.17	30.7	-3.4	11 1.4	11 1.4	15 1.4	PMS	f
47	8683-242-1	UCL	14:37:50.23 -54:57:41.1	7.59(94)	20	K0+IV	3.715(15)	0.08(11)	0.30(6)	0.1	0.32	30.6	-3.0	8 1.3	14 1.1	18 1.2	PMS	...
48	8283-264-1	UCL	14:41:35.00 -47:00:28.8	9.11(52)	94	G4IV	3.759(13)	0.20(6)	0.02(7)	1.2	0.23	30.9	-2.8	18 1.2	22 1.1	25 1.2	PMS	...
49	8283-2795-1	UCL	14:47:31.77 -48:00:05.7	7.68(81)	1	G2.5IV	3.766(8)	-0.05(9)	0.43(7)	1.8	0.17	30.2	-3.4	.....	44 1.0	...1.0	PMS	...
50	7305-380-1	UCL	14:50:25.81 -35:06:48.6	5.27(87)	73	K0IV	3.723(15)	0.52(15)	0.21(8)	0.0	0.28	30.6	-3.3	3 1.8	5 1.6	7 1.7	PMS	g
51	7828-2913-1	UCL	14:52:41.98 -41:41:55.2	6.89(75)	84	K1IVe	3.701(10)	0.10(10)	0.61(10)	-0.6	0.35	30.5	-3.2	5 1.3	11 1.2	13 1.3	PMS	...
52	7310-2431-1	UCL	14:57:19.63 -36:12:27.4	7.59(61)	13	G6IV	3.750(11)	0.18(7)	0.15(6)	1.4	0.25	30.3	-3.4	16 1.2	20 1.1	24 1.2	PMS	g
53	7310-503-1	UCL	14:58:37.70 -35:40:30.4	7.36(77)	82	K2-IVe	3.689(8)	0.21(9)	0.23(11)	-0.3	0.37	30.3	-3.4	3 1.3	6 1.4	7 1.5	PMS	g
54	7824-1291-1	UCL	14:59:22.76 -40:13:12.1	8.17(57)	85	G3IV	3.764(8)	0.32(6)	0.40(6)	1.5	0.23	30.5	-3.4	15 1.2	17 1.2	21 1.2	PMS	g
55	7833-2037-1	UCL	15:00:51.88 -43:31:21.0	6.14(72)	78	G9IV	3.731(12)	0.16(11)	0.30(9)	0.1	0.33	30.4	-3.2	11 1.3	15 1.1	20 1.2	PMS	g
56	7829-504-1	UCL	15:01:11.56 -41:20:40.6	4.67(62)	94	G0.5IV	3.774(8)	0.64(12)	0.48(8)	1.5	0.24	31.0	-3.3	10 1.5	10 1.4	13 1.4	PMS	g
57	8297-1613-1	UCL	15:01:58.82 -47:55:46.4	6.43(62)	25	G1.5IV	3.770(6)	0.29(9)	0.22(10)	2.0	0.20	30.2	-3.8	18 1.2	21 1.2	24 1.2	PMS	...
58	7319-749-1	UCL	15:07:14.81 -35:04:59.6	9.92(82)	12	G9.5IV	3.727(11)	-0.12(8)	0.44(10)	1.2	0.25	30.0	-3.4	21 1.0	33 0.9	38 1.0	PMS	h
59	7833-2400-1	UCL	15:08:37.75 -44:23:16.9	5.55(72)	81	G1.5IVe	3.770(11)	0.29(12)	0.13(11)	-0.8	0.27	30.9	-2.9	18 1.2	21 1.2	24 1.2	PMS	h
60	7833-2559-1	UCL	15:08:38.50 -44:00:52.1	7.46(71)	85	G1.5IV	3.771(9)	0.20(9)	0.11(7)	1.2	0.24	30.4	-3.3	21 1.1	26 1.1	30 1.2	PMS	h

Table 2.6—Continued

(1)	(2)	(3)	(4)	(5)	(6)	(7)	(8)	(9)	(10)	(11)	(12)	(13)	(14)	(15)	(16)	(17)	(18)	(19)
ID	Name	OB	α, δ (ICRS)	π_{sec}	P_1	Spec.	$\log(T_{eff})$	$\log L/L_\odot$	A_V	EW(Hα)	EW(Li)	$\log(L_X)$	$\log(L_X/$	DM97	PS01	SDF00	Class	Notes
#	TYC	Grp	h m s ° ′ ″	(mas)	%	Type	(K)	(dex)	(mag)	(Å)	(Å)	(erg s^{-1})	$L_{bol})$	$\tau, \mathcal{M}$	$\tau, \mathcal{M}$	$\tau, \mathcal{M}$	...	...
61	8294-2230-1	UCL	15:12:50.18 -45:08:04.5	6.61(72)	100	G5IV	3.756(8)	0.19(10)	0.27(7)	1.7	0.24	30.6	-3.1	18 1.2	22 1.1	25 1.2	PMS	h
62	8694-1685-1	UCL	15:18:01.74 -53:17:28.8	9.74(93)	14	G7IV	3.746(9)	0.08(9)	0.77(7)	1.2	0.27	30.4	-3.3	19 1.1	25 1.0	28 1.1	PMS	...
63	7822-158-1	UCL	15:18:26.91 -37:38:02.1	7.89(86)	97	G9IV	3.729(16)	0.05(10)	0.72(8)	0.4	0.26	30.4	-3.0	14 1.2	21 1.1	24 1.1	PMS	h
64	8295-1530-1	UCL	15:25:59.65 -45:01:15.8	6.73(73)	40	G8IV	3.740(12)	-0.02(10)	0.19(5)	1.1	0.26	30.1	-3.5	21 1.0	30 1.0	35 1.1	PMS	h
65	7326-928-1	UCL	15:29:38.58 -35:46:51.3	7.39(71)	93	K0+IV	3.718(10)	0.17(9)	0.16(5)	0.1	0.25	30.3	-3.4	7 1.4	12 1.2	15 1.2	PMS	h
66	7327-1934-1	UCL	15:37:02.14 -31:36:39.8	7.41(59)	32	G6IV	3.750(9)	0.42(7)	0.43(5)	0.4	0.23	30.9	-3.0	9 1.4	11 1.3	15 1.3	PMS	i
67	7840-1280-1	UCL	15:37:11.30 -40:15:56.8	6.11(67)	99	G8.5IVe	3.736(14)	0.25(10)	0.40(10)	-0.9	0.30	30.7	-3.2	10 1.3	13 1.2	17 1.2	PMS	h
68	7848-1659-1	UCL	15:38:43.06 -44:11:47.4	8.04(58)	82	G8.5IV	3.736(8)	0.08(7)	0.62(5)	0.5	0.27	30.3	-3.4	15 1.2	21 1.1	25 1.1	PMS	h
69	6785-510-1	UCL	15:39:24.41 -27:10:21.9	7.89(61)	72	G5IV	3.755(7)	0.46(7)	0.28(6)	1.7	0.21	30.7	-3.3	9 1.4	11 1.3	15 1.4	PMS	j
70	7331-782-1	UCL	15:44:03.77 -33:11:11.2	8.08(86)	99	K0IVe	3.723(13)	0.01(10)	0.47(6)	-1.1	0.30	30.2	-3.3	13 1.2	21 1.1	25 1.1	PMS	...
71	7845-1174-1	UCL	15:45:52.25 -42:22:16.5	7.71(58)	32	K2-IVe	3.690(7)	0.12(7)	0.80(8)	-0.8	0.39	30.9	-2.9	4 1.3	8 1.3	10 1.3	PMS	h
72	8317-551-1	UCL	15:46:51.79 -49:19:04.7	7.55(59)	96	G7.5IV	3.744(7)	0.21(7)	0.29(8)	1.5	0.26	30.5	-3.3	13 1.2	17 1.1	21 1.2	PMS	...
73	7842-250-1	UCL	15:56:59.05 -39:33:43.1	5.74(70)	99	G9.5IV	3.726(7)	0.21(11)	0.35(6)	1.2	0.21	30.5	-3.4	8 1.4	12 1.2	16 1.2	PMS	...
74	7333-1260-1	UCL	16:01:07.93 -32:54:52.5	7.60(55)	87	G0IV	3.779(6)	0.33(6)	0.15(7)	2.3	0.11	30.6	-3.4	18 1.2	22 1.2	25 1.3	PMS	...
75	7333-719-1	UCL	16:01:08.97 -33:20:14.2	5.69(74)	64	G5IV	3.756(12)	0.41(12)	0.16(6)	0.7	0.26	30.6	-3.1	11 1.4	12 1.3	16 1.3	PMS	h
76	7863-1629-1	UCL	16:03:45.37 -43:55:49.2	5.63(51)	62	G9.5IV	3.725(14)	0.75(8)	0.51(6)	0.7	0.35	31.2	-3.1	2 2.1	4 1.8	4 2.0	PMS	h,k
77	7855-1106-1	UCL	16:03:52.50 -39:39:01.3	7.14(79)	83	K2-IVe	3.687(10)	0.09(10)	0.18(6)	-0.4	0.38	30.4	-3.2	4 1.2	8 1.3	10 1.3	PMS	h
78	7851-1-1	UCL	16:05:45.00 -39:06:06.5	7.69(75)	61	G6.5IV	3.749(10)	0.13(9)	0.19(5)	0.3	0.32	30.5	-3.1	18 1.1	23 1.1	26 1.1	PMS	h
79	7355-317-1	UCL	16:13:58.02 -36:18:13.4	8.10(71)	90	G9IVe	3.732(14)	-0.13(8)	0.31(9)	-0.5	0.27	30.4	-2.9	24 1.0	37 0.9	45 1.0	PMS	l
80	8319-1687-1	UCL	16:14:52.01 -50:26:18.5	7.77(72)	81	G9.5IV	3.726(10)	0.34(8)	0.39(7)	0.6	0.32	30.6	-3.1	6 1.5	10 1.3	12 1.4	PMS	...

We can rule out most of the pre-MS candidates being Li-rich *post-MS* stars. Based on the surveys of Li abundances in field subgiants by Randich et al. (1999) and Pallavicini et al. (1987), we do not expect to find any post-MS subgiants with EW(λ6707) $>$ 100 mÅ. Even if our measured EWs for the Li I λ6707 line are over-estimated due to low spectral resolution, the overestimate would have to be greater than a factor of two to reconcile our sources with even the most Li-rich subgiants found in the Randich et al. survey. Our spectral analysis suggests that the majority of our sample stars are both Li-rich and above the main sequence (i.e. pre-MS).

Could some of our stars be *post*-MS chromospherically active binaries (CABs) or RS CVn systems? The light from an RS CVn system would be dominated by a rapidly rotating, evolved (subgiant) primary. Only six of our targets are Li-poor subgiants (HIP 63797, 81775, TYC 8293-92-1, 7833-1106-1, 7858-526-1, and 8285-847-1). The first three appear to be normal subgiants. TYC 7833-1106-1 is possibly a spectroscopic binary. TYC 7858-526-1 has a wide, broad Hα absorption line. It appears to be a multiple late-F star (we classify it as F8.5; Houk (1982) classify it as F5), so the star could hide a cosmic Li abundance due to the increased ionization of Li I in F stars (and correspondingly lower EW(Li)). The system could be a legitimate member, but we exclude it from the pre-MS sample. The subgiant TYC 8285-847-1 (HIP 69781 = V636 Cen) is probably a CAB. It is a previously known grazing, eclipsing binary (e.g. Popper, 1966) and its saturated X-ray emission argues for being a true CAB. Finally, the Li-rich star TYC 8992-605-1 (star #19; K0+III) is the only RASS-ACT/TRC star that appears in the giant regime of Fig. 2.1. The star is an obvious spectroscopic binary of nearly equal mass. We believe this star is probably a pre-MS binary, and include it in our "pre-MS?"

Table 2.6—Continued

(1)	(2)	(3)	(4)	(5)	(6)	(7)	(8)	(9)	(10)	(11)	(12)	(13)	(14)	(15)	(16)	(17)	(18)	(19)
ID	Name	OB	α, δ (ICRS)	π_{sec}	P_1	Spec.	$\log(T_{eff})$	$\log L/L_\odot$	A_V	EW(Hα)	EW(Li)	$\log(L_X)$	$\log(L_X/$	DM97	PS01	SDF00	Class	Notes
#	TYC	Grp	h m s ° ′ ″	(mas)	%	Type	(K)	(dex)	(mag)	(Å)	(Å)	(erg s^{-1})	L_{bol})	$\tau, \mathcal{M}$	$\tau, \mathcal{M}$	$\tau, \mathcal{M}$	...	...
81	7852-51-1	UCL	16:18:38.56 -38:39:11.8	9.30(54)	5	F9IV	3.780(6)	0.33(5)	0.32(4)	2.6	0.13	30.3	-3.8	19 1.2	22 1.2	26 1.3	PMS	...
82	7857-648-1	UCL	16:21:12.19 -40:30:20.6	6.43(54)	1	G8IV	3.738(7)	0.23(8)	0.69(6)	1.4	0.25	30.5	-3.3	11 1.3	14 1.2	19 1.2	PMS	i
83	7857-514-1	UCL	16:23:29.55 -39:58:00.8	5.91(72)	91	G3IV	3.764(7)	0.11(11)	0.95(8)	2.0	0.20	30.4	-3.4	23 1.1	30 1.1	66 1.2	PMS?	i
84	7853-227-1	UCL	16:27:30.55 -37:49:21.6	5.55(85)	66	G9.5IV	3.726(10)	0.21(14)	0.50(6)	0.6	0.35	30.5	-3.3	8 1.4	12 1.2	16 1.2	PMS	...
85	7353-2640-1	UCL	16:31:42.03 -35:05:17.2	7.01(69)	92	G7.5IV	3.742(9)	0.05(9)	0.33(5)	1.2	0.24	30.4	-3.3	19 1.1	25 1.0	28 1.1	PMS	...
86	7349-2191-1	UCL	16:35:35.99 -33:26:34.7	5.22(69)	7	K2-IV	3.687(7)	0.35(12)	0.34(6)	0.1	0.35	30.9	-3.0	2 1.3	4 1.5	5 1.6	PMS	...
87	7858-830-1	UCL	16:39:59.30 -39:24:59.2	4.63(75)	100	G4IV	3.760(10)	0.74(14)	0.27(7)	1.5	0.24	30.7	-3.3	6 1.8	5 1.7	9 1.6	PMS	...
88	7871-1282-1	UCL	16:42:24.00 -40:03:29.7	5.02(54)	92	G1IV	3.772(11)	0.92(10)	0.74(8)	0.3	0.18	30.7	-3.7	5 1.9	4 1.9	7 1.8	PMS	...

Note. — Columns: (1) short ID, (2) Tycho-2 name, (3) OB subgroup, (4) Tycho-2 position (ICRS, epoch 2000.0), (5) Secular parallax estimate (mas) (see §2.6.3), (6) Membership probability (with v_{disp} = 1 km s^{-1}), (7) Spectral type (see §2.4.1), (8) Effective temperature (see §2.6.2), (9) Luminosity (see §2.6.5), (10) Extinction A_V (see §2.6.5), (11) Equivalent Width of Hα λ6562.8 (Å) (see §2.4.2.1), (12) Corrected EW of Li I λ6707.8 (Å) (see §2.4.2.2) , (13) X-ray luminosity (erg s^{-1}) (see §2.2.2), (14) Logarithm of ratio between X-ray and bolometric luminosities, (15) Age τ (in Myr) and Mass $\mathcal{M}$ (in $M/M_\odot$) using DM97 tracks, (16) Age τ (in Myr) and Mass $\mathcal{M}$ (in $M/M_\odot$) using PS01 tracks, (17) Age τ (in Myr) and Mass $\mathcal{M}$ (in $M/M_\odot$) using SDF00 tracks, (18) Class – PMS = pre-main sequence, PMS? = pre-main sequence? (see §2.5.1), (19) Notes: (a) Star #10 = HIP 59721 is a common proper motion pair ($\rho = 24''$) with HD 106444 = HIP 59716 (F5V, $\pi = 9.92 \pm 2.53$). (b) Star #19 = Einstein Slew Survey source 1ES 1233-63.4. (c) Star #23 = HD 311894 = 2E 1241.6-6315 = Eclipsing binary discovered in The All Sky Automated Survey (Pojmanski, 1998): ASAS J124435-6331.8 (Per. = 2.6 days). (d) Star #27 = 2E 1255.1-7012 = EUVE J1258-70.4. (e) Star #34 = PDS 66 = Hen 3-892 = IRAS 13185-6922. This is the lone classical T Tauri star identified in this survey. [O I] λ6300 is seen in emission (EW = 0.2Å). (f) Star #46 = CCDM J1437-4145AB. Unresolved binary ($\rho = 0.4''$). (g) Young *ROSAT* star identified by Wichmann et al. (1997b) (h) Young *ROSAT* star identified by Krautter et al. (1997) (i) Star #66 = CCDM J15370-3127A = RX J1537.0-3136 = 2E 1533.9-3126?. Our spectrum is of the bright (V = 10) primary; the BC components (both V = 13) are 4″ away, and off-slit. (j) Star #69 = CCDM J15394-2710AB. Unresolved binary ($\rho = 0.4''$). (k) Star #76 = CCDM J16038-4356AB. Unresolved binary ($\rho = 0.3''$). (l) Star #79. Faint companion off-slit ($\rho \simeq 4''$).

Table 2.7. RASS-ACT/TRC & *Hipparcos* Stars Rejected as Sco-Cen Members

(1)	(2)	(3)	(4)	(5)	(6)	(7)	(8)
Name	α, δ (ICRS)	P_1	SpT	EW(Hα)	EW(Li)	log(L_X /	Type
	h m s ° ′ ″	%	...	(Å)	(Å)	(L_{bol})	...
TYC 8222-105-1	11:35:03.76 -48:50:22.0	71	F8.5V	2.7	0.19	-3.4	ZAMS
TYC 8982-3046-1	12:04:14.42 -64:18:51.7	97	G1V	2.0	0.20	-3.1	ZAMS
TYC 8990-701-1	13:13:28.11 -60:00:44.6	9	F9V	2.2	0.11	-3.4	ZAMS
TYC 8285-847-1	14:16:57.91 -49:56:42.3	43	G2.5IV	2.2	0.00	-3.9	subgiant (CAB)
TYC 7833-1106-1	15:08:00.55 -43:36:24.9	4	G2IV	0.6	0.00	-3.5	active subgiant
TYC 8293-92-1	15:09:27.93 -46:50:57.2	28	K0IV	0.7	0.05	-3.4	active subgiant
TYC 7318-593-1	15:31:21.93 -33:29:39.5	94	G9.5V	0.0	0.15	-3.3	active dwarf
TYC 7858-526-1	16:38:38.47 -39:33:03.5	98	F8.5IV	2.5	0.02	-4.0	active subgiant (CAB)
HIP 63797	13:04:30.96 -65:55:18.5	9	G3.5IV	2.4	0.00	<-4.5	subgiant
HIP 65423	13:24:35.12 -55:57:24.2	99	G0V	2.1	0.18	-3.6	ZAMS[a]
HIP 68726	14:04:07.12 -37:15:50.5	60	G0.5III	1.9	0.00	<-5.1	giant
HIP 72070	14:44:30.96 -39:59:20.6	62	G1V	2.6	0.16	<-4.2	ZAMS
HIP 74501	15:13:29.22 -55:43:54.6	3	G1.5III	2.4	0.03	<-4.9	giant
HIP 77015	15:43:29.86 -38:57:38.6	61	G0.5V	2.8	0.06	<-4.1	dwarf
HIP 79610	16:14:43.02 -38:38:43.5	37	G0.5V	2.7	0.03	<-4.2	dwarf
HIP 81775	16:42:10.36 -31:30:15.0	14	G1IV	2.8	0.04	<-4.1	subgiant

Note. — *Columns:* (1) Name from Tycho-2 or *Hipparcos* catalogs, (2) position (ICRS, epoch 2000.0), (3) Membership probability (with v_{disp} = 1 km s^{-1}), (4) Spectral type (see §2.4.1), (5) Equivalent width of Hα λ6562.8 (Å), (6) Corrected EW of Li I λ6707.8 (Å), (7) Logarithm of ratio between X-ray and bolometric luminosities (approximate upper limits assume RASS PSPC detection limit of 0.05 ct s^{-1} and *HR1* = 0), (8) Class of object

[a]HIP 65423 = HD 116402. Cutispoto et al. (2002) measure EW(Li) = 220 mÅ, and $v\sin i$ = 35 km s^{-1}.

sample. It appears that CABs are a negligible contaminant when using X-ray and kinematic selection in tandem with medium dispersion spectroscopy to identify pre-MS populations.

2.5.3 Sample Completeness

We can make a rough estimate how many stars our selection procedure should have detected by counting the number of massive Sco-Cen members in a certain mass range, and assuming an initial mass function. We assume a complete membership census within a limited mass range (the revised B-star *Hipparcos* membership from Z99), and then extrapolate how many stars we should have seen in our survey. We produce a theoretical H-R diagram for the subgroups' B stars (discussed at length in §2.7.2), and calculate masses from the evolutionary tracks of Bertelli et al. (1994) (Z = 0.02). We choose 2.5 $M_{\odot}$ as our lower mass boundary (roughly the lower limit for B stars), and adopt 13 $M_{\odot}$ as the upper mass boundary (slightly higher than the highest inferred mass from the main sequence members). In this mass range, we count 32 LCC members and 56 UCL members. We use a Kroupa (2001) IMF to predict how many low-mass stars might belong to the OB subgroups. Down to the hydrogen-burning limit (0.08 $M_{\odot}$), a total population of 1200^{+200}_{-300} stars in LCC and 2200 ± 300 stars in UCL is predicted (Poisson errors)[4]. Between 1.1-1.4 $M_{\odot}$, the mass range of a 15 Myr-old population that our survey can probe (see §2.7.1 and Fig. 2.8), the Kroupa IMF predicts a population of 29^{+6}_{-5} stars in LCC, and 51^{+8}_{-7} stars in UCL. In this mass range, our survey detects 36 pre-MS stars in LCC and 40 pre-MS stars in UCL. The number of observed pre-MS stars with 1.1-1.4 $M_{\odot}$ corresponds to +1.1σ and -1.6σ of the

[4]For low-number statistical uncertainties, we use the 1σ values from Gehrels (1986) throughout.

predicted number, for LCC and UCL respectively. This suggests that our survey is fairly complete for LCC, but we might be missing ~10 members with masses of 1.1-1.4 $M_{\odot}$ in the more distant UCL subgroup if the subgroup mass function is consistent with the field star IMF. The missing members of the UCL OB subgroup could be X-ray faint ($L_X \leq 10^{30.2}$ erg s^{-1}) stars which we were capable of detecting in the closer LCC subgroup. The IMF extrapolation does suggest that we have likely found at least the majority of stars in this mass range in both OB subgroups (if not a complete census for LCC) and that our samples are representative of the total population.

2.6 The H-R Diagram

In order to investigate the star-formation history of the LCC and UCL OB subgroups, we convert our observational data (spectral types, photometry, distances) into estimates of temperature and luminosity. We then use theoretical evolutionary tracks to infer ages and masses for our stars.

2.6.1 Photometry

The primary sources of photometry for our sample of association member candidates are the Tycho-2 catalog (Høg et al., 2000a,b) and 2MASS catalog (Cutri et al., 2003). However, the Tycho and 2MASS bandpasses are non-standard, and must be converted to standard photometric systems to enable comparison with intrinsic colors of normal stars and the interstellar reddening vector. To convert the Tycho photometry to the Johnson system, we fit low-order polynomials to the data in Table 2 of Bessell (2000) (relations given in Appendix C). A caveat is that Bessell's calibrations are for B–G dwarfs and K–M giants. The majority of our

stars appear to be pre-MS G–K stars, whose intrinsic colors should more closely match those of dwarfs rather than giants. To convert the 2MASS JHK_s data to the system of Bessell & Brett (1988), we use the conversions of Carpenter (2001). The original optical and near-IR photometry for our target stars is given in Tables 2.2 and 2.1.

2.6.2 Temperature Scale

To fix stellar properties as a function of spectral type, we adopt relations (i.e. intrinsic colors, BCs) from Table A5 of Kenyon & Hartmann (1995). Previous studies have shown that colors and BCs as a function of T_{eff} are largely independent of surface gravity over the range of interest for this study (e.g. Bessell, Castelli, & Plez, 1998). However, T_{eff} decreases with lower $\log g$ for FGK stars. After some investigation (see Appendix A), we decided to adopt the dwarf T_{eff} scale of Schmidt-Kaler (1982) (which Kenyon & Hartmann (1995) also use) with a -35 K offset to account for the effects of lower $\log g$ in our sample stars. The scatter in published dwarf T_{eff} scales is 60 K (1σ) among G stars, so while the shift is systematic, its magnitude is of the order of the uncertainties. The uncertainties in T_{eff} given in column 9 of Tables 5 and 6 include the uncertainty in spectral type and the scatter in published T_{eff} scales. The typical 1σ uncertainties in T_{eff} for the pre-MS stars is $\approx$100 K.

2.6.3 Secular Parallaxes

All of the stars in our sample have published proper motions, but only a few dozen have trigonometric parallaxes measured by *Hipparcos*. The stars are distributed over hundreds of square degrees of sky, and inhabit stellar associations

which are tens of parsecs in depth. Adopting a standard distance for all of the stars in the association introduces unwanted scatter in the H-R diagram. With accurate proper motions available, we calculate individual distances to the pre-MS candidates using moving cluster or "secular" parallaxes (e.g. Smart, 1968). We adopt the equations and formalism of de Bruijne (1999b), as well as his space motions and convergent points for the LCC and UCL OB subgroups. The uncertainties in the secular parallaxes are dominated by the uncertainties in the proper motion ($\sigma_\pi \propto \sigma_\mu$), but contain a term added in quadrature accounting for a projected $1\,\mathrm{km\,s^{-1}}$ internal velocity dispersion (see §4 of de Bruijne, 1999b). The secular parallax is only meaningful if the star is indeed a member of the group. Our spectroscopic survey has confirmed that most of the candidate stars are legitimately pre-MS, and that they are most likely members of the OB subgroups. Secular parallaxes for older, interloper stars are meaningless and ignored. In Tables 2.5 and 2.6, we list the secular parallaxes and membership probabilities for the pre-MS stars in our survey. We calculate membership probability P_1 (using formulae 4 and 6 from Z99), which have assumed an internal velocity dispersion of $1\,\mathrm{km\,s^{-1}}$ (de Bruijne, 1999b; Madsen, Dravins, & Lindegren, 2002) respectively. We independently confirm that $1\,\mathrm{km\,s^{-1}}$ is a good estimate of the internal velocity dispersion for low-mass stars in §2.6.4.

The robustness of our method can be illustrated (Fig. 2.4) by comparing the secular parallaxes (π_{sec}) to the *Hipparcos* trigonometric parallaxes (π_{HIP}). The uncertainties are typically 1-2 mas for the *Hipparcos* parallaxes, and 0.5-1 mas for our secular parallax estimates. The secular and trigonometric parallaxes agree quite well for the few pre-MS stars in our sample for which *Hipparcos* measured the parallax. The secular parallaxes yield distance uncertainties of ~5-15 % for most

of the pre-MS stars.

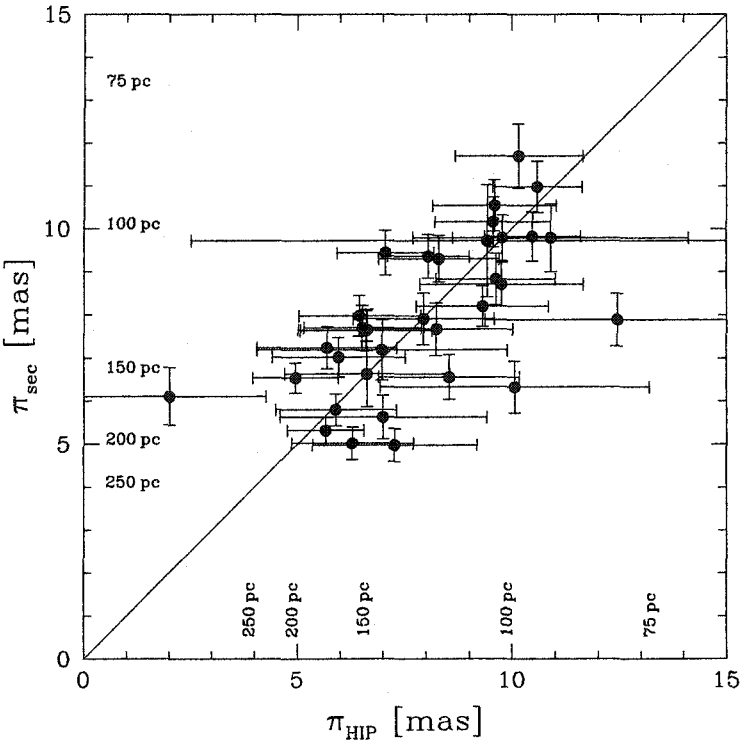

Figure 2.4: Comparison between *Hipparcos* astrometric parallaxes and our secular parallaxes calculated using the moving group method. Data points are Pre-MS (and Pre-MS?) association members from Tables 2.6 and 2.5.

2.6.4 Independent Confirmation of $v_{disp} \simeq 1\,\mathrm{km\,s^{-1}}$ for Low-Mass Members.

With a new, high-quality astrometric catalog now available (Tycho-2), one can address the question: is the internal velocity dispersion of the post-T Tauri members the same as that for the high mass members ($\sim$1 km s^{-1})? We would like to answer this question as a check. The secular parallaxes that we calculate in §2.6.3 assume that the subgroup velocity dispersions for the low-mass stars are the same as that observed for the high mass stars ($\simeq$1 km s^{-1}; de Bruijne, 1999b;

Madsen, Dravins, & Lindegren, 2002). In principle, one can calculate an *upper limit* to the velocity dispersion with the Tycho-2 astrometry alone.

As previously demonstrated, pre-main sequence members of the OB subgroups can be efficiently selected by their strong X-ray emission and convergent proper motions. To identify low-mass member candidates, we construct a cross-referenced catalog of all Tycho-2 stars with *ROSAT* All-sky Survey BSC and FSC X-ray sources within 40″ radius (hereafter RASS-TYC2), and analyze the distribution of their proper motions. Within the LCC and UCL regions (defined by de Zeeuw et al. 1999), we find 271 RASS-TYC2 stars with $(B - V) > 0.60$ (G-type or later) in LCC and 328 in UCL. For simplicity, we do not apply a magnitude restriction other than the Tycho-2 magnitude limit. The vast majority are consistent with being pre-MS or ZAMS at d = 100-200 pc.[5]

To search for subgroup members, we plot the proper motions for the RASS-TYC2 stars in (μ_v, μ_τ) space instead of (μ_α, μ_δ). The proper motion components represent the motion toward the subgroup convergent point (μ_v) and perpendicular to the great circle between the star and the convergent point (μ_τ) (Smart, 1968). The expectation value of μ_τ for an ensemble of bona fide cluster members is zero, and μ_v scales with distance and angular separation from the convergent point. We adopt the space motion for the LCC and UCL subgroups from de Bruijne (1999b) (the g_{lim} = 9 solutions in their Table 5, where the space motion vector can be converted to a convergent point solution using eqn. 10 of de Bruijne

[5]In principle, this analysis could have produced an *original* list of pre-MS candidate subgroup members independent of Hoogerwerf's (1999) work. The availability of improved astrometry (namely the Tycho-2 catalog; made publicly available early 2000), and a deeper catalog of X-ray sources (the *Rosat* All-Sky *Faint* Source Catalog ; made publicly available mid-2000), have enabled this analysis.

(1999b)). Low-mass members of the OB subgroups stand out clearly in (μ_v, μ_τ) space (Fig. 2.5). The mean subgroup proper motion values (de Bruijne 1999a; Table 4) are shown as dashed vertical lines, where $\bar{\mu}$ for members is approximately equal to $\bar{\mu}_v$. We define boxes around the loci in Fig. 2.5 to select probable association members for statistical study (70 stars in LCC, 105 in UCL).

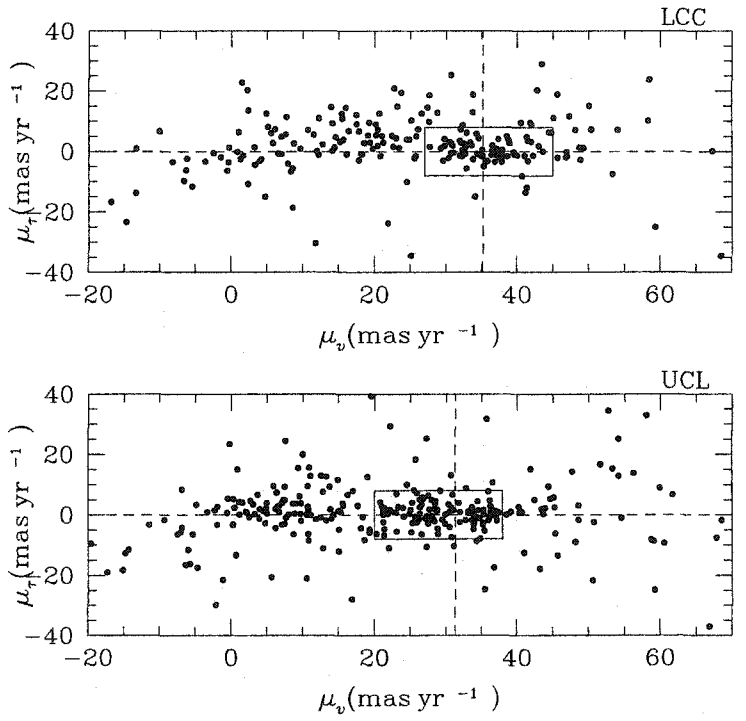

Figure 2.5: Proper motions of RASS-TYC2 stars with $(B-V) > 0.60$, lying within the boundaries of the LCC and UCL OB subgroups defined by de Zeeuw et al. (1999). The mean $\bar{\mu}_v$ values for the OB subgroups are shown by vertical dashed line (from de Bruijne 2000). Association members should have a mean value of $\bar{\mu}_\tau = 0$, with small scatter $\sigma(\mu_\tau)$.

In order to estimate the observed dispersion in μ_τ in a way that is insensitive to the boundaries of the subjectively drawn selection box (Fig. 2.5) and the

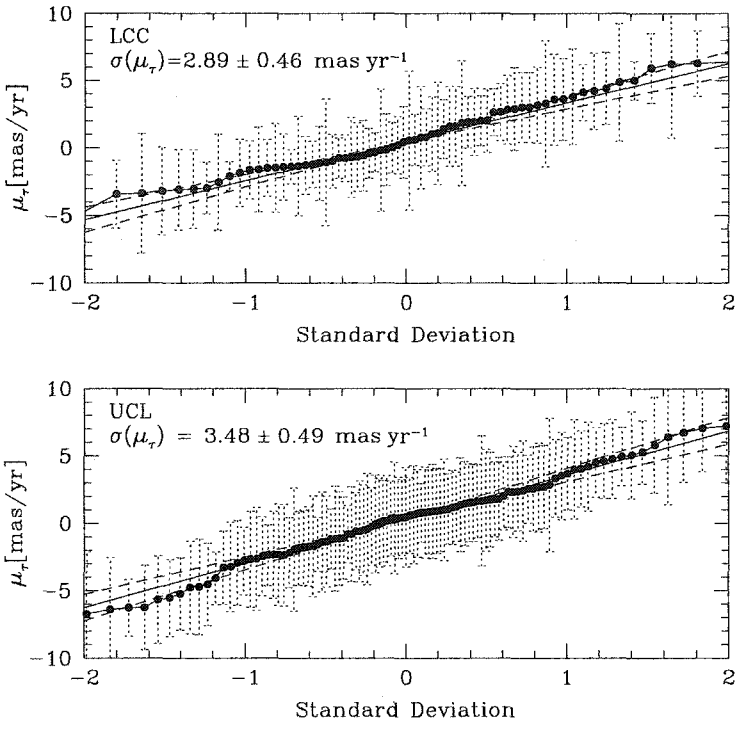

Figure 2.6: Probability plots for μ_τ for stars in the boxes defined in Fig. 2.5. A Gaussian profile will produce a straight line, where the slope gives the standard deviation. The observed distributions are consistent with the Tycho-2 proper motion errors combined with intrinsic velocity dispersions of $0.6^{+0.5}_{-0.6}$ km s^{-1} (LCC) and $1.0^{+0.6}_{-1.0}$ km s^{-1} (UCL).

presense of outliers, we use probability plots (Fig. 2.6). We follow the analysis method outlined in §3 of Lutz & Upgren (1980). In a probability (or "probit") plot, the abscissa is the expected deviation from the mean predicted for the ith sorted data point in units of the standard deviation, and the ordinate is the data value in question (μ_τ). The slope of the probability plot distribution yields the standard deviation, and the y-intercept is the median. To fit a line to the probability plots in Fig. 2.6, we use the Numerical Recipes least-squares routine *fit*, and trim 10% from both sides of the distribution to mitigate against the effects of outliers. The

probability plots yield standard deviations of $\sigma(\mu_\tau) = 2.9 \pm 0.5$ mas yr^{-1} (LCC) and 3.5 ± 0.5 mas yr^{-1} (UCL). The mean values of μ_τ are close to zero (0.7 ± 0.3 mas yr^{-1} for LCC, 0.3 ± 0.3 mas yr^{-1} for UCL), consistent with the expectation that most of the RASS-TYC2 stars in the boxes in Fig. 2.5 are subgroup members.

An upper limit to the velocity dispersions of the low-mass subgroup memberships can be estimated as follows. The observational errors in μ_τ range widely from 1-7 mas yr^{-1} (3.0 ± 0.9 mas yr^{-1}). We use Monte Carlo simulations to estimate the observed scatter expected in μ_τ accounting for both the Tycho-2 proper motion errors and the intrinsic velocity dispersion of the association. The intrinsic velocity dispersion $\sigma^\star_{int}$ (in km s^{-1}) translates into a proper motion dispersion $\sigma(\mu_\tau^{int})$ (in mas yr^{-1}) as a function of mean subgroup parallax π (adapted from de Bruijne (1999) eqn. 20):

$$\sigma(\mu_\tau^{int}) = \pi\, \sigma^\star_{int}/A \tag{2.1}$$

where A = 4.74 km s^{-1} yr^{-1}, the astronomical unit expressed in km divided by the seconds in a Julian year. For the simulations, we model velocity dispersions ranging from $\sigma^\star_{int}$ = 0-3 km s^{-1} in 0.5 km s^{-1} steps. We adopt the mean distances to LCC and UCL from de Zeeuw et al. (1999). We generate 10^4 Gaussian deviates for each star with zero mean and a standard deviation equal to the square root of the observed value of $\sigma(\mu_\tau)$ and the model $\sigma(\mu_\tau^{int})$ values added in quadrature. Statistical testing showed that clipping the Monte Carlo data at the box boundaries in Fig. 2.5 ($|\mu_\tau| < 8$ mas yr^{-1}) had negligible effect on the probability plot determinations of $\sigma(\mu_\tau)$, so all Monte Carlo values were retained.

Table 2.8. Estimates of $\sigma(\mu_\tau)$ from Monte Carlo Simulations and Observations

(1) Sample ...	(2) LCC $\sigma(\mu_\tau)$ (mas yr^{-1})	(3) UCL $\sigma(\mu_\tau)$ (mas yr^{-1})
Observed RASS-TYC2 sample	2.89 ± 0.46	3.48 ± 0.49
Model $\sigma^\star_{int} = 0.0$ km s^{-1}	2.62	3.18
Model $\sigma^\star_{int} = 0.5$ km s^{-1}	2.78	3.27
Model $\sigma^\star_{int} = 1.0$ km s^{-1}	3.24	3.48
Model $\sigma^\star_{int} = 1.5$ km s^{-1}	3.84	3.89
Model $\sigma^\star_{int} = 2.0$ km s^{-1}	4.53	4.35
Model $\sigma^\star_{int} = 2.5$ km s^{-1}	5.30	4.86
Model $\sigma^\star_{int} = 3.0$ km s^{-1}	6.08	5.41

A comparison between the $\sigma(\mu_\tau)$ values for the Monte Carlo simulations and the observations is shown in Table 2.8. It appears that the internal velocity dispersions of the subgroups are indeed detectable. The observed $\sigma(\mu_\tau)$ values for LCC and UCL are consistent with internal velocity dispersions of $\sigma^\star_{int} = 0.6^{+0.5}_{-0.6}$ km s^{-1} and $1.0^{+0.6}_{-1.0}$ km s^{-1}, respectively. The 95% confidence level upper limits to the velocity dispersions are <1.6 km s^{-1} (LCC) and <2.2 km s^{-1} (UCL). We can rule out velocity dispersions of 3 km s^{-1} (de Zeeuw et al. 1999), as this would have produced a dispersion of $\sigma(\mu_\tau) \simeq$ 5-6 mas yr^{-1} in both subgroups.

The velocity dispersions determined from the Monte Carlo simulations are strictly upper limits only. The MML02 survey observed *most* of the stars in the selection boxes in Fig. 2.5, and some of those are known not to be pre-MS members. Interlopers will evenly populate the Fig. 2.5 selection boxes, leading to slightly inflated dispersions in μ_τ, although the use of probability plots largely mitigates against this effect. Taking into account the lack of spectroscopic confirmation of

pre-MS status for all of the RASS-TYC2 candidate members, We conservatively conclude the following: *The intrinsic velocity dispersion $\sigma^{\star}_{int}$ of post-T Tauri stars in the LCC and UCL OB subgroups is $\leq$2 km s^{-1}, and consistent with the value (1 km s^{-1}) measured for the early-type members by de Bruijne (1999b) and Madsen, Dravins, & Lindegren (2002).* Currently, there is no evidence for mass-dependent dynamical evolution. A future radial velocity survey of the subgroup members will enable us to determine whether these unbound associations are expanding, and possibly determine an independent "expansion age" estimate.

2.6.5 Luminosities

With five-band photometry, a temperature / spectral type estimate, and a secular parallax, we calculate stellar luminosities for the pre-MS candidates. We adopt the absolute bolometric magnitude of the Sun ($M_{\rm bol\odot}$ = 4.64) from Schmidt-Kaler (1982). In order to compromise between the uncertainties in luminosity due to reddening, photometric uncertainties, and possible K-band excess, we calculate the $M_{\rm bol}$ using the dereddened 2MASS J magnitude. We estimate the visual extinction from a weighted mean of A_V estimates from the color excess in $(B-V)$and $(V-J)$. We took the E$(B-V)$ formula from Drilling & Landolt (2000) and the value of A_J/A_V(= 0.294) was taken from the near-IR extinction law of Mathis (1990) for a central wavelength 1.22 μm. The reddening A_J typically ranged from 0 to 0.35 mag with formal uncertainties of $\sim$0.1 mag. The typical uncertainty in log L/L$_\odot$ for the pre-MS candidates is $\approx$0.08 dex. With the luminosities and X-ray fluxes from the RASS BSC catalog (Voges et al., 1999), we calculate the ratio of X-ray/bolometric radiation for the stars with X-ray counterparts. The derived values of log(L_X/L_{bol}) are in the range of $10^{-2.8} - 10^{-3.8}$, indicating coronal X-ray emission elevated above most ZAMS G-type stars (e.g.

Pleiads; Stauffer et al., 1994).

2.6.6 Evolutionary Tracks

In order to infer theoretical masses and ages from our pre-MS candidates, we use the evolutionary tracks from D'Antona & Mazzitelli (1997) (DM97; Z = 0.02, x_D = 2×10^{-5}), Siess, Dufour, & Forestini (2000) (SDF00; Z = 0.02), and Palla & Stahler (2001, ; PS01). Ages and masses for a given $\log T_{eff}$ and $\log L/L_\odot$ were calculated using an interpolation algorithm. Given the mean observational errors ($\sigma(\log T_{eff}$, $\log L/L_\odot$) = 0.007, 0.078 dex for LCC Pre-MS stars, and $\sigma(\log T_{eff}$, $\log L/L_\odot$) = 0.009, 0.084 dex among UCL Pre-MS stars), we estimate the isochronal age uncertainties for an individual star to be approximately 4, 5, 7 Myr (DM97, PS01, SDF00) in LCC, and 4, 5, 5 Myr (DM97, PS01, SDF00) in UCL, as illustrated in Fig. 2.7. The uncertainties in the interpolated masses are 0.1 $M_\odot$ for all three sets of tracks. Fig. 2.8 shows the H-R diagram for the pre-MS candidates overlayed with the evolutionary tracks of DM97.

2.7 Results

The ages of the low-mass population of LCC and UCL have not been estimated before, though de Geus et al. (1989) and de Zeeuw & Brand (1985) give main sequence turn-off ages. In §2.7.1 we estimate the pre-MS ages for the two subgroups, and put an upper limit on the intrinsic age spread. In §2.7.2 we calculate new turn-off ages for the subgroups using early B stars from the revised *Hipparcos* membership lists of Z99.

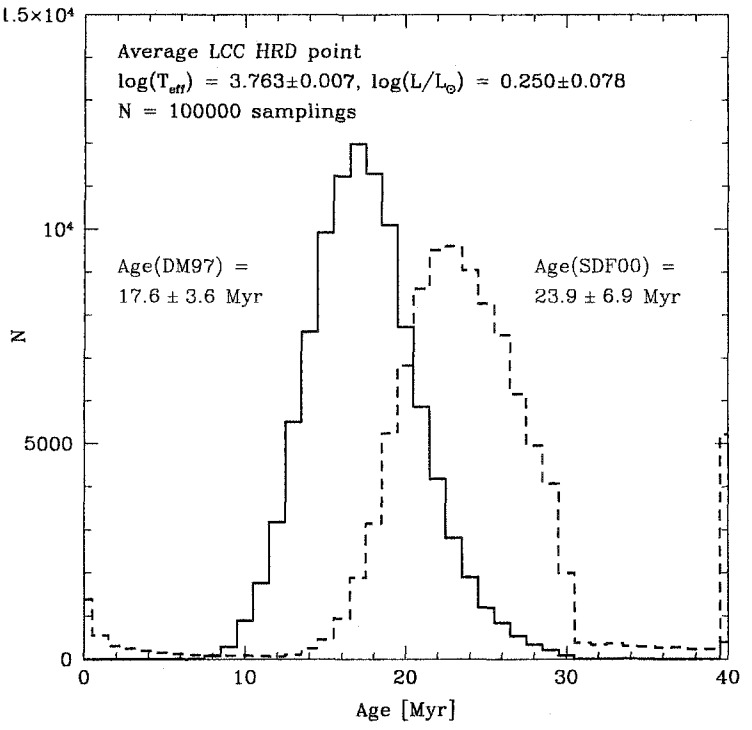

Figure 2.7: A histogram of the inferred ages from the DM97 and SDF00 tracks for a hypothetical LCC Pre-MS star with average H-R diagram point (T_{eff},log L/L$_\odot$) and gaussian uncertainties. The extreme right bin retains all points older than 40 Myr. The standard deviations are calculated using only stars with ages between 1-100 Myr.

2.7.1 Pre-MS Ages and Age Spread

The H-R diagram for our "pre-MS" and "pre-MS?" stars is shown in Fig. 2.8, overlayed with the evolutionary tracks of D'Antona & Mazzitelli (1997). The temperatures and luminosities of the pre-MS stars are given in Columns 9 and 10 of Tables 2.6 and 2.5, along with their inferred masses and ages (columns 15 through 17). One notices immediately that the bulk of isochronal ages are in the range of ~10-20 Myr. The age range is nearly identical for both groups. To assess the effects of our magnitude limit in biasing our mean age estimates, in Fig. 2.9 we

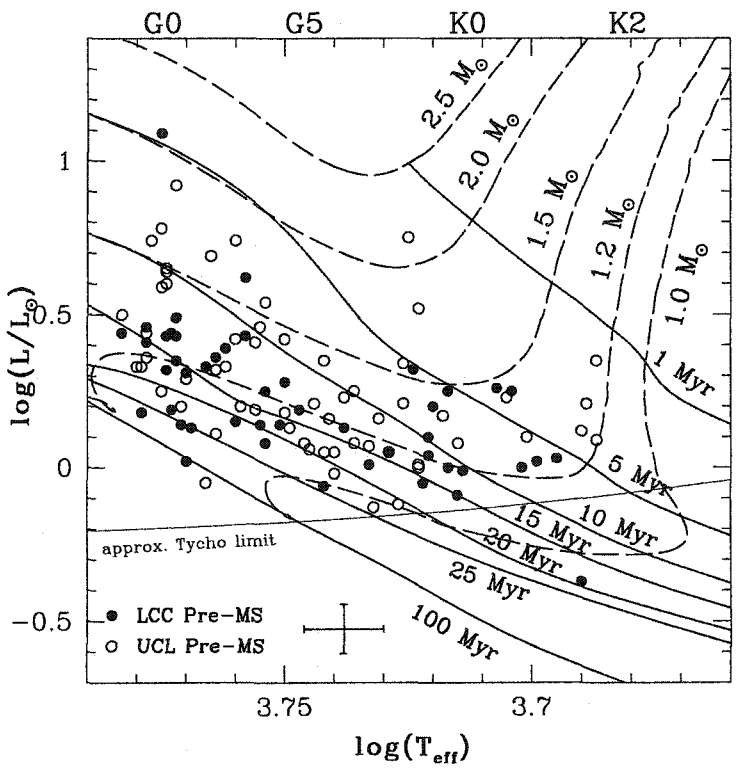

Figure 2.8: Theoretical H-R diagram for stars identified as Pre-MS or Pre-MS? in Tables 2.5 and 2.6 in the UCL (open circles) and LCC samples (filled circles). The pre-MS evolutionary tracks of DM97 are overlayed. The ACT/TRC magnitude limit (V = 11 mag) is shown for a distance of 150 pc (A_V = 0.3 assumed). The star in the bottom right corner (TYC 8648-446-1) is one of the faintest stars in our sample (V = 11.2 mag) with larger than average errors in $\log L/L_\odot$ - hence its unusual position. The average 1σ error bars in $\log T_{eff}$ and $\log L/L_\odot$ are shown.

plot the mean pre-MS age (with standard errors of the mean) for the pre-MS subgroup samples as a function of minimum $\log T_{eff}$ cut-off. The magnitude bias of our survey is clearly apparent: the mean age systematically decreases when stars with $\log T_{eff} < 3.73$ are included in the calculation. In calculating the pre-MS ages of the OB subgroups, we explicitly omit the pre-MS stars with $\log T_{eff} < 3.73$ (30% of our sample). This temperature threshold intersects our magnitude

limits at ages of ~25 Myr for stars of 1 $M_{\odot}$ on the DM97 tracks. That the lines in Fig. 2.9 are nearly flat for $\log T_{eff} > 3.73$, suggests that (detectable) stars with ages of >25 Myr are not a significant component of either subgroup (also see discussion in §2.8.1).

Fig. 2.10 displays histograms of the isochronal ages for the pre-MS stars in the LCC and UCL subgroups derived using DM97 and SDF00 evolutionary tracks. These tracks represent the extrema in age estimates for our sample (DM97 is youngest, SDF00 is oldest). The 1σ age dispersion among the unbiased samples ($\log T_{eff} > 3.73$) is 5-9 Myr for both groups. If we remove the known spectroscopic binaries (see notes in Tables 2.6 and 2.5), the age dispersions are 4-8 Myr. Because there may be additional unresolved binaries, this *observed* age spread places an upper limit on the *intrinsic* age spread. As illustrated in Fig. 2.7, the individual H-R diagram positions of the pre-MS samples have $\log T_{eff}$ and $\log L/L_{\odot}$ errors which fold onto the evolutionary tracks with age uncertainties of 4-7 Myr. From this analysis, we conclude that the *intrinsic* 1σ age dispersions in each subgroup must be less than 2-8 Myr (i.e. ~2/3rds of the star-formation took place in <4-16 Myr). Using the DM97 pre-MS ages, which agree best with the turn-off age estimates (§2.7.2), we find intrinsic 1σ age dispersions of 2 Myr (LCC) and 3 Myr (UCL).*This implies that 68% of the low-mass star-formation took place within <4-6 Myr, and 95% within <8-12 Myr in the OB subgroups.* Our observational uncertainties and lack of knowledge about the unseen binarity of the pre-MS sample stars do not allow us to constrain the age spread more precisely than this. The mean age estimates for our unbiased pre-MS samples ($\log T_{eff}$> 3.73, SBs removed) are shown in Table 2.9. Counter to previous studies, we find that LCC is slightly older than UCL by 1-2 Myr (at 1-3σ significance), indepen-

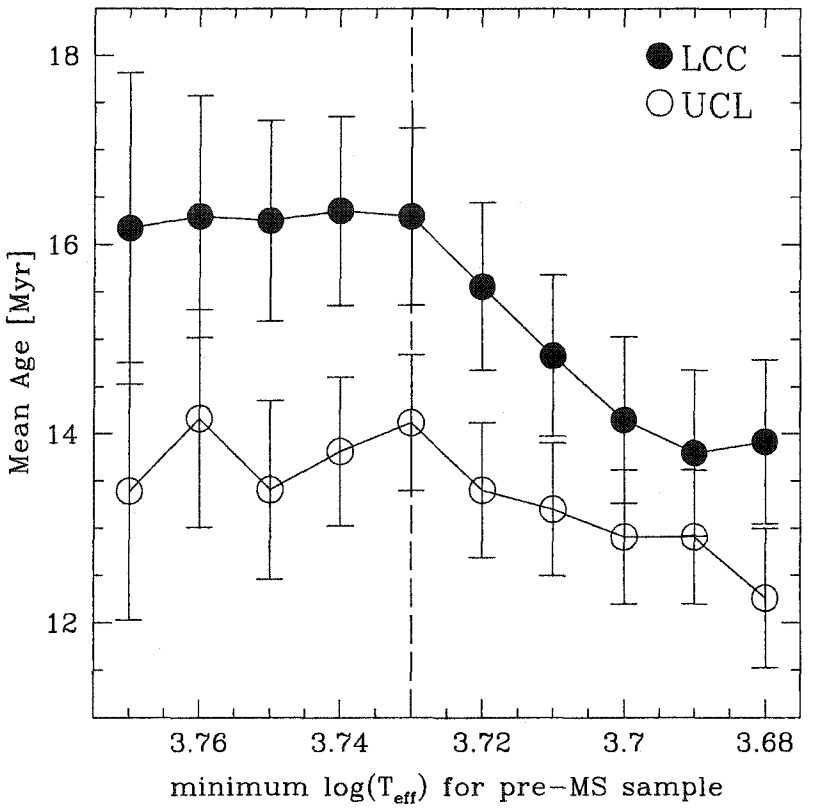

Figure 2.9: Illustration of the effects of magnitude bias on our mean age estimates for the pre-MS populations. The abscissa is the minimum $\log(T_{eff})$ threshold for evaluating the mean sample ages (using DM97 tracks). The ordinate is calculated mean age with standard errors of the mean (shown; typically $\approx$1 Myr). At cooler temperatures (later than K0), the magnitude limit of our survey biases the sample towards more luminous stars, thereby decreasing the mean age estimate. From this diagram, we choose $\log T_{eff} = 3.73$ (vertical dashed line) as the lower T_{eff} cut-off for evaluating the mean pre-MS ages. Known spectroscopic binaries are included here, but excluded in the final age estimates presented in Table 8. The *observed* isochronal ages and spread are 16 ± 5 Myr for LCC and 14 ± 5 Myr for UCL.

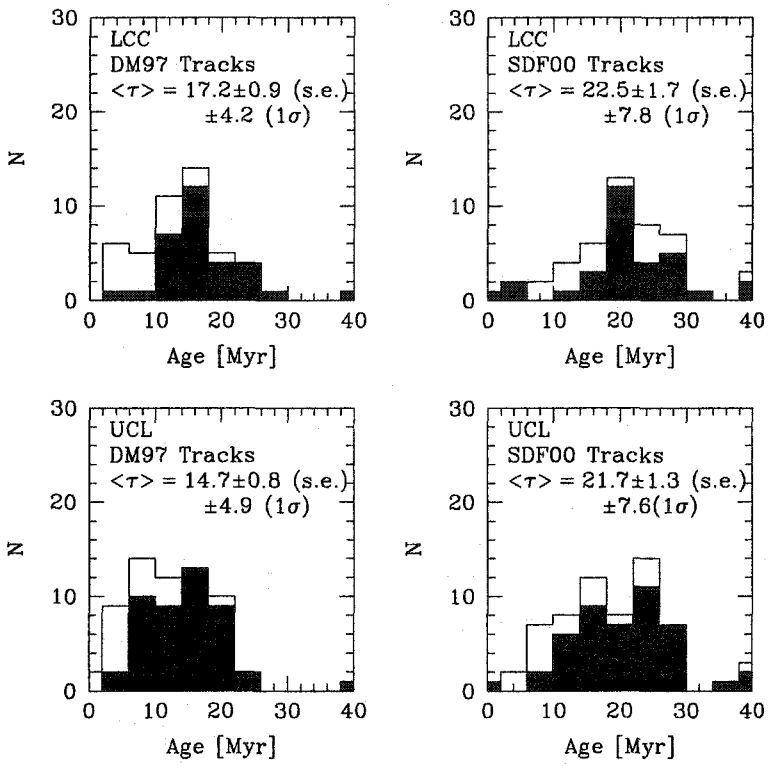

Figure 2.10: Histograms of the isochronal ages for pre-MS and "pre-MS?" candidates in Tables 2.5 and 2.6 from the models of DM97 and SDF00. The filled bins are for stars with $\log T_{eff} > 3.73$, and the unfilled bins are for the entire (magnitude-biased) sample. Mean isochronal ages (with standard errors of the means and 1σ uncertainties) are given for the unbiased sample ($\log T_{eff} > 3.73$). Outliers with isochronal ages of >40 Myr are counted within the 40 Myr bin.

dent of which evolutionary tracks we use. From Fig. 2.10, we also conclude that star-formation ceased approximately ~5-10 Myr ago in the subgroups.

2.7.2 Turn-off Ages

De Geus et al. (1989) published the most recent age estimates for the LCC and UCL groups, but in light of the new *Hipparcos* distances and subgroup member-

Table 2.9. Age Estimates of LCC & UCL

Ref.	Tracks	method	age(LCC) (Myr)	age(UCL) (Myr)
1	4	pre-MS	17 ± 1	15 ± 1
1	5	pre-MS	21 ± 2	19 ± 1
1	6	pre-MS	23 ± 2	22 ± 1
1	7	turn-off	16 ± 1	17 ± 1
2	8	turn-off	11-12	14-15
3	8,9	turn-off	10-11	12-13

Note. — Uncertainties are standard errors of the mean. Pre-MS age estimates exclude known SBs and stars with $\log T_{eff} < 3.73$, which bias the calculated ages. The turn-off ages from this work are determined using only early-B stars classified as members by de Zeeuw et al. (1999).

References. — (1) this work, (2) de Geus et al. (1989), (3) de Zeeuw & Brand (1985), (4) D'Antona & Mazzitelli (1997), (5) Palla & Stahler (2001), (6) Siess, Dufour, & Forestini (2000), (7) Bertelli et al. (1994), (8) Maeder (1981), (9) Cogan (priv. comm.)

ship lists, we feel it is worthwhile reevaluating the subgroups' turn-off ages. We construct a theoretical H-R diagram for the B-type subgroup members of UCL and LCC listed both in Table C1 of Z99 and Tables A2 and A3 of de Bruijne (1999b). Several of the "classical" [6] members rejected as members by *Hipparcos* from Z99 are included as well. For input data, we use the following databases in order of availability: (1) $ubvy\beta$ photometry from the database of Hauck & Mermilliod (1997), (2) UBV photometry from Slawson, Hill, & Landstreet (1992), and (3) UBV photometry from SIMBAD. For distances we use the secular parallaxes (π_{sec}) given in column 4 of Tables A2 and A3 of de Bruijne (1999b) when available, or the *Hipparcos* parallaxes (π_{HIP}). We deredden the stars with $ubvy\beta$ photometry to the B-star sequence of Crawford (1978) using the prescription of Shobbrook (1983). For stars with Stromgren photometry, we calculate T_{eff} using the temperature relation of Napiwotzki, Schönberner, & Wenske (1993). If no $ubvy\beta$ photometry was available, we use UBV photometry to calculate the reddening-free index Q (Crawford & Mandwewala , 1976) to infer the star's unreddened color. A polynomial fit to Table 15.7 from Drilling & Landolt (2000) is used to calculate T_{eff} as a function of $(B-V)_\circ$. The BC versus T_{eff} relation of Balona (1994) is used for all stars. We linearly interpolate between the isochrones from Bertelli et al. (1994) (Y = 0.28, Z = 0.02, convective overshoot) to infer ages for the subgroup B stars. The theoretical H-R diagram is shown in Fig. 2.11.

UCL has a well-defined MS turn-off composed of the *Hipparcos* members HIP 67464 (ν Cen; B2IV), HIP 68245 (ϕ Cen; B2IV), HIP 68282 (ν^1 Cen; B2IV-V), HIP 71860 (α Lup; B1.5III), HIP 75141 (δ Lup; B1.5IV), HIP 78384 (η Lup; B2.5IV), and HIP 82545 (μ^2 Sco; B2IV), as well as "classical" members (but *Hipparcos* non-

[6] "Classical" members are early-type stars which were included in Sco-Cen membership lists before the *Hipparcos* studies of Z99.

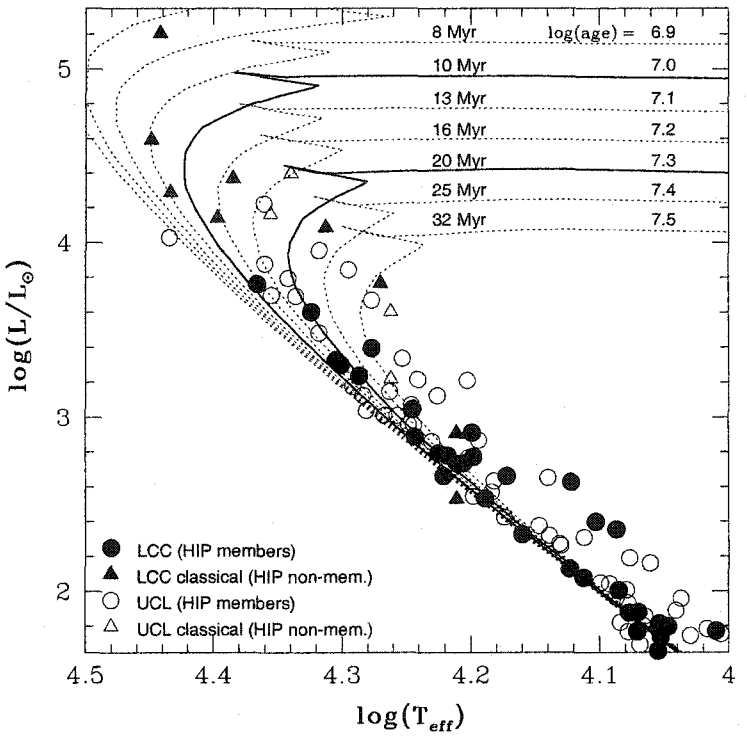

Figure 2.11: Theoretical H-R diagram for the B-star candidate members of the LCC & UCL memberships using the evolutionary tracks of Bertelli et al. (1994). Only the most massive *Hipparcos* members were included in the age estimates. The unusual variable HIP 67472 (μ Cen; B2Vnpe; $\log L/L_{\odot}$, $\log T_{eff}$ = 4.43, 4.0) was excluded from the UCL turn-off age estimate.

members) HIP 82514 (μ_1 Sco; B1.5Vp) and 73273 (β Lup; B2III)[7]. The variable star HIP 67472 (μ Cen; B2Vnpe) was excluded. Using the Bertelli et al. (1994) tracks, the mean age of the 7 turn-off *Hipparcos* members is 17 ± 1 Myr. Including the two "classical" members has negligible effect on the mean age estimate. Our MS turn-off age estimate for UCL is slightly older than de Geus et al.'s (14-15 Myr), and is close to the mean pre-MS ages that we found in §2.7.1 (15-22 Myr).

[7]Note that the two *Hipparcos* non-members were found to be probable members by Hoogerwerf (2000) if the long-baseline ACT (HIP 73273) and TRC (HIP 82514) proper motions were used instead of the *Hipparcos* values.

LCC lacks a well-defined turn-off, however we have enough early-B stars in the middle of their MS phase with which to make an age estimate. We estimate the age for LCC from the following main sequence B stars: HIP 59747 (δ Cru; B2IV), HIP 60823 (σ Cen; B2V), HIP 61585 (α Mus; B2IV-V), HIP 63003 (μ^1 Cru; B2IV-V), and HIP 64004 (ξ^2 Cen; B1.5V). The mean age for these five stars is 16 ± 1 Myr; similar to what we found for UCL, and it agrees well with the younger end of our pre-MS age estimates (17-23 Myr). This age estimate is significantly older than previous estimates (10-12 Myr), and warrants more critical examination (§2.8.3).

The new results yielded by our age analysis of the OB subgroups are: (1) two-thirds of the low-mass star-formation in each subgroup took place in less than a $\sim$5 Myr span (and 95% took place within $\sim$10 Myr), (2) the pre-MS and B-star ages for LCC and UCL are in approximate agreement, (3) the B-star subgroup memberships defined by *Hipparcos* have ages of 16 ± 1 Myr and 17 ± 1 Myr for LCC and UCL, respectively. We discuss the implications of these results in §2.8.

2.7.3 The Census of Accretion Disks

An important question both for star and planet formation is the lifetime of accretion disks around young stars. Statistics for the frequency of active accretion disks around low-mass stars come predominantly from near-IR surveys of young associations and clusters (Hillenbrand & Meyer, 1999; Haisch, Lada, & Lada, 2001a). The samples of low-mass stars surveyed are dominated by embedded associations with ages of <3 Myr (e.g. Tau-Aur, Cha I, etc.), and older open clusters with ages of 30-100 Myr (e.g. Pleiades, IC 2602, α Per, etc.). Few well-studied

pre-MS stars of 3-30 Myr-old ages have been surveyed. The situation has recently been slightly ameliorated by the discoveries of the TW Hya association and η Cha cluster (Kastner et al., 1997; Webb et al., 1999; Mamajek, Lawson, & Feigelson, 1999). Yet these samples are small (~10-20 stars) and dominated by K and M-type stars with masses of 0.1-0.8 $M_{\odot}$. Our pre-MS star sample is unique in its mass (~1-1.5 $M_{\odot}$) and age range (~10-20 Myr), so measuring its disk-frequency provides a valuable datum.

Stars with EW(Hα) > 10Å in emission are usually called Classical T Tauri stars (CTTSs), which show spectroscopic signatures of accretion as well as near-IR excesses (e.g. Hartigan, Edwards, & Ghandour, 1995). Stars lacking the strong Hα emission and near-IR excesses are called Weak-lined T Tauri stars (WTTSs). This can be explained as a correlation between the presence of magnetospheric accretion columns and an inner accretion disk (e.g. Meyer, Calvet, & Hillenbrand, 1997; Muzerolle, Hartmann, & Calvet, 1998). Our Hα EW measurements are discussed in §2.4.2.1, and here we quantify the K-band excess of our targets. We calculate the intrinsic $(J-K_s)$ color excess $E(J-K_s)_\circ$ as defined by Meyer, Calvet, & Hillenbrand (1997):

$$E(J-K)_\circ = (J-K)_{obs} - (J-K)_\circ - A_V \times (A_J - A_K) \qquad (2.2)$$

where $(J-K_s)_{obs}$ is the observed color and $(J-K_s)_\circ$ is the intrinsic color of an unreddened dwarf star of appropriate spectral type (Kenyon & Hartmann, 1995). Uncertainties in each quantity were propagated in order to estimate the signal-to-noise of the intrinsic color excess. The distribution of measured $E(J-K_s)_\circ$ values indicate a systematic offset of a few hundredths of a mag. We subtract the small

offset, with the result being that the distribution of $E(J-K_s)_\circ$ values is symmetric about zero, with a few positive and negative $\sim 2\sigma$ points. There is only one star with a $E(J-K_s)_\circ$ color excess with S/N > 2.5: star #34 = TYC 9246-971-1 has an intrinsic color excess of $E(J-K_s)_\circ = 0.26 \pm 0.06$ implying a K-band excess. This star also happens to be the only CTT identified in our optical spectra (EW(Hα) = -39 Å). TYC 9246-971-1 (= PDS 66, Hen 3-892) was originally identified as an emission line star by Henize (1976), and classified as a CTT in the Pico dos Dias survey of stars in the IRAS PSC catalog (Gregorio-Hetem et al., 1992). By virtue of its position, proper motion, and spectral characteristics, we find that TYC 9246-971-1 is a $\approx$8 Myr-old, $\approx 1.2\,M_\odot$ (DM97 tracks) member of the LCC subgroup. Our secular parallax for TYC 9246-971-1 yields a distance of 86^{+8}_{-7} pc; the third nearest of the LCC pre-MS stars in our sample, and among the nearest CTTSs known. Only 1/58 ($1.7^{+4.0}_{-1.4}$%; 1σ Poisson) of pre-MS stars in LCC are classified as bona fide CTTS, along with none (0/42) of the pre-MS members of UCL. For our accretion disk frequency statistics, we use the isochronal ages derived from the DM97 evolutionary tracks (which agree well with the turn-off ages), and include the entire sample of 110 pre-MS stars (including the cooler stars which bias the mean to younger ages). Only 1/110 ($0.9^{+2.1}_{-0.8}$%; 1σ) of $1.3 \pm 0.2\,(1\sigma)\,M_\odot$ stars with ages of 13 ± 1 (s.e.) $\pm 6\,(1\sigma)$ Myr are CTTSs. This implies that accretion terminates in solar-type stars within the first 15 Myr of their evolution.

2.7.4 Is There a Sco-Cen OB Subgroup in Chamaeleon?

A recent study (Sartori, Lépine, & Dias, 2003, hereafter SLD03) proposed that another, previously undiscovered, and nearby, OB subgroup lay just to the south of LCC in Chamaeleon. If the subgroup were real, the putative association could possibly add a significant new piece to the puzzle of the star-formation history of

the Sco-Cen region.

SLD03 presented a membership list of 21 B stars in the Chamaeleon region that they claim constitute a new OB subgroup of Sco-Cen (§2.3 and Table 5 of their paper). The putative Cha OB members were selected solely by distance (120-220 pc) and projected proximity to the Chamaeleon molecular clouds. We present two observations which demonstrate that either the Cha subgroup membership list of SLD03 is severely contaminated by field stars, or that the group doesn't exist.

SLD03 measured a velocity dispersion for their Cha B-star sample of (σ_U, σ_V, σ_W) = (8, 11, 6) km s^{-1}. Observations of nearby OB associations show that their velocity dispersions are small – typically $\leq$1 km s^{-1} (de Bruijne, 1999b; Madsen, Dravins, & Lindegren, 2002). Torra, Fernández, & Figueras (2000) find that young (<100 Myr-old), nearby (d = 100-600 pc) field OB stars *distributed all over the sky* have a velocity dispersion of (σ_U, σ_V, σ_W) $\simeq$ (8, 9, 5) km s^{-1}. This is similar to the velocity dispersion for the Cha B stars, and suggests that *if* the sample contains a bona fide OB association, it is probably severely contaminated by field B stars.

There is also a discrepancy in the numbers of Cha OB members versus non-members in the Chamaeleon region. If one searches the *Hipparcos* catalog for B stars in the 180 deg^2 region surveyed for Chamaeleon *ROSAT* T Tauri stars by Alcalá et al. (1995), constrained to distances between 120-220 pc, one finds that all 12 B stars within these constraints are considered Cha OB members by SLD03. How many non-member field B-type stars would one expect? The projected density of

Hipparcos B stars with distances of 120-220 pc at Galactic latitude –18° is ~0.057 deg^{-2} (calculated in a 10°-wide band centered on b = –18°, covering all Galactic longitudes). Over the 180 deg^2 Cha region defined by Alcalá et al. (1995), one expects to find $10 \pm \sqrt{10}$ B-type field stars. One finds 12, consistent with the density of field B-stars, and within the Poisson error bar. It is difficult to accept that all 12 B-type *Hipparcos* stars in this region are members of a new OB association, when 10 B-type field stars are predicted to exist. These numbers also suggest that there is not a statistically significant over-density of B stars in the Chamaeleon region. Along with the high velocity dispersion of the putative Cha OB membership list, the evidence presented here suggests that there is no kinematic OB subgroup in Chamaeleon, associated with Sco-Cen.

2.8 Discussion

We can address several interesting questions regarding the star-formation history of Sco-Cen with data from our survey. Could the Sco-Cen progenitor giant molecular cloud (GMC) have produced a substantial population of low-mass stars for an extended period (>5-10 Myr) *before* conditions were right to form an OB population? Conversely, is there evidence for any low-mass star-formation *after* the bulk of the high-mass OB stars formed? The OB star-formation in LCC and UCL has apparently destroyed the progenitor GMC through supernovae and stellar winds (e.g. de Geus, 1992; Preibisch & Zinnecker, 2000). However the region is not totally devoid of molecular gas (e.g. the Lupus complex). We will first examine whether there is any evidence of star-formation prior to the formation of the OB subgroups (§2.8.1), and then assess the evidence for more recent star-formation in the UCL region (§2.8.2). We will address the age of LCC in §2.8.3,

and discuss the formation of the subgroups in §2.8.4. Throughout the discussion, we adopt the DM97 ages, as they agree more closely with the turn-off ages than do the SDF00 and PS01 ages.

2.8.1 Is There Evidence for Star-Formation Before the Primary Bursts?

Is our survey sensitive to older stars which may have preceded the primary star-formation episode? Three pre-MS stars in our sample have isochronal ages of >25 Myr (or undefined as lying below the ZAMS), however given the uncertainties in T_{eff} and $\log L/L_{\odot}$ (Fig. 2.7), even a coeval ≈15 Myr-old population would be expected to have *statistical* outliers. Here we explore three possible ways in which older ZAMS stars could have escaped our attention.

One could argue that our surface gravity indicator is biasing our sample against identifying ZAMS stars members (if they exist). If we disregard surface gravity as a criterion, we gain only 4 more RASS-ACT/TRC stars (all between F8.5 and G1), and only *one* of those would have an isochronal age > 25 Myr (TYC 8222-105-1; ∼30 Myr). If they were legitimate, older members with real ages of > 25 Myr, they should also be among the stars with the oldest *isochronal ages* in our sample, which they are not. This suggests that their secular parallaxes, hence their luminosities, are unjustified, and that they are not members of the OB subgroups. Coincidently, TYC 8222-105-1 is one of the earliest type stars in our sample (F8.5), where our surface gravity indicator has the least fidelity (Fig. 2.1). We can state that only *one* of the Li-rich stars showing dwarf gravity signatures that is co-moving with LCC and UCL has an H-R diagram position *and* gravity suggestive of ZAMS status.

If a significant ZAMS population existed in LCC and UCL, would our magnitude and X-ray flux limits allowed their detection? X-ray surveys of the ZAMS-age clusters IC 2602 and IC 2391 (~30-50 Myr) by Randich et al. (1995) and Patten & Simon (1996) found that late-F and early-G stars ZAMS stars have X-ray luminosities of $L_X \simeq 10^{29.0} - 10^{30.5}$ erg s^{-1}, with L_X/L_{bol} ranging from $10^{-3.0}$ to $10^{-4.8}$. The X-ray and optical flux limits imposed by the *ROSAT* All-Sky Survey and the Tycho catalog allow us to detect ZAMS sources with $L_X/L_{bol} > 10^{-3.2}$ within 140 pc if they exist. If we adopt the X-ray luminosities of the G stars in IC 2602 and IC 2391 as representative for a ~30 Myr-old population, we should have detected roughly one-third of a putative Sco-Cen ZAMS population between masses of 1 and 1.2 $M_\odot$. We can put a rough upper limit on the number of >25 Myr-old stars in our mass range. Assuming that TYC 8222-105-1 *is* a ZAMS member, and that its H-R diagram position is not a statistical fluctuation from the locus of ~15 Myr-old stars, we detect one ZAMS star with age >25 Myr in the mass range (1-1.2 $M_\odot$). Accounting for the two-thirds of the ZAMS stars which would have undetectable X-ray emission, and extrapolating over a Kroupa (2001) IMF, this implies a population of ~100 stars with masses greater than 0.1 $M_\odot$. This is ≤10% of the stellar population predicted to exist in each OB subgroup (~1000-2000; §2.5.3).

Could such ZAMS stars have left the region we probed? If we postulate that the population was very centrally concentrated and gravitationally bound until the OB stars destroyed the giant molecular cloud (GMC) some ~10 Myr ago (de Geus, 1992), then a 2 km s^{-1} motion radially away from the subgroup center would have moved the star 20 pc in the past 10 Myr. This distance is the approximate radius of both of the subgroups today (see Fig. 9 of Z99). Hence

if an older population was concentrated at center of the gravitationally-bound GMC until the high mass stars destroyed the cloud, we would find them within the projected boundaries of the subgroups so long as they inherited velocities of <2 km s^{-1}. The kinematic selection procedure of Hoogerwerf (2000) would have selected such stars, since a large velocity dispersion (3 km s^{-1}) was initially assumed.

We conclude that there is no evidence for significant star-formation in the LCC and UCL progenitor giant molecular clouds before the primary star-formation episodes. Our findings are consistent with the idea that molecular clouds form stars over a wide range of masses, and dissipate within timescales of $\sim$10 Myr.

2.8.2 On-going Star-Formation?

Two obvious sources of young stars may be contaminating the UCL pre-MS sample. The youngest, unembedded OB subgroup of Sco-Cen is Upper Sco (US), with a nuclear age of 5-6 Myr (de Geus et al., 1989). US borders UCL near Galactic longitude 343°, and its space motion and distance are very similar to that of UCL (Z99). The Lupus molecular clouds are also in the western region of UCL (roughly between $335° < \ell < 345°$ and $+5° < b < 25°$). The T Tauri star population within the major Lupus clouds was surveyed by Hughes et al. (1994), and the region was recently mapped in ^{12}CO by Tachihara et al. (2002). Dozens of pre-main sequence stars were identified outside of the main cores by a pointed *ROSAT* survey (Krautter et al., 1997), and the All-Sky Survey (Wichmann et al., 1997b). The clouds lie at d = 140 pc (Hughes, Hartigan, & Clampitt, 1993), situated spatially between the US and UCL subgroups of Sco-Cen (both $d \simeq 145$ pc). Fig. 2.12 illustrates the positions of the primary Lupus clouds, the pre-*ROSAT* Lupus T Tauri

star population, the pre-MS stars from our survey, and the B-star population of the OB subgroups.

How does the presence of US and the Lupus molecular clouds (and their associated T Tauri stars) affect our findings regarding the mean age of the UCL subgroup? We split our unbiased ($\log T_{eff} > 3.73$) "pre-MS" and "pre-MS?" members of UCL into two groups using the Galactic longitude line 335° as a division. Most of the molecular cloud mass in the Lupus region lies between $335° < \ell < 345°$ (see Fig. 2 of Tachihara et al. (2002)). Using the DM97 tracks, we find that the "eastern" UCL pre-MS sample surrounding the Lupus clouds has a mean age of 13 ± 1 Myr, while the "western" UCL sample is somewhat older (16 ± 1 Myr). The UCL stars with ages of <10 Myr are found in greater numbers near the Lupus clouds and US border, supporting the idea that our UCL sample is probably contaminated by more recent star-formation. The age estimate of UCL for the stars west of $\ell = 335°$ is probably more representative of the underlying UCL population.

Three of the youngest stars (HIP 81380, TYC 7858-830-1, and TYC 7871-1282-1; 5-9 Myr; DM97 tracks) in our entire survey are positioned near a clump of 8 B stars at (ℓ, b) = (343°, +4°). These three pre-MS stars also have secular parallax distances of ~200 pc, similar to what de Bruijne (1999b) found for the group of B stars. The secular parallaxes may be biased, however, if this clump has slightly different kinematics than the average UCL motion. This clump may represent substructure within UCL. However de Bruijne (1999b) was unable to demonstrate that the clump had distinct kinematics or age. The mean *Hipparcos* distance of the clump B stars is 175 pc, with HIP 82514 (μ^1 Sco; B1.5Vp) and HIP 82545 (μ^2 Sco;

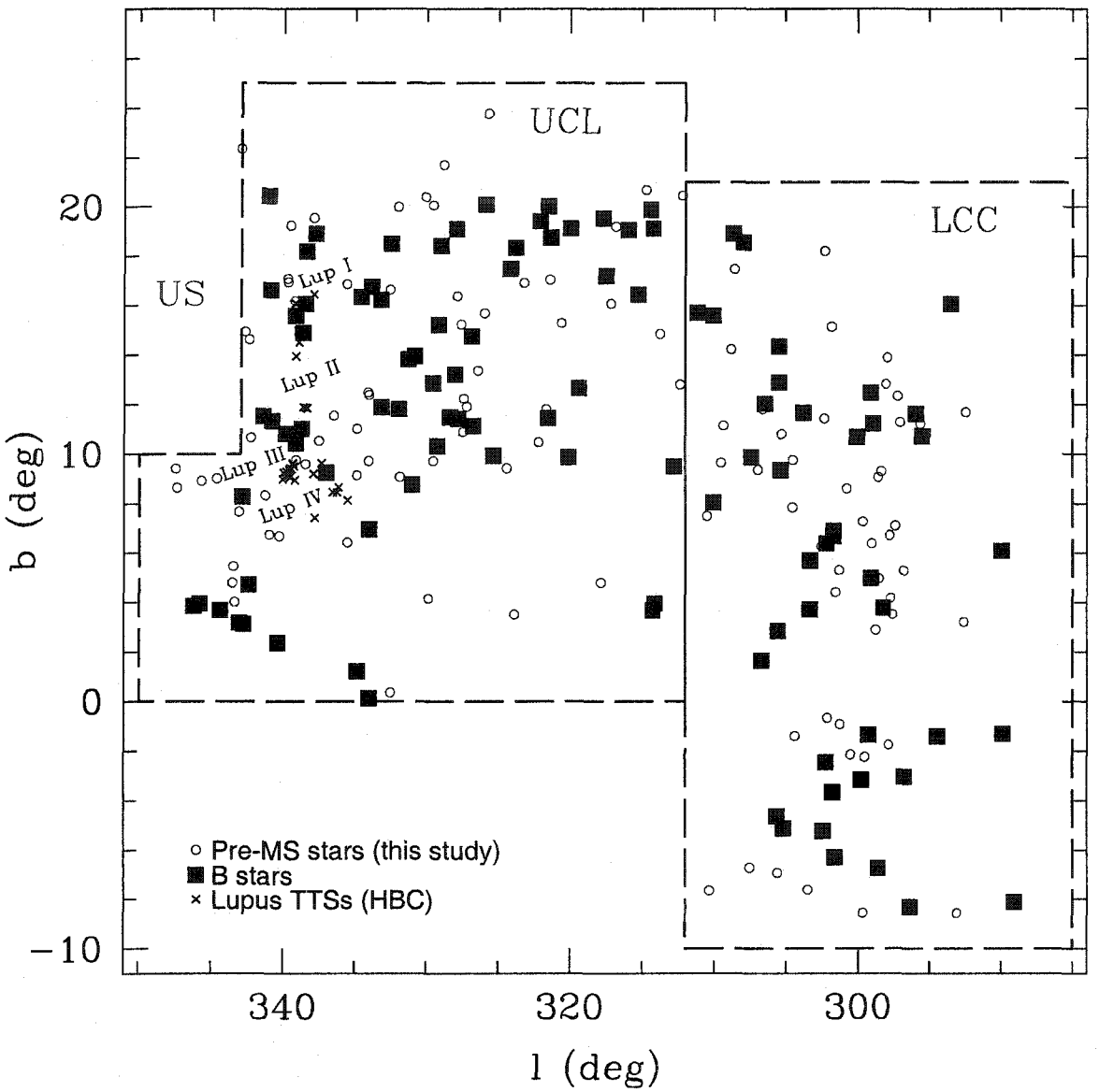

Figure 2.12: Map of the UCL and LCC subgroups of the Sco-Cen OB association (Sco OB2). The B-star population from de Zeeuw et al. (1999) is shown by filled squares. The pre-MS (and pre-MS?) sample from this survey is shown as open circles. Pre-*ROSAT* T Tauri stars in the HBC catalog associated with the Lupus cloud are shown as Xs (Herbig & Bell, 1988).

B2IV) as the most massive members. Our identification of 3 new pre-MS stars in the same region with similar secular parallaxes supports the notion that this may be a separate subgroup.

Some of our pre-MS stars were also identified in the *ROSAT* surveys of the Lupus region by Krautter et al. (1997) and Wichmann et al. (1997b) (see notes in Table 2.6). The presense of a significant population of pre-MS stars outside of star-forming molecular clouds has been attributed by various authors to be due to one or more of the following: (1) slow diffusion (1-2 $\mathrm{km\,s^{-1}}$) from existing molecular clouds (e.g. Wichmann et al., 1997a), (2) ejection from small-N body interactions (Sterzik & Durisen, 1995), (3) formation *in situ* from short-lived cloudlets (Feigelson, 1996), or (4) fossil star-formation associated with the Gould Belt (e.g. Guillout et al., 1998). Wichmann convincingly showed that most of the young RASS stars in the Lupus region are at a distance of around $\sim$150 pc (similar to previously published distances for the Lupus clouds and UCL), and that the stars are roughly 10 Myr-old. Wichmann concludes that the dispersed pre-MS population is most likely a manifestation of the Gould Belt. The OB subgroups of Sco-Cen are major sub-structures of the Gould Belt (as defined by age and kinematics; Frogel & Stothers, 1977), i.e. UCL is the dominant Gould Belt substructure in the Lupus region. We interpret the presence of dozens of pre-MS stars near the Lupus clouds to be primarily the low-mass membership of the UCL OB subgroup. Our analysis suggests that younger US or Lupus stars are a minor contaminant to our UCL sample.

2.8.3 Is LCC Older than UCL?

Although our pre-MS and turn-off age estimates for LCC agree rather well, they are substantially older (by ~50%) than previous values. The de Geus et al. (1989) age estimate (11-12 Myr) appears to hinge primarily on the H-R diagram position of ϵ Cen, with δ Cru, α Mus, and ξ^2 Cen defining the rest of the turn-off isochrone. The latter three stars were confirmed as members by Z99, however ϵ Cen (the most massive) was rejected. Although our age for ϵ Cen is consistent with de Geus's, we omitted it from our LCC age estimate. If one uses the long-baseline proper motion for ϵ Cen from the new Proper Motions of Fundamental Stars (PMFS) catalog (Gontcharov et al., 2001), and adopt the LCC space motion, convergent point, and formulae of Z99 (with $v_{int} = 3\,\mathrm{km\,s^{-1}}$), ϵ Cen has a 100% membership probability. The resulting secular parallax ($\pi_{sec} = 9.6 \pm 2.0$ mas) agrees well with the *Hipparcos* astrometric parallax ($\pi_{HIP} = 8.7 \pm 0.8$ mas), further strengthening the interpretation that ϵ Cen is a bona fide LCC member. Including ϵ Cen with the other 5 turn-off stars discussed in §2.7.2 does not change our turn-off age estimate, however (16 ± 1 Myr). If one ignores the stars with masses less than that of ϵ Cen, then the 12-Myr Bertelli isochrone would appear to be an acceptable fit for LCC. Because the turn-off is poorly defined, we give equal weight to the next five *Hipparcos* members down the mass spectrum (δ Cru, σ Cen, α Mus, μ^1 Cru, and ξ^2 Cen), which yields an age older than de Geus's.

ϵ Cen is one of several "classical" LCC early B-type member candidates rejected as members of Sco-Cen using the *Hipparcos* astrometry. These stars have been included in Sco-Cen candidate membership lists on and off over the past half-century: HIP 59196 (δ Cen; B2IVne), HIP 60718A (α^1 Cru A; B0.5IV), HIP 62434 (β Cru; B0.5IV), and HIP 68702 (β Cen; B1III). These stars are ~10-20 $M_\odot$

star, with inferred ages of ~5-15 Myr, and distances of ~100-150 pc. Such stars are extremely rare, and their presense in the LCC region appears to be more than coincidental. Are they all LCC members whose *Hipparcos* proper motions are perturbed due to binarity? *All* five systems are flagged (field #59) in the *Hipparcos* catalog as stars with unusual motions due to either unseen companions or variability. A kinematic investigation of these stars, and their potential membership in LCC is beyond the scope of this study, but necessary for understanding the global star-formation history of the Sco-Cen region. Are these stars bona fide members? If so, why are they so much younger than the other members (both pre-MS and mid-B stars)? If they are not bona fide members, where did they come from? Although our age estimates for the pre-MS sample and *Hipparcos* early-B members appear to be consistent, the presense of these young, B0-B2 classical members (*Hipparcos* non-members) hints that the story of star-formation in Sco-Cen is more complex than our results reveal.

2.8.4 A Star-Formation History of Sco-Cen?

Preibisch & Zinnecker (2000) reviewed the recent star-formation history of Sco-Cen (<5-10 Myr) in the region of US, UCL, and ρ Oph. They present evidence for external supernovae triggering in the formation of the subgroups. They claim that supernovae shock waves from UCL passed through the US progentior GMC approximately 5 Myr ago, and caused the cloud to collapse. The US group appears to have had at least one supernova in the past ~1 Myr, possibly a deceased massive companion to the runaway O9.5V star ζ Oph. This supernova contributed to destroying the GMC and producing the US superbubble (de Geus, 1992; Hoogerwerf, de Bruijne, & de Zeeuw, 2001). The US subgroup appears to be currently triggering star-formation in the ρ Oph cloud core. Here we speculate

on the global star-formation history of the Sco-Cen complex.

The formation of LCC and/or UCL may have been similarly triggered. However it is unclear if one triggered the formation of the other or vice versa. Our pre-MS age estimates are consistent with LCC being slightly older than UCL by a few Myr, though they could be coeval. What was the origin of these large OB subgroups? The gas associated with the Sco-Cen complex appears to be part of the Lindblad Ring, a torus of H I and molecular clouds hundreds of pc in radius. It is centered roughly near the α Persei cluster and Cas-Tau OB association (Blaauw, 1991; Pöppel , 1997). The young stars that have formed from this gas complex (i.e. the Gould Belt) share a systematic expansion consistent with a localized origin for the whole complex – possibly an expanding gas shell from a large star-formation event (e.g. Moreno, Alfaro, & Franco, 1999). The gas associated with Sco-Cen appears to be part of a "spur" of neutral hydrogen and molecular clouds that runs from near LCC (including Coalsack, Musca, and Chamaeleon clouds), through Lupus, Ophiuchus, and into the Aquila and Vulpecula Rift regions (see Fig. 3-18 of Pöppel , 1997). It is likely that LCC and UCL were among the first clumps in the Lindblad Ring to collapse and form stars (see §4 of Blaauw, 1991), either from self-gravity or from triggered from external supernovae events. The LCC and UCL regions formed a large population of OB stars and their stellar winds and supernovae may indeed have triggered the collapse of the US group. The process might continue over the next 10 Myr as the supernovae from the US and ρ Oph subgroups send shock waves into the vast reservoir of atomic and molecular gas associated with the Aquila Rift (see §3.4 of Pöppel , 1997, and references therein). On the other side of Sco-Cen, there appears to be little gas westward of LCC until one reaches the Vela complex some 400 pc away. The lack of a suffi-

cient gas reservoir probably explains why triggering did not proceed to form OB subgroups west of LCC.

The Sco-Cen subgroups have formed their own network of superbubbles with radii of $\sim$100 pc (de Geus, 1992). The superbubbles appear to be largely H I, presumably gas from the progenitor Sco-Cen GMC as well as the swept-up interstellar medium. In some regions, they are associated with well-known nearby molecular cloud complexes: Coalsack, Musca, Chamaeleon, Corona Australis, Lupus, and numerous small high Galactic latitude clouds (e.g. Bhatt, 2000). The Lupus clouds are spatially coincident with the western side of the US superbubble, however no kinematic analysis has been yet undertaken to determine whether the Lupus clouds share in the bubble expansion. The CrA molecular clouds are embedded within the UCL superbubble shell, and the space motion of the T Tauri star population is moving radially away from UCL (Mamajek & Feigelson, 2001). Other young stars in the field toward the 4th Galactic quadrant, including the η Cha cluster, TW Hya association, and β Pic group, all have ages of $\sim$10 Myr and are moving radially away from LCC and UCL. Perhaps these stars formed in small molecular clouds that accumulated within the expanding LCC/UCL superbubble shells.

2.9 Conclusions

From our spectroscopic survey of an X-ray- and kinematically-selected sample of late-type stars in the Sco-Cen OB association, we summarize our main findings as follows:

- We have identified a population of low-mass stars in the Lower Centaurus-Crux (LCC) and Upper Centaurus-Lupus (UCL) OB subgroups with the following properties: (1) G-K spectral types, (2) subgiant surface gravities, (3) Lithium-rich, (4) strong X-ray emission ($L_X \simeq 10^{30}$ - 10^{31} erg s^{-1}), and (5) proper motions consistent with the high-mass members. We classify stars which show these characteristics as bona fide pre-MS stars or "post-T Tauri" stars. X-ray and kinematic selection (the RASS-ACT/TRC sample) yielded a hit rate of 93% for selecting probable pre-MS stars, while kinematic selection alone (*Z99 Hipparcos* sample G-K dwarfs and subgiants) yielded 73%.

- We estimate the mean age of the pre-MS population in the LCC subgroup to be 17 $\pm$ 1 Myr (DM97 tracks), 21 $\pm$ 2 Myr (PS01), and 23 $\pm$ 2 Myr (SDF00). For UCL, the pre-MS population's mean age is 15 $\pm$ 1 Myr (DM97), 19 $\pm$ 1 Myr (PS01), and 22 $\pm$ 1 Myr (SDF00). The UCL pre-MS estimate appears to be slightly biased towards younger ages (by $\sim$1 Myr) through contamination by Lupus or US members. We also calculate new MS turn-off ages of 16 $\pm$ 1 Myr for LCC and 17 $\pm$ 1 Myr for UCL using the *Z99 Hipparcos* membership and Bertelli et al. (1994) evolutionary tracks. The UCL pre-MS and turn-off age estimates are roughly self-consistent, and similar to previously published estimates. Our age estimates for LCC (pre-MS and turn-off) are older than previous estimates, and are equal to or slightly older than UCL.

- We find that 68% of the low-mass star-formation in each subgroup took place within a <4-6 Myr span, and 95% took place within <8-12 Myr (using DM97 tracks). Hence, we have a strong upper limit of $\sim$10 Myr on the duration of low-mass star-formation in the LCC and UCL progenitor molecular clouds.

- Using the Tycho-2 proper motions, we determine that the internal velocity dispersion of the post-T Tauri population in both LCC and UCL has strong 95% confidence upper limits of 1.6 km s^{-1} and 2.2 km s^{-1}, respectively. The best estimates of the post-T Tauri population velocity dispersion in LCC and UCL are $\sigma^*_{int} = 0.6^{+0.5}_{-0.6}$ km s^{-1} and $1.0^{+0.6}_{-1.0}$, respectively. These values are consistent with the values ($\sim$1 km s^{-1}) found for the higher mass stars (de Bruijne, 1999b; Madsen, Dravins, & Lindegren, 2002).

- Based on star counts and kinematic arguments, we demonstate that a new OB subgroup of Sco-Cen proposed to exist in Chamaeleon by Sartori, Lépine, & Dias (2003) probably does not exist.

- We find the frequency of CTTSs among a pre-MS population in an OB association with masses of 1.3 ± 0.2 (1σ) $M_\odot$ and ages of 13 ± 1 (s.e.) ± 6 (1σ) Myr (DM97 tracks) to be only $0.9^{+2.1}_{-0.8}$% (1/110). The younger age results from using our entire (i.e. magnitude-biased) sample of pre-MS stars. Only one star in our sample showed both strong Hαemission and a K-band excess: the previously known CTTS TYC 9246-971-1 (#34 = PDS 66 = Hen 3-892). This suggests that the disk accretion phase lasts $\leq$10-20 Myr in the evolution of solar-type stars in OB associations.

- We demonstrate that a surface gravity indicator for classifying field G and K stars (Sr II λ4077 to Fe I λ4071) can be used to distinguish whether Li-rich stars are pre-MS or ZAMS in nature. When this indicator is used in tandem with other youth diagnostics (Li abundance, X-ray emission, Hα emission, and kinematics), one can confidently classify a star as pre-MS in nature.

CHAPTER 3

CONSTRAINING THE LIFETIME OF CIRCUMSTELLAR DISKS IN THE TERRESTRIAL PLANET ZONE: A MID-IR SURVEY OF THE 30-MYR-OLD TUCANA-HOROLOGIUM ASSOCIATION

This chapter was previously published in Mamajek et al. (2004).

3.1 Introduction

Although the phenomenon of optically-thick accretion disks appears to be isolated to the first ~few Myr of a star's life, numerous examples of older stars with optically-thin dust disks have been found over the past two decades, primarily using space-based IR telescopes, e.g. *InfraRed Astronomical Satellite* (IRAS) and *Infrared Space Observatory* (ISO) (Backman & Paresce, 1993; Lagrange, Backman, & Artymowicz, 2000). Optically-thin disks have been found around stars over a wide range of ages and masses, but those with the highest fractional luminosity ($f_d = L_{disk}/L_\star$) are mostly confined to those younger than <few×100 Myr in age (Habing et al., 2001; Spangler et al., 2001). These dusty "debris" disks are inferred to be created by the collisions of larger bodies, rather than primordial ISM dust (Harper, Loewenstein, & Davidson, 1984; Backman & Paresce, 1993). For micron-size dust grains orbiting between ~0.1-10 AU, the timescale for Poynting-Robertson drag to pull the grains into the star ($\sim 10^{1-5}$ yr) is short compared to typical stellar ages ($\sim 10^{7-10}$ yr), implying that either the observed phenomena is short-lived, or that grains must be replenished through collisions of larger bodies. There is preliminary evidence for a monotonic decrease in dust disk optical

depth with age (Spangler et al., 2001), or possibly a more precipitous drop in optical depth after age ~400 Myr (Habing et al., 2001). Most of the known debris disks have been identified by excess far-IR emission above that of the stellar photosphere (e.g. Silverstone, 2000), with characteristic dust temperatures of ~30-100 K. Despite efforts to find warm (T ~ 200-300 K) dust disks around field stars, precious few examples with detectable 10-12μm excesses are known (Aumann & Probst, 1991).

Observational constraints on the evolution of circumstellar dust in the terrestrial planet zone are currently scarce. Planned observations with the recently launched *Spitzer Space Telescope* (SST) by the *Formation and Evolution of Planetary Systems* (FEPS) Legacy Science program[1], among others, will remedy this situation. FEPS plans to systematically trace the evolution of circumstellar gas and dust around sun-like stars between the epoch of optically-thick accretion disks (ages ~ few Myr) to the epoch of mature planetary systems (ages ~ few Gyr; Meyer et al., 2002, 2004).

Although SST promises to provide a leap in our understanding of the circumstellar environs of stars, we can address a basic question about disk evolution using currently available ground-based facilities. *How much dust remains within a few AU of young stars during the epoch of terrestrial planet formation?* We address this question through a mid-IR survey of a sample of young, low-mass stars with ages of ~30 Myr: the Tuc-Hor Association.

Dynamical simulations suggest that, given the surface mass density of the minimum-mass solar nebula, runaway growth can take place and form Moon-sized planetary "embryos" within ~10^5 yr (Wetherill & Stewart, 1993). When the largest embryos reach radii of ~1000 km, gravitational interactions increase

[1]http://feps.as.arizona.edu

the eccentricities and collision velocities of smaller planetesimals, causing more dust-producing collisions (Kenyon & Bromley, 2004). Over the next $\sim 10^7$-10^8 yr, the growth of the largest embryos is dominated by giant impacts, which consolidate the embryos into a small number of terrestrial planets (Agnor, Canup, & Levison, 1999; Chambers, 2001). During this epoch in our own solar system, the proto-Earth is hypothesized to have been impacted by a Mars-sized planetesimal, which formed the Earth-Moon system (Hartmann & Davis, 1975; Stevenson, 1987). Chronometry studies using radioactive parent-daughter systems (such as ^{182}Hf-^{182}W) suggest that the Earth-Moon impact occurred 25-35 Myr after the formation of the solar system (Kleine et al., 2002; Kleine, Mezger, & Münker, 2003). We know that around at least one star (our Sun), terrestrial planets were forming at age $\sim$30 Myr.

In §3.2 we describe the sample, our mid-IR observations, and data reduction. §3.3 presents the results of our photometry. We present three simple circumstellar disk models in §3.4, and calculate upper limits to the amount of dust orbiting within $\lesssim$10 AU of the stars observed. In §3.5 we discuss our results in light of previous observational and theoretical efforts in order to better understand disk evolution around young stars. In the Appendix, we present information related to the photometric calibration of the MIRAC-BLINC system, as well as details regardings stars for which mid-IR excesses were detected.

3.2 Observations

3.2.1 The Sample

Our mid-IR survey contains 14 low-mass stars that we argue are probable members of the $\sim$30-Myr-old Tuc-Hor Association. The observations of the Tuc-Hor stars are presented in Table 3.1. Observations of some Tuc-Hor candidates that

Table 3.1. MIRAC Observations of Tuc-Hor Members

(1) UT Date	(2) Star Name	(3) Band ...	(4) On-Source Time (s)	(5) Flux Standards
2001 Aug 8	HIP 105388	N	300	ι Cet, α CMa
...	HIP 105404	N	600	ι Cet, α CMa
...	HIP 107947	N	600	ι Cet, α CMa
...	HIP 108195	N	360	ι Cet, α CMa
...	HIP 116748AB	N	600	ι Cet, α CMa
...	HIP 1481	N	480	ι Cet, α CMa
...	HIP 1910	N	840	ι Cet, α CMa
...	HIP 2729	N	840	ι Cet, α CMa
2001 Aug 9	HIP 490	N	420	ι Cet, η Sgr, α CMa
...	HIP 6485	N	600	ι Cet, η Sgr, α CMa
...	HIP 6856	N	660	ι Cet, η Sgr, α CMa
...	HIP 9892	N	840	ι Cet, η Sgr, α CMa
...	ERX 37N	N	1020	ι Cet, η Sgr, α CMa
2001 Aug 10	HIP 9685	N	690	α Cen, ι Cet, η Sgr
2002 Aug 21	HIP 1910	N	180	γ Cru, η Sgr, ι Cet

we reject as members, and other young stars (some of which are FEPS SST Legacy Science targets) are included in Table 3.2. Here we discuss some technical aspects of the Tuc-Hor sample.

The Tucana and Horologium associations are young stellar moving groups that were identified nearly contemporaneously by Zuckerman & Webb (2000, ZW00) and Torres et al. (2000, TDQ00). Zuckerman, Song, & Webb (2001, ZSW01) present an updated membership list and photometry, and suggest that the similar ages, kinematics, and positions of the Tucana and Horologium associations allow us to consider them a single group ("Tuc-Hor"). We adopt ~30 Myr as a reasonable age estimate for Tuc-Hor based on recent values in the literature (see

Table 3.2. MIRAC Observations of Other Stars

(1) UT Date	(2) Star Name	(3) Band ...	(4) On-Source Time (s)	(5) Flux Standards
2001 Aug 6	GJ 799 AB	11.6	135	ι Cet
...	GJ 803	11.6	165	ι Cet
...	HIP 108195	11.6	60	ι Cet
2001 Aug 7	HIP 99273	11.6	255	α Car, α PsA, γ Cru
2001 Aug 8	HD 143006	N	60	ι Cet, α CMa
...	HD 143006	11.6	120	γ Cru
...	[$PZ99$] J161318.6-221248	N	600	ι Cet, α CMa
...	HD 181327	N	240	ι Cet, α CMa
...	HR 7329	N	60	ι Cet, α CMa
2001 Aug 9	RX J1853.1-3609	N	960	ι Cet, η Sgr, α CMa
...	RX J1917.4-3756	N	660	ι Cet, η Sgr, α CMa
2001 Aug 10	HIP 63797	N	300	α Cen, ι Cet, η Sgr
...	[$PZ99$] J161411.0-230536	N	360	α Cen, ι Cet, η Sgr
...	ScoPMS 214	N	450	α Cen, ι Cet, η Sgr
...	ScoPMS 5	N	450	α Cen, ι Cet, η Sgr
...	HIP 95149	N	360	α Cen, ι Cet, η Sgr
...	HIP 113579	N	510	α Cen, ι Cet, η Sgr
...	HIP 1134	N	480	α Cen, ι Cet, η Sgr
2002 Aug 21	HIP 93815	N	180	γ Cru, η Sgr, ι Cet
...	HIP 99803 A	N	690	γ Cru, η Sgr, ι Cet
...	HIP 99803 B	N	165	γ Cru, η Sgr, ι Cet
...	HIP 105441	N	360	γ Cru, η Sgr, ι Cet
...	HIP 107649	N	240	γ Cru, η Sgr, ι Cet
...	PPM 366328	N	180	γ Cru, η Sgr, ι Cet
...	HIP 108809	N	360	γ Cru, η Sgr, ι Cet
...	HIP 108422	N	300	γ Cru, η Sgr, ι Cet
...	GJ 879	N	240	γ Cru, η Sgr, ι Cet

Table 3.3. Age Estimates for Tucana-Horologium Association

(1) Reference	(2) Group	(3) Age (Myr)	(4) Method	(5) Notes
Zuckerman & Webb (2000)	Tuc	40	Hα Emission	Comparing Hα of 3 members to α Per members
Torres et al. (2000)	Hor	30	Isochrones	Siess, Forestini, & Dougados (1997) tracks
Torres et al. (2001)	Tuc-Hor	20	Velocity Disp.	"GAYA" = Tuc-Hor
Stelzer & Neuhäuser (2001)	Tuc	10-30	X-ray Emission	Member L_X values similar to TWA, Tau-Aur, & IC 2602
Zuckerman, Song, & Webb (2001)	Tuc	10-40	Isochrones	K & M stars; Siess, Dufour, & Forestini (2000) tracks

Table 3.3).

The published membership lists for Tuc-Hor appear to be somewhat subjective and contain some stars that are unlikely to be members. In order to include stars that are plausibly members of Tuc-Hor as part of our study, we used kinematics as the primary membership criterion (in addition to the other criteria used in previous studies). For the combined Tuc-Hor membership lists of TDQ00, ZW00, ZSW01, we calculate membership probabilities using the equations of de Bruijne (1999a), the heliocentric space motion of the Tucana nucleus from ZW00, and the best long-baseline proper motions available at present (preferably Tycho-2 or UCAC2; Høg et al., 2000a; Zacharias et al., 2003). We reserve rigorous discussion of membership and kinematics for a separate future study. For this study, we retain only those stars whose membership we could not reject based on proper motion data. We find that ~30% of the stars proposed as members of Tuc-Hor have proper motions inconsistent with the motion of the assumed Tucana "nucleus" (centered on the β Tuc mini-cluster; using space motion vector given by Zuckerman & Webb, 2000). The published membership lists appear to contain several field stars, a handful of which we observed with MIRAC (Table 3.2) be-

fore appreciating that they were probable non-members. Care should be used by investigators employing samples of recently-discovered, diffuse stellar associations (e.g. Tuc-Hor) for the study of age-dependent stellar phenomena.

We include in our Tuc-Hor sample the active dwarf HD 105 (= HIP 490). HD 105 is in the same region of sky (α, δ(ICRS) = 00^h05^m,–41°45′) as the other proposed Tuc-Hor stars, and has a Hipparcos distance of d = 40 pc. For our calculations we adopt the long baseline Tycho-2 proper motion (Høg et al., 2000a) and the Tuc-Hor space motion vector from Zuckerman & Webb (2000). In subjecting HD 105 to the same kinematic tests as the other Tuc-Hor candidates, we are unable to reject its membership. The calculated cluster parallax (25.3 mas) and predicted radial velocity (0 km s^{-1}) agree very well with the observed trigonometric parallax (24.9 ± 0.9 mas; ESA, 1997) and measured RV (+1.7 ± 2.5 km s^{-1}; Wichmann, Schmitt, & Hubrig, 2003). The equivalent width of the Li I λ6707 line (165 mÅ; Cutispoto et al., 2002) is similar to that for early-G-type members of ∼50 Myr-old IC 2602 and IC 2391 clusters (Randich et al., 2001), and stronger than that found in ∼120-Myr-old Pleiades stars (Soderblom et al., 1993). Finally, the X-ray luminosity of HD 105 (log(L_X) = 29.4 erg s^{-1}; Cutispoto et al., 2002) is similiar to what is expected for early-G stars with ages of 10-100 Myr (Briceño et al., 1997). Therefore, we conclude that HD 105 is a likely member of the Tuc-Hor association.

3.2.2 Data Acquisition

Mid-IR images of the Tuc-Hor members and other young stars were obtained during the nights of 6-10 August 2001 and 22 August 2002 (UT) with the MIRAC-BLINC instrument on the Magellan I (Baade) 6.5-m alt-az telescope at Las Campanas Observatory, Chile. The *Mid-InfraRed Array Camera* (MIRAC-3) contains a Rockwell HF16 128 × 128 hybrid BIB Si:As array, and was built at the Stew-

ard Observatory, University of Arizona, and the Harvard-Smithsonian Center for Astrophysics (Hoffmann et al., 1998). The *BracewelL Infrared Nulling Cryostat* (BLINC) is a nulling interferometer mated to MIRAC-3 (Hinz et al., 2000). In our observing mode, however, BLINC is used as a re-imaging system, reducing the f/11 beam from the Magellan tertiary mirror to a f/20 beam required for the MIRAC-3 instrument. The pixel scale is 0.123″/pixel, resulting in a FOV of 15.7″.

Our intent was to survey for circumstellar dust surrounding our target stars in the terrestrial planet zone (~0.3-3 AU), with characteristic temperatures of ~300 K, and corresponding Wien emission peak at ~10 μm. Observations were obtained with either the wide-band N filter (λ_{iso} = 10.34μm for an A0 star, where λ_{iso} is the isophotal wavelength, e.g. Golay, 1974) or narrow-band "11.6" filter (λ_{iso} = 11.57μm for an A0 star) in standard chop-nod mode (4 position beam switching; see Appendix 1 of Hoffmann & Hora, 1999). The nod and chop separations were 8″, and the chop (frequency of 3-10 Hz) was in a direction perpendicular to the nod vector. The chop-nod imaging technique produces two positive and two negative images of the star in a square configuration on the detector. The nod separation was chosen so that all four images of the star appear on the detector with sufficient room for determination of the background flux in annuli surrounding each star image. We found that using chop frequencies between 3 and 10 Hz mitigated the effects of poorly subtracted sky background (background noise increases as chop frequency decreases) while maintaining observing efficiency (increasing the chop frequency adds overhead time, with minimal improvement in background subtraction). Chopping was done with an internal pupil plane beam-switching mirror within BLINC. The frame time (on-chip integration time) was either 10 ms (N-band) or 40 ms (11.6-band), and these frames were co-added in 15-30 s long integrations per nod beam. We found that derotating the MIRAC-BLINC instru-

ment (i.e. freezing the cardinal sky directions on the detector) in the Nasmyth port during observations resulted in poorer background subtraction compared to turning the derotation off. Hence, for the majority of observations taken during these nights, the instrument derotation was turned off. The ability to guide the telescope while derotating the instrument, was not available during our observing runs. Hence the telescope was not guiding during most of our observations. This had negligible impact on the achieved image quality, but limited our ability to reliably co-add data for faint sources.

3.2.3 Reduction

The MIRAC images were reduced using the custom program *mrc2fts* (Hora, 1991) and IRAF[2] routines. Flat fields were constructed from images of high (dome) and low (sky) emissivity surfaces. A median sky frame was produced and subtracted from the individual ($N \simeq 10$) dome frames. The results were then median combined to produce the final flat field. The pixel-to-pixel variation in sensitivity ($\sim$2% r.m.s.) of the MIRAC detector is small enough that flat-fielding had negligible effect on our derived photometry.

Aperture photometry was derived using the IRAF *phot* package. We used aperture radii of either 0.62″ (5 px) or 1.23″ (10 px), depending on which flux had the higher S/N ratio after the photometric errors were fully propagated (dominated by sky noise for large aperture or uncertainty in aperture correction for smaller apertures). The photometry derived with aperture radii of 5 px and 10 px were consistent within the errors for all of the stars observed. The background level was determined by measuring the mean sky value per pixel in an annulus centered on the star with inner radius 1.85″ (15 pix) and outer radius 3.08″ (25

[2]IRAF is distributed by the National Optical Astronomy Observatories, which are operated by the Association of Universities for Research in Astronomy, Inc., under cooperative agreement with the National Science Foundation. http://iraf.noao.edu

pix) for subtraction. The background annulus radii were chosen so as to sample a negligible contribution of the star's PSF, but to avoid the PSFs from the other images of the same star. For the faintest sources, an aperture radius of 5 px was usually used, in which case an aperture correction was applied to place all photometry on the 10 px system. The aperture corrections were determined nightly using standard stars, and the typical correction to the 5 px aperture radius photometry was -0.32 ± 0.05 mag. Photometric solutions (zero points and airmass corrections) were determined for every night of observations. The typical airmass corrections at N-band were 0.1-0.2 mag airmass^{-1}. The conversion between fluxes (in mJy) and magnitudes is simply $mag_\lambda(\mathrm{star}) = -2.5 \log\{f_\lambda(\mathrm{star})/f_\lambda(0)\}$, where $f_\lambda(\mathrm{star})$ is the star's flux at wavelength λ, and $f_\lambda(0)$ is the flux of a zero-magnitude star (see Appendix D). The sensitivity was such that we could detect a star with of magnitude 7.5 in N-band, at S/N $\simeq 5$, with 600 s of on-source integration time.

We observed standard stars taken from the MIRAC manual (Hoffmann & Hora, 1999), the list of ESO IR standards (van der Bliek, Manfroid, & Bouchet, 1996), and the list of Cohen et al. (1999). Martin Cohen calculated an independent calibration of the MIRAC photometric system, using the approach identical to that described in Cohen, Wheaton, & Megeath (2003). Discussion on the input data for the absolute photometric calibration, the zero-magnitude attributes of the MIRAC filter systems, and standard star fluxes, are given in Appendix D. The absolute accuracy of the standard star fluxes among the four filters ranges from 1.7-4.5%.

3.3 Results

N-band photometry for young stars in Tuc-Hor is presented in Table 3.4, while photometry for stars in other regions (most belonging to young, nearby associations) is presented in Table 3.5. Near-infrared (JHK_s) photometry from the 2MASS catalog (Cutri et al., 2003) was used to help predict the brightness of the stellar photospheres at 10μm. For the range of spectral types investigated, models predict that $([11.6] - N) \simeq 0.00$ within our photometric errors (typically $\sim$0.05-0.10 mag), hence we plot $(K_s - N)$ and $(K_s - [11.6])$ on the same color-color plot, and generically refer to these colors as "$(K_s - N)$" throughout. A color-color plot of the Tuc-Hor stars is illustrated in Fig. 3.1.

Table 3.4. N-band Photometry of Tuc-Hor Members

(1) Name ...	(2) Name ...	(3) Spec. Type	(4) K_s (mag)	(5) Pred. F_ν (mJy)	(6) Meas. F_ν (mJy)	(7) E(N) (mJy)	(8) Dev. (σ)
HIP 490	HD 105	G0	6.12 ± 0.02	139	138 ± 8	-1 ± 8	–0.2
HIP 1481	HD 1466	F8	6.15 ± 0.02	135	151 ± 20	$+16 \pm 20$	+0.8
HIP 1910	BPM 1699	M0	7.49 ± 0.02	51	49 ± 7	-2 ± 7	–0.3
HIP 2729	HD 3221	K4	6.53 ± 0.02	111	102 ± 5	-9 ± 5	–1.7
HIP 6485	HD 8558	G6	6.85 ± 0.03	71	82 ± 4	$+11 \pm 4$	+2.4
HIP 6856	HD 9054	K2	6.83 ± 0.02	72	85 ± 4	$+13 \pm 4$	+3.0
HIP 9685	HD 12894	F4	5.45 ± 0.02	258	207 ± 17	-51 ± 18	–2.9
HIP 9892	HD 13183	G5	6.89 ± 0.02	68	67 ± 6	-1 ± 6	–0.2
ERX 37N	AF Hor	M3	7.64 ± 0.03	42	46 ± 3	$+4 \pm 3$	+1.3
HIP 105388	HD 202917	G5	6.91 ± 0.02	67	65 ± 9	-2 ± 9	–0.3
HIP 105404	HD 202947	K0	6.57 ± 0.02	92	74 ± 9	-18 ± 9	–1.9
HIP 107947	HD 207575	F6	6.03 ± 0.02	151	155 ± 12	$+4 \pm 12$	+0.3
HIP 108195	HD 207964	F3	4.91 ± 0.02	424	394 ± 20[a]	-30 ± 21	–1.4
HIP 116748A	HD 222259A	G6	6.68 ± 0.03	83	75 ± 12	-8 ± 12	–0.7
HIP 116748B	HD 222259B	K	7.03 ± 0.06	60	53 ± 14	-7 ± 14	–0.5

Note. — Columns (1) Hipparcos name, (2) other name, (3) spectral type, from either ZW00, TDQ00, or ZSW01, (4) K_s magnitude from 2MASS (Cutri et al., 2003), (5) measured MIRAC N-band flux, (6) predicted photospheric flux, (7) flux excess and uncertainty, (8) residual deviation = $E(N)/\sigma(E(N))$. ERX 37N is given in SIMBAD as [TDQ2000] ERX 37N. Predicted N-band photospheric fluxes use or assume: 2MASS K_s magnitudes, A_V = 0, dwarf color relations from §3.3, and zero magnitude flux of 37.25 Jy for N-band.

[a]HIP 108195 was also imaged at 11.6μm with a flux of 284 ± 40 mJy.

Table 3.5. Measured Photometry for Other Stars

(1) Name	(2) Name	(3) Spec. Type	(4) K_s (mag)	(5) Band	(6) Pred. F_ν (mJy)	(7) Meas. F_ν (mJy)	(8) E(N) (mJy)	(9) Dev. (σ)
Tuc-Hor Rejects								
HD 177171	HIP 93815	F7	3.81 ± 0.10[a]	*N*	1171	1236 ± 103	$+65 \pm 149$	+0.4
HD 191869 A[b]	HIP 99803 A	F7	6.81 ± 0.02	*N*	74	87 ± 9	$+13 \pm 9$	+1.5
HD 191869 B[b]	HIP 99803 B	...	6.86 ± 0.03	*N*	70	63 ± 14	-7 ± 14	–0.5
HD 202746	HIP 105441	K2	6.40 ± 0.02	*N*	107	116 ± 11	$+9 \pm 11$	+0.8
HD 207129	HIP 107649	G0	4.12 ± 0.02[c]	*N*	880	837 ± 70	-43 ± 72	–0.6
PPM 366328	TYC 9129-1361-1	K0	7.61 ± 0.02	*N*	35	63 ± 24	$+28 \pm 24$	+1.1
HD 208233[d]	HIP 108422	G8	6.75 ± 0.02	*N*	78	89 ± 14	$+11 \pm 14$	+0.8
Upper Sco Members + FEPS								
[*PZ*99] J161411.0-230536	TYC 6793-819-1	K0	7.46 ± 0.03	*N*	48	273 ± 11	$+225 \pm 11$	+20.3
ScoPMS 214	NTTS 162649-2145	K0	7.76 ± 0.02	*N*	42	37 ± 5	-5 ± 5	–1.0
ScoPMS 5	HD 142361	G3	7.03 ± 0.02[e]	*N*	60	58 ± 6	-2 ± 6	–0.4
HD 143006	HBC 608	G6/8	7.05 ± 0.03	*N*	134	648 ± 31	$+514 \pm 31$	+16.5
HD 143006	HBC 608	G6/8	7.05 ± 0.03	11.6	104	640 ± 34	$+536 \pm 34$	+15.7
[*PZ*99] J161318.6-221248	TYC 6213-306-1	G9	7.43 ± 0.02	*N*	45	32 ± 6	-13 ± 6	–2.2
β Pic Group Members								
GJ 799 A	HIP 102141 A	M4.5	5.70 ± 0.10[f]	11.6	202	259 ± 24	$+57 \pm 30$	+1.9
GJ 799 B	HIP 102141 B	M4	5.70 ± 0.10[f]	11.6	202	260 ± 25	$+58 \pm 31$	+1.9
GJ 803	HIP 102409	M0	4.53 ± 0.02	11.6	627	608 ± 32	-19 ± 34	–0.6
HD 181327	HIP 95270	F5/6	5.91 ± 0.03	*N*	169	200 ± 18	$+31 \pm 19$	+1.7
HR 7329	HIP 95261	A0	5.01 ± 0.03	11.6	301	343 ± 31	$+42 \pm 32$	+1.3
HR 7329	HIP 95261	A0	5.01 ± 0.03	*N*	387	466 ± 52	$+79 \pm 53$	+1.5

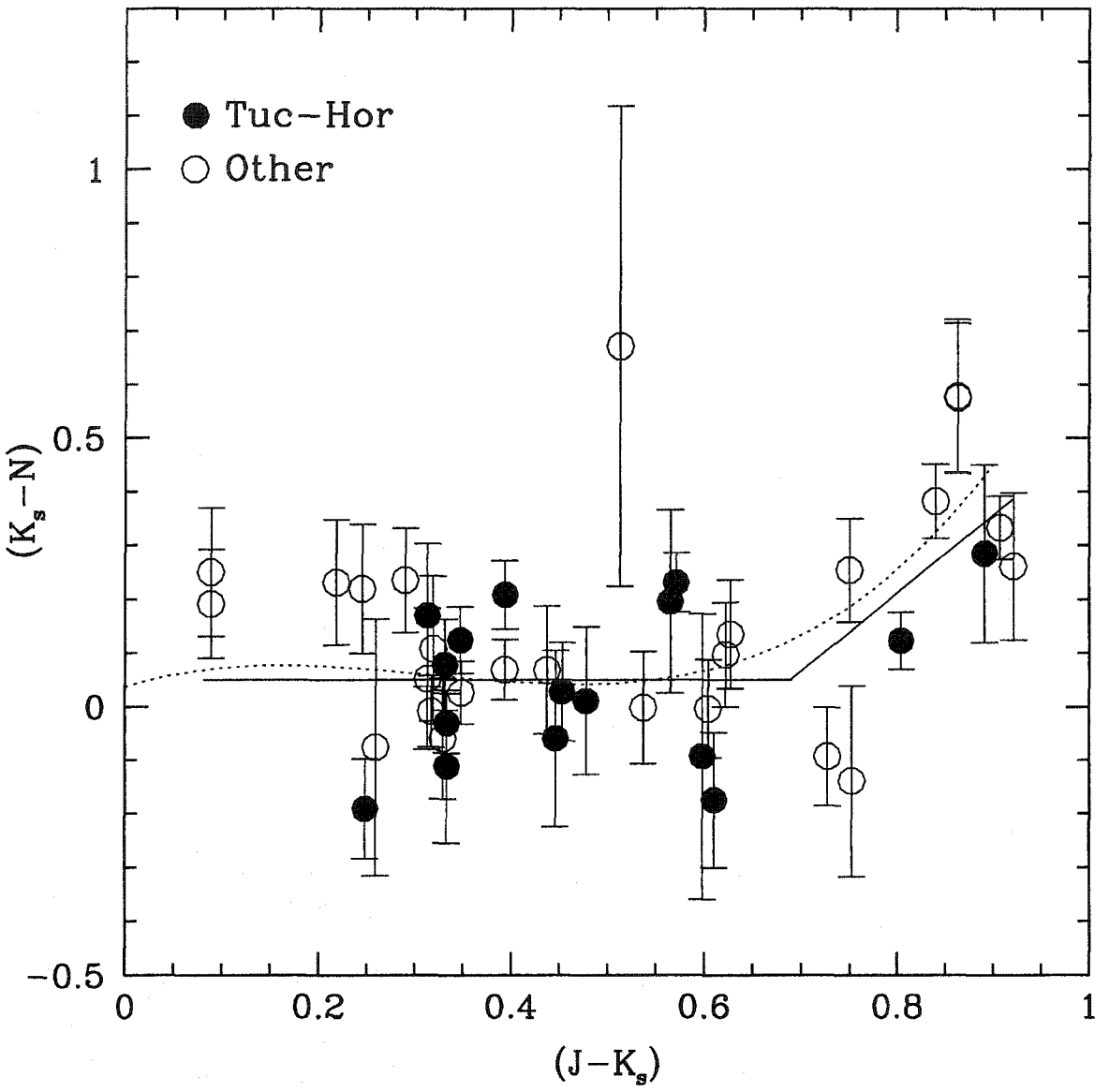

Figure 3.1: Color-color diagram for Tuc-Hor members (*filled circles*) and other stars observed in this study (*open circles*). Two stars (not members of Tuc-Hor) with significantly red $(K_s - N)$ colors are not shown (HD 143006 and J161411). The *solid line* is our adopted photosphere color relation (§3.3). The *dashed line* is a smoothed fit to the $(K_{CIT} - [12])$ dwarf sequence of Kenyon & Hartmann (1995), where we calculate $(K_s - N) \simeq (K_{CIT} - [12])_{KH95}$ - 0.06.

Table 3.5—Continued

(1) Name	(2) Name	(3) Spec. Type	(4) K_s (mag)	(5) Band	(6) Pred. F_ν (mJy)	(7) Meas. F_ν (mJy)	(8) E(N) (mJy)	(9) Dev. (σ)
CrA Off-Cloud Stars + FEPS								
RX J1853.1-3609	HD 174656	G6	7.28 ± 0.02	N	48	46 ± 4	-2 ± 4	–0.4
RX J1917.4-3756	SAO 211129	K2	7.47 ± 0.03	N	44	45 ± 4	$+1 \pm 4$	+0.3
Sco-Cen Reject								
HD 113376[g]	HIP 63797	G3	6.70 ± 0.02	N	81	83 ± 9	$+2 \pm 9$	+0.2
Other FEPS Targets								
HD 181321	HIP 95149	G5	4.93 ± 0.02	N	418	425 ± 21	$+7 \pm 22$	+0.3
HD 191089	HIP 99273	F5	6.08 ± 0.03	11.6	113	132 ± 15	$+19 \pm 15$	+1.3
HD 209253	HIP 108809	F6/7	5.39 ± 0.02	N	273	255 ± 21	-18 ± 22	–0.8
HD 216803	GJ 879	K4	3.81 ± 0.02[c]	N	1233	1027 ± 85	-206 ± 88	–2.3
HD 217343	HIP 113579	G3	5.94 ± 0.03	N	164	160 ± 8	-4 ± 9	–0.4
HD 984	HIP 1134	F5	6.07 ± 0.02	N	145	131 ± 14	-14 ± 14	–1.0

Note. — (1) Hipparcos name, (2) other name, (3) spectral type (from SIMBAD unless otherwise noted) (4) K_s magnitude from 2MASS (Cutri et al., 2003), unless otherwise noted, (5) measured MIRAC N-band flux, (6) predicted photospheric flux, (7) flux excess and uncertainty, (8) residual deviation = $E(N)/\sigma(E(N))$.

[a]Star is saturated in 2MASS. We adopt the V magnitude from Hipparcos (ESA, 1997), and the intrinsic $(V-J)$ and $(J-K_s)$ color for F7 stars from Kenyon & Hartmann (1995) (converted to 2MASS system via Carpenter 2001), to calculate a rough K_s magnitude. We assume an uncertainty of 0.10 mag.

[b]Zuckerman et al. (2001) calls the pair HIP 99803 NE and SW. A = SE and B = NW.

[c]2MASS photometry is saturated. We take the K_{CIT} magnitude from Aumann & Probst (1991) and transform it to the 2MASS system via equation (12) of Carpenter (2001).

[d]We can not rule out HIP 108422 as a Tuc-Hor member based on its proper motion, or the agreement between the calculated cluster parallax and Hipparcos trigonometric parallax. However, we conservatively exclude the star as a member at present, since no spectroscopic evidence of youth has been presented in the literature. If it is co-moving with the Tucana nucleus, we predict a RV of +3 $\mathrm{km\,s^{-1}}$.

[e]A 0.8" binary discovered by Ghez, Neugebauer, & Matthews (1993) and seen in MIRAC K-band images. MIRAC N and 2MASS K_s magnitudes are for unresolved pair.

[f]The 2MASS K_s magnitudes from Reid, Kilkenny, & Cruz (2002) appear to be at odds with the combined magnitude for A & B measured by Cutri et al. (2003), Nelson et al. (1986), and Probst (1983). The system is essentially an equal brightness binary at optical bands as well as at N, so we split the 2MASS K_s magnitude evenly and adopt a generous 0.10 mag error. Spectral types are from Hawley, Gizis, & Reid (1996)

[g]Rejected as a Sco-Cen member by Mamajek, Meyer, & Liebert (2002)

Fig. 3.1 indicates that $(K_s - N)$ colors are fairly uniform for stars with $(J - K_s)$ < 0.7, i.e. for FGK stars. We decided to analyze the M stars separately from the FGK stars. We surmise that much of the structure in the published color-color relations for dwarfs is probably due to statistical fluctuations (e.g. Cohen et al., 1987; Waters, Cote, & Aumann, 1987; Mathioudakis & Doyle, 1993; Kenyon & Hartmann, 1995). After examining our data and those from previous studies of large dwarf samples, we decided to assume a constant $(K_s - N)$ color for the photospheres of FGK stars. In calculating a mean intrinsic $(K_s - N)$ color, we include the FGK stars in Tables 3.4 and 3.5, but exclude the FGK stars HD 143006, [PZ99] J161411 (both with $(K_s - N) \simeq 2$), and HIP 95270 and HIP 99273 (known to have far-IR excesses which may contaminate N-band flux, e.g. Zuckerman & Song, 2004). The median, unweighted mean, and weighted mean $(K_s - N)$ color for the FGK stars are all similar (0.05, 0.04 ± 0.02, and 0.07 ± 0.02, respectively). These estimates agree well with the mean FGK dwarf color found by Fajardo-Acosta, Beichman, & Cutri (2000, $(K_s - [12]) \simeq +0.04$ implies $(K_s - N) \simeq +0.05$) and are close to the value for AFGK-type dwarfs found by Aumann & Probst (1991, $(K_{CIT} - [12]) = +0.02$ implying $(K_s - N) = +0.01$) [3]. Within the uncertainties, *our measured mean* $(K_s - N)$ *color for FGK dwarfs is consistent with previous determinations. The mean colors for the young stars in our observing program do not appear to be biased toward red* $(K_s - N)$ *colors due to the presence of circumstellar material.* We adopt $(K_s - N)_{phot} = +0.05$ as the photospheric color for FGK-type stars with $(J - K_s) < 0.69$.

The observed $(K_s - N)$ colors of the M-type stars are systematically redder

[3] Although not explicitly stated, the K photometry from Aumann & Probst (1991) appears to be on the CIT system, where 2MASS $K_s = K_{CIT} - 0.019$ (Carpenter, 2001). The MIRAC N-band photometric system assumes N = 0.00 for Vega, whereas Aumann & Probst (1991) list [12] = +0.01 for Vega. We ignore any color terms in converting [12] to a predicted N magnitude, and derive $(K_s - N) \simeq (K_{CIT}\text{–}[12]) - 0.01$.

than those of the FGK stars, as well as the M-giant standards. We looked for independent confirmation that the turn-up in $(K_s - N)$ color for the coolest dwarfs is a real effect, and not due to circumstellar material. We measure a color of $(K_s - [11.6]) = 0.33 \pm 0.06$ for the ~12-Myr-old M0 star GJ 803. Song et al. (2002) studied the spectral energy distribution of GJ 803 and concluded that the observed cold dust excess detected by IRAS at 60μm does not contribute significant flux at 12μm, and that the IRAS 12μm flux is consistent with a NextGen model photosphere. Our observed 11.6μm flux (608 ± 32 mJy) agrees very well with the predicted photospheric flux (633 mJy at 11.6μm), as well as the color-corrected IRAS 12μm flux (537 ± 32 mJy). These observations confirm that the observed $(K_s - [11.6])$ color for GJ 803 is photospheric, and that the turn-up in $(K_s - N)$ color for M stars is real. It appears that none of the M-type stars has a statistically significant mid-IR excess. For the purposes of calculating upper limits on mid-IR excess, we fit a line to the mean $(K_s - N)$ colors for the KM-type stars with $(J - K_s) > 0.6$ (excluding the T Tauri star [PZ99] J161411), and model the M-type dwarf photosphere colors as: $(K_s - N)_{phot} = -0.947 + 1.448 \times (J - K_s)$ $(0.69 < (J - K_s) < 0.92)$.

We determine whether a star has detectable excess at N or 11.6 through calculating the excess as:

$$E(N) = N - N_{phot} = N - K_s + (K_s - N)_{phot} \tag{3.1}$$

$$\sigma^2[E(N)] = \sigma^2[N] + \sigma^2[K_s] + \sigma^2[(K_s - N)_{phot}] \tag{3.2}$$

The contribution to the N-band excess from interstellar extinction will only become similar in size to our photometric errors if $A_V \gtrsim$ 1-2 mag, hence we can safely ignore extinction for the stars observed. We examined the residuals (defined as $E(N)/\sigma[E(N)]$) in order to identify statistically-significant outliers (i.e. possible N-band excess stars). The ~5-Myr-old Upper Sco members HD 143006

and [PZ99] J161411 (Preibisch & Zinnecker, 1999) both stand out with definite N-band excesses ($\simeq$ 15-20σ), and they are discussed further in Appendix B. There are two stars with positive 2-3σ excesses (HIP 6485 and HIP 6856), however there are three stars with 2-3σ deficits (HIP 9685, GJ 879, and [PZ99] J161318). Hence, the weak excesses for HIP 6485 and HIP 6856 are probably statistical and not real. Excluding the two Upper Sco stars with strong N-band excesses, we find that $56 \pm 12\%$ of the excesses E(N) are within 1σ of zero, and $88 \pm 15\%$ are within 2σ (uncertainties reflect Poisson errors). It does not appear necessary to introduce a non-zero uncertainty in the intrinsic $(K_s - N)_{phot}$. If one wanted to force 68% of the residuals to be within $\pm 1\sigma$ and 95% to be within $\pm 2\sigma$, then either $\sigma[(K_s - N)_{phot}] \simeq$ 0.07-0.09 mag, or our observational uncertainties are underestimated by $\sim$40%. We searched for, and could not find, a plausible reason why our photometric errors would be underestimated by such a large amount. The observations of our standard stars certainly do not support a significant increase in our quoted photometric errors. More calibration observations are required to see if this dispersion can be attributed to actual structure in the intrinsic $(K_s - N)$ colors of normal dwarf stars as a function of spectral type.

Among the Tuc-Hor stars, only one star has as observed N-band flux $\geq 3\sigma$ above that expected for stellar photosphere: HIP 6856 (3.0σ excess). However, there is a Tuc-Hor member with a similarly sized flux *deficit* (HIP 9685; –2.9σ), so it is difficult to claim that the excess for HIP 6856 is statistically significant. *We find that none of the 14 Tuc-Hor members has an N-band excess more than 3σ offset from the dwarf color relation.* We estimate a conservative upper limit to the N-band excess due to a hypothetical dust disk as 3$\times$ the uncertainty in the flux excess ($\sigma[E(N)]$; given in column 8 of Table 3.4).

3.4 Disk Models

Our survey was designed to be sensitive enough to detect the photospheres of young stars, hence we can place meaningful constraints on the census of even optically-thin circumstellar disks in our target sample. We analyze the upper limits to possible mid-IR excess for the Tuc-Hor stars using three different models. The first model assumes a geometrically-thin, optically-thick disk with a large inner hole. The second model assumes emission from an optically-thin disk of single-sized grains. The third model treats the hypothetical disks as a scaled-up version of the zodiacal dust disk in our solar system.

3.4.1 Optically-Thick Disk With Inner Hole

Infrared and submillimeter observations of T Tauri stars in dark clouds show that roughly half are orbited by an optically-thick circumstellar dust disk (see review by Beckwith, 1999). While the stars in our sample are roughly an order of magnitude older (~30 Myr) than typical T Tauri stars in dark clouds (≤3 Myr), we can ask the question: If the Tuc-Hor stars have optically-thick, geometrically-thin disks, what is the minimum inner hole radius allowed by observations?

To answer this question for each star, we adopt the axisymmetric, geometrically-thin, optically-thick disk model of Adams, Lada, & Shu (1987), and follow the formalism of Beckwith et al. (1990). While we assume a face-on orientation ($\theta = 0$), our results are not strongly dependent on this assumption. We also assume that the disk is optically-thick between r_{in} and r_{out} (300 AU is assumed for all models) and at all frequencies ($1 - e^{-\tau_\nu} \sim 1$). This is a safe assumption for T Tauri star disks in the wavelength regime probed in this study ($\lambda \leq 100\,\mu$m; Beckwith et al., 1990).

Our N-band photometry alone allows us to rule out optically-thick disks with inner hole radii of $\sim$0.1 AU for the Tuc-Hor stars. Stronger constraints on inner disk radius for a hypothetical optically-thick circumstellar disk can be calculated by including IRAS photometry. For IRAS point sources, we adopt 25 μm, 60 μm, and 100 μm fluxes and upper limits from the Faint Source Catalog (Moshir et al., 1990). Where no IRAS point source is detected, we adopt the IRAS Point Source Catalog upper limits of 0.5 Jy (25 μm), 0.6 Jy (60 μm), and 1.0 Jy (100 μm) (IPAC, 1986). For the brightest stars, the IRAS 60 μm and 100 μm data provide the strongest constraints on the existence of an optically thick disk, whereas for the fainter K and M-type stars, the MIRAC photometry provides the strongest constraint. IRAS did not map the region around HD 105, hence the inner hole radius we derive for this star is based only on the MIRAC N-band 3σ upper limit. In Fig. 3.2, we illustrate a typical example (HIP 1481) of how the MIRAC and IRAS photometry constrain the existence of optically-thick disks around the Tuc-Hor stars. The values we derive for the minimum inner hole radius for a hypothetical optically-thick disk are given in column 5 of Table 3.6. The median value of the minimum inner hole radius is $\sim$0.3 AU (range: 0.1-7.9 AU). The N-band and IRAS upper limits place the strongest constraints on inner hole size for the luminous F stars ($r_{in} \gtrsim 5$ AU), and the weakest constraints for the faint K/M stars ($r_{in} \gtrsim 0.1$ AU). *The MIRAC and IRAS photometry easily rule out the existence of optically-thick disks with inner hole radii of $\sim$0.1 AU of the $\sim$30 Myr-old Tuc-Hor stars.*

3.4.2 Optically-Thin Disk

In the absence of circumstellar gas, a putative mid-IR excess around a $\sim$30-Myr-old star would be most likely to be due to an optically-thin debris disk rather than an optically-thick T Tauri-type disk. The stellar ages ($\sim 10^{7.5}$ yr) are orders of magnitude greater than the Poynting-Robertson drag timescale ($\sim 10^{3-4}$ yr) for

Table 3.6. Model Parameters for Tuc-Hor Members

(1)	(2)	(3)	(4)	(5)	(6)	(7)	(8)	(9)	(10)	(11)
Name	π	log	log	r_{hole}	$\bar{a}$	$r_{in} - r_{out}$	Σ_o	M_{disk}	log	Zodys
...	(mas)	T_{eff}	$L/L_\odot$	(AU)	(μm)	(AU)	(g cm^{-2})	($M_\oplus$)	(L_d/L_*)	($\mathcal{Z}$)
HIP 490	24.9	3.776	+0.17	0.3	0.50	0.05-13.9	3.4E-06	7.8E-05	-3.25	2.6E3
HIP 1481	24.4	3.780	+0.21	1.8	0.53	0.06-13.8	8.2E-06	1.9E-04	-2.89	6.4E3
HIP 1910	21.6	3.585	–0.81	0.1	0.10	0.03-10.8	1.4E-05	1.9E-04	-2.20	2.9E3
HIP 2729	21.8	3.643	–0.32	0.7	0.27	0.04-12.4	5.0E-06	9.2E-05	-2.80	2.1E3
HIP 6485	20.3	3.744	–0.04	0.3	0.34	0.05-14.4	3.2E-06	7.7E-05	-3.10	2.0E3
HIP 6856	26.9	3.707	–0.55	0.1	0.12	0.04-15.3	2.6E-06	7.1E-05	-2.85	1.1E3
HIP 9685	21.2	3.829	+0.71	4.9	1.44	0.09-12.0	6.9E-06	1.2E-04	-3.45	7.5E3
HIP 9892	19.9	3.752	–0.08	0.2	0.31	0.05-14.9	4.5E-06	1.2E-04	-2.91	3.0E3
ERX 37N	22.6	3.540	–0.89	0.1	0.14	0.02-8.6	8.3E-06	7.1E-05	-2.48	1.2E3
HIP 105388	21.8	3.746	–0.16	0.2	0.26	0.05-15.3	5.4E-06	1.5E-04	-2.75	3.6E3
HIP 105404	21.7	3.719	–0.21	0.2	0.26	0.04-14.6	6.4E-06	1.6E-04	-2.68	3.8E3
HIP 107947	22.2	3.795	+0.38	2.1	0.75	0.06-13.0	6.3E-06	1.3E-04	-3.16	4.8E3
HIP 108195	21.5	3.817	+0.91	7.9	2.40	0.11-11.7	1.0E-05	1.6E-04	-3.53	8.6E3
HIP 116748A	21.6	3.746	–0.09	1.0	0.31	0.05-14.8	8.0E-06	2.1E-04	-2.65	5.0E3
HIP 116748B	21.6	3.645	–0.46	0.2	0.19	0.04-13.0	1.4E-05	2.9E-04	-2.24	5.8E3

Note. — (1) Star name. (2) Parallax. ERX 37N parallax calculated via cluster parallax method, the other values are from Hipparcos (ESA, 1997). (3) Stellar effective temperature. (4) Luminosity in solar units. (5) Lower limits on inner hole radius for a hypothetical optically-thick disk (§3.4.1). (6) Mean calculated grain size, where $\bar{a} = 5a_{min}/3$, where a_{min} is the blow-out grain size (Eqn. 1; §3.4.2). (7) Inner and outer radii for calculation of optically-thin disk (§3.4.2). (8) Disk surface mass density for optically-thin disk model (§3.4.2); independent of radius for our adopted model with ($\Sigma = \Sigma_o r_{AU}^{-p}; p = 0$). (9) Upper limit on disk mass (in grains of size $\bar{a}$) for optically-thin model (§3.4.2). (10) Upper limit to fractional luminosity of scaled-up zodiacal dust model (§3.4.3). (11) Upper limit to emitting area of scaled-up zodiacal dust model (in units of "zodys", where 1 $\mathcal{Z} = 10^{21}$ cm^2; §3.4.3).

typical interplanetary dust grains orbiting ~1 AU from a solar-type star. Small dust grains must be continually replenished by collisions of larger bodies, or else they would be only detectable for astrophysically short timescales. Using a simple, single grain-size model, we place upper limits on the amount of orbiting dust within several AU of the ~30-Myr-old Tuc-Hor stars.

Circumstellar dust grains surrounding young main sequence stars should most likely have radii somewhere between the scale of typical ISM grains (~0.01-1 μm; Mathis, Rumpl, & Nordsieck, 1977) and solar system zodiacal dust (~10-100 μm; Grün et al., 1985). Theoretically, an ensemble of dust grains produced from a collisional cascade of fragments is predicted to follow the equilibrium power-law size distribution (Dohnanyi, 1969): $n(a)\,\mathrm{d}a = n_o\, a^{-p}\,\mathrm{d}a$, where $p = 3.5$. Indeed this power law distribution is observed for ISM grains (Mathis, Rumpl, & Nordsieck, 1977) and asteroids (Greenberg & Nolan, 1989). With $p = 3.5$, most of the mass is in the largest (rarest) grains, but most of the surface area in the smallest (most common) grains. If the grain size distribution has a minimum cut-off, the mean grain size is calculated to be $\bar{a} = 5a_{min}/3$ (e.g. Metchev, Hillenbrand, & Meyer, 2004). A limit on the minimum grain size a_{min} can be estimated from consideration of radiation pressure blow-out (e.g. Artymowicz, 1988):

$$a_{min} = \frac{3L_* Q_{pr}}{16\pi G M_* c \rho} \tag{3.3}$$

Where L_* is the luminosity of the star, Q_{pr} is the radiation pressure efficiency factor averaged over the stellar spectral energy distribution, G is the Newtonian gravitational constant, M_* is the mass of the star, c is the speed of light, and ρ is the grain density (assumed to be 2.5 g cm^{-3}; Grün et al., 1985). The minimum grain size corresponds to the case where the ratio of the radiation pressure force to the stellar gravitational force is $F_{rad}/F_{grav} = 1$. For this calculation we assume

the geometric optics case where $Q_{pr} = 1$. For the idealized grain orbiting the Sun at 1 AU, we calculate $a_{min} = 0.2\ \mu$m and $\bar{a} = 0.4\ \mu$m. The grain size lower limit may be larger if the momentum imparted by stellar winds dominates radiation pressure. The minimum grain size will be somewhat lower if we calculate Q_{pr} using Mie theory and stellar spectral energy distributions, instead of adopting the geometric optics case. Highlighting the uncertainty in this calculation, we note that the value of $\bar{a}$ that we calculate for the Sun is $\sim 10^2\times$ smaller than the mean interplanetary dust particle orbiting in the Earth's vicinity (Grün et al., 1985). This is largely due to a complex interplay between Poynting-Robertson drag and collisions. Increasing the cross-section of dust particles in the solar system zodiacal dust cloud by $\sim 10^4$ (i.e. comparable to what we are sensitive to in Tuc-Hor, see §3.4.3), will decrease the collision timescale, and correspondingly decrease the mean particle size to comparable to the blow-out grain size (Dominik & Decin, 2003).

We model the thermal emission from an optically-thin disk of single-sized dust grains of radius $\bar{a}$ orbiting in an annulus between inner radius r_{in} and outer radius r_{out}. Spherical grains emit thermally at a temperature T_d where the incident energy flux from the star is equal to the isotropically emitted output energy flux of the grain. We approximate the emissivity ϵ_λ of the single-size dust grains by using the simple model of Backman & Paresce (1993): emissivity $\epsilon_\lambda = 1$ for $\lambda < 2\pi a$, and $\epsilon_\lambda = (\lambda/2\pi a)^{-\beta}$ for longer wavelengths, where we assume $\beta = 1.5$. Our adopted value of β is similar to that observed for zodiacal dust (see Fig. 2 of Fixsen & Dwek, 2002) and ISM grains (Backman & Paresce, 1993). The mass opacity is calculated as $\kappa_\lambda = 3\epsilon_\lambda/4a\rho$. The optical depth of emission through the disk annulus is $\tau_\lambda = \Sigma\kappa_\lambda$, where Σ is the surface density of the disk in g cm^{-2}. We calculate the orbital distance from the star (r) of dust grains heated to temperature

T using equation #5 from Wolf & Hillenbrand (2003). We verify that this relation is valid by comparing our calculations with Backman & Paresce (1993) for grains much larger than the Wien peak of incident light (blackbody case) and for grains much smaller than the Wien peak of incident light (e.g. ISM grains). For the Tuc-Hor stars, the Wien peak of incident starlight is comparable to $\bar{a}$. We assume a flat mass surface density profile ($\Sigma = \Sigma_o r_{AU}^{-p}$; $p = 0$), which is appropriate for a population of dust grains in circular orbits subject to Poynting-Robertson drag (see discussion in §4.1 of Wolf & Hillenbrand, 2003, and references therein). This predicted power law is close to what is observed for the zodiacal dust disk in our own solar system ($p = 0.34$; Kelsall et al., 1998).

Where exactly to define the inner and outer radii of a hypothetical dust disk requires some basic modeling. Among the Tuc-Hor stars, 90% of the thermal emission from our hypothetical disk model at N-band comes from within ≈1.5-2.2×r_W of the star, where r_W is the radius at which the dust is at the Wien temperature (T_W) for the isophotal wavelength of the N-band filter, and $T_W = 2898\ \lambda_{\mu\mathrm{m}}^{-1}\ (5/(\beta + 5))$ (eqn. 6.9 of Whittet, 2003). For simplicity, we adopt a consistent definition of the outer radius for all stars as $2\times r_W$. Beyond $2\times r_W$, the hypothetical dust disk contributes negligible flux (≲10%) to what is observed in the N-band filter. Approximately 50% of the thermal emission observed in N-band from a hypothetical dust disk comes from within ≲0.4-0.5× r_W of the star. For r_{in}, we adopt the radius for which the grain temperature is 1400 K – approximately the silicate dust sublimation limit. The temperatures of the inner edges of typical T Tauri star disks appear to be near this value (Muzerolle et al., 2003). For the Tuc-Hor stars, $r_{in} \sim 0.05$ AU and $r_{out} \sim 10 - 15$ AU. Hence we are most sensitive to dust at orbital radii comparable to our inner solar system.

Results for a typical set of fitted model parameters for our optically-thin disk

model are illustrated in Fig. 3.2. Our calculations suggest that the survey was sensitive to dust disk masses of $\sim 2 \times 10^{-6}\, M_{\oplus}$ ($\sim 10^{22}$ g) in a single-sized dust grain population (of uniform size $\bar{a}$, typically 0.1-2 μm). Our optically-thin model puts upper limits of $\Sigma_o \simeq 10^{-6}$-10^{-5} g cm^{-2} on the surface density of micron-sized dust grains in the ~0.1-10 AU region around the Tuc-Hor stars. *For the masses and surface densities quoted, we assume that all of the mass is in dust grains of size $\bar{a}$.* In order to convey how sensitive our assumptions are for our final results, we show the effects of changing various parameters on our results in Table 3.7. The dust disk masses that we calculate are similar to those found by other studies (Chen & Jura, 2001; Metchev, Hillenbrand, & Meyer, 2004) which also use the single grain-size approximation. The dust mass surface density upper limits that we calculate are ~10^{-7}-$10^{-6}\times$ that of the solids in the minimum mass solar nebula (Weidenschilling, 1977), however we are not sensitive to bodies much larger than the wavelength of our observations, or to gas.

3.4.3 Single-Temperature Zody Disk

Another simple model to apply to our data is that of a scaled-up version of the terrestrial-zone zodiacal dust cloud in our own solar system. Though the detailed zodiacal dust model for the inner solar system is quite complex (Kelsall et al., 1998), it can also be approximated by a single temperature blackbody (T = 260 K) with bolometric luminosity 8×10^{-8} L$_{\odot}$ (Gaidos, 1999). This luminosity and temperature imply an equivalent surface area of 5×10^{-6} AU^2 $\simeq 1 \times 10^{21}$ cm^2. Gaidos (1999) defines this area as 1 "zody" (1 $\mathcal{Z}$). The unit is useful for comparing relative amounts of exozodiacal dust between the Sun and other stars.

With none of our stars having statistically significant N-band excesses, we calculate upper limits to the number of zodys present using 3$\times$ the uncertainty in the excess measurement, assuming $T_d = 260\, K$, and blackbody emission from

Table 3.7. Effects of Changing Adopted Values on Model Output

(1) Parameter	(2) Δr_{in}	(3) Δr_{out}	(4) $\Delta\Sigma_o$	(5) ΔM_{dust}	(6) Notes
$\beta = 2$	×(1.00-1.17)	×(1.4-2.3)	/(1.3-0.26)	×(1.5-21)	crystalline case
$\beta = 1$	/(1.00-1.16)	/(1.4-2.3)	×(1.2-0.24)	/(1.6-22)	amorphous case
$\beta = 0$	/(1.01-1.74)	/(2.7-12)	×(1.5-0.013)	/(4.7-10700)	blackbody case
$\bar{a} \times 10$	/(1.01-1.73)	/(1.6-4.4)	×(9.5-0.32)	×(3.8-0.017)	···
$\bar{a} \times 100$	/(1.01-1.75)	/(1.6-7.1)	×(95-2.7)	×(38-0.054)	···
$p = 0.34$	no change	no change	×(1.3-0.6)	/(1.5-2.8)	zodiacal case
$p = 1$	no change	no change	×(1.3-0.17)	/(4.7-26)	···
$p = 1.5$	no change	no change	/(1.1-21)	/(13-140)	min. mass solar nebula case

Note. — Columns: (1) model parameter, (2-5) range of factors acted upon model values in Table 3.6 if parameter in column #1 is adopted, (6) case name.

large grains (i.e. analogous to the situation for the solar system zodiacal dust disk). An upper limit on the fraction of grain thermal emission to stellar emission ($f_d = L_{dust}/L_*$) was also calculated for each star using these assumptions. While the MIRAC photometry is capable of detecting ~4000 $\mathcal{Z}$ disks at T = 260 K (equivalent $log(f_d) < -2.9$) around the Tuc-Hor members observed, no convincing mid-IR excesses were detected.

For completeness, we note that the fraction of disk luminosity to stellar luminosity ($f_d = L_d/L_*$) has been observed to fall off as $f_d \propto age^{-1.76}$ (Spangler et al., 2001). The disk fractional luminosity is predicted to follow $f_d \propto age^{-2}$ if the observed amount of dust is proportional to the collision frequency of large particles, and P-R drag is the dominant dust removal mechanism. Recently, Dominik & Decin (2003) argue that for the very luminous debris disks that have been detected so far, the collision timescales are much shorter than the P-R drag

timescales, all the way down to the blow-out grain size. For this collision-dominated scenario, Dominik & Decin (2003) predict that the dust luminosity evolves as $f_d \propto age^{-1}$. While these models ignore effects like, e.g., gravitational perturbations, or ejections, of dust-producing planetesimals by planets (which likely had an enormous effect on the early evolution of the asteroid belt in our solar system), they provide simple, physically plausible models with which to compare observations.

If one takes the solar system zodiacal dust disk ($log(f_d) \simeq -7.1$, at $\log(age_{yr})$ = 9.66), and scale it backward in time according to Spangler et al's relation ($f_d \propto age^{-1.76}$) or the theoretical P-R drag-dominated evolution ($f_d \propto age^{-2}$), one would predict at age 30 Myr zodiacal dust disks with $log(f_d) \simeq -3.3$ (6900 $\mathcal{Z}$) or $log(f_d) \simeq -2.7$ (23000 $\mathcal{Z}$), respectively. Hence, for the simple model of collisionally replenished, P-R-drag-depleted disks, *we should have easily detected the solar system's zodiacal dust disk at age 30 Myr*. For the empirical relation (Spangler et al., 2001), we could have detected the Sun's zody disk around most (13/15) of the ~30-Myr-old Tuc-Hor stars in our sample. Backward extrapolation of the Sun's zodiacal dust disk luminosity using Dominik & Decin's relation for collisionally-dominated disks would yield $log(f_d) \simeq -4.9$ (150 $\mathcal{Z}$). Such a disk would not have been detectable in our survey, consistent with our null result. *If* analogs of the Sun's zodiacal dust disk are common around 30-Myr-old stars, f_d must evolve as a shallower power law (<1.65) than either Spangler et al.'s empirical relation or the P-R-drag-dominated dust depletion model.

3.5 Discussion

In Fig. 3.3, we plot the incidence of N-band excess versus stellar age for samples of low-mass stars. While ~80% of ~1-Myr-old stars have in Taurus have N-band

excesses (Kenyon & Hartmann, 1995), only ~10% of ~10-Myr-old stars in the TW Hya Association and β Pic Moving Group show comparable excess emission (Jayawardhana et al., 1999; Weinberger et al., 2003a,b). Of these ~10-Myr-old stars, only a few are known to have optically-thick disks (TW Hya, Hen 3-600), while the others are optically-thin disks. Our survey imaged a small number (N = 5) of Upper Sco members (~5-Myr-old) as well, among which two have clear N-band excesses. By an age of ~30 Myr, we find that N-band excesses due to optically-thick *or* optically-thick disks, are rare ($\lesssim$7%). Excluding the ~10-Myr-old star β Pic, Aumann & Probst (1991) find only one star (ζ Lep) among a sample of 548 field AFGK stars ($\approx$0.2%) with a convincing 12μm excess. These results seem to imply that *dust appears to be efficiently removed from <5-10 AU of young stars on timescales similar to that of the cessation of accretion.* While accretion terminates over a wide range of ages (~1-10 Myr; Haisch, Lada, & Lada, 2001a; Hillenbrand et al., 2004), the *duration* of the transition from optically-thick to optically-thin has been observed to be remarkably short (~10^5 yr; Skrutskie et al., 1990; Wolk & Walter, 1996).

Gravitational perturbations of small planetesimals (~0.1-100 km radius) by growing planetary embryos (~2000 km radius) can theoretically cause collisional cascades of dust grains that produce observable mid-IR signatures (Kenyon & Bromley, 2004). Simulations show that when the largest planetary embryos reach radii of ~3000 km, the population of dust-producing ~0.1-100 km-size planetesimals in the planet-forming zone becomes collisionally depleted, and N-band excesses become undetectable. The timescale over which the N-band excess would be detectable during this phase of terrestrial planet formation is of order ~1 Myr. With a larger sample size (e.g. FEPS Spitzer Legacy survey), one might be able to probe whether this is occurring around stars at age ~30 Myr. With 10% of

$\sim$10 Myr-old stars having detectable N-band excesses (Jayawardhana et al., 1999; Weinberger et al., 2003a,b), we may be witnessing the signature from runaway protoplanet growth in the terrestrial planet zone (Kenyon & Bromley, 2004). This would agree with the isotopic evidence in our own solar system that Moon- to Mars-sized protoplanetary embryos accreted within the first $\sim$10-20 Myr (Kleine et al., 2002; Kleine, Mezger, & Münker, 2003), ultimately leading to the formation of the Earth-Moon system.

3.6 Conclusions

We have undertaken a mid-IR survey of 14 young stars in the nearby $\sim$30-Myr-old Tuc-Hor Association in order to search for emission from warm circumstellar disks. No excess emission at 10 μm was detected around any Tuc-Hor members. If optically-thick disks do exist around these stars, their inner holes must be large (range: 0.2-5.8 AU). Combining our photometric results with optically-thin dust disk models, we place the following physical constraints on dust orbiting within $\sim$10 AU of these $\sim$30-Myr-old stars: fractional disk luminosities of $L_{dust}/L_* < 10^{-2.9}$ and dust emitting surface areas $<$4000$\times$ that of the inner solar system zodiacal dust. The disk masses of micron-size dust grains with orbital radii between the silicate dust sublimation point and $\sim$10 AU must be less than $\sim 10^{-6}\ M_\oplus$. The photometric upper limits also suggest that the upper limit on the surface density of micron-sized grains is $\sim 10^{-7}$ g cm^{-2}. These results imply that inner disks dissipate on timescales comparable to the cessation of accretion.

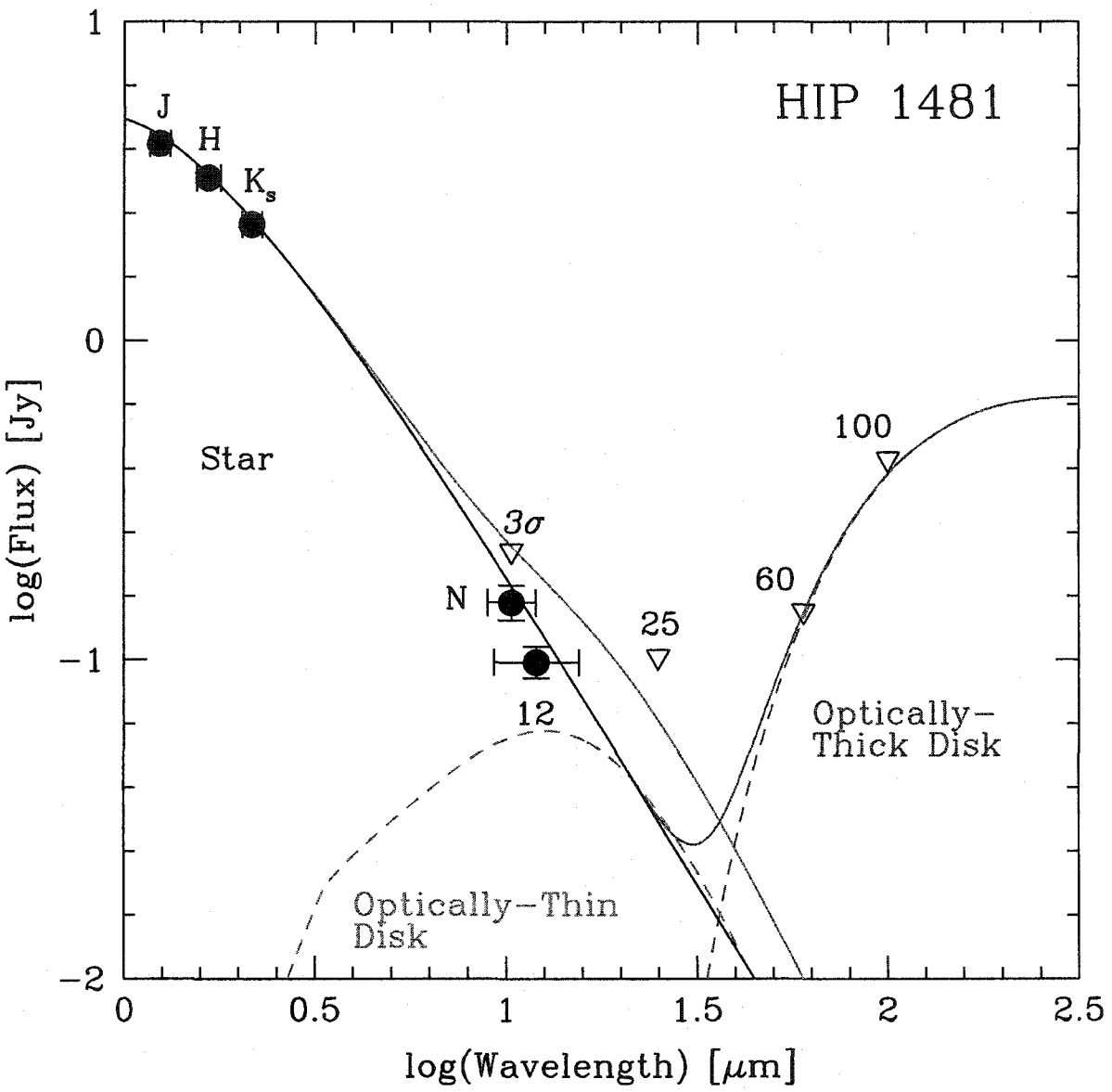

Figure 3.2: Optically-thin and thick dust models fit to the MIRAC and IRAS photometry for a typical Tuc-Hor star (HIP 1481). If the star has an optically-thick disk, its inner hole radius must be >1.8 AU (constrained by IRAS PSC 60μm upper limits). The stellar SED is approximated here as a 6026 K blackbody. The optically-thin disk model is conservatively matched to the 3× the uncertainty in the N-band excess $E(N)$. The kink in the spectral energy distribution for the optically-thin model occurs at $\lambda = 2\pi\bar{a}$ due to our simple treatment of dust emissivity (§3.4.2).

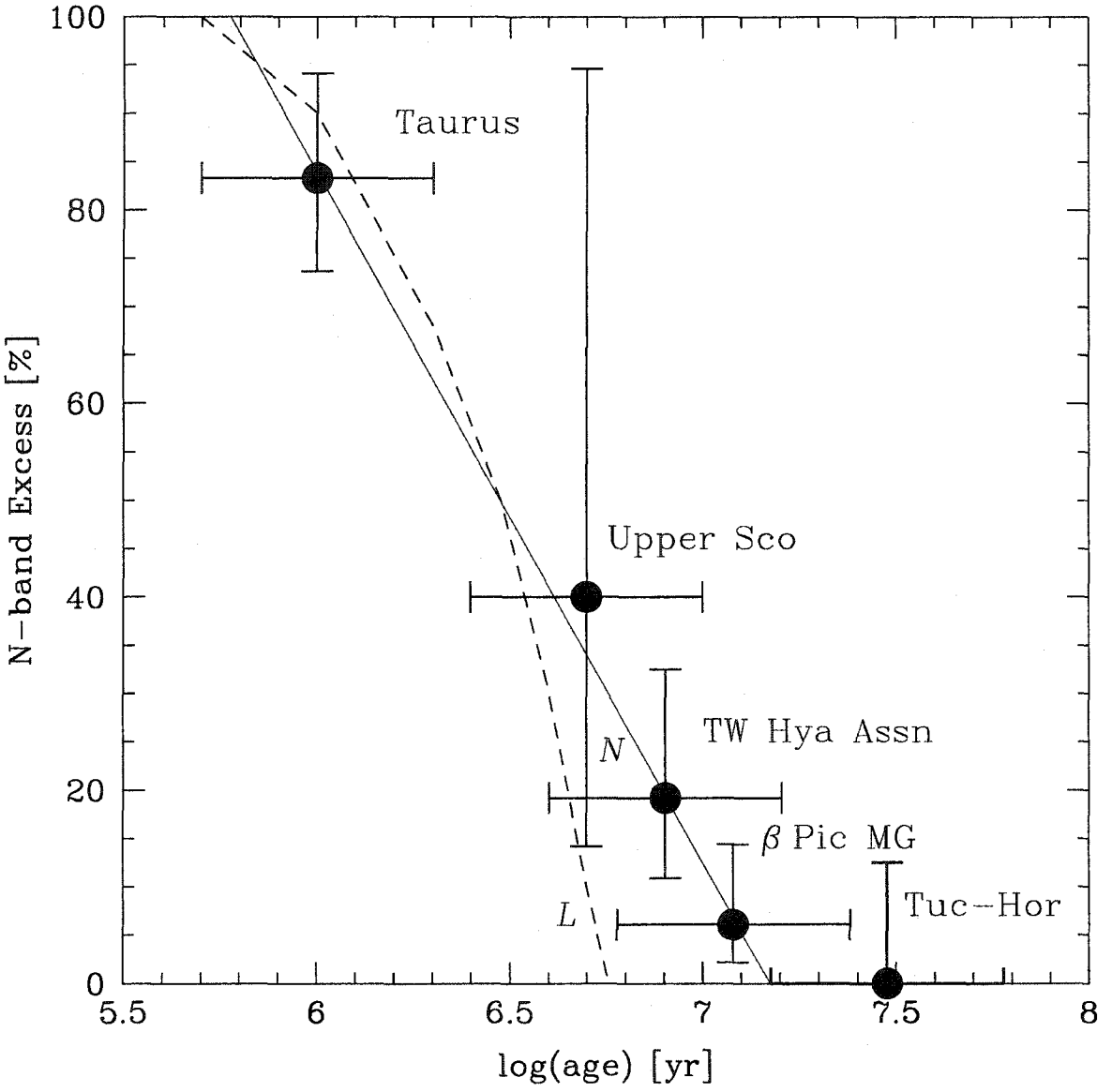

Figure 3.3: N-band excess versus age for stellar samples of varying ages. Data are plotted for the following samples: Taurus-Auriga (Kenyon & Hartmann, 1995), TW Hya Association (Jayawardhana et al., 1999; Weinberger et al., 2003a), β Pic group (Weinberger et al., 2003b), Upper Sco, and Tuc-Hor (both this study). Data from the IRAS study of AFGK-type field stars by Aumann & Probst (1991) shows that N-band excesses among mostly older ($\gtrsim$100 Myr) field stars are extraordinarily rare ($\sim$0.2%). *Dashed line* is the L-band disk fraction measured by Haisch, Lada, & Lada (2001a). The *solid line* is a fit to the N-band disk fraction for the four youngest groups. It appears that N-band excesses are only detectable for timescales marginally longer than that of L-band excesses, however the statis-

CHAPTER 4

KINEMATIC DISTANCES TO YOUNG FIELD STARS

4.1 Introduction

4.1.1 Motivation

Often in astronomy, one is interested in studying the nearest objects of a sample. The primary reasons are (1) greatest sensitivity in a fixed integration time, and (2) the highest possible spatial resolution. Both enable searches for resolved extended emission (e.g. circumstellar disks) and extremely faint companions at small physical separations (e.g. brown dwarfs and extrasolar planets).

The measurement of stellar distances is very important for other reasons. A measurement of distance, along with a determination of the star's bolometric flux, can be used to infer its luminosity. Combined with theoretical evolutionary tracks, the luminosity of a star can be used to infer an age and mass. Age can be especially difficult to estimate through other means. For regions in the Hertzsprung-Russell diagram where stars evolve relatively quickly (e.g. the pre-MS Hayashi and radiative tracks), luminosity can be a useful indicator of youth – especially when combined with corroborating evidence (e.g. stellar activity, Li abundances). For pre-MS stars in particular, trigonometric parallaxes are rare (Wichmann et al., 1998; Bertout, Robichon, & Arenou, 1999). In order to understand the recent star-formation history of the solar neighborhood, as well as identify the nearest, youngest stars for high spatial resolution imaging, we need reliable methods for assessing distances and ages for field stars.

If one has a model for the velocity field of a stellar group, and can demonstrate

that a star plausibly belongs to that kinematic group, then one can estimate the distance to an object from its proper motion. The calculation of these so-called *secular parallaxes* or *cluster parallaxes*[1] has been fundamental to establishing the cosmological distance scale and understanding stellar evolution. This technique has been most successfully applied to members of star clusters and associations (e.g. de Bruijne, 1999b; Madsen, Dravins, & Lindegren, 2002). Theoretically, it should work for any long-lived over-density in velocity space, whether the stellar members are born together or not. Olin Eggen used the cluster parallax technique with stars that he claimed were members of "superclusters" (e.g. Eggen, 1995). Although the existence of Eggen's superclusters was rather controversial before his death in 1998 (see Griffin, 1998; Taylor, 2000, for critical reviews of his work), many of Eggen's groups have been independently found by several studies using *Hipparcos* data (e.g. Dehnen, 1998; Skuljan, Hearnshaw, & Cottrell, 1999; Chereul et al., 1999). Among the most reliable identifications are three of the youngest of Eggen's groups: the Local Association (or "Pleiades Supercluster"), the Hyades supercluster, and the Ursa Major supercluster (or "Sirius supercluster").

4.1.2 The Local Association

Spectroscopic follow-up of point sources in EUV and X-ray all-sky surveys have identified a population of Li-rich, late-type stars in the solar neighborhood – presumably young pre-MS or ZAMS field stars. Most of these objects have been detected in all-sky surveys conducted by the *ROSAT* satellite at EUV (Pye et al., 1995) and X-ray (Voges et al., 1999) wavelengths. Many of these young field stars

[1] In a strict sense, the parallaxes calculated in this work are not *moving-cluster parallaxes, secular parallaxes,* or *statistical parallaxes,* as defined in §2.2 of Binney & Merrifield (1998). In a general sense, our method involves two steps: (1) statistically assessing whether a star is a plausible member of a group, and (2) estimating the distance using a predicted tangential velocity and the observed proper motion. Following de Bruijne (1999a), we will simply call parallaxes that are based on a kinematic model and observed proper motion data as *secular parallaxes.*

are more Li-rich than Pleiades members of similar spectral type, so they are likely to be <125-Myr-old (Stauffer, Schultz, & Kirkpatrick, 1998). The *ROSAT* All-Sky Survey contains $\sim 10^4$ stellar x-ray sources, the majority of which are likely to be previously unknown, young, active stars (Guillout et al., 1999).

Studies over the past decade reveal that the Li-rich stars found all over the sky have similar space motion vectors, and a relatively small velocity dispersion ($\sim 5\,\mathrm{km\,s^{-1}}$) compared to older field stars ($\sim 30\,\mathrm{km\,s^{-1}}$) (Jeffries, 1995; Wichmann, Schmitt, & Hubrig, 2003; Makarov, 2003). Since these objects were identified in flux-limited surveys (i.e. X-ray or EUV emission), the kinematic properties of these objects should be free of kinematic bias. Jeffries & Jewell (1993) and Jeffries (1995) proposed that the majority of Li-rich field stars found in the *ROSAT* EUV all-sky survey are likely to be low-mass members of Eggen's "Local Association" or "Pleiades Supercluster" (Eggen, 1961, 1975, 1995, 1998). Similarly, Wichmann & Schmitt (2003) used the X-ray *ROSAT* all-sky survey to investigate ~750 mostly G and K-type stars with Tycho proper motions, and found that 10 of the stars were definitely more Li-rich than the Pleiades (and hence younger). They also formed a tight kinematic group with a mean space motion similar to Eggen's Local Association. Wichmann, Schmitt, & Hubrig (2003) suggest that their group of 10 Li-rich stars could be evidence for the dissolution the Sco-Cen (~15 Myr-old) or Per OB3 (~50 Myr-old) associations into the field. Regardless of their origin, it is clear that the nearby, active stars with ages younger than the Pleiades have remarkably similar space motions within some small velocity dispersion, and can be considered a kinematic group. Following the work of Eggen, Jeffries, Wichmann, and other authors, we will refer to this particular concentration[2] of

[2]There is often confusion in the literature regarding the "Local Association" and "Gould Belt." What is commonly referred to as the Gould Belt is a younger (<30-90 Myr) subset of the Local Association which demonstrates peculiar kinematics (a positive K term implying expansion), and appears to be spatially isolated to tilted plane (Lindblad et al. , 1997). The definition of

Table 4.1. Parameters for the "Local Association"

Reference	Age Myr	U_o km s^{-1}	V_o km s^{-1}	W_o km s^{-1}	σ_U km s^{-1}	σ_V km s^{-1}	σ_W km s^{-1}	Notes
Eggen (1998)	0-160?	-11.6	-21.0	-11.4	NA	NA	NA	[a]
Chen et al. (1997)	70 ± 40	-10.0	-19.0	-8.1	7.9	8.6	5.8	[b]
Wichmann, Schmitt, & Hubrig (2003)	$\lesssim$125	-11.0	-21.4	-5.5	2.5	3.4	3.0	[c]
Jeffries (1995)	$\lesssim$300	-10	-21	-13	5.7	5.7	5.7	[d]

[a]The age estimate comes from interpretation of remarks in Eggen's papers (1975,1992,1998), including a manuscript ("The Local Association of Very Young Stars") submitted to AJ which went unpublished due to Eggen's death in October 1998. Eggen claimed that the LA was comprised of young field stars and members of some local clusters, OB and T associations. Eggen claimed that the oldest cluster constituent of the LA was either the Pleiades (125 Myr; Stauffer, Schultz, & Kirkpatrick, 1998) or possibly NGC 2516 (160 Myr; Sung et al., 2002).

[b]Chen et al. (1997) studied the kinematics of 1,924 BAF-type *Hipparcos* stars. They found four major clumps in velocity-age space, of which the Pleiades supercluster was one.

[c]Wichmann, Schmitt, & Hubrig (2003) surveyed 748 *ROSAT*-Tycho stars and identified 10 which were more Li-rich than the Pleiades. Their space motions were remarkably coherent, as listed.

[d]Jeffries (1995) identified a subsample of $\sim$25 very Li-rich, active, EUV-luminous, stars in the *ROSAT* WFC All-Sky Survey, and noted that their kinematic properties were similar to Eggen's LA.

stars in velocity-age space as the "Local Association" (or "LA"), and we list its vital characteristics in Table 4.1.

We maintain that if a late-type, field star is demonstrably more Li-rich than the Pleiades open cluster (and hence <125-Myr-old), there exists an excellent, empirically-measured kinematic model for such objects. We exploit the kinematic coherence of young stars, and use the observed proper motion vector to derive secular parallax distances to individual objects. In this chapter, we describe a technique for calculating secular parallaxes for the instance where a proper motion (μ_α^*, μ_δ) and radial velocity (ρ) have been measured for a star at some equa-

the Local Association appears to reflect the fact that the mean space motions of stars in the solar neighborhood younger than 125-160 Myr appear to be reasonably coherent within a small velocity dispersion.

torial position on the celestial sphere (α, δ), and one has a plausible model of a stellar velocity field (heliocentric Galactic space motion vector (U_0, V_0, W_0), velocity dispersion tensor $(\sigma_U, \sigma_V, \sigma_W)$, plus Oort parameters (A, B, C, K) to which the star may belong. The question of whether the star "belongs" to the group, or should be "rejected" as a field star, can be answered through statistical hypothesis testing.

In 4.2, we start by reviewing basic vector astrometry, and discuss how cluster parallaxes are calculated, and how cluster membership is commonly assigned. We follow this introductory material with §4.3, where we discuss how to generalize these techniques for velocity fields with anisotropic velocity dispersions and non-zero Oort constants. We also describe an iterative technique to derive kinematic distances to field stars that are statistically consistent with membership in a kinematic group. In §4.4, we discuss our test case (young stars from the FEPS Spitzer Legacy Science program), and the results (§4.5) for testing the membership of these stars to the Local Association. In §4.6, we summarize our findings and discuss future applications of this technique.

4.2 Astrometry Background Material

4.2.1 Rectangular Equatorial Coordinates

In the *rectangular equatorial system*, the unit vector $\vec{x}$ points toward Right Ascension 0 hours ($\alpha = 0°, \delta = 0°$), $\vec{y}$ points towards Right Ascension 6 hours on the celestial equator ($\alpha = 90°, \delta = 0°$), and $\vec{z}$ towards the North Celestial Pole ($\delta = 90°$). The Right Ascensions and declination coordinates are assumed to be on the International Celestial Reference System (ICRS), as adopted by the *Hipparcos and Tycho Catalog* (see §1.2.2 of ESA, 1997). The ICRS is coincident with the equinox and equator of the J2000 system (defined by the FK5 catalog) within ~80 mas (Arias

et al., 1995), but is tied to several hundred extragalactic radio sources, and is thus independent of the effects of the Earth's motion. The *Hipparcos* and *Tycho* astrometry catalogs are effectively the most accurate realization of the ICRS at optical wavelengths, and have provided the reference grid for the recent optical/near-IR sky surveys like 2MASS, Sloan Digital Sky Survey, etc.

The (x, y, z) vector components are related to the Right Ascension α, declination δ, and distance d through the following relations:

$$\begin{bmatrix} x \\ y \\ z \end{bmatrix} = d \begin{bmatrix} \cos\,\delta\,\cos\,\alpha \\ \cos\,\delta\,\sin\,\alpha \\ \sin\,\delta \end{bmatrix} \tag{4.1}$$

4.2.2 Heliocentric Galactic Coordinates

In our discussion, we use the right-handed heliocentric Galactic coordinate system. The unit vector $\vec{X}$ points toward the Galactic center (ℓ = 0°), vector $\vec{Y}$ points towards the direction of Galactic rotation (ℓ = +90°), and the vector $\vec{Z}$ points toward the North Galactic Pole (b = +90°), perpendicular to the Galactic plane. The position of a star in the heliocentric Galactic frame is (X, Y, Z) and its velocity vector is given by (U, V, W), where $U \equiv \dot{X}$, $V \equiv \dot{Y}$, and $W \equiv \dot{Z}$ (dot implies a time derivative). The position of a star in Galactic coordinates (ℓ, b), with distance d has a position (X, Y, Z) of:

$$\begin{bmatrix} X \\ Y \\ Z \end{bmatrix} = d \begin{bmatrix} \cos\,b\,\cos\,\ell \\ \cos\,b\,\sin\,\ell \\ \sin\,b \end{bmatrix} \tag{4.2}$$

The rectangular equatorial coordinates (x, y, z) and velocity $(\dot{x}, \dot{y}, \dot{z})$ can be converted to the corresponding Galactic system coordinate (X, Y, Z) and velocity

(U, V, W) components through the following matrix relations:

$$\begin{bmatrix} X \\ Y \\ Z \end{bmatrix} = \mathbf{G} \begin{bmatrix} x \\ y \\ z \end{bmatrix} \qquad \begin{bmatrix} x \\ y \\ z \end{bmatrix} = \mathbf{G^{-1}} \begin{bmatrix} X \\ Y \\ Z \end{bmatrix} \tag{4.3}$$

$$\begin{bmatrix} U \\ V \\ W \end{bmatrix} = \mathbf{G} \begin{bmatrix} \dot{x} \\ \dot{y} \\ \dot{z} \end{bmatrix} \qquad \begin{bmatrix} \dot{x} \\ \dot{y} \\ \dot{z} \end{bmatrix} = \mathbf{G^{-1}} \begin{bmatrix} U \\ V \\ W \end{bmatrix} \tag{4.4}$$

where $\boldsymbol{G^{-1}}$ implies the matrix inverse of $\boldsymbol{G}$ and

$$\mathbf{G} = \begin{bmatrix} -0.0548755604 & +0.4941094279 & -0.8676661490 \\ -0.8734370902 & -0.4448296300 & -0.1980763734 \\ -0.4838350155 & +0.7469822445 & +0.4559837762 \end{bmatrix} \tag{4.5}$$

The elements of the $\boldsymbol{G}$ matrix come from eqn. 1.5.11 of the *Hipparcos and Tycho Catalog* (ESA, 1997) and define the Galactic system on the International Celestial Reference System (see discussion in §1.5.3 of that reference). The transformation matrix $\boldsymbol{G}$ is orthogonal, so $\boldsymbol{G^{-1}}$ is simply equal to the transpose of $\boldsymbol{G}$ $(= \boldsymbol{G^T})$. On the ICRS, the North Galactic Pole is at $\alpha_G = 192^\circ.85948$ and $\delta_G = +27^\circ.12825$, and the ascending node (where the Galactic equator intercepts the equatorial "Celestial" equator) is $\ell_\Omega = 32^\circ.93192$. The transformation between equatorial coordinates (α, δ) and Galactic coordinates can be found in numerous astronomy texts (e.g. Atanasijević, 1971), or can be derived from equations 4.1, 4.2, and 4.3.

4.2.3 The Normal Triad

One can define a coordinate system known as the *normal triad* (§1.2.8; ESA, 1997) with the star at the origin on the celestial sphere, and axes $\vec{p}, \vec{q}, \vec{r}$ (see Fig. 4.1).

The vectors $\vec{p}$ and $\vec{q}$ are tangent to the celestial sphere, and $\vec{r}$ is normal to it. Component $\vec{p}$ points "east" in positive Right Ascension (α), $\vec{q}$ points towards "north" in positive declination (δ), and $\vec{r}$ connects the center of the celestial sphere to the star, moving positively with increasing radius from the sphere center[3]. The velocity component $\dot{r}$ corresponds to a star's radial velocity. The *tangential velocity* of a star is related to the velocity components in the $\vec{p}$ and $\vec{q}$ directions:

$$V_{tan}^2 = \dot{p}^2 + \dot{q}^2 \tag{4.6}$$

and the uncertainty in V_{tan} is:

$$\sigma^2(V_{tan}) = \frac{\dot{p}^2\sigma_{\dot{p}}^2 + \dot{q}^2\sigma_{\dot{q}}^2}{\dot{p}^2 + \dot{q}^2} \tag{4.7}$$

The velocity vector components $(\dot{p}, \dot{q}, \dot{r})$ can be derived from the observed quantities

(proper motions $\mu_\alpha^* (\equiv \mu_\alpha cos(\delta))$, μ_δ, distance d, and radial velocity ρ) through the following relations:

$$\begin{bmatrix} \dot{p} \\ \dot{q} \\ \dot{r} \end{bmatrix} = \begin{bmatrix} \dot{x} \\ \dot{y} \\ \dot{z} \end{bmatrix} \begin{bmatrix} -\sin\alpha & +\cos\alpha & 0 \\ -\sin\delta\cos\alpha & -\sin\delta\sin\alpha & +\cos\delta \\ +\cos\delta\cos\alpha & +\cos\delta\sin\alpha & +\sin\delta \end{bmatrix} \tag{4.8}$$

The usefulness of the normal triad system and our definition of V_{tan} will become more apparent in §4.2.6. First, we must cover the relationship between space motion and convergent points, as well as how one tests a star for membership in a kinematic group.

[3]This coordinate system is sometimes called the *astronomical trihedral* in units of $\vec{\alpha}, \vec{\delta}, \vec{r}$ (e.g. Atanasijević, 1971). We instead adopt the usage of $\vec{p}, \vec{q}, \vec{r}$, following the convention of the Hipparcos and Tycho Catalog (ESA, 1997), and some recent influential astrometry papers (e.g. de Bruijne, 1999b; Lindegren, Madsen, & Dravins, 2000)

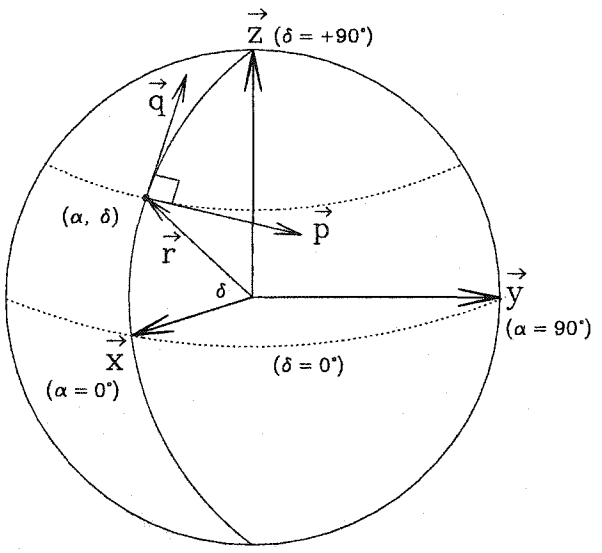

Figure 4.1: The orientation of the normal triad $(\vec{p}, \vec{q}, \vec{r})$ with respect to the rectangular equatorial system $(\vec{x}, \vec{y}, \vec{z})$ and the celestial sphere. Here, the fiducial star is at $\alpha = 0°$ and at some positive declination δ. The $\vec{p}$ and $\vec{q}$ axes are tangent to the surface of the celestial sphere. The rectangular equatorial system is heliocentric, is defined by International Celestial Reference Frame (ICRF).

4.2.4 Convergent Points and Velocity Vectors

The proper motions $(\mu_{\alpha^*}, \mu_\delta)$ for a group of stars with identical space motion vectors $(\dot{x}, \dot{y}, \dot{z})$ will appear to converge towards a *convergent point* (or *vertex*). If the position of the convergent point $(\alpha_{cp}, \delta_{cp})$ is estimated through another method (e.g. de Bruijne, 1999a), and the radial velocities (ρ) for some of the members have been determined, then one can calculate the magnitude of the group's space motion S:

$$S = \rho \sec \lambda \tag{4.9}$$

$$\cos \lambda = \cos \delta_{cp} \cos \delta \cos(\alpha_{cp} - \alpha) + \sin \delta_{cp} \sin \delta \tag{4.10}$$

where λ is the angular separation between the star and the convergent point on the sphere. Conversely, if the space motion and convergent point of the cluster is known, and the cluster is not expanding or contracting, the radial velocity ρ of a cluster member can be predicted as $\rho = S \cos \lambda$. The velocity vector for a moving group is related to the convergent point and space motion by the relation:

$$\begin{bmatrix} \dot{x} \\ \dot{y} \\ \dot{z} \end{bmatrix} = S \begin{bmatrix} \cos \delta_{cp} \cos \alpha_{cp} \\ \cos \delta_{cp} \sin \alpha_{cp} \\ \sin \delta_{cp} \end{bmatrix} \tag{4.11}$$

If need be, the equatorial velocity vector can be transformed to the Galactic system via eqn. 4.4. If a published estimate of the space motion vector for a moving group exists, one can calculate the corresponding convergent point and space motion:

$$\alpha_{cp} = \tan^{-1}\left(\frac{\dot{y}}{\dot{x}}\right) \qquad \delta_{cp} = \tan^{-1}\left(\frac{\dot{z}}{\sqrt{\dot{x}^2 + \dot{y}^2}}\right) \qquad S = \sqrt{\dot{x}^2 + \dot{y}^2 + \dot{z}^2} \tag{4.12}$$

Throughout this discussion, we assume that the velocity vectors of the stellar members of a kinematic group are normally distributed around the centroid velocity vector within some intrinsic velocity dispersion.

4.2.5 Testing for Group Membership

How do we test whether a star "belongs" to a kinematic group? Ultimately, assigning a star membership to a kinematic group is an exercise in statistical hypothesis testing. The best we can do is reject statistical outliers as non-members, and retain those objects whose properties are consistent with membership as members. An ideal kinematic group member will have all of its proper motion pointed toward the convergent point, and none of it perpendicular to the great

circle joining the star and the convergent point. We can use this as the basis for testing the hypothesis of group membership.

The proper motion components (μ_{α^*}, μ_δ) can be rotated to see how much of the stellar proper motion is oriented towards the convergent point (μ_v) and how much is perpendicular to the great circle between the star and the convergent point (μ_τ) [4]. Following de Bruijne (1999a), the rotation is calculated as:

$$\begin{bmatrix} \mu_v \\ \\ \mu_\tau \end{bmatrix} = \begin{bmatrix} +\sin\theta & +\cos\theta \\ \\ -\cos\theta & +\sin\theta \end{bmatrix} \begin{bmatrix} \mu_{\alpha^*} \\ \\ \mu_\delta \end{bmatrix} \tag{4.13}$$

where the rotation angle θ is calculated by:

$$\tan\theta = \frac{\sin(\alpha_{cp} - \alpha)}{\cos\delta \tan\delta_{cp} - \sin\delta\cos(\alpha_{cp} - \alpha)} \tag{4.14}$$

The proper motion errors are propagated as:

$$\sigma^2_{\mu_v} = \sin^2\theta\,\sigma^2_{\mu^*_\alpha} + \cos^2\theta\,\sigma^2_{\mu_\delta} \tag{4.15}$$

$$\sigma^2_{\mu_\tau} = \cos^2\theta\,\sigma^2_{\mu^*_\alpha} + \sin^2\theta\,\sigma^2_{\mu_\delta} \tag{4.16}$$

The expectation value of μ_τ for a cluster member is zero. Stellar moving groups have an intrinsic velocity dispersion, and all proper motion determinations will have measurement uncertainties, so one must determine how close μ_τ is to zero statistically.

In his work assigning membership of *Hipparcos* stars to nearby clusters and associations, de Bruijne (1999a) and de Zeeuw et al. (1999) calculate the unitless quantity $t_\perp$ which measures the deviation of the star's proper motion from that oriented exactly towards the convergent point.

$$t_\perp \equiv \frac{\mu_\tau}{\sqrt{\sigma^2_{\mu_\tau} + \sigma^{*2}_{int}}} \tag{4.17}$$

[4] We use Kapteyn's original nomenclature of these terms (μ_v,μ_τ) rather than ($\mu_\parallel$,$\mu_\perp$) used by de Bruijne (1999a). The primary motivation is so that we can adopt these letters v and τ for unique axis labels which point in the same directions as the proper motion vector (μ_v, μ_τ). The notation ($\vec{v}, \vec{\tau}$) is arguably more transparent than the cryptic ($\vec{\parallel}$,$\vec{\perp}$)

σ^*_{int} is defined as the 1D velocity dispersion of the cluster expressed in proper motion (mas yr^{-1}). In this calculation, the velocity dispersion is assumed to be isotropic. The quantity σ^*_{int} is related to the 1D velocity dispersion (σ_{int}) in velocity units (km s^{-1}) by:

$$\sigma^*_{int} = \frac{\sigma_{int}\,\bar{\pi}}{A} \tag{4.18}$$

where $\bar{\pi}$ is the mean parallax of the kinematic group (a good assumption for spatially compact groups), and A is the astronomical unit (4.74047 km yr s^{-1}).

de Bruijne (1999a) assumes that for a given position on the sky, members of a cluster will be distributed as a χ^2 distribution with ν=2 degrees of freedom about mean values of μ_v and μ_τ. In their analysis, μ_v is ignored, and the membership analysis is totally dependent on the distribution of μ_τ.

The probability that a true member of the cluster would have a $t^2_\perp$ higher than that observed can be calculated. We generically call this probability (Q) the *membership probability*. Following the notation of Press et al. (1986), one can calculate the probability from the complement to the incomplete gamma function:

$$Q \equiv \frac{1}{\Gamma(\nu/2)} \int_{t^2_\perp/2}^{\infty} e^{-t}\, t^{\nu/2-1}\, dt \;=\; e^{-t^2_\perp/2} \quad for\ \nu = 2 \tag{4.19}$$

It is apparent from eqns. 4.17 and 4.19 that stars with low accuracy proper motions (either those with large σ_{μ_τ} or small μ_τ, or both) will have small values of $t_\perp$ and large membership probability Q. The result is that large numbers of distant field stars with small proper motions moving in the same direction as a cluster convergent point, fail to be rejected as members. This was a ever-present problem for selecting members of nearby clusters and associations using Hipparcos data (e.g. de Zeeuw et al., 1999). While clusters and associations can be isolated as regions of high stellar density, supercluster members can plausibly be found

anywhere on the sky. At this point, we do not initially ignore or reject stars with low S/N proper motions.

In order to assess whether an object is considered a member or non-member, one must assign in advance a *level of significance* α. In statistical parlance, α is the probability of a Type I error, where a hypothesis is true, but rejected by the statistical test (Trumpler & Weaver, 1953). In our case, α is the fraction of bona fide cluster members that will be accidentally rejected and considered non-members. Decreasing α too much means that more and more contaminants (field stars) will not be able to be rejected as non-members, and will be considered members by the test. Increasing α too much causes more true cluster members to be rejected. We follow (Trumpler & Weaver, 1953) and adopt $\alpha = 0.05$ as our fiducial value.

4.2.6 Calculating a Cluster Parallax

The cluster parallax distances for members of moving clusters are some of the best determined distances in astronomy. The cosmological distance ladder is critically dependent on its first few rungs – the distances to the nearest open clusters. In this work, we are not interested in determining the convergent point solution or space velocity for kinematic groups – we rely on previous studies for this input. For detailed discussions on *how* to determine the convergent point for a stellar group or association, we refer the reader to Atanasijević (1971) and de Bruijne (1999a). We are mainly interested in using published convergent point solutions and high-quality proper motion and radial velocity determinations to (1) determine whether a given star is a likely member of a stellar group, and (2) if its membership can not be rejected, estimate its distance. Here we briefly discuss the cluster parallax technique and present the basic equations. In the following section we will build upon this technique for use with other velocity fields.

With knowledge of the convergent point and the proper motion of a cluster

member, the star's cluster parallax can be calculated:

$$\pi_c = \frac{A\,\mu}{S\,\sin\,\lambda} = \frac{A\,\mu}{V_{tan}} \tag{4.20}$$

where the constant A = 4.74047 is the astronomical unit (AU) in units of km yr s^{-1}, and μ is the total proper motion ($\mu^2 = \mu_{\alpha^*}^2 + \mu_\delta^2$). The quantity $S\,sin\,\lambda$ can be identified as the tangential velocity V_{tan} (Eqn. 4.6). In order to extract useful cluster parallaxes, one needs accurate μ values, and work with kinematic groups which have small intrinsic velocity dispersions compared to S.

4.3 Generalization of the Secular Parallax Technique

With the basic astrometry tools and equations presented in §4.2, one can test a star for membership in a kinematic group, and calculate a cluster parallax if the star is a member. In this section, we build on the these techniques, and generalize the calculation of secular parallaxes for stars which belong to groups with non-isotropic velocity dispersions, and non-zero Oort parameters. We also formalize the calculation of membership probability to include radial velocity information. The motivation for this project is to estimate distances to stars in the FEPS Legacy Science program, and we are fortunate to be blessed with many radial velocity determinations for these stars (Hillenbrand, in prep.). Instead of relying solely on proper motions, we incorporate radial velocity as an another criterion for membership.

This section is outlined as follows. In §4.3.1, we calculate supercluster velocity vectors when the space motion at the position of the Sun is known, as well as the Oort parameters. In §4.3.2, we generalize the calculation of the velocity dispersion in the direction tangential to the star-convergent point great circle, in order to take into account in instance of an anisotropic velocity dispersion tensor. In §4.3.3 we give a generalized kinematic criterion for supercluster membership.

Lastly, §4.3.4 discusses an iterative technique for determining secular parallaxes to supercluster members. We follow this section with our test case for this technique in §4.4.

4.3.1 Velocity Fields

When calculating a membership probability and cluster parallax for a putative member of a cluster or association, recent studies assume that the velocity dispersion is isotropic, and that the mean space motion vector for the group is independent of position (e.g. de Bruijne, 1999b; de Zeeuw et al., 1999; Madsen, Dravins, & Lindegren, 2002). For compact open clusters with small velocity dispersion, this is probably a good assumption. For OB associations, this assumption starts to breaks down, as the unbound associations are almost certainly expanding (Madsen, Dravins, & Lindegren, 2002), and can cover ~10s-100 pc is dimension (de Zeeuw et al., 1999). On these scales, the effects of differential Galactic rotation are similar in magnitude to the accuracy of space motion vectors, calculated using *Hipparcos* astrometry and published radial velocities[5]. For characterizing the space motion of a member of a supercluster, which can be situated anywhere on the sky, and plausibly anywhere within a few hundred pc of the Sun (due to the flux limits inherent in one's input sample, here the *ROSAT* All-Sky Survey and the Tycho-2 catalog), one can account for first-order corrections to the mean

[5]A simple calculation demonstrates this. Assume a hypothetical OB association 100 pc in length, whose space motion matches the Local Standard Rest (on a perfectly circular orbit of the Galaxy). Assume the near side is situated at the Sun, and the far side situated 100 pc distant toward $(\ell, b = +90°, +0°)$. The effects of differential Galactic rotation (assuming A and B Oort constants from Feast & Whitelock, 1997) on the far side will result in a difference of space motion of $\Delta U = +2.7\,\mathrm{km\,s^{-1}}$. This is similar in magnitude to the modern accuracy of radial and tangential velocities for members of nearby young groups. The typical errors for published radial velocities for young late-type stars are ~1 $\mathrm{km\,s^{-1}}$. The uncertainty in the tangential velocities for young stars at $d \sim 100$ pc with Hipparcos astrometry is similarly ~2 $\mathrm{km\,s^{-1}}$ ($V_{tan} \propto D\mu$; for accurate μ, then $\sigma_{V_{tan}}/V_{tan} \sim \sigma_D\mu/D\mu \sim \sigma_D/D \sim 1\,\mathrm{mas}/10\,\mathrm{mas} \sim 0.1$. For $V_{tan} \sim 20\,\mathrm{km\,s^{-1}}$, then $\sigma_{V_{tan}} \sim 2\,\mathrm{km\,s^{-1}}$). Hence the typical uncertainty in the any velocity component ($\sigma_U, \sigma_V, \sigma_W$) will typically be at minimum ~1-2 $\mathrm{km\,s^{-1}}$.

supercluster velocity vector.

We define the *velocity field* as a model for the space motion vector of an object as a function of its position. For a given velocity field, one can calculate the space motion as a function of Galactic coordinates and distance ($\ell, b, d \Leftrightarrow X, Y, Z$) following the first-order linear approximation of the velocity field summarized in §10.3.3 of Binney & Merrifield (1998) and §2.1 of Pöppel (1997). As a function of position (X, Y), the mean U and V velocity components can be corrected using the Oort parameters:

$$\begin{bmatrix} U \\ V \end{bmatrix} = \begin{bmatrix} U_0 \\ V_0 \end{bmatrix} + \begin{bmatrix} \delta U \\ \delta V \end{bmatrix} = \begin{bmatrix} U_0 \\ V_0 \end{bmatrix} + \begin{bmatrix} K+C & A-B \\ A+B & K-C \end{bmatrix} \begin{bmatrix} X \\ Y \end{bmatrix} \tag{4.21}$$

Where the "$_0$" subscript implies that the values are given for the origin, i.e. the Sun, and corrected for first-order effects like Galactic differential rotation. K and C are usually statistically consistent with zero for older stellar samples, consistent with an axisymmetric Galactic potential. The values of K and C are not necessarily zero for the youngest stellar samples which may still show irregularities due to the motions of the ISM from which they were born (Torra, Fernández, & Figueras , 2000). For our test case (§4.4), we adopt the space motion (U_0, V_0, W_0) of the Local Association from Wichmann, Schmitt, & Hubrig (2003), the A and B Oort parameters from Feast & Whitelock (1997), and assume $C = K = 0$. In calculating the space velocity as a function of position, we propagate the uncertainties in the mean Galactic velocity components (U_0, V_0, W_0) and the Oort parameters (A, B, C, K).

4.3.2 The Perpendicular Velocity Dispersion $\sigma_{\dot{\tau}}$

The kinematic parameters of superclusters in the literature are nearly always presented in Galactic coordinates. Recall that in calculating membership probabil-

ities for stars in open clusters and OB associations (§4.2.5; following de Bruijne, 1999a), an isotropic velocity dispersion tensor was assumed[6]. The published velocity dispersion tensors for superclusters (e.g. Asiain et al., 1999) suggest that isotropy can be a poor assumption. For superclusters, it would be more appropriate to estimate the velocity dispersion in the direction perpendicular to the great circle joining the star and the convergent point (parallel to μ_τ). We therefore generalize our membership criterion to reflect the fact that supercluster velocity dispersions can be anisotropic.

To this end we define (yet) another coordinate system tangential to the celestial sphere, which is a simple rotation of the $(\vec{p}, \vec{q}, \vec{r})$ system. We leave the radial component $\vec{r}$ unaltered. This rotation will look familiar as we previously did the same rotation in transforming the equatorial proper motions (μ_{α^*}, μ_δ) into the (μ_υ, μ_τ) system (i.e. the proper motions towards the convergent point, and perpendicular to it).

$$\begin{bmatrix} \dot{\upsilon} \\ \dot{\tau} \\ \dot{r} \end{bmatrix} = \begin{bmatrix} +\sin\theta & +\cos\theta & 0 \\ -\cos\theta & +\sin\theta & 0 \\ 0 & 0 & 1 \end{bmatrix} \begin{bmatrix} \dot{p} \\ \dot{q} \\ \dot{r} \end{bmatrix} \tag{4.22}$$

The primary purpose of this coordinate transformation is to calculate the quantity $\sigma_{\dot{\tau}}$ – the projected intrinsic velocity dispersion of the supercluster in the direction perpendicular to the star-convergent point line. This quantity is needed for the revised membership probability calculated in the next section. For clarity, we

[6]While we have been referring to the published velocity dispersion for kinematic groups (i.e. $\sigma_U, \sigma_V, \sigma_W$) as velocity dispersion *tensors*, in reality we are only dealing with the diagonal elements of such a tensor. We are currently not tracking covariances in our calculations, and the cross-terms of supercluster velocity dispersions are usually not published. Despite this, we plan on eventually eventually including covariance terms in a future version of the kinematics code.

note that an ideal supercluster member would satisfy:

$$\dot{v} = V_{tan} = S \sin \lambda \tag{4.23}$$

$$\dot{\tau} = 0 \tag{4.24}$$

$$\dot{r} = S \cos \lambda \tag{4.25}$$

i.e. only motion towards the convergent point ($\dot{v}$), and in the in the radial direction ($\dot{r}$).

4.3.3 Revised Membership Probability

We are now prepared to calculate a revised membership probability for candidate supercluster members. We incorporate both proper motion and radial velocity data, as both are readily available for our test case. We assume that for *bona fide* supercluster members the observed perpendicular proper motions μ_τ (as a function of distance), and observed radial velocities ρ, will be distributed about mean values (zero and $\dot{r}$, respectively) following a χ^2 distribution with two degrees of freedom:

$$\chi^2 = \frac{\mu_\tau^2}{\sigma_{\mu_\tau}^2 + \sigma_{\dot{\tau}}^{*\,2}} + \frac{(\rho - \dot{r})^2}{\sigma_\rho^2 + \sigma_{\dot{r}}^2} \tag{4.26}$$

The definition for each variable is as follows: $\mu_\tau\,(\pm\sigma_{\mu_\tau})$ is the observed proper motion in the τ direction (eqn. 4.13), $\rho\,(\pm\sigma_\rho)$ is the observed radial velocity, and $\dot{r}\,(\pm\sigma_{\dot{r}})$ is the predicted radial velocity (and uncertainty) from the model velocity field (from Eqn. 4.8, and simple error propagation of that expression). The quantity $\sigma_{\dot{\tau}}^*$ is the *intrinsic 1D velocity dispersion of the supercluster in the direction perpendicular to the star-convergent point line* at the estimated distance to the star in proper motion units:

$$\sigma_{\dot{\tau}}^* = \frac{\sigma_{\dot{\tau}}\,\hat{\pi}}{A} \tag{4.27}$$

where σ_{τ} is the velocity dispersion in the τ direction in $\mathrm{km\,s^{-1}}$(Eqn. 4.22), $\hat{\pi}$ is the estimated stellar parallax in milliarcseconds, and A is the astronomical unit (4.74...) as before. The value σ^*_{τ} is analogous to the σ^*_{int} term used by de Bruijne (1999a) for the isotropic 1D velocity dispersion of a cluster or association. We define σ^*_{τ} differently from σ^*_{int} since we are dealing with (1) anisotropic velocity dispersions, and (2) supercluster members do not necessarily clump at some mean distance, as do members of open clusters or OB associations. The secular parallax estimate $\hat{\pi}$ (and uncertainty) is:

$$\hat{\pi} = \frac{A\,\mu}{V_{tan}} \tag{4.28}$$

$$\sigma_{\hat{\pi}} = \frac{A}{V_{tan}}\sqrt{\sigma^2_{\mu} + \sigma^2_{V_{tan}}\mu^2 V_{tan}^{-2}} \tag{4.29}$$

The membership probability can be derived from the complement to the incomplete gamma function with $\nu = 2$ degrees of freedom (Press et al., 1986), analogous to Eqn. 4.19. Instead of the variable $t_{\perp}$ used in Eqn. 4.17 and 4.19, we intuitively retain use of the χ^2 value:

$$Q \equiv \frac{1}{\Gamma(\nu/2)}\int_{\chi^2/2}^{\infty} e^{-t}\,t^{\nu/2-1}\,dt = e^{-\chi^2/2} \quad for\ \nu = 2 \tag{4.30}$$

For a star that is not rejected as a member, we estimate the distance D (in pc) from the calculated secular parallax $\hat{\pi}$ (in mas) from:

$$\hat{D} = \frac{1000}{\hat{\pi}} \tag{4.31}$$

4.3.4 Iterative Algorithm

Since the mean velocity vector for a supercluster is position-dependent, and the distance to the candidate supercluster members is unknown *a priori*, we devise an iterative scheme for converging on values of the membership probability and

secular parallax for a given star.

[1] Start with an initial guess of the distance (nominally 100 pc – the final value will be quite insensitive to the initial guess) and calculate the space motion (U, V, W) from the velocity field parameters $(U_0, V_0, W_0, A, B, C, K)$ evaluated at the star's coordinates (ℓ, b) and initial guess distance d (§4.3.1).

[2] Transform the calculated space motion (U, V, W) to rectangular equatorial coordinates $(\dot{x}, \dot{y}, \dot{z})$ (§4.2.2). Calculate the convergent point $(\alpha_{cp}, \delta_{cp})$ and space motion (S) from $(\dot{x}, \dot{y}, \dot{z})$ (§4.2.4). Calculate the predicted tangential motion V_{tan} for a supercluster member at that position (§4.2.3).

[3] Use the convergent point solution $(\alpha_{cp}, \delta_{cp}, S)$, the predicted tangential motion (V_{tan}), and the star's proper motion (μ) to calculate a membership probability and new secular parallax estimate $(\hat{\pi})$ (§4.3.3).

[4] Using the new secular parallax, repeat steps [1] through [3] until the difference between the old and new secular parallaxes is smaller than some threshold value.

We find that the secular parallaxes converge to a precision of 10^{-6} within $\mathrm{N} \simeq 5 \pm 1$ iterations for the LA convergent point solution. Secular parallax distances are only to be taken seriously for stars whose membership probabilities Q are above some rejection threshold (α; §4.2.5). Since the membership probability definition is distance-dependent, and cycling through these calculations on a modern computer takes a trivial amount of time, we calculate the membership

probabilities at each step, but do not reject a star as a member until the final iteration.

4.4 Sample Selection

Next we examine the efficacy of our technique for estimating the distances to young field stars. From a large parent sample (stars from the "Formation and Evolution of Planetary Systems" (FEPS) Spitzer Space Telescope (SST) Legacy Science program[7] (Meyer et al., 2004)), we select stars that are plausibly <125-Myr-old by virtue of their Li data, and then kinematically test these stars for membership in the $\lesssim$125-160 Myr-old Local Association. The Li selection is an efficient means of excluding older interlopers from consideration as members.

There are 353 stars in the FEPS program, and the stars were originally selected by age, populating six logarithmically-spaced bins between 3 Myr and 3 Gyr. From this parent sample of 353 FEPS stars with extensive ancillary data, we apply a lithium criteria for isolating those that are plausibly $\lesssim$125 Myr-old. The majority of the FEPS stars considered have measurements of the equivalent width of the Li I λ6707Å line taken at high resolution (R = 20,000) with the Palomar 60" by Hillenbrand et al. (in prep.). The same study measured radial velocities for one or more epochs for these stars, with typical accuracy of $\sim$0.6 km s^{-1}. We omitted most of the young FEPS stars that had reliable membership assignments (members of Sco-Cen, IC 2602, etc.), but included some as "tracers" as a check of our technique.

We placed statistical constraints on the ages of the FEPS stars by comparing their T_{eff} and EW(Li) data to that for the 125-Myr-old Pleiades cluster. First, we combine all of the high-resolution measurements of EW(Li) for Pleiades FGK

[7] http://feps.as.arizona.edu

stars from the literature (Butler et al., 1987; Pilachowski, Booth, & Hobbs, 1987; Boesgaard, Budge, & Ramsay, 1988; Soderblom et al., 1993; Garcia Lopez, Rebolo, & Martin, 1994; Jones et al., 1996; Jeffries, 1999). If multiple measurements were available for any star, we preferred the values taken at higher resolution or higher signal-to-noise. Overall, 153 Pleiades members had high resolution EW(Li) measurements. Three stars (HII 948, HII 1794, HII 2208) were rejected as Li-poor outliers, and were noted as such in previous studies. We fit a polynomial to the data in the region devoid of EW(Li) upper limits, between 4300 K $< T_{eff} <$ 6720 K, where we have 119 data points. The distribution of log(EW(Li)) values for Pleiades members is well represented by a quadratic fit with different variances on either side of 5300 K.

$$log(EW(Li)) = -5.962278 + (3.133483E-3)\,x - (2.986343E-7)\,x^2 \qquad (4.32)$$

Where $x \equiv$ log(EW(Li)), the EW(Li) values are in units of mÅ, and their published error estimates are typically ~0.02 dex. The observed rms scatter for Pleiades members between 4300 K $<$ T_{eff} $<$ 5300K is 0.213 dex, and only 0.066 for those with 5300 K $<$ T_{eff} $<$ 6720 K.

We classify stars as younger than the Pleiades when their EW(Li) value is higher than 95% of Pleiades for a given effective temperature. For a normal distribution, 5% of Pleiades members will have EW(Li) values more than +1.645σ above equation 4.32. In other words, with data for bona fide Pleiades cluster members, we would consider 95% as being consistent with the age of the Pleiades, and 5% would fall above +1.645σ, and be incorrectly considered younger than the Pleiades. Indeed, testing the 119 Pleiades members in the temperature range where our fit is relevant, we find that 4/119 (3.4%) are rejected as Li-rich outliers. This is within the Poisson noise, and consistent with our prediction. Our

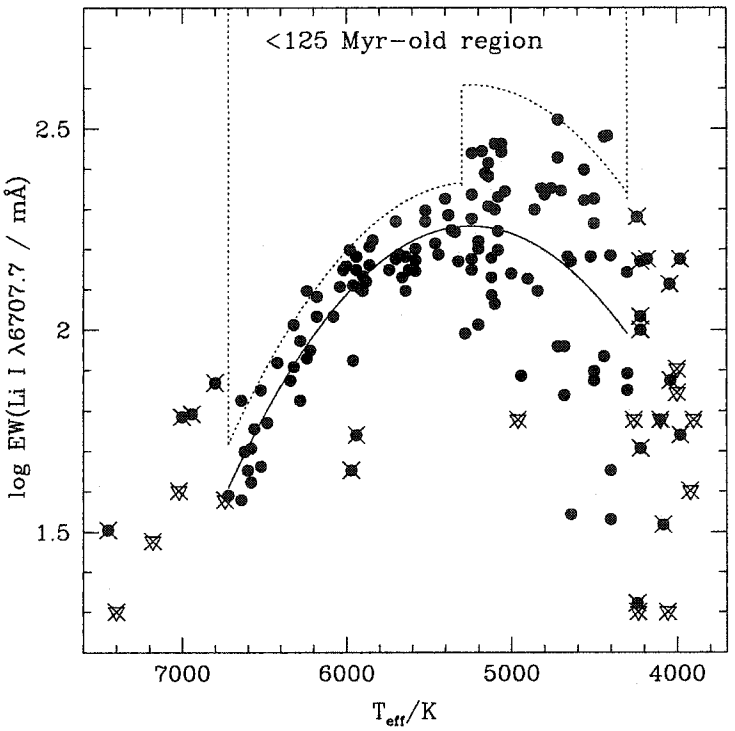

Figure 4.2: The distribution of T_{eff} vs. EW(Li) values for Pleiades members. The region for selecting stars that we consider <125-Myr-old is outlined in a dashed line.

test will, however, reject many stars whose ages are likely to be <125 Myr, but whose EW(Li) values lie in the locus of Pleiades data points. For example, a ~50-Myr-old Li-poor star may have a EW(Li) value within the locus of points for the 125-Myr-old Pleiades. Such a star would *not* be selected as younger than the Pleaides.

Of the 353 stars in the FEPS Legacy Science survey, 287 (81%) currently have measurements of the Li I λ6707Å line. Of these 287 stars, 72 have lithium values within the "<125 Myr" selection region in Fig. 4.2, i.e. are more Li-rich than 95% of Pleiades for a given T_{eff}.

Of these 72 Li-rich stars, we chose roughly half (32) that had accurate ra-

dial velocity measurements (required for our kinematic analysis). Most of these remaining stars that were previously known to be members of clusters or associations were omitted, but a few were retained for independent verification. Hence, our sample consists of ~10% of the original FEPS sample, but includes the youngest stars in the program. The input astrometry and photometric data for these stars are listed in Table 4.2. As mentioned in §4.3.1, we adopt the Local Association as defined by Wichmann, Schmitt, & Hubrig (2003, parameters given in Table 4.1) as the supercluster to which we test membership for the young FEPS stars.

Table 4.2. Sample of FEPS Targets Younger than the Pleiades (<125 Myr-old)

Name	α(ICRS)	δ(ICRS)	$\mu_{\alpha*}$	μ_δ	π_{trig}	Spec.	T_{eff}	EW(Li)	RV	A_V	Prob.	Kin.
...	h m s	° ′ ″	mas yr^{-1}	mas yr^{-1}	mas	Type	K	mÅ	km s^{-1}	mag	%	Mem.?
RE J0137+18A	01:37:39.41	+18:35:33.16	+65.8 ± 1.9	-46.0 ± 2.5	...	K3Ve	4837	416 ± 7	+1.8 ± 2.2	0.00	72.3	Y
1RXS J025751.8+115759	02:57:51.68	+11:58:05.83	+31.4 ± 1.2	-28.4 ± 1.2	...	G7V	5509	232 ± 12	+12.0 ± 2.2	0.72 ± 0.08	41.9	Y
1RXS J031644.0+192259	03:16:43.89	+19:23:04.11	+11.2 ± 1.3	-8.5 ± 1.3	32 ± 44	G2V	5856	190 ± 10	+8.2 ± 1.2	0.04 ± 0.07	35.6	Y
1E 0324.1-2012	03:26:22.05	-20:01:48.81	+25.0 ± 1.6	+7.4 ± 1.6	-74 ± 39	G4V	5717	203 ± 13	+26.0 ± 0.6	0.07 ± 0.05	0.0	N
RX J0331.1+0713	03:31:08.38	+07:13:24.78	+13.7 ± 1.5	-13.1 ± 1.3	...	K4Ve	4632	371 ± 11	+15.4 ± 0.3	0.00	34.1	Y
HD 22179	03:35:29.91	+31:13:37.45	+42.6 ± 0.6	-46.0 ± 0.7	15 ± 11	G5IV	5986	179 ± 9	+11.6 ± 0.6	0.12 ± 0.10:	4.5	N
1RXS J035028.0+163121	03:50:28.40	+16:31:15.19	+26.2 ± 1.3	-23.4 ± 2.1	...	G5IV	5681	206 ± 11	+8.0 ± 0.6	0.37 ± 0.06	66.8	Y
RX J0357.3+1258	03:57:21.39	+12:58:16.83	+22.7 ± 1.8	-21.9 ± 1.5	-20 ± 98	G0	5970	245 ± 16	+6.8 ± 0.6	0.58 ± 0.06	31.4	Y
HD 285281	04:00:31.07	+19:35:20.70	+2.7 ± 1.1	-12.9 ± 1.2	-37 ± 40	K1	5123	409 ± 9	+16.1 ± 0.6	0.69 ± 0.05	0.1	N
HD 285372	04:03:24.95	+17:24:26.12	+4.8 ± 2.0	-14.4 ± 2.0	...	K3V	4759	653 ± 13	+10.2 ± 0.7	0.78 ± 0.12	15.6	Y
HD 284135	04:05:40.58	+22:48:12.14	+6.0 ± 0.6	-14.9 ± 0.6	16 ± 19	G3V	5793	208 ± 8	+12.8 ± 1.2	0.09 ± 0.04	4.8	N
HD 279788	04:26:37.40	+38:45:02.37	+5.8 ± 1.1	-28.6 ± 1.0	114 ± 67	G5V	5681	267 ± 14	+11.4 ± 0.4	0.68 ± 0.07	0.1	N
1RXS J043243.2-152003	04:32:43.51	-15:20:11.39	+2.3 ± 1.1	+14.2 ± 1.1	80 ± 35	G4V	5779	278 ± 12	+17.6 ± 0.6	0.37 ± 0.05	0.0	N
RX J0442.5+0906	04:42:32.09	+09:06:00.86	+28.9 ± 2.4	-22.3 ± 2.0	132 ± 52	G5V	5661	247 ± 12	+19.7 ± 0.6	0.45 ± 0.09	10.8	Y
HD 286179	04:57:00.65	+15:17:53.09	-1.8 ± 1.5	-17.3 ± 1.4	-13 ± 31	G3V	5705	205 ± 15	+13.8 ± 0.4	0.41 ± 0.06	0.0	N
HD 31950	05:00:24.31	+15:05:25.28	+0.3 ± 1.1	-15.2 ± 1.1	-41 ± 31	...	6104	150 ± 8	+13.9 ± 0.6	0.12 ± 0.10:	0.5	N
HD 286264	05:00:49.28	+15:27:00.68	+20.0 ± 1.4	-59.0 ± 1.4	...	K2IV	4995	423 ± 7	+18.1 ± 0.6	1.09 ± 0.08	19.5	Y
1RXS J051111.1+281353	05:11:10.53	+28:13:50.38	+6.0 ± 0.8	-24.0 ± 0.7	36 ± 64	K0V	5267	464 ± 9	+11.6 ± 1.2	0.92 ± 0.07	37.3	Y
HD 245567	05:37:18.44	+13:34:52.52	+7.5 ± 0.9	-33.2 ± 0.9	26 ± 22	G0V	6050	276 ± 9	+14.4 ± 0.5	0.63 ± 0.04	44.8	Y
SAO 150676	05:40:20.74	-19:40:10.85	+19.2 ± 1.2	-12.9 ± 1.2	4 ± 10	G2V	5827	216 ± 8	+24.8 ± 0.5	0.00	95.7	Y
AO Men	06:18:28.24	-72:02:41.56	-7.9 ± 1.0	+74.3 ± 1.0	26 ± 1	K3V	4359	357:	+16.2 ± 0.7	0.00	20.4	Y

4.5 Results

In subjecting the astrometric and radial velocity data for the young FEPS stars to our iterative procedure in §4.3.4, we found that 24/32 (75%) of the objects *are statistically consistent with Local Association membership*. Since the stars were pre-selected to be more Li-rich than the Pleiades, we already know that their true ages (as inferred from Li abundances) are probably consistent with being Local Association members.

With the availability of color-magnitude information, reddening estimates, and effective temperatures, we would like to plot these stars on the HR diagram to see if they are consistent with being very young, i.e. pre-MS. In order to do this, we calculate how much above the ZAMS a particular star is using both empirical isochrones and theoretical evolutionary tracks. It has been recently found that *no set of widely-used, modern isochrones can fully fit the observed color-magnitude data for open clusters across the full main sequence* (Grocholski & Sarajedini, 2003). The systematic differences between the different theoretical ZAMS lines (in $(V - K_s)$ vs. M_V) are of the order $\Delta(V - K_s) \simeq 0.05 - 0.1$ mag, which can translate into luminosity offsets of $\Delta \log \mathrm{L/L_\odot} \simeq$ 0.05-0.1 dex for solar-type stars. To mitigate against the systematic differences between theoretical tracks and observed color-magnitude data, we do the following:

[1] Using the available V and K_s photometry, and reddening estimate A_V from the FEPS database (Carpenter, in prep.), we deredden the observed V magnitude and $(V - K_s)$ color to produce V_o and $(V - K_s)_o$.

[2] Estimate the absolute magnitude M_V for a ZAMS star of similar $(V - K_s)_o$.

Table 4.2—Continued

Name	α(ICRS)	δ(ICRS)	μ_{α^*}	μ_δ	π_{trig}	Spec.	T_{eff}	EW(Li)	RV	A_V	Prob.	Kin.
...	h m s	$^\circ$ ′ ″	mas yr^{-1}	mas yr^{-1}	mas	Type	K	mÅ	km s^{-1}	mag	%	Mem.?
RX J0850.1-7554	08:50:05.41	-75:54:38.11	-18.5 ± 1.5	$+33.1 \pm 1.3$	-14 ± 27	G5	5711	250 ± 15	$+15.5 \pm 2.0$	0.31 ± 0.02	80.1	Y
HD 86356	09:51:50.70	-79:01:37.73	-25.9 ± 1.1	$+39.0 \pm 1.5$	68 ± 19	G6/K0	5611	260 ± 15	$+12.2 \pm 2.0$	0.52 ± 0.03	10.8	Y
RX J1111.7-7620	11:11:46.32	-76:20:09.21	-17.2 ± 5.2	$+6.9 \pm 5.2$	...	K1	4621	500:	$+19.0 \pm 2.0$	1.30 ± 0.05	17.2	Y
HD 104467	12:01:39.15	-78:59:16.85	-41.0 ± 1.0	-4.4 ± 1.1	2 ± 7	G5III/IV	5690	255:	$+21.7 \pm 4.0$	0.14 ± 0.02	6.9	Y
HD 141943	15:53:27.29	-42:16:00.81	-42.2 ± 1.1	-65.3 ± 1.1	8 ± 13	G0/2V	5805	230:	$+1.9 \pm 5.6$	0.00	62.0	Y
HD 142361	15:54:59.86	-23:47:18.26	-29.3 ± 1.1	-38.8 ± 1.1	6 ± 15	G3V	5833	260 ± 7	-4.6 ± 0.8	0.45 ± 0.02	42.8	Y
ScoPMS 214	16:29:48.70	-21:52:11.91	-5.6 ± 3.6	-22.1 ± 1.8	...	K0IV	5318	426 ± 11	-7.6 ± 0.9	1.69 ± 0.03	12.1	Y
HD 174656	18:53:05.99	-36:10:22.91	$+3.8 \pm 1.3$	-24.7 ± 1.1	-63 ± 29	G6IV	5629	348 ± 6	-5.1 ± 0.6	0.84 ± 0.04	25.2	Y
RX J1917.4-3756	19:17:23.83	-37:56:50.52	$+8.3 \pm 1.3$	-27.3 ± 1.0	37 ± 31	K2	5001	443 ± 9	-2.4 ± 0.6	0.49 ± 0.05	6.1	Y
HD 191089	20:09:05.22	-26:13:26.63	$+39.3 \pm 1.1$	-68.2 ± 1.2	19 ± 1	F5V	6441	96 ± 5	-7.8 ± 2.2	0.00	17.8	Y
HD 202917	21:20:49.95	-53:02:03.05	$+30.2 \pm 1.5$	-97.2 ± 1.6	22 ± 1	G5V	5553	233:	-5.3 ± 1.0	0.00	5.3	Y

Note. — Columns: (1) Name, (2) Right Ascension (ICRS), (3) declination (ICRS), (4-5) proper motion in R.A. and dec, from UCAC2 catalog if available (Zacharias et al., 2003), or Tycho-2 (Høg et al., 2000a), or Hipparcos (ESA, 1997), (6) trigonometric parallax from Hipparcos or Tycho-1 (ESA, 1997). Those with errors in parallax of >5 mas are from Tycho-1, the rest from Hipparcos. Columns (7-11) are from the "Formation and Evolution of Planetary Systems" (FEPS) Spitzer Legacy Science database. (7) spectral type (mostly from Michigan Spectral Atlas Vols. 1-5; e.g. Houk & Cowley, 1975), (8) effective temperature (Carpenter et al., in prep.), (9) equivalent width of Li I λ6707.7Å(Hillenbrand et al., in prep.), (10) radial velocity (Hillenbrand et al., in prep.), (11) V magnitude extinction A_V (Carpenter et al., in prep.), (12) Membership probability Q defined in §4.3.3, (13) Is the star selected as member of the Local Association based on kinematic criteria ($Q > 5\%$)?

[3] Calculate the difference in absolute magnitude (ΔM_V) between that predicted with the secular parallax distance (M_V(sec)) vs. that predicted with the empirical ZAMS (M_V(ZAMS)).

[4] Estimate the difference in bolometric luminosity between the secular parallax solution and the ZAMS solution as $\Delta log(L) = -0.4\Delta M_V$. To calculate a luminosity "calibrated" for use with the evolutionary tracks, add $\Delta log(L)$ to the luminosity of an object with similar T_{eff} on the 625 Myr-old solar metallicity isochrone.

For the empirical ZAMS, we adopt the high-quality, single-star ZAMS for the Hyades from Pinsonneault et al. (2004) ($(V - K_s)_o$ vs. M_V). We then corrected this ZAMS to solar metallicity using the $(V - K_s)$ vs. [Fe/H] correction from Sarajedini et al. (2004), and assuming the Hyades metallicity ([Fe/H] = +0.13) from Paulson, Sneden, & Cochran (2003). The color shift to solar metallicity was $\Delta(J - K_s)$ = -0.024 mag. For the solar metallicity 625-Myr-old isochrone, we interpolate values from the evolutionary tracks of D'Antona & Mazzitelli (1997), and normalize these tracks to the Hyades locus for solar metallicity.

Since our stars were selected to be <125-Myr-old by virtue of their lithium, we predict that the HRD for these stars should mostly consist of ZAMS stars, with some pre-MS stars. The pre-MS epoch for a 1 $M_\odot$ stars is ~40 Myr, so if the sample stars were equally distributed in age between 0-125 Myr, we would naively expect ~2/3rds to be ZAMS, and 1/3rd to be pre-MS, and no stars below the ZAMS. In order to estimate an *isochronal age* for each star, we take the estimated T_{eff} and "calibrated" log L/L$_\odot$ values, and generate 10^4 Monte Carlo HRD positions for each star with the associated uncertainties in $\sigma_{T_{eff}}$ and $\sigma_{log(L/L_\odot)}$. We

interpolate ages and masses for these Monte Carlo points on the D'Antona & Mazzitelli (1997) evolutionary tracks. Due to the results of our lithium test in §4.4, we *rejected those Monte Carlo-generated ages and masses when the isochronal ages wer >125 Myr*. We also reject isochronal ages of <0.1 Myr, as these HRD positions would lie above the stellar birthline and be inconsistent with the appearance of an unembedded star with little reddening. The fraction of the Monte Carlo data points that are rejected due to our Li criterion is listed in column (8) of Table 4.3. For the remaining Monte Carlo values of age and mass, we calculate the median value and assign 68.3% (1σ) confidence intervals. These values are given in columns (6) and (7) of Table 4.3. The HRD for the FEPS stars that we select as Local Association members is shown in Fig. 4.3.

As seen in Fig. 4.3, none of the FEPS stars selected as Local Association members is more than 1.2σ below the ZAMS. Some of the stars appear to be very young (<10 Myr). We see that roughly half of the stars (11) are within 2σ of the ZAMS. Only three of the stars in Table 4.2 have accurate *Hipparcos* distances. The predicted secular parallax distances versus the *Hipparcos* distances are as follows: AO Men (37 ± 1 pc vs. 50 ± 9 pc; $+1.4\sigma$), HD 191089 (54 ± 3 pc vs. 59 ± 9 pc; $+0.6\sigma$), and HD 202917 (46 ± 2 pc vs. 53 ± 7 pc; $+1.0\sigma$).

Can the isochronal ages listed in Table 4.3 be independently verified by other means? AO Men is claimed to be a member of the ~12 Myr-old β Pic Moving Group (Zuckerman, Song, Bessell, & Webb, 2001). Using the iterative secular parallax calculated for AO Men, we derive an isochronal age for AO Men of 11^{+12}_{-6} Myr, in agreement with Zuckerman et al.'s assessment. HD 202917 is claimed to be a member of the ~30 Myr-old Tucana-Horologium association (Zuckerman, Song, & Webb, 2001, we agree with this assessment in §3 of this thesis). The iterative secular parallax calculated for HD 202917 leads to an isochronal age of 28^{+12}_{-8}

Table 4.3. Kinematically-Selected Local Association Members

Name	Distance	ΔM_V	$\log(T_{eff})$	$\log L/L_\odot$	Isochronal Age	Mass	Fraction
...	pc	mag	K	...	log(yr)	$M_\odot$	%
RE J0137+18A	64 ± 8	-1.14 ± 0.31	3.685 ± 0.005	-0.20 ± 0.12	$6.97^{+0.22}_{-0.21}$	$1.05^{+0.06}_{-0.09}$	100
1RXS J025751.8	118 ± 16	-0.11 ± 0.45	3.741 ± 0.004	-0.18 ± 0.18	$7.38^{+0.17}_{-0.22}$	$1.00^{+0.11}_{-0.03}$	67
1RXS J031644.0	365 ± 60	-1.30 ± 0.50	3.768 ± 0.004	0.53 ± 0.20	$7.03^{+0.17}_{-0.18}$	$1.42^{+0.23}_{-0.18}$	99
RX J0331.1+0713	250 ± 40	-3.12 ± 0.38	3.666 ± 0.005	0.45 ± 0.15	$5.65^{+0.23}_{-0.19}$	$0.80^{+0.09}_{-0.07}$	100
1RXS J035028.0	138 ± 21	-0.24 ± 0.41	3.754 ± 0.004	-0.01 ± 0.17	$7.36^{+0.10}_{-0.15}$	$1.06^{+0.11}_{-0.05}$	72
RX J0357.3+1258	149 ± 23	0.54 ± 0.45	3.776 ± 0.004	-0.12 ± 0.18	$7.41^{+0.06}_{-0.10}$	1.15 ± 0.02	13
HD 285372	343 ± 69	-2.78 ± 0.52	3.678 ± 0.005	0.39 ± 0.21	$5.95^{+0.30}_{-0.27}$	$1.05^{+0.12}_{-0.11}$	100
RX J0442.5+0906	119 ± 21	0.72 ± 0.58	3.753 ± 0.004	-0.41 ± 0.23	$7.43^{+0.15}_{-0.14}$	$1.02^{+0.05}_{-0.03}$	12
HD 286264	71 ± 11	-0.51 ± 0.44	3.699 ± 0.004	-0.35 ± 0.18	$7.34^{+0.25}_{-0.27}$	$0.92^{+0.16}_{-0.10}$	90
1RXS J051111.1	199 ± 29	-2.36 ± 0.40	3.722 ± 0.004	0.55 ± 0.16	$6.44^{+0.20}_{-0.21}$	$1.83^{+0.22}_{-0.21}$	100
HD 245567	119 ± 21	-0.58 ± 0.42	3.782 ± 0.004	0.37 ± 0.17	$7.23^{+0.14}_{-0.12}$	$1.26^{+0.13}_{-0.08}$	91
SAO 150676	78 ± 30	-0.07 ± 0.89	3.765 ± 0.004	0.02 ± 0.36	$7.26^{+0.16}_{-0.24}$	$1.17^{+0.25}_{-0.08}$	53
AO Men	50 ± 9	-1.14 ± 0.38	3.639 ± 0.005	-0.49 ± 0.15	$7.04^{+0.32}_{-0.34}$	$0.84^{+0.04}_{-0.07}$	100
RX J0850.1-7554	112 ± 18	0.23 ± 0.35	3.757 ± 0.004	-0.18 ± 0.14	$7.44^{+0.12}_{-0.09}$	$1.04^{+0.04}_{-0.03}$	28
HD 86356	99 ± 15	-0.30 ± 0.34	3.749 ± 0.004	-0.03 ± 0.14	$7.37^{+0.10}_{-0.13}$	$1.04^{+0.09}_{-0.04}$	82
RX J1111.7-7620	291 ± 91	-4.01 ± 0.71	3.665 ± 0.005	0.80 ± 0.28	$5.35^{+0.26}_{-0.21}$	$0.84^{+0.16}_{-0.10}$	84
HD 104467	118 ± 15	-1.89 ± 0.29	3.755 ± 0.004	0.65 ± 0.12	$6.79^{+0.13}_{-0.17}$	$1.68^{+0.23}_{-0.17}$	100
HD 141943	67 ± 9	-1.04 ± 0.29	3.764 ± 0.004	0.39 ± 0.12	7.12 ± 0.11	$1.32^{+0.11}_{-0.12}$	100
HD 142361	101 ± 14	-1.08 ± 0.32	3.766 ± 0.004	0.42 ± 0.13	7.10 ± 0.12	1.34 ± 0.12	100
ScoPMS 214	215 ± 41	-2.45 ± 0.42	3.726 ± 0.004	0.62 ± 0.17	6.41 ± 0.21	$1.94^{+0.25}_{-0.25}$	100
HD 174656	193 ± 29	-2.40 ± 0.37	3.750 ± 0.004	0.81 ± 0.15	$6.48^{+0.24}_{-0.12}$	$2.08^{+0.28}_{-0.32}$	100
RX J1917.4-3756	173 ± 25	-2.72 ± 0.34	3.699 ± 0.004	0.52 ± 0.14	$6.14^{+0.19}_{-0.18}$	$1.53^{+0.11}_{-0.10}$	100
HD 191089	59 ± 9	-0.13 ± 0.34	3.809 ± 0.003	0.47 ± 0.14	$7.24^{+0.16}_{-0.12}$	$1.41^{+0.08}_{-0.07}$	68
HD 202917	53 ± 7	-0.05 ± 0.28	3.745 ± 0.004	-0.17 ± 0.12	7.44 ± 0.16	$0.99^{+0.04}_{-0.02}$	66

Note. — Columns (1) Name, (2) distance from secular parallax estimate, (3) difference in absolute magnitude between unreddened star at secular parallax distance and ZAMS, (4) effective temperature (Carpenter, in prep.), (5) luminosity of star calculated according to description in §4.5, (6) median value of log(age/Myr) and 68.3% confidence limits from HRD position on D'Antona & Mazzitelli (1997) tracks (assuming Gaussian errors in $\log T_{eff}$ and $\log L/L_\odot$), (7) median value of mass and 68.3% confidence limits from HRD position on D'Antona & Mazzitelli (1997) tracks (assuming Gaussian errors in $\log T_{eff}$ and $\log L/L_\odot$), and (8) percentage of Monte Carlo points (N=10^4) which gave reasonable isochronal ages between 0.1-125 Myr, and were included in the estimation of ages and masses for columns (6) and (7).

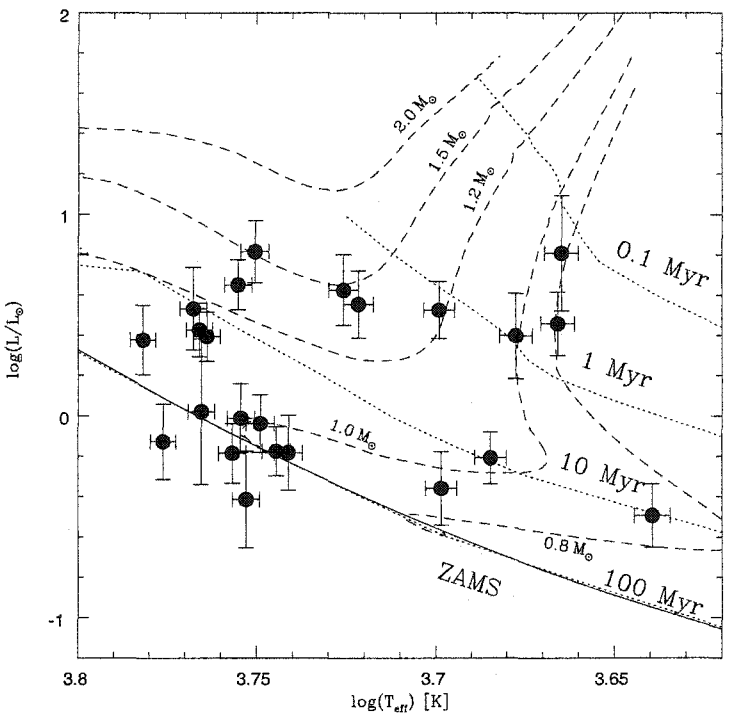

Figure 4.3: HRD for FEPS stars selected as Local Association members. The luminosities were calculated using secular parallax distances following the discussion in §4.5. Evolutionary tracks are from D'Antona & Mazzitelli (1997) and a 1998 update for $<1\,M_{\odot}$ stars.

Myr, in agreement with the mean age for its assigned group. Two stars in Table 4.3 have been previously classified as members of the ~5-Myr-old (Preibisch et al., 2002) Upper Sco OB subgroup (HD 142361 and ScoPMS 214). The iterative secular parallax distances lead to isochronal ages of 13^{+4}_{-3} Myr and 3^{+2}_{-1} Myr for HD 142361 and ScoPMS 214, respectively. We conclude that for the instances where FEPS stars in Table 4.3 have been previously classified as members of other groups, our technique leads to isochronal ages consistent with published estimates of the group ages.

A few stars in our subsample appear to be extremely young (<1 Myr), but

not embedded in known star-forming clouds. Can we truly believe that some of the FEPS stars (RX J0331.1+0713, HD 285372, RX J1111.7-7620) have ages of <1 Myr? Two effects may be conspiring to produce what might seem to be an unusually high number of <1-Myr-old stars. First, one of the sources for FEPS targets was spectroscopic surveys of *ROSAT* All-Sky Survey X-ray sources in the vicinity of star-forming molecular clouds. The first two (RX J0331 and HD 285372) are south of the Taurus-Auriga clouds, where isolated Classical T Tauri stars have been found (Wichmann et al., 1996). The third source (RX J1111.7-7620) is actually on the outskirts of the Chamaeleon I cloud. While these stars have not been kinematically linked to these star-forming clouds, it is plausible that they were recently formed in molecular clouds related to Taurus or Chamaeleon (within the past <few Myr). So we can not dismiss these very young age estimates easily. Note that we have also ignored stellar multiplicity. RX J0331 has been resolved as binary at K-band (Palomar 200" AO survey; Metchev, Hillenbrand, & White, in prep.) with the companion being roughly half the brightness of the primary. HD 285372 is a single-lined spectroscopic binary candidate (Wichmann et al., 2000). However, RX J1111.7 appears to be single according to multi-epoch radial velocity monitoring (Melo, 2003) and a speckle search for companions (Köhler, 2001). Hence, the first two stars may be somewhat older stars ($\sim$10 Myr) whose unresolved binarity (according to our Tycho-2 and 2MASS photometry) makes them appear younger on evolutionary tracks. Unresolved binarity among *bona fide* stars may be responsible for scattering some stars into the pre-MS part of the HRD, but it is doubtful that is responsible for all of the high luminosity stars in Fig. 4.3.

4.6 Conclusions & Future Work

For the few instances where Local Association stars in the FEPS database have previously published distances and age estimates, we find satisfactory agreement between our values and those previously published. For many of the stars in Table 4.3, verification (or negation) of these secular parallax estimates will have to await the next astrometric space mission that will conduct an all-sky survey: GAIA (Perryman, 2003).

The tools developed in §4.2 and 4.3 can be used as a powerful engine to identify the nearest, youngest stars in the solar neighborhood. If one cross-references a deep proper motion catalog (like the UCAC2 catalog ; Zacharias et al., 2003) and an all-sky X-ray survey (i.e. *ROSAT* ; Voges et al., 1999), one can identify active stars whose proper motions are consistent with membership in the Local Association. The Local Association velocity field is appropriate for the young B-type population (Chen et al., 1997) and the Li-rich field stars (Wichmann, Schmitt, & Hubrig, 2003), and so provides an excellent kinematic model with which to compare the motions of candidate young stars.

Although a previous survey of *ROSAT*-Tycho stars with statistically significant trigonometric parallaxes yielded only ~10 <125-Myr-old stars out of a sample of ~750 targets (Wichmann, Schmitt, & Hubrig, 2003), this search was biased against identifying pre-MS K and M stars due to the flux-limit of the Tycho-2 proper motion catalog ($V < 12^{mag}$). The recently available UCAC2 catalog (Zacharias et al., 2003) will allow us to probe three magnitudes deeper than Tycho-2, and should allow kinematic selection of the nearest K and M-type pre-MS stars within ~50 pc of the Sun. Spectroscopic follow-up of hundreds of candidates will be necessary to confirm whether the X-ray active stars co-moving with the Local Association are indeed pre-MS. We conclude that it is now practical to search for

the nearest, isolated pre-MS stars in the solar neighborhood, without having to wait 1-2 decades for the next dedicated space-based astrometric mission.

CHAPTER 5

CONCLUSIONS & FUTURE WORK

The stated goals of this thesis were to investigate the fossil record of star-formation in the nearest OB association and to study the evolution of circumstellar environments within 10 AU of young solar-type stars. In order to do this, we needed to develop new techniques necessary for identifying elusive post-T Tauri stellar populations. We have succeded in achieving these goals, and in the process created a tool which can be used for the next generation of surveys to identify the nearest, youngest stars to the Sun.

We identified a large sample of nearby post-T Tauri stars in the nearest OB association to the Sun (Sco-Cen). Our study of this young, solar-type population in §2 found that the duration of star-formation in the LCC and UCL OB subgroups was short (<5-10 Myr), consistent with the idea that star-formation in giant molecular clouds takes place over timescales shorter than the ambipolar diffusion time scale (>10 Myr). Hence, one does not expect large numbers of ~10-30 Myr-old post-T Tauri stars on the periphery of modern star-forming clouds.

The answer to the question *"Where are the post-T Tauri stars?"* is this: Post-T Tauri stars are found in ghostly kinematic groups devoid of obvious molecular clouds. They can be found as low-mass members of OB associations (like Sco-Cen), and in kinematic groups that escaped detection until recently (e.g. η Cha cluster, TW Hya association, Tuc-Hor association). The idea that post-T Tauri stars may be found in "halos" surrounding long-lived molecular clouds

that are currently forming stars, appears to lack observational support. Molecular clouds appear to form stars during brief bursts (<few Myr), followed by disruption of the cloud by the new stellar population, and termination of further star-formation. In the 20th century, Classical T Tauri stars (CTTS) were discovered in large quantities by objective prism surveys of star-forming clouds, and weak-lined T Tauri stars were discovered in X-ray surveys of those same clouds. In the 21st century, we are now capable of finding the long-sought post-T Tauri stars in large numbers using all-sky X-ray and proper motion datasets.

As a by-product of our spectroscopic survey of pre-MS stars in Sco-Cen in §2, we found that the incidence of accretion disks among $\sim$1 $M_{\odot}$ stars in a stellar population with mean age $\sim$13 Myr is $\sim$1 %, indicating that it is very rare for young solar-type stars to exhibit Classical T Tauri star activity beyond this age. Building on this work, in §3 we surveyed a group of post-T Tauri stars whose age corresponded with the epoch of terrestrial planet formation in our solar system (Tucana-Horologium association; age $\sim$30 Myr). We found no indication of warm dust emission from circumstellar material within $\sim$10 AU of these young stars. Through modeling of the flux upper limits with plausible circumstellar disk and dust grain models, we conclude that these post-T Tauri stars have less than $\lesssim$3000 times the dust grain surface area of our solar system's zodiacal dust disk. If the stars have optically-thick dust disks, then our photometry rules out inner hole radii of <0.2-6 AU. Combining our survey results from other recent surveys suggests that detectable $\sim$10 μmemission from circumstellar disks (either optically-thick T Tauri accretion disks or optically-thin debris disks like that orbiting β Pic) disappears by age $\sim$20 Myr. Theoretical models of terrestrial planet-formation suggest that dust is generated collisionally in copious amounts by perturbations from Ceres-sized planetesimals. The effects are observable as

mid-IR excess emission compared to the stellar photosphere. This dust generation mechanism dies off within a short time (~1 Myr) after the planetesimals reach this threshold size. Those models, combined with observations from our survey and other published surveys, suggest that planetesimals reach ~1000 km in radii before ~20 Myr age. At the age of the Tuc-Hor association (~30 Myr), the oligarchical accretion of the largest planetesimals has probably swept up the hoards of smaller, dust-generating bodies.

In §4, we developed a revised method of assigning membership and calculating kinematic distances (from an iterative secular parallax technique) to putative members of superclusters. Our results show that the isochronal ages that we derive using these distances are consistent with previously published ages. Hence, we have developed a technique for identifying pre-MS field stars that currently lack trigonometric parallax information. One could, in principle, apply these techniques to identify the nearest, youngest stars in the solar neighborhood. The basic ingredients for such a search are available today: the *ROSAT* All-Sky Survey can identify active stars by virtue of their X-ray activity, and the Tycho-2 or UCAC2 proper motion catalogs provide photometry and proper motion information. Using this input data, and employing a reliable kinematic model for the <100-Myr-old stars in the solar neighborhood (i.e. the Local Association), one can statistically test whether the stars have motions consistent with membership in the group. Spectroscopic follow-up of the kinematically-selected stars would be necessary to identify those that are Li-rich, and to measure radial velocities, which can be used to further refine the probability of membership. Finding the nearest, youngest, stars is crucial for advancing our knowledge regarding the formation and evolution of planetary systems, and for placing our own solar system in context.

APPENDIX A

THE PRE-MAIN SEQUENCE T_{eff} SCALE

Pre-main sequence stars lie between dwarfs (V) and subgiants (IV) on color-absolute magnitude or temperature-luminosity H-R diagrams. A given visual spectral type will correspond to cooler temperatures as surface gravity decreases (e.g. Gray, 1991; de Jager & Nieuwenhuijzen, 1987). Dwarf temperature scales are often adopted for pre-MS populations, however it is prudent to account for the effects of surface gravity.

We quantify the effects of $\log g$ on the SpT vs. T_{eff} relation using two datasets. First, we fit a polynomial surface to T_{eff}(SpT, $\log g$) using the data from Gray (1991, Table 2). As with most compilations of T_{eff}(SpT) in the FGK-star regime, we find that a trinomial is the best low-order fit, and that a linear dependence on $\log g$ adequately accounts for the effects of surface gravity on temperature. Our second method finds a similar surface fit to T_{eff}(SpT, $\log g$) using published T_{eff} and $\log g$ values (Cayrel de Strobel et al., 2001) for the GK standards of Keenan & McNeil (1989) and F standards of Garcia (1989) (those within 0.3 dex of solar [Fe/H], and luminosity class IV and V only). We adopt the isochrones from D'Antona & Mazzitelli (1997) for a fiducial $\log g$ value as a function of T_{eff} for a coeval 15-Myr-old population.

Both assessments yield essentially the same result: dwarf temperature scales for G-K stars should be lowered by 35 K for a 15 Myr-old population. The temperature decrement increases for younger ages: 70 K-40 K for G0-K2 10-Myr-old stars, 235 K-105 K for G0-K2 5-Myr-old stars, and 260 K-180 K for G3-K2 1-Myr-

old stars. Both techniques yielded a linear dependence of $\log g$ on T_{eff}(SpT, $\log g$), and the slopes were similar: $\partial T_{eff}/\partial \log g \simeq 220$ K/log(cm s^{-1}) for the Keenan standards with Cayrel de Strobel stellar atmosphere data, and $\partial T_{eff}/\partial \log g \simeq 190$ K/log(cm s^{-1}) for the interpolation of Gray's (1991) Table 2. As the evolutionary model isochrones are parallel to the main sequence when the stars are on the radiative tracks (i.e. $\sim$10-30 Myr for $\sim$1 $M_{\odot}$ stars), the $\Delta \log g$ between a 15 Myr-isochrone and the main sequence is fairly constant over the G-K spectral types. Hence one naively expects a linear offset in T_{eff}(SpT, $\log g$) between the 15-Myr isochrone and the MS.

With the 1σ scatter between published T_{eff}(SpT) relations being $\sim$60 K amongst G stars, the systematic shift is nearly negligible. Upon comparing several temperature scales from the literature, we adopt the dwarf T_{eff} scale from Schmidt-Kaler (1982), and apply a -35 K offset to correct for the effects of lower surface gravity for a putative 15-Myr-old population. We conclude that adopting dwarf T_{eff} vs. SpT scales for pre-MS stars younger than $\sim$10 Myr will systematically overestimate their T_{eff} values, and in turn, their masses inferred from evolutionary tracks. This could have deleterious systematic effects on derived initial mass functions for young associations.

APPENDIX B

STANDARDS WITH QUESTIONABLE LUMINOSITY CLASS

Several of the standard stars we observed had H-R diagram positions, published $\log g$ values, and Sr II λ4077/Fe I λ4071 ratios (SrFe) which differed from what is expected for their luminosity classes given in Keenan & McNeil (1989). The differences are only at the half of a luminosity-class level. We adopt the Keenan temperature types for all of his standard stars, however we revised the luminosity classes of these stars to bring their H-R diagram positions, SrFe index, and published $\log g$ estimates into harmony (Table B.1). The SrFe indices for the vast majority of the standards formed loci according to luminosity class (Fig. 2.1), so we are comfortable using the index as an additional descriminent. The dwarf regression line in the gravity indicator vs. temperature indicator plot (Fig. 2.1) was constructed using only Keenan standards for which his luminosity classification agreed with published $\log g$ values and the H-R diagram position.

Table B.1. Revised Luminosity Classes of Standard Stars

Star	Published	$\log g$	Sr/Fe	HRD	adopted
...	Lum. class	estimates	class	pos.	Lum. class
HR 5072	V	3.8-3.9 (IV-V)	IV-V	IV-V	IV-V
HR 4995	IV-V	3.0-3.7 (III/IV)	IV	IV	IV
HR 5409	IV	3.3-3.9 (III/IV)	III-IV	III-IV	III-IV
HR 6608	IIIb	...	IV	IV	IV

Note. — Published luminosity classes from Keenan & McNeil (1989). The range of published $\log g$ estimates come from the compilation of Cayrel de Strobel et al. (2001). "Sr/Fe class" is from measuring the Fe I λ4071/Sr II λ4071 ratio in our spectra and intercomparison to the spectral standards in Table 2.3 (see Fig. 2.1). The luminosity class from the HRD position uses the V and $(B-V)$data from it Hipparcos and the standard relations from Appendix B of Gray (1991).

APPENDIX C

POLYNOMIAL FITS

• *MI6 vs. Spectral Type*: This flux ratio is Index 6 of Malyuto & Schmidt-Kaler (1997). We measure the index in magnitudes (MI6 = -2.5log(f($\lambda\lambda$5125-5245)/f($\lambda\lambda$5245-5290))), and find the following relation for Keenan and Garcia F0-K6 III-IV standards (Table 2.3) within 0.3 dex of solar metallicity:

$$+0.06 < MI6 < 0.26:$$
$$SpT = 33.26 \pm 0.07 + (22.75 \pm 0.48) \times MI6$$
$$-0.04 < MI6 < 0.06:$$
$$SpT = 30.82 \pm 0.16 + (105.38 \pm 8.28) \times MI6 - (711.74 \pm 173.81) \times MI6^2 \quad \text{(C.1)}$$

where SpT is the spectral type on Keenan's (1984) scale, i.e. F5 = 28, F8 = 29, G0 = 30, G2 = 31, G5 = 32, G8 = 33, K0 = 34, K1 = 35, and K2 = 36. Intermediate types can be assigned e.g. G9 = 33.5, G9.5 = 33.75, K0+ = 34.25, K0.5 = 34.5, etc. The first equation applies to K0-K6 stars, and the second equation applies to F0-K0 stars. The 1σ dispersion in these fits is 0.6 subtypes.

• *λ4374/λ4383 vs. Spectral Type*: This band ratio consists of two 3Å bands centered on 4374.5Å and 4383.6Å. We measure the index in magnitudes as YFe = -2.5$\times$log(f(λ4374.5)/f(λ4383.6)). We find the following relation between the band ratio and SpT for F0-K6 III-V stars:

$$SpT = 25.97 \pm 0.30 + (20.47 \pm 0.90) \times YFe \quad \text{(C.2)}$$

The residual standard deviation to the fit (using 20 Keenan F0-K5 III-V standards within 0.3 dex of solar metallicity) is 0.6 subtypes.

• *Surface Gravity Index Fe* I *λ4071/Sr* II *λ4077 vs. Spectral Type*: We measure a surface gravity index using the flux ratio of two 3Å bands centered on Fe I λ4071.4 and Sr II λ4076.9. We measure the flux ratio in magnitudes: SrFe = -2.5×log(f(λ4071)/f(λ4077)), and plot against our MI6 spectral type index. The Keenan standard dwarfs confirmed as being main sequence stars define a narrow locus:

$$SrFe = -0.078 \pm 0.005 + (2.123 \pm 0.261) \times MI6 - (8.393 \pm 2.945) \times MI6^2 + (15.487 \pm 8.672) \times MI6^3 \quad \text{(C.3)}$$

The 1σ sample standard deviation of this fit is 0.0094 mag in SrFe. The boundary between dwarfs and subgiants in Fig. 2.1 is -2σ of the dwarf locus. This relation is valid for F9-K6 stars.

• *EW(Hα) vs. Spectral Type*: In Fig. 2.2, we fit the equivalent widths of the Hα feature (at low resolution, the photospheric absorption plus the chromospheric emission) as a function of spectral type for F0-K6 dwarf and subgiant standard stars (Table 2.3) with the following polynomial:

$$EW(H\alpha) = 2.983 \pm 0.066 - (0.456 \pm 0.027) \times (SpT - 30) + (2.574 \pm 0.378) \times 10^{-2} \times (SpT - 30)^2 \quad \text{(C.4)}$$

EW(Hα) is measured in Å. SpT is spectral type on Keenan's scale (as before). The sample standard deviation of the polynomial fit to 11 standards was 0.20Å.

• *Converting Tycho* $(B - V)$ *to Cousins-Johnson* $B-V$: The *Hipparcos* catalog gives linear relations between $(B_T - V_T)$, $(B - V)$, V, and V_T for stars of a wide range in spectral types. Bessell (2000) compared the *Hipparcos*/Tycho photometry

and that of the E-region photometric standards, and refined the relations between the two systems. Table 2 of Bessell (2000) gives a standard relation between ($B_T - V_T$) Cousins-Johnson ($B - V$) and (V - V_T) for B-G dwarfs and K-M giants. We fit the following relations to Bessell's tables:

$$V = V_T + 9.7 \times 10^{-4} - 1.334 \times 10^{-1}(B_T - V_T) + 5.486 \times 10^{-2}(B_T - V_T)^2 - 1.998 \times 10^{-2}(B_T - V_T)^3 \quad \text{(C.5)}$$

$$(B - V) = (B_T - V_T) + 7.813 \times 10^{-3}(B_T - V_T) - 1.489 \times 10^{-1}(B_T - V_T)^2 + 3.384 \times 10^{-2}(B_T - V_T)^3 \quad \text{(C.6)}$$

$$(B - V) = (B_T - V_T) - 0.006 - 1.069 \times 10^{-1}(B_T - V_T) + 1.459 \times 10^{-1}(B_T - V_T)^2 \quad \text{(C.7)}$$

The V(V_T,($B_T - V_T$)) polynomial equation C.5 applies to stars from -0.25 < ($B_T - V_T$) < 2.0 (B-M types). Equation C.6 is for stars with 0.5 < ($B_T - V_T$) < 2.0, and equation C.7 is for stars with -0.25 < ($B_T - V_T$) < 0.5. We do not quote uncertainties in the polynomial coefficients since the Bessell relations are already smoothed. These equations fit Bessell's standard relations to 1-2 millimagnitudes.

APPENDIX D

MIRAC PHOTOMETRIC CALIBRATION

With a significant body of MIRAC-BLINC observations acquired during the 2001-2003 observing runs at Magellan I, it was decided to calculate the photometric attributes of commonly used MIRAC bands on the Cohen-Walker-Witteborn (CWW) system of absolute infrared calibration (e.g. Cohen, Wheaton, & Megeath, 2003, and references therein)[1]. The photometric standard system for previously published MIRAC studies is given in Appendix 2 of the MIRAC3 User's Manual (Hoffmann & Hora, 1999).

Relative spectral responses (RSRs) for each combination of filter and window were constructed. The throughput chain consists of the following groups of components: atmosphere, telescope optics, BLINC optics, MIRAC optics, and MIRAC detector. The complete throughput equation consists of the following components multiplied together: atmosphere, 3 aluminum mirrors (Magellan), dewar window (KRS-5 or KBr), KBr lens (in BLINC), 5 gold mirrors (3 in BLINC, 2 in MIRAC), filter, and the Si:As array. Most of the MIRAC observations were taken in just four of the seventeen filters currently available in the three MIRAC filter wheels: L, N, 11.6, and Q_s, and these were the filters we absolutely calibrated. For each MIRAC filter, we list a manufacturer's name, mean filter wavelength (λ_o),

[1]This appendix was previously published in Mamajek et al. (2004) so as to provide an absolute photometric calibration of the publicly-available MIRAC camera for the community. The author completed the work regarding digitizing archived printouts of filter transmission profiles and gathering optical throughput measurements, however Martin Cohen is credited with calculating the zero-magnitude attributes and absolute photometric calibration provided in Tables D.1 and D.2. Many thanks go to Phil Hinz and Bill Hoffmann for providing critical information that made this calibration possible.

bandwidth ($\Delta\lambda/\lambda$; defined as the FWHM of the normalized transmission curve divided by the mean wavelength), and the temperature at which the filter profile was measured (or extrapolated). The transmission profiles for the filters are plotted in Fig. D.1. While we list *mean* filter wavelengths (λ_o) in this discussion, the *isophotal* wavelengths (λ_{iso}) are given in Table D.1.

The L filter (OCLI "Astro L"; $\lambda_o = 3.84\mu$m; $\Delta\lambda/\lambda = 16.2\%$; 77 K) is the same one used in all previous and current MIRAC L-band observations, and the transmission curve is plotted in Fig. A2.2 of Hora (1991). The N filter (OCLI code W10773-8; $\lambda_o = 10.75\,\mu$m; $\Delta\lambda/\lambda = 47.2\%$; Ambient) was purchased in 1994 in preparation for comet Shoemaker-Levy-9 observations, and has been in use ever since. Pre-1994 MIRAC observations employed a slightly bluer wideband N filter whose characteristics we only present here for completeness (OCLI code W10575-9; $\lambda_o = 10.58\,\mu$m; $\Delta\lambda/\lambda = 45.8\%$; Ambient). The narrow 11.6 μm filter (OCLI "Astronomy R"; $\lambda_o = 11.62\,\mu$m; $\Delta\lambda/\lambda = 9.5\%$; extrapolated to 5 K) has been used since MIRAC was commissioned (Hora, 1991). Its transmission curve includes the effects of a BaF_2 blocker, and it is the only filter of the four that we were able to linearly extrapolate its transmission characteristics to the detector's operating temperature (5 K; data at Ambient and 77 K were available). The Q_s or "Q-short" filter has also been used for the lifetime of MIRAC, and its characteristics are only currently known at ambient temperature: $\lambda_o = 17.50\,\mu$m; $\Delta\lambda/\lambda = 10.6\%$).

We followed Cohen et al. (1999) in using PLEXUS (Clark, 1996) to assess mean, site-specific atmospheric transmission. Transmission curves for KRS-5 and KBr were taken from the Infrared Handbook (Wolfe & Zissis, 1985). We used a KRS-5 window during the August 2001 and May 2002 runs, and a KBr window for the August 2002 and March 2003 runs. The reflectivities of the gold and aluminum mirrors were assumed to be flat in the wavelength range of interest (2-20 μm). The

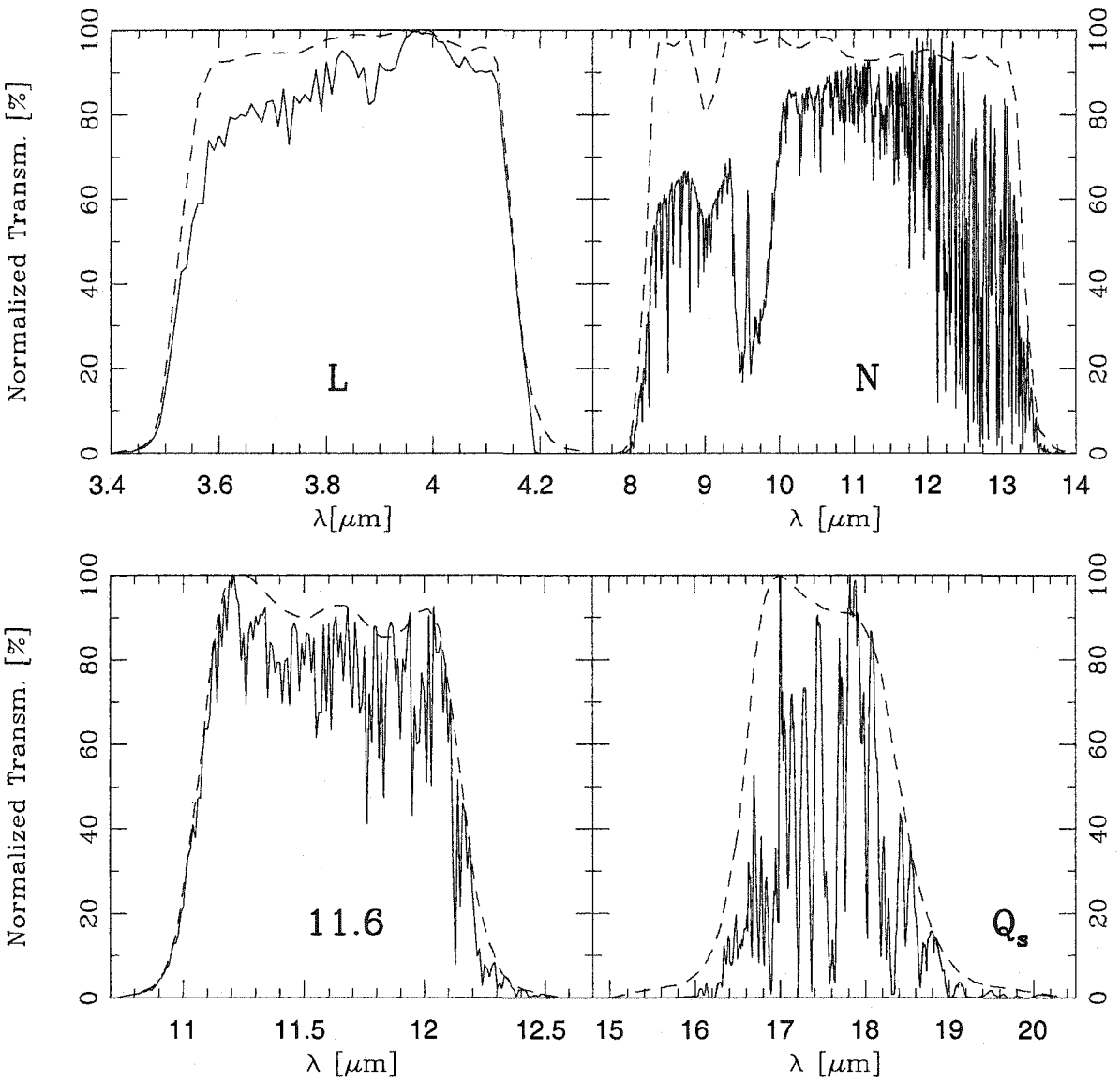

Figure D.1: Transmission profiles for the MIRAC L, N, 11.6, and Q_s filters. *Dashed lines* are the normalized filter transmission profiles. *Solid lines* are the relative spectral response curves (= "RSRs", details given in Appendix A), and represent the product of transmissions for the filters, detector, optics, KRS-5 dewar window, and atmosphere. The RSRs were used for absolutely calibrating MIRAC on the CWW system.

Table D.1. Zero-Magnitude Attributes of MIRAC Photometric Bands

(1)	(2)	(3)	(4)	(5)	(6)	(7)	(8)
MIRAC	λ_{iso}	Bandwidth	In-Band	F_λ(iso)	Bandwidth	F_ν(iso)	ν(iso)
Band	(μm)	(μm)	(W cm^{-2})	(W cm^{-2} μm^{-1})	(Hz)	(Jy)	(Hz)
L	3.844	0.5423	2.631E-15	4.852E-15	1.102E+13	238.8	7.793E+13
uncert.	0.018	0.0037	1.609%	8.469E-17	6.820E+10	4.1	7.361E+11
N	10.35	3.228	3.263E-16	1.011E-16	8.760E+12	37.25	2.946E+13
uncert.	0.05	0.022	1.632%	1.789E-18	4.170E+10	0.60	2.416E+11
11.6	11.57	0.8953	5.816E-17	6.496E-17	2.006E+12	29.00	2.592E+13
uncert.	0.08	0.0135	2.110%	1.686E-18	2.149E+10	0.61	2.827E+11
Q_s	17.58	0.9130	1.123E-17	1.230E-17	8.834E+11	12.72	1.706E+13
uncert.	0.14	0.0185	2.494%	3.951E-19	1.263E+10	0.32	2.171E+11

Note. — Columns (1) name of MIRAC band, (2) isophotal wavelength, (3) wavelength bandwidth of RSR, (4) In-band flux for zero-magnitude star, (5) isophotal monochromatic intensity (wavelength units), (6) frequency bandwidth of RSR, (7) isophotal monochromatic intensity (frequency units), (8) isophotal frequency. Note that the stated quantities assume that a KRS-5 dewar window is used. If the KBr dewar window is used, the values are nearly identical. For KBr, every stated value is within 5% of the stated uncertainty for the L, 11.6, and Q_s bands, and within 36% of the stated uncertainty for N-band.

quantum efficiency for the MIRAC doped-silicon blocked-impurity-band (BIB) array was taken from Stapelbroek et al. (1995), following Hoffmann et al. (1998). The zero magnitude attributes of the MIRAC filter systems are given in Table D.1. Standard star fluxes on the CWW system for the four primary MIRAC filters (with the KRS-5 dewar window) are given in Table D.2. When the KBr dewar window is used on MIRAC-BLINC, the standard star fluxes are nearly identical (to within <7% of the quoted flux uncertainties), so the same fluxes and magnitudes can be safely adopted. The flux densities in Tables 3.4 and 3.5 are referenced to this system.

Table D.2. Predicted MIRAC Standard Star Fluxes on CWW system

(1) HD Name	(2) Alt. Name	(3) Band ...	(4) Mag ...	(5) unc. ...	(6) F_λ ($W\,cm^{-2}\,\mu m^{-1}$)	(7) unc. ($W\,cm^{-2}\,\mu m^{-1}$)	(8) F_ν (mJy)	(9) unc. (mJy)	(10) unc. (%)
1522	ι Cet	L	0.800	0.022	2.32E-15	4.99E-17	1.14E+05	2.46E+03	2.15
1522	ι Cet	N	0.807	0.021	4.81E-17	9.98E-19	1.77E+04	3.68E+02	2.08
1522	ι Cet	11.6	0.772	0.026	3.19E-17	9.01E-19	1.42E+04	4.02E+02	2.83
1522	ι Cet	Q_s	0.775	0.030	6.02E-18	2.08E-19	6.23E+03	2.16E+02	3.46
12929	α Ari	L	-0.762	0.021	9.79E-15	2.01E-16	4.82E+05	9.88E+03	2.05
12929	α Ari	N	-0.754	0.020	2.02E-16	4.00E-18	7.46E+04	1.47E+03	1.98
12929	α Ari	11.6	-0.789	0.025	1.34E-16	3.70E-18	6.00E+04	1.65E+03	2.75
12929	α Ari	Q_s	-0.787	0.030	2.54E-17	8.63E-19	2.62E+04	8.93E+02	3.40
29139	α Tau	L	-3.045	0.021	8.01E-14	1.62E-15	3.94E+06	7.99E+04	2.03
29139	α Tau	N	-3.013	0.020	1.62E-15	3.21E-17	5.97E+05	1.18E+04	1.98
29139	α Tau	11.6	-3.074	0.025	1.10E-15	3.03E-17	4.92E+05	1.35E+04	2.75
29139	α Tau	Q_s	-3.058	0.029	2.06E-16	6.91E-18	2.13E+05	7.14E+03	3.36
45348	α Car	L	-1.289	0.019	1.59E-14	3.04E-16	7.83E+05	1.50E+04	1.91
45348	α Car	N	-1.309	0.020	3.38E-16	6.53E-18	1.24E+05	2.41E+03	1.94
45348	α Car	11.6	-1.307	0.025	2.17E-16	6.03E-18	9.67E+04	2.69E+03	2.78
45348	α Car	Q_s	-1.307	0.029	4.10E-17	1.37E-18	4.24E+04	1.42E+03	3.35
48915	α CMa	L	-1.360	0.017	1.70E-14	2.96E-16	8.36E+05	1.46E+04	1.75
48915	α CMa	N	-1.348	0.018	3.50E-16	6.19E-18	1.29E+05	2.28E+03	1.77
48915	α CMa	11.6	-1.346	0.023	2.24E-16	5.82E-18	1.00E+05	2.60E+03	2.59
48915	α CMa	Q_s	-1.341	0.027	4.23E-17	1.36E-18	4.38E+04	1.41E+03	3.21
81797	α Hya	L	-1.362	0.019	1.70E-14	3.19E-16	8.37E+05	1.57E+04	1.88
81797	α Hya	N	-1.309	0.019	3.38E-16	6.39E-18	1.24E+05	2.36E+03	1.89
81797	α Hya	11.6	-1.351	0.027	2.25E-16	6.59E-18	1.01E+05	2.94E+03	2.92
81797	α Hya	Q_s	-1.350	0.030	4.26E-17	1.46E-18	4.41E+04	1.51E+03	3.42
106849	ϵ Mus	L	-1.594	0.029	2.11E-14	5.83E-16	1.04E+06	2.87E+04	2.77
106849	ϵ Mus	N	-1.647	0.027	4.61E-16	1.17E-17	1.70E+05	4.32E+03	2.54
106849	ϵ Mus	11.6	-1.708	0.031	3.13E-16	1.01E-17	1.40E+05	4.53E+03	3.24
106849	ϵ Mus	Q_s	-1.700	0.039	5.89E-17	2.42E-18	6.09E+04	2.50E+03	4.10
108903	γ Cru	L	-3.299	0.039	1.01E-13	3.71E-15	4.99E+06	1.83E+05	3.66
108903	γ Cru	N	-3.354	0.038	2.22E-15	7.95E-17	8.18E+05	2.93E+04	3.58

Table D.2—Continued

(1) HD Name	(2) Alt. Name	(3) Band	(4) Mag	(5) unc.	(6) F_λ ($W\,cm^{-2}\,\mu m^{-1}$)	(7) unc. ($W\,cm^{-2}\,\mu m^{-1}$)	(8) F_ν (mJy)	(9) unc. (mJy)	(10) unc. (%)
108903	γ Cru	11.6	-3.413	0.041	1.51E-15	6.13E-17	6.73E+05	2.74E+04	4.07
108903	γ Cru	Q_s	-3.403	0.043	2.83E-16	1.27E-17	2.92E+05	1.31E+04	4.49
128620	α Cen A	L	-1.562	0.018	2.04E-14	3.58E-16	1.01E+06	1.76E+04	1.75
128620	α Cen A	N	-1.564	0.018	4.27E-16	7.57E-18	1.57E+05	2.79E+03	1.77
128620	α Cen A	11.6	-1.565	0.023	2.75E-16	7.13E-18	1.23E+05	3.18E+03	2.60
128620	α Cen A	Q_s	-1.566	0.027	5.20E-17	1.67E-18	5.38E+04	1.73E+03	3.21
133216	σ Lib	L	-1.565	0.025	2.05E-14	5.00E-16	1.01E+06	2.46E+04	2.44
133216	σ Lib	N	-1.619	0.022	4.49E-16	9.79E-18	1.66E+05	3.61E+03	2.18
133216	σ Lib	11.6	-1.680	0.028	3.05E-16	9.03E-18	1.36E+05	4.03E+03	2.96
133216	σ Lib	Q_s	-1.670	0.036	5.73E-17	2.23E-18	5.92E+04	2.30E+03	3.89
135742	β Lib	L	2.874	0.019	3.44E-16	6.39E-18	1.69E+04	3.14E+02	1.86
135742	β Lib	N	2.899	0.019	7.00E-18	1.32E-19	2.58E+03	4.85E+01	1.88
135742	β Lib	11.6	2.904	0.025	4.48E-18	1.23E-19	2.00E+03	5.49E+01	2.75
135742	β Lib	Q_s	2.915	0.029	8.40E-19	2.78E-20	8.68E+02	2.88E+01	3.32
150798	α TrA	L	-1.337	0.022	1.66E-14	3.50E-16	8.18E+05	1.72E+04	2.11
150798	α TrA	N	-1.329	0.021	3.44E-16	6.99E-18	1.27E+05	2.58E+03	2.03
150798	α TrA	11.6	-1.364	0.026	2.28E-16	6.38E-18	1.02E+05	2.85E+03	2.80
150798	α TrA	Q_s	-1.361	0.030	4.31E-17	1.48E-18	4.46E+04	1.53E+03	3.44
167618	η Sgr	L	-1.731	0.022	2.39E-14	5.08E-16	1.18E+06	2.50E+04	2.13
167618	η Sgr	N	-1.696	0.021	4.82E-16	9.86E-18	1.78E+05	3.63E+03	2.04
167618	η Sgr	11.6	-1.753	0.026	3.26E-16	9.13E-18	1.46E+05	4.08E+03	2.80
167618	η Sgr	Q_s	-1.786	0.031	6.37E-17	2.25E-18	6.59E+04	2.33E+03	3.53
216956	α PsA	L	1.002	0.019	1.93E-15	3.62E-17	9.49E+04	1.78E+03	1.88
216956	α PsA	N	1.001	0.019	4.02E-17	7.65E-19	1.48E+04	2.82E+02	1.90
216956	α PsA	11.6	1.004	0.025	2.58E-17	7.11E-19	1.15E+04	3.18E+02	2.76
216956	α PsA	Q_s	1.008	0.029	4.86E-18	1.62E-19	5.02E+03	1.67E+02	3.33

Note. — All stated quantities assume that a KRS-5 dewar window is used. If the KBr window is used, the values are nearly identical (to within 7% of the stated uncertainties).

APPENDIX E

COMMENTS ON INDIVIDUAL SOURCES

The only young stars in our survey to show a significant N-band excess were the T Tauri stars HD 143006 and [PZ99] J161411.0-230536, both members of the ~5-Myr-old Upper Sco OB subgroup. Both stars are targets in the FEPS Spitzer Legacy Science program, but only HD 143006 was previously known to possess a circumstellar disk. Both were detected by IRAS, and the MIRAC N-band fluxes are consistent with the color-corrected 12 μm measurements in the IRAS FSC (Moshir et al., 1990). Here we discuss these stars in more detail.

E.1 [PZ99] J161411.0-230536

J161411 is a K0-type weak-lined T Tauri (EW(Hα) = 0.96Å) star discovered by Preibisch et al. (1998). In a spectroscopic survey to identify new members of Upper Sco (Mamajek, Meyer, & Liebert, in prep.), the authors obtained a red, low-resolution spectrum of J161411 in July 2000, which shows an asymmetric Hα feature with blueshifted emission and redshifted absorption (net EW(Hα) = 0.36Å). We confirm the strong lithium absorption (EW(Li λ6707) = 0.45 Å) observed by Preibisch et al. (1998). The UCAC2 proper motion (Zacharias et al., 2003) for J161411 is consistent with membership in the Upper Sco subgroup. The $(K_s - N)$ color (=2.1) is similar to that of classical T Tauri stars in Taurus-Auriga (Kenyon & Hartmann, 1995). The photometric and spectroscopic evidence suggest that this ~5-Myr-old, ~1 $M_\odot$ star is actively accreting from a circumstellar disk.

E.2 HD 143006

HD 143006 is a G5Ve (Henize, 1976) T Tauri star with strong Li absorption (EW(Li λ6707) = 0.24Å; Dunkin, Barlow, & Ryan, 1997). The star is situated in the middle of the Upper Sco OB association, and its proper motion (μ_α, μ_δ = -11, -20 mas/yr; Zacharias et al., 2003) and radial velocity (-0.9 km/s; Dunkin, Barlow, & Ryan, 1997) are indistinguishable from other association members (de Bruijne, 1999b). Several studies have classified HD 143006 as a distant G-type supergiant or "pre-planetary nebula" (Carballo, Wesselius, & Whittet, 1992; Kohoutek, 2001), however we believe this is erroneous. If HD 143006 were indeed a supergiant at d = 3.4 kpc (Pottasch & Parthasarathy, 1988), its tangential velocity would be ~370 km/s – extraordinarily fast for a population I star. The MIRAC N and 11.6 photometry agrees well with the data points in the SED for HD 143006 plotted in Fig. 2 of Sylvester et al. (1996). The spectral energy distribution for HD 143006 and its optically-thick disk is well-studied from 0.4-1300 μm, so we do not discuss this object further.

REFERENCES

Adams, F. C., Lada, C. J., & Shu, F. H. 1987, ApJ, 312, 788

Agnor, C. B., Canup, R. M., & Levison, H. F. 1999, Icarus, 142, 219

Alcalá, J. M., Krautter, J., Schmitt, J. H. M. M., Covino, E., Wichmann, R., & Mundt, R. 1995, A&AS, 114, 109

Arias, E. F., Charlot, P., Feissel, M., & Lestrade, J.-F. 1995, A&A, 303, 604

Artymowicz, P. 1988, ApJ, 335, L79

Asiain, R., Figueras, F., Torra, J., & Chen, B. 1999, A&A, 341, 427

Atanasijević, I. 1971, *Selected Exercises in Galactic Astronomy*, Astrophysics and Space Science Library, Dordrecht: Reidel, 1971

Aumann, H. H. & Probst, R. G. 1991, ApJ, 368, 264

Backman, D. E. & Paresce, F. 1993, Protostars and Planets III, 1253

Ballesteros-Paredes, J., Hartmann, L., & Vázquez-Semadeni, E. 1999, ApJ, 527, 285

Balona, L. A., 1994, MNRAS, 268, 119

Basri, G., Marcy, G. W., & Graham, J. R., 1996, ApJ, 458, 600

Beckwith, S. V. W. 1999, NATO ASIC Proc. 540: The Origin of Stars and Planetary Systems, 579

Beckwith, S. V. W., Sargent, A. I., Chini, R. S., & Guesten, R. 1990, AJ, 99, 924

Beichman, C. A., Myers, P. C., Emerson, J. P., Harris, S., Mathieu, R., Benson, P. J., & Jennings, R. E. 1986, ApJ, 307, 337

Beichman, C. A., Neugebauer, G., Habing, H. J., Clegg, P. E., & Chester, T. J. 1988, NASA RP-1190, Vol. 1

Bertelli, G., Bressan, A., Chiosi, C., Fagotto, F., & Nasi, E., 1994, A&AS, 106, 275

Bertout, C., 1989, ARA&A, 27, 351

Bertout, C., Robichon, N., & Arenou, F. 1999, A&A, 352, 574

Bessell, M.S., 2000, PASP, 112, 961

Bessell, M. S. & Brett, J. M. 1988, PASP, 100, 1134

Bessell, M.S., Castelli, F., & Plez, B., 1998, A&A, 333, 231

Bhatt, H. C., 2000, A&A, 362, 715

Binney, J. & Merrifield, M. 1998, Galactic Astronomy, Princeton, NJ : Princeton University Press.

Blaauw, A., 1946, Ph.D. Thesis, Gronningen University

Blaauw, A., 1991, in The Physics of Star Formation and Early Stellar Evolution, NATO ASI Series C, Vol. 342, eds. C.J. Lada & N.D. Kylafis (Dordrecht: Kluwer), 125

Blitz, L. & Shu, F. H. 1980, ApJ, 238, 148

Boesgaard, A. M., Budge, K. G., & Ramsay, M. E. 1988, ApJ, 327, 389

Bouvier, J., Wichmann, R., Grankin, K., Allain, S., Covino, E., Fernandez, M., Martin, E. L., Terranegra, L., Catalano, S., Marilli, E., 1997, A&A, 318, 495

Briceño, C., Hartmann, L. W., Stauffer, J. R., Gagne, M., Stern, R. A., & Caillault, J. 1997, AJ, 113, 740

Briggs, R. E. 1962, AJ, 67, 710

Burns, J. A., Lamy, P. L., & Soter, S. 1979, Icarus, 40, 1

Butler, R. P., Marcy, G. W., Cohen, R. D., & Duncan, D. K. 1987, ApJL, 319, L19

Carballo, R., Wesselius, P. R., & Whittet, D. C. B. 1992, A&A, 262, 106

Carpenter, J. M. 2001, AJ, 121, 2851

Cayrel de Strobel, G. & Cayrel, R. 1989, A&A, 218, L9

Cayrel de Strobel, G., Soubiran, C., Ralite, N., 2001, A&A, 373, 159

Chambers, J. E. 2001, Icarus, 152, 205

Chen, B., Asiain, R., Figueras, F., & Torra, J. 1997, A&A, 318, 29

Chen, C. H. & Jura, M. 2001, ApJ, 560, L171

Chereul, E., Crézé, M., & Bienaymé, O. 1999, A&AS, 135, 5

Chiang, E. I. & Goldreich, P. 1997, ApJ, 490, 368

Clark, F. O. 1996, PLEXUS Version 2.1a, CD-ROM (Hanscom AFB, MA: Phillips Lab., Dir. Geophys., Air Force Mater. Command).

Cohen, M. & Kuhi, L. V. 1979, ApJS, 41, 743

Cohen, M., Schwartz, D. E., Chokshi, A., & Walker, R. G. 1987, AJ, 93, 1199

Cohen, M., Walker, R. G., Barlow, M. J., & Deacon, J. R. 1992, AJ, 104, 1650

Cohen, M., Walker, R. G., Carter, B., Hammersley, P., Kidger, M., & Noguchi, K. 1999, AJ, 117, 1864

Cohen, M., Megeath, S. T., Hammersley, P. L., Martín-Luis, F., & Stauffer, J. 2003, AJ, 125, 2645

Cohen, M., Wheaton, W. A., & Megeath, S. T. 2003, AJ, 126, 10

Covino, E., Alcalá, J. M., Allain, S., Bouvier, J., Terranegra, L., & Krautter, J., 1997, A&A, 328, 187

Crawford, D. L., 1978, AJ, 83, 48

Crawford, D. L. & Mandwewala, N., 1976, PASP, 88, 917

Cutispoto, G., Pastori, L., Pasquini, L., de Medeiros, J. R., Tagliaferri, G., & Andersen, J. 2002, A&A, 384, 491

Cutri, R. M. et al. 2003, 2MASS All-Sky Catalog of Point Sources, VizieR Online Data Catalog, 2246, 0

D'Antona, F. & Mazzitelli, I., 1997, Mem. Soc. Astr. Ital., 68, 807 (DM97)

de Bruijne, J. H. J., 1999a, MNRAS, 306, 381

de Bruijne, J. H. J., 1999b, MNRAS, 310, 585

de Geus, E., 1992, A&A, 262, 259

de Geus, E., de Zeeuw, P. & Lub, J., 1989, A&A, 216, 44

Dehnen, W. 1998, AJ, 115, 2384

de Jager, C. & Nieuwenhuijzen, H., 1987, A&A, 177, 217

de Zeeuw, P. T. & Brand, J., 1985, in Birth and Evolution of Massive Stars and Stellar Groups; Proceedings of the Symposium, Dwingeloo, Netherlands, September 24-26, 1984, (Dordrecht: D. Reidel), 102

de Zeeuw, P. T., Hoogerwerf, R., de Bruijne, J. H. J., Brown, A. G. A., & Blaauw, A., 1999, AJ, 117, 354 (dZ99)

Dohnanyi, J. W. 1969, J. Geophys. Res., 74, 2531

Dominik, C. & Decin, G. 2003, ApJ, 598, 626

Drilling, J. S., & Landolt, A. U., 2000, in Allen's Astrophysical Quantities, 4th. Ed., ed. Arthur C. Cox, (New York: AIP Press, Springer)

Dunkin, S. K., Barlow, M. J., & Ryan, S. G. 1997, MNRAS, 290, 165

Eggen, O. J. 1961, Royal Greenwich Observatory Bulletin, 41, 245

Eggen, O. J. 1975, PASP, 87, 37

Eggen, O. J. 1995, AJ, 110, 1749

Eggen, O. J. 1998, unpublished manuscript

ESA 1997, The Hipparcos and Tycho Catalogues, ESA SP-1200

Evans, N. J. 1999, ARA&A, 37, 311

Fajardo-Acosta, S. B., Beichman, C. A., & Cutri, R. M. 2000, ApJ, 538, L155

Feast, M. & Whitelock, P. 1997, MNRAS, 291, 683

Feigelson, E. D., 1996, ApJ, 468, 306

Feigelson, E. D. & Kriss, G. A. 1981, ApJL, 248, L35

Fixsen, D. J. & Dwek, E. 2002, ApJ, 578, 1009

Fleming, T. A., Molendi, S., Maccacaro, T., & Wolter, A., 1995, ApJS, 99, 701

Frink, S. 1999, Ph.D. Thesis, Astronomisches Rechen-Institut Heidelberg

Frogel, J. A., & Stothers, R., 1977, AJ, 82, 890

Gaidos, E. J. 1999, ApJ, 510, L131

Garcia, B., 1989, Bull. Inform. CDS 36, 27

Garcia Lopez, R. J., Rebolo, R., & Martin, E. L. 1994, A&A, 282, 518

Gehrels, N., 1986, ApJ, 303, 336

Ghez, A. M., Neugebauer, G., & Matthews, K. 1993, AJ, 106, 2005

Golay, M. 1974, Astrophysics and Space Science Library, 41

Gontcharov, G. A., Andronova, A. A., Titov, O. A., & Kornilov, E. V., 2001, A&A, 265, 222

Gray, D. F., 1991, The Observation and Analysis of Stellar Photospheres, 2nd ed., (New York: Cambridge)

Gray, R.O., 2000, A Digital Spectral Classification Atlas, http://nedwww.ipac.caltech.edu/level5/Gray/

Gray, R.O., Graham, P.W., & Hoyt, S.R., 2001, AJ, 121, 2159

Greenberg, R. & Nolan, M. C. 1989, Asteroids II, 778

Gregorio-Hetem, J., Lépine, J. R. D., Quast, G. R., Torres, C. A. O., & de la Reza, R., 1992, AJ, 103, 549

Griffin, R. F. 1998, The Observatory, 118, 223

Grocholski, A. J. & Sarajedini, A. 2003, MNRAS, 345, 1015

Grün, E., Zook, H. A., Fechtig, H., & Giese, R. H. 1985, Icarus, 62, 244

Guillout, P., Sterzik, M. F., Schmitt, J. H. M. M., Motch, C., & Neuhäuser, R., 1998, A&A, 337, 113

Guillout, P., Schmitt, J. H. M. M., Egret, D., Voges, W., Motch, C., & Sterzik, M. F. 1999, A&A, 351, 1003

Habing, H. J. et al. 2001, A&A, 365, 545

Haisch, K. E., Lada, E. A., & Lada, C. J. 2001a, ApJ, 553, L153

Haisch, K. E., Lada, E. A., & Lada, C. J. 2001b, AJ, 121, 2065

Hamuy, M., Suntzeff, N. B., Heathcote, S. R., Walker, A. R., Gigoux, P., & Phillips, M. M., 1994, PASP, 106, 566

Harper, D. A., Loewenstein, R. F., & Davidson, J. A. 1984, ApJ, 285, 808

Hartigan, P., Edwards, S., & Ghandour, L., 1995, ApJ, 452, 736

Hartmann, L. 2001, AJ, 121, 1030

Hartmann, L., Ballesteros-Paredes, J., & Bergin, E. A. 2001, ApJ, 562, 852

Hartmann, W. K. & Davis, D. R. 1975, Icarus, 24, 504

Hartmann, L., Stauffer, J. R., Kenyon, S. J., & Jones, B. F. 1991, AJ, 101, 1050

Hauck, B. & Mermilliod, M., 1997, A&AS, 129, 431

Hawley, S. L., Gizis, J. E., & Reid, I. N. 1996, AJ, 112, 2799

Henize, K. G. 1976, ApJS, 30, 491

Herbig, G. H., 1978, in Problems of Physics and Evolution of the Universe, ed. L. V. Mirzoyan (Yervan: Acad. Sci. Armenian SSR), 171

Herbig, G. H., Bell, K. Robin, 1988, Lick Obs. Bulletin No. 1111, (Santa Cruz: Lick Observatory)

Herbig, G. H., Vrba, F. J., & Rydgren, A. E. 1986, AJ, 91, 575

Hillenbrand, L. A., Strom, S. E., Calvet, N., Merrill, K. M., Gatley, I., Makidon, R. B., Meyer, M. R., & Skrutskie, M. F. 1998, AJ, 116, 1816

Hillenbrand, L. A., et al. 2004, in prep

Hillenbrand, L. A. & Meyer, M. R., 1999, BAAS, 195, #209

Hinz, P. M., Angel, J. R. P., Woolf, N. J., Hoffmann, W. F., & McCarthy, D. W. 2000, Proc. SPIE, 4006, 349

Hoffmann, W. F., Hora, J. L., Fazio, G. G., Deutsch, L. K., & Dayal, A. 1998, Proc. SPIE, 3354, 647

Hoffmann, W. F. & Hora, J. L. 1999, MIRAC3 User's Manual, http://cfa-www.harvard.edu/~jhora/mirac/mrcman.pdf

Høg, E., Kuzmin, A., Bastian, U., Fabricius, C., Kuimov, K., Lindegren, L., Makarov, V.V., & Roeser, S., 1998, A&A, 335, L65

Høg, E., Fabricius, C., Makarov, V.V., Urban, S., Corbin, T., Wycoff G., Bastian U., Schwekendiek P., Wicenec A. 2000a, A&A, 355, L27

Høg, E., Fabricius, C., Makarov, V.V., Bastian, U., Schwekendiek, P., Wicenec, A., Urban, S., Corbin, T., Wycoff, G. 2000b, A&A, 357, 367

Hollenbach, D. J., Yorke, H. W., & Johnstone, D. 2000, Protostars and Planets IV, 401

Hoogerwerf, R. 2000, MNRAS, 313, 43

Hoogerwerf, R. & Aguilar, L. A., 1999, MNRAS, 306, 394

Hoogerwerf, R., de Bruijne, J. H., J., & de Zeeuw, P. T., 2001, 365, 49

Hora, J. L. 1991, Ph.D. Thesis, The University of Arizona

Houk, N., 1978, Michigan Catalogue of Two-Dimensional Spectral Types for HD Stars. (Vol. 2, -52° < -40°), (Ann Arbor: Univ. Michigan)

Houk, N., 1982, Michigan Catalogue of Two-Dimensional Spectral Types for HD Stars. (Vol. 3, -40° < -26°), (Ann Arbor: Univ. Michigan)

Houk, N. & Cowley, A. P., 1975, Michigan Catalogue of Two-Dimensional Spectral Types for HD Stars. (Vol. 1, -90° < -53°), (Ann Arbor: Univ. Michigan)

Houk, N. & Smith-Moore, M., 1988, Michigan Catalogue of Two-Dimensional Spectral Types for HD Stars. (Vol. 4, -26° < -12°), (Ann Arbor: Univ. Michigan)

Houk, N. & Swift, C., 1999, Michigan Catalog of Two-Dimensional Spectral Types for the HD Stars. (Vol. 5., -12° < +5°), (Ann Arbor: Univ. Michigan)

Hughes, J., Hartigan, P., Krautter, J., & Kelemen, J., 1994, AJ, 108, 1071

Hughes, J., Hartigan, P., Clampitt, L., 1993, AJ, 105, 571

IPAC, 1986, IRAS Point Source Catalog

Jayawardhana, R., Hartmann, L., Fazio, G., Fisher, R. S., Telesco, C. M., & Piña, R. K. 1999, ApJ, 521, L129

Jeffries, R. D. 1995, MNRAS, 273, 559

Jeffries, R. D. 1999, MNRAS, 309, 189

Jeffries, R. D. & Jewell, S. J. 1993, MNRAS, 264, 106

Jensen, E., 2001, in Young Stars Near Earth: Progress & Prospects, eds. R. Jayawardhana & T. Greene, ASP Conf. Ser. Vol. 244, (San Francisco: ASP), 3

Johnson, H. L, & Morgan, W. W., 1953, ApJ, 117, 313

Jones, B. F., Shetrone, M., Fischer, D., & Soderblom, D. R. 1996, AJ, 112, 186

Jones, B. F., Fischer, D., Shetrone, M., & Soderblom, D. R., 1997, AJ, 114, 352

Jones, B. F. & Herbig, G. H. 1979, AJ, 84, 1872

Jourdain de Muizon, M., et al. 1999, A&A, 350, 875

Joy, A. H. 1945, ApJ, 102, 168

Jura, M., Zuckerman, B., Becklin, E. E., & Smith, R. C. 1993, ApJL, 418, L37

Kastner, J. H., Zuckerman, B., Weintraub, D. A., &Forveille, T., 1997, Science, 227, 67

Keenan, P.C., 1984, in The MK Process and Stellar Classification, ed. R. F. Garrison, (Toronto: Univ. of Toronto), 29

Keenan, P.C. & Barnbaum, C., 1999, ApJ, 518, 859

Keenan, P.C. & McNeil, R.C. 1976, An Atlas of Spectra of the Cooler Stars, (Columbus: Ohio State Univ.)

Keenan, P.C. & McNeil, R.C., 1989, ApJS, 71, 245

Keenan, P.C. & Yorka, S.B., 1988, Bull. Inform. CDS 35, 37

Kelsall, T. et al. 1998, ApJ, 508, 44

Kenyon, S. J. & Bromley, B. C. 2004, ApJ, 602, L133

Kenyon, S. J. & Hartmann, L. 1995, ApJS, 101, 117

Kleine, T., Münker, C., Mezger, K., & Palme, H. 2002, Nature, 418, 952

Kleine, T., Mezger, K., & Münker, C. 2003, Meteoritics & Planetary Science, vol. 38, Supplement, abstract no.5212, 38, 5212

Kleinmann, S. G., Cutri, R. M., Young, E. T., Low, F. J., & Gillett, F. C. 1986, IRAS Serendipitous Survey Catalog, Tucson, Univ. of Arizona

Koenigl, A. 1991, ApJL, 370, L39

Köhler, R., Kunkel, M., Leinert, C., & Zinnecker, H., 2000, A&A, 356, 541

Köhler, R. 2001, AJ, 122, 3325

Kohoutek, L. 2001, A&A, 378, 843

Krautter, J., Wichmann, R., Schmitt, J.H.M.M., Alcalá, J.M., Neuhauser, R., & Terranegra, L., 1997, A&AS, 123, 329

Kroupa, P., 2001, MNRAS, 322, 231

Lachaume, R., Dominik, C., Lanz, T., & Habing, H. J. 1999, A&A, 348, 897

Lada, C. J. 1987, IAU Symp. 115: Star Forming Regions, 115, 1

Lada, C. J. & Wilking, B. A. 1984, ApJ, 287, 610

Lagrange, A.-M., Backman, D. E., & Artymowicz, P. 2000, Protostars and Planets IV, 639

Lawson, W. A., Crause, L. A., Mamajek, E. E., & Feigelson, E. D. 2002, MNRAS, 329, L29

Lawson, W. A., Lyo, A.-R., & Muzerolle, J., 2004, MNRAS, in press

Lesh, J. R. 1968, ApJS, 17, 371

Lindblad, P. O., Palous, J., Loden, K., & Lindegren, L., 1997, ESA SP-402: Hipparcos - Venice '97, 402, 507

Lindegren, L., Madsen, S., & Dravins, D. 2000, A&A, 356, 1119

Lowrance, P. J., Schneider, G., Kirkpatrick, J. D., Becklin, E. E., Weinberger, A. J., Zuckerman, B., Plait, P., Malmuth, E. M., Heap, S. R., Schultz, A., Smith, B. A., Terrile, R. J., & Hines, D. C., 2000, ApJ, 541, 390

Lyo, A.-R., Lawson, W. A., Mamajek, E. E., Feigelson, E. D., Sung, E., & Crause, L. A. 2003, MNRAS, 338, 616

Madsen, S., Dravins, D., & Lindegren, L. 2002, A&A, 381, 446

Maeder, A., 1981, A&A, 101, 385

Makarov, V. V. 2003, AJ, 126, 1996

Malyuto, V. & Schmidt-Kaler, Th. 1997, A&A, 693, 699

Mamajek, E.E., 2003, proceedings of "Open Issues in Local Star Formation and Early Stellar Evolution", Ouro Preto (astro-ph/0305209)

Mamajek, E.E., Meyer, M.R., Hinz, P.M., Hoffmann, W.F., Cohen, M., Hora, J.L., 2004, ApJ, in press (astro-ph/0405271)

Mamajek, E.E., Feigelson, E.D., 2001, Young Stars Near Earth: Progress & Prospects, ASP Conf. Ser. Vol. 244, eds. R. Jayawardhana & T. Greene, (San Francisco: ASP), 104.

Mamajek, E.E., Lawson, W.A. & Feigelson, E.D. 1999, ApJ, 516, L77

Mamajek, E. E., Meyer, M. R., & Liebert, J. 2002, AJ, 124, 1670

Marcy, G. W. & Butler, R. P. 2000, PASP, 112, 137

Marsakov, V. A. & Shevelev, Y. G. 1995, Bulletin d'Information du Centre de Donnees Stellaires, 47, 13

Mashonkina, L. & Gehren, T., 2001, A&A, 376, 232

Mathioudakis, M. & Doyle, J. G. 1993, A&A, 280, 181

Mathis, J. S., 1990, ARA&A, 28, 37

Mathis, J. S., Rumpl, W., & Nordsieck, K. H. 1977, ApJ, 217, 425

McCaughrean, M. J. & O'Dell, C. R. 1996, AJ, 111, 1977

McKee, C. F., Zweibel, E. G., Goodman, A. A., & Heiles, C. 1993, Protostars and Planets III, 327

Melo, C. H. F. 2003, A&A, 410, 269

Mendoza, E. E. 1968, ApJ, 151, 977

Metchev, S. A., Hillenbrand, L. A., & Meyer, M. R. 2004, ApJ, 600, 435

Meyer, M. R., Calvet, N., & Hillenbrand, L. A., 1997, AJ, 114, 288

Meyer, M. R. et al. 2002, The Origins of Stars and Planets: The VLT View. Proceedings of the ESO Workshop held in Garching, Germany, 24-27 April 2001, p. 463.

Meyer, M. R. et al., 2004, ApJS, in press

Montmerle, T., Koch-Miramond, L., Falgarone, E., & Grindlay, J. E. 1983, ApJ, 269, 182

Moreno, E., Alfaro, E. J., & Franco, J., 1999, ApJ, 522, 276

Moshir, M. & et al. 1990, IRAS Faint Source Catalogue, version 2.0

Motte, F., Andre, P., & Neri, R. 1998, A&A, 336, 150

Mukai, T. & Yamamoto, T. 1982, A&A, 107, 97

Mundt, R., Walter, F. M., Feigelson, E. D., Finkenzeller, U., Herbig, G. H., & Odell, A. P. 1983, ApJ, 269, 229

Muzerolle, J., Calvet, N., Briceño, C., Hartmann, L., & Hillenbrand, L. 2000, ApJ, 535, L47

Muzerolle, J., Calvet, N., Hartmann, L., & D'Alessio, P. 2003, ApJ, 597, L149

Muzerolle, J., Hartmann, L., & Calvet, N., 1998, AJ, 116, 455

Myers, P. C. 1999, NATO ASIC Proc. 540: The Origin of Stars and Planetary Systems, 67

Napiwotzki, R., Schönberner, D., & Wenske, V., 1993, A&A, 268, 653

Nelson, G. J., Robinson, R. D., Slee, O. B., Ashley, M. C. B., Hyland, A. R., Tuohy, I. R., Nikoloff, I., & Vaughan, A. E. 1986, MNRAS, 220, 91

Nordström, B., et al. 2004, A&A, 418, 989

Palla, F. & Galli, D. 1997, ApJL, 476, L35

Palla, F., & Stahler, S. W., 2001, ApJ, 553, 299 (PS01)

Pallavicini, R., Cerruti-Sola, M., & Duncan, D.K., 1987, A&A, 174, 116

Patten, B. H., & Simon, T., 1996, ApJS, 106, 489

Paulson, D. B., Sneden, C., & Cochran, W. D. 2003, AJ, 125, 3185

Perryman, M. A. C. 2003, ASP Conf. Ser. 298: GAIA Spectroscopy: Science and Technology, 3

Pilachowski, C. A., Booth, J., & Hobbs, L. M. 1987, PASP, 99, 1288

Pinsonneault, M. H., Terndrup, D. M., Hanson, R. B., & Stauffer, J. R. 2004, ApJ, 600, 946

Pojmanski, G., 1998, Acta Astron., 48, 35

Pöppel, W., 1997, Fund. Cosmic Phys., 18, 1

Popper, D. M., 1966, AJ, 71, 175

Pottasch, S. R. & Parthasarathy, M. 1988, A&A, 192, 182

Preibisch, T., Guenther, E., Zinnecker, H., Sterzik, M., Frink, S., & Roeser, S. 1998, A&A, 333, 619

Preibisch, T., Brown, A. G. A., Bridges, T., Guenther, E., & Zinnecker, H. 2002, AJ, 124, 404

Preibisch, T. & Zinnecker, H., 1999, AJ, 117, 2381

Preibisch, T. & Zinnecker, H., 2000, in Stellar Clusters and Associations: Convection, Rotation, and Dynamos, ASP Conf., Vol.198., eds. by R. Pallavicini, G. Micela, and S. Sciortino, 219

Press, et al. 1986, Numerical Recipes in Fortran 77, 2nd Edition, Vol. 1 of Fortran Numerical Recipes, Cambridge University Press, New York

Pye, J. P., et al. 1995, MNRAS, 274, 1165

Probst, R. G. 1983, ApJS, 53, 335

Randich, S., Schmitt, J. H. M. M., Prosser, C. F., & Stauffer, J. R., 1995, A&A, 300, 134

Randich, S., Aharpour, N., Pallavicini, R., Prosser, C. F., & Stauffer, J. R., 1997, A&A, 323, 86

Randich, S., Gratton, R., Pallavicini, R., Pasquini, L., & Carretta, E., 1999, A&A, 348, 487

Randich, S., Pallavicini, R., Meola, G., Stauffer, J. R., & Balachandran, S. C. 2001, A&A, 372, 862

Reach, W. T., Morris, P., Boulanger, F., & Okumura, K. 2003, Icarus, 164, 384

Rebull, L. M., Wolff, S. C., Strom, S. E., & Makidon, R. B., 2001, ApJ, in press

Reid, I. N., Kilkenny, D., & Cruz, K. L. 2002, AJ, 123, 2822

Rodgers, A. W., Conroy, P., & Bloxham, G., 1988, PASP, 100, 626

Rose, J.A., 1984, AJ, 89, 1238

Sarajedini, A., Brandt, K., Grocholski, A. J., & Tiede, G. P. 2004, AJ, 127, 991

Sartori, M. J., Lépine, J. R. D., & Dias, W. S. 2003, A&A, 404, 913

Schmidt-Kaler, Th., 1982, in Landolt-Börnstein: Numerical Data and Functional Relationships in Science and Technology, eds. K. Schaífers & H. H. Voigt, (Berlin: Springer-Verlag)

Shobbrook, R. R., 1983, MNRAS, 205, 1215

Shu, F. H., Adams, F. C., & Lizano, S. 1987, ARA&A, 25, 23

Shu, F. H., Allen, A., Shang, H., Ostriker, E. C., & Li, Z. 1999, NATO ASIC Proc. 540: The Origin of Stars and Planetary Systems, 193

Siess, L., Dufour, E. & Forestini, M., 2000, A&A, 358, 593 (SDF00)

Siess, L., Forestini, M., & Dougados, C. 1997, A&A, 324, 556

Silverstone, M. D. 2000, Ph.D. Thesis, UCLA

Skrutskie, M. F., Dutkevitch, D., Strom, S. E., Edwards, S., Strom, K. M., & Shure, M. A. 1990, AJ, 99, 1187

Skuljan, J., Hearnshaw, J. B., & Cottrell, P. L. 1999, MNRAS, 308, 731

Slawson, R. W., Hill, R. J., & Landstreet, J. D., 1992, ApJS, 82, 117

Smart, W. M., 1968, Stellar Kinematics, (London:Longmans)

Soderblom, D. R., Jones, B. F., Balachandran, S., Stauffer, J. R., Duncan, D. K., Fedele, S. B., & Hudon, J. D. 1993, AJ, 106, 1059

Soderblom, D. R., King, J. R., & Henry, T. J., 1998, AJ, 116, 396

Song, I., Weinberger, A. J., Becklin, E. E., Zuckerman, B., & Chen, C. 2002, AJ, 124, 514

Song, I., Zuckerman, B., & Bessell, M. S. 2003, ApJ, 599, 342

Spangler, C., Sargent, A. I., Silverstone, M. D., Becklin, E. E., & Zuckerman, B. 2001, ApJ, 555, 932

Spergel, D. N., et al. 2003, ApJS, 148, 175

Stapelbroek, M. G., Seib, D. H., Huffman, J. E., & Florence, R. A. 1995, Proc. SPIE, 2475, 41

Stauffer, J. R., Caillault, J.-P., Gagné, M., Prosser, C. F., & Hartmann, L. W., 1994, ApJS, 91, 625

Stauffer, J. R., Schultz, G., & Kirkpatrick, J. D. 1998, ApJL, 499, L199

Stelzer, B. & Neuhäuser, R. 2001, A&A, 372, 117

Sterzik, M. F., & Durisen, R. H., 1995, A&A, 304, L9

Stevenson, D. J. 1987, Annual Review of Earth and Planetary Sciences, 15, 271

Strom, K. M., Wilkin, F. P., Strom, S. E., & Seaman, R. L. 1989, AJ, 98, 1444

Sung, H., Bessell, M. S., Lee, B., & Lee, S. 2002, AJ, 123, 290

Sylvester, R. J., Skinner, C. J., Barlow, M. J., & Mannings, V. 1996, MNRAS, 279, 915

Tachihara, K., Toyoda, S., Onishi, T., Mizuno, A., Fukui, Y., & Neuhäuser, R., 2002, PASJ, in press.

Taylor, B. J. 2000, A&A, 362, 563

Torra, J., Fernández, D., & Figueras, F., 2000, A&A, 359, 82

Torres, C. A. O., da Silva, L., Quast, G. R., de la Reza, R., & Jilinski, E. 2000, AJ, 120, 1410 (TDQ00)

Torres, C. A. O., da Quast, G. R., de la Reza, R., da Silva, L., & Melo, C. H. F. 2001, ASP Conf. Ser. 244: Young Stars Near Earth, 43.

Torres, C. A. O., Quast, G. R., de La Reza, R., da Silva, L., & Melo, C. H. F. 2003, ASP Conf. Ser. 287: Galactic Star Formation Across the Stellar Mass Spectrum, 439

Trumpler, R. J. & Weaver, H. F., 1953, Statistical Astronomy, Dover Books on Astronomy and Space Topics, New York: Dover Publications

Urban, S.E., Corbin, T.E., & Wycoff, G.L. 1998, AJ, 115, 2161

van der Bliek, N. S., Manfroid, J., & Bouchet, P. 1996, A&AS, 119, 547

Voges, W., et al., 1999, A&A, 349, 389

Wallace, L., Hinkle, K., & Livingston, W. 1998, An Atlas of the Spectrum of the Solar Photosphere from 13,500 to 28,000 cm^{-1} (3570 to 7405 Å),(Tucson: NOAO)

Walter, F. M., Brown, A., Mathieu, R. D., Myers, P. C., & Vrba, F. J. 1988, AJ, 96, 297

Walter, F. M. & Kuhi, L. V. 1981, ApJ, 250, 254

Waters, L. B. F. M., Cote, J., & Aumann, H. H. 1987, A&A, 172, 225

Webb, R., A., Zuckerman, B., Platais, I., Patience, J., White, R. J., Schwartz, M. J., McCarthy, C., 1999, ApJ, 512, L63

Weidenschilling, S. J. 1977, Ap&SS, 51, 153

Weinberger, A. J., Becklin, E. E., Zuckerman, B., & Song, I. 2003, BAAS, 202, #34.01

Weinberger, A. J., Becklin, E. E., Zuckerman, B., & Song, I. 2003, BAAS, 203, #13.03

Westin, T. N. G., 1985, A&AS, 60, 99

Wetherill, G. W. & Stewart, G. R. 1993, Icarus, 106, 190

Whittet, D. C. B. 2003, Dust in the Galactic Environment, 2nd ed., Bristol: Institute of Physics (IOP) Publishing, Series in Astronomy and Astrophysics

Wichmann, R., et al. 1996, A&A, 312, 439

Wichmann, R., Krautter, J., Covino, E., Alcalá, J. M., Neuhäuser, R., Schmitt, J. H. M. M., 1997, A&A, 320, 185

Wichmann, R., Sterzik, M., Krautter, J., Metanomski, A., & Voges, W., 1997b, A&A, 326, 211

Wichmann, R., Bastian, U., Krautter, J., Jankovics, I., & Rucinski, S. M., 1998, MNRAS, 301, L39

Wichmann, R., et al. 2000, A&A, 359, 181

Wichmann, R. & Schmitt, J. H. M. M. 2003, MNRAS, 342, 1021

Wichmann, R., Schmitt, J. H. M. M., Hubrig, S., 2003, A&A, 399, 983

Wilking, B. A., Lada, C. J., & Young, E. T., 1989, ApJ, 340, 823

Wolfe, W. L. & Zissis, G. J. 1985, Arlington: Office of Naval Research, Department of the Navy

Wolf, S. & Hillenbrand, L. A. 2003, ApJ, 596, 603

Wolk, S. J. & Walter, F. M. 1996, AJ, 111, 2066

Wood, B. E., Müller, H., Zank, G. P., & Linsky, J. L. 2002, ApJ, 574, 412

Zacharias, N., Urban, S. E., Zacharias, M. I., Wycoff, G. L., Hall, D. M., Germain, M. E., Holdenried, E. R., & Winter, L. 2003, VizieR Online Data Catalog, 1289, 0

Zuckerman, B., Song, I., Bessell, M. S., & Webb, R. A. 2001, ApJ, 562, L87

Zuckerman, B., Song, I. 2004, ApJ, 603, 738

Zuckerman, B., Song, I., Bessell, M. S., & Webb, R. A. 2001, ApJ, 562, L87

Zuckerman, B., Song, I., & Webb, R. A., 2001, ApJ, 559, 388 (ZSW01)

Zuckerman, B. & Webb, R. A., 2000, ApJ, 535, 959 (ZW00)